TITLE PAGE

New ultrasonic methods for detecting damage in metals and composite materials.

Submitted by Peter Robert Armitage, to the University of Exeter as a thesis for the degree of Doctor of Philosophy in Engineering, February 2009

I certify that all material in this thesis which is not my own work has been identified and that no material has previously been submitted and approved for the award of a degree by this or any other University

(signature)……

ABSTRACT

Recent requirements in the field of non-destructive testing are techniques that quantify micro-structural damage in a wide variety of materials during their manufacture and life cycle for ensuring both their quality and durability. Traditional evaluation techniques such as acoustic pulse echo, impact echo, resonance, ultrasonic transmission, electromagnetic and visual inspection methods are not sufficiently sensitive to the presence and development of domains of incipient and progressive damage. The research presented in this thesis details work undertaken by the author while working at the University of Exeter and is concerned with the development and validation of innovative methods to inspect micro-damage. Various non-linear acoustic measurement techniques, such as detecting defects by measuring the generation of harmonic and inter-modulation products, pulse inversion and resonant frequency deviation has been investigated. In addition to the experimental work new transducers and instrumentation has been developed and used in experimental validation tests on a variety of objects and differing materials. It has been found that the non-linear acoustic testing method provides a practical means by which low levels of progressive damage can be detected and quantified with sensitivities far in excess of that provide by conventional ultrasonic testing methods.

ACKNOWLEDGEMENTS

The author wishes to thank Koen Van Den Abeele of the Katholieke Universiteit Leuven, Belgium, who provided inspiration to this work and to the other members of the Aeronews research consortium. Thanks are also given to the Aeronautical Research and Test Institute (VZLU) in Prague, Czech Republic, who provided test samples and facilities for two of the large scale validation testing programs. I also wish to acknowledge the contribution of David Baker (XAT, University of Exeter, UK) who took my back of fag packet design sketches for the mechanical construction of the NBOX modules and produced professional CAD drawings and prototypes in plastic using their laser sinter station. To Mike Sloan also of XAT who assisted with the tensile tests and Luke Savage who dealt with all the business and financial aspects for this research project at Exeter, also my thanks is given to Roget Perrett (Technical services, University of Exeter, UK) who gave assistance in the construction of the power supplies and prototype printed circuit boards and all the students involved with testing the radio modules. Lastly a special thanks to my supervisor David Wright who helped in the final presentation of this thesis.

TABLE OF CONTENTS

LIST OF FIGURES

[sch] = schematic, [ph] = photograph, [gp] graphical plot

[ill] = illustration, [vsi] = video screen image

LIST OF TABLES

LIST OF SYMBOLS AND ACRONYMS

Institutional acronyms:-

KULAK: Catholic University of Leuven Campus Kortrijk, Belgium

VUB: Free University of Brussels, Belgium

ASCO: N.V. ASCO Industries, Belgium

MA: Masquito Aircarft, Belgium

DAKEL: ZD Rpety Czech Republic

IT AS CR: Institute of Thermomechanics, Czech Republic

VZLU: Aeronautical Research and Test Institute, Czech Republic

GIP Ultrasons, France

NDT Expert, France

IZFP: Fraunhofer Institute for Nondestructive Testing, Germany

POLITO: Politecnico of Turin, Italy

UNI-Na DPA: University of Naples, Italy

IA-CSIC: Instituto de Acustica, Spain

BR&TC: Boeing Research & Technology Center, Spain

CSM: CSM Materialteknik AB, Sweden

UNEXE: Exeter University, UK

UNIVBRIS: University of Bristol, UK (part of UK RCNDE)

UNOTT: University of Nottingham, UK (part of UK RCNDE)

CU: Cranfield University, UK

Material acronyms:-

PT = Lead Titanate

PZT = Lead Zirconate Titanate

PMN = Lead Magnesium Niobate

LM = Lead Metaniobate

PMN-PT = Lead Magnesium Niobate-Lead Titanate

PNN-PT = Lead Nickel Niobate-Lead Titanate

LGS = Lanthanum Gallium Silicon Oxide

LTA = Lithium Tantalate

BT = Barium Titanate

ADP = Ammonium Dihydrogen Phosphate

PVDF = Polyvinylidene Fluoride

GMM = Giant magnetostrictive materials

MSM = Magnetically shaped memory materials

CFRP = Carbon fibre reinforced polymer

Other acronyms

NEWS = Non-linear Elastic Wave Spectroscopy

NDT = Non-destructive testing

MEMS = micro-electro-mechanical-system

EMAT = Electromagnetic acoustic transducer

PLL = Phase Locked Loop

Acoustic symbols:-

Z = Acoustic impedance (P / V.A) [$Pa.s.m^{-3}$]

Z_o = Characteristic acoustic impedance ($C_L.\rho$) [$kg.m^{-2}.s^{-1}$]

z = Specific acoustic impedance (P/V) [$Pa.s.m^{-1}$]

C = General acoustic wave velocity

C_L = Longitudinal acoustic velocity, p-wave velocity [$m.s^{-1}$]

C_S = Shear wave acoustic velocity, s-wave velocity [$m.s^{-1}$]

C_R = Rayleigh wave velocity, surface wave velocity [$m.s^{-1}$]

C_E = Rod wave velocity, dimensions << wavelength ($\checkmark E/\rho$) [$m.s^{-1}$]

C_{rod} = General rod or bar acoustic velocity, dimensions << wavelength

C_T = Torsional wave velocity [$m.s^{-1}$]

C_F = Flexural wave velocity [$m.s^{-1}$]

C_{plate} = Longitudinal plate wave velocity [$m.s^{-1}$]

C_{lamb} = Lamb wave velocity [$m.s^{-1}$]

V = General particle velocity [$m.s^{-1}$]

ρ = Density [$kg.m^{-3}$]

P = Sound pressure (force/area) [Pa] or [$N.m^{-2}$] or [$m^{-1}.kg.s^{-2}$]

A = Area [m^2]

a = generally a linear dimension in the x-axis [m]

b = generally a linear dimension in the y-axis [m]

c = generally a linear dimension in the z-axis [m]

u = Displacement in the x-direction [m]

v = Displacement in the y-direction [m]

w = Displacement in the z-direction [m]

I = Second moment of a cross-section

K = Radius of gyration

Λ = Wavelength [m]

γ = Wavenumber ($2\pi / \Lambda$) cycles per meter

E = Young's modulus

ν = Poisson's ratio [dimensionless]

λ = Lame's first constant

μ = Lame's second constant, shear modulus

Φ = General phase angle

θ = Dilatation, change in volume of a unit cube

σ = Stress (force / unit area)

ε = Strain (change in dimension / original dimension)

$\varepsilon_{xx}, \varepsilon_{yy}, \varepsilon_{zz},$ = Strains in the x, y and z directions

$\sigma_{xx}, \sigma_{yy}, \sigma_{zz}$ = Stresses in the x, y and z directions

B = Bulk modulus

M = P-wave modulus

ω = Angular frequency ($2\pi f$)

Θ = general angle measurement (degrees or radians)

f = Frequency, cycles per second or Hertz $[s^{-1}]$

Ψ = Ratio of Rayleigh wave velocity to Shear wave velocity [dimensionless]

α = Material constant $(1 - 2\upsilon) / (2 - 2\upsilon)$

q,s = Attenuation factors

V_p = Phase velocity of acoustic wave

V_g = group velocity of acoustic wave

Np = Attenuation in Nepers

Ri = motional analogue of damping, due to internal losses

Rr = motional analogue of damping, due to radiation losses

F_p = parallel resonant frequency (for piezoelectric crystal)

F_s = series resonant frequency (for piezoelectric crystal)

β = non-linear ultrasonic parameter (A_2/A_1^2)

A_1 = amplitude of fundamental frequency

A_2 = amplitude of second harmonic

Electrical symbols:-

C_o = Static capacitance of a PZT material

Z_e = Electrical Impedance

Q = Quality factor

L = general electrical inductance

C = general electrical capacitance

R = general electrical resistance

ε_{pzt} = permittivity of piezoelectric (farads/m)

X_c = Capacitive reactance ($1/2\pi.f.C$)

X_L = Inductive reactance ($2\pi.f.L$)

PREFACE

The main funding for the research detailed in this thesis was provided by the European Sixth framework programme, AST3-CT-2003-502927 Aeronautics and space, and titled AERONEWS. This project was to enhance and implement new experimental and simulation tools necessary to measure, characterize, predict, quantify, and locate early stage damage in aircraft components and structures, based on the non-linear response of a material. The Non-linear Elastic Wave Spectroscopy (NEWS) technique developed in this thesis has proved to be a very sensitive and effective method in detecting micro-damage in materials at the early stages of failure, and long before linear acoustic properties show any signs of material degradation.

The AERONEWS research program was split into seven work packages (WP1 to WP7). WP1 being concerned with an optimisation study of the NEWS technique to detect micro-scale damage in aircraft components and structures, this included the selection of suitable components to test, methods of testing and an investigation of failure scenarios. WP2 involved simulations and theoretical evaluation of non-linear behaviour in micro-damaged structures, this being to supplement the experimental investigations. WP3 involved a market survey of suitable transducers, including an analysis of their capabilities and limitations for use in NEWS testing. The work package also included the design and development of new transducers and "SMART" components.

WP4 was concerned with producing a specification for an instrument that would perform all the NEWS testing and measurement methods together with the construction of such an instrument. In addition this work package was to include and investigation in to remote control and wireless communication links.

WP5 was the experimental implementation of the NEWS method and included demonstrations of the application to small and large aircraft components. This experimental work involved three development tests, one conducted at Exeter and the other two at VZLU in Prague, Czech Republic, involving large test objects. Other small scale experimental validation tests were performed at each partners own laboratories. WP6 involved the academic and industrial dissemination of the research work, mainly through papers, conferences and patents and WP7 the project management.

This thesis concentrates on the work contributed by the author while working for University of Exeter who were the leaders for work package WP4 and played significant roles within work packages WP3 and the experimental work of WP5.

The AERONEWS research focus was on the expansion of the present knowledge of the non-linear behaviour of progressive fatigue damage in aircraft parts and structures, the development of explicit sensor systems and advanced self-monitoring components, the formulation of an integrated design for a testing procedure and a unique engineered monitoring system for micro-damage inspection including remote control and communication tools, together with the validation of the applicability of the system to real time in-situ inspection of a full-scale model on the ground. This activity included a study of integrating these techniques into existing engine and control health monitoring strategies. The photograph below shows the author and other Aeronews partners putting a steel bracket through cyclic loading and using non-linear and various other techniques to detect the onset of damage.

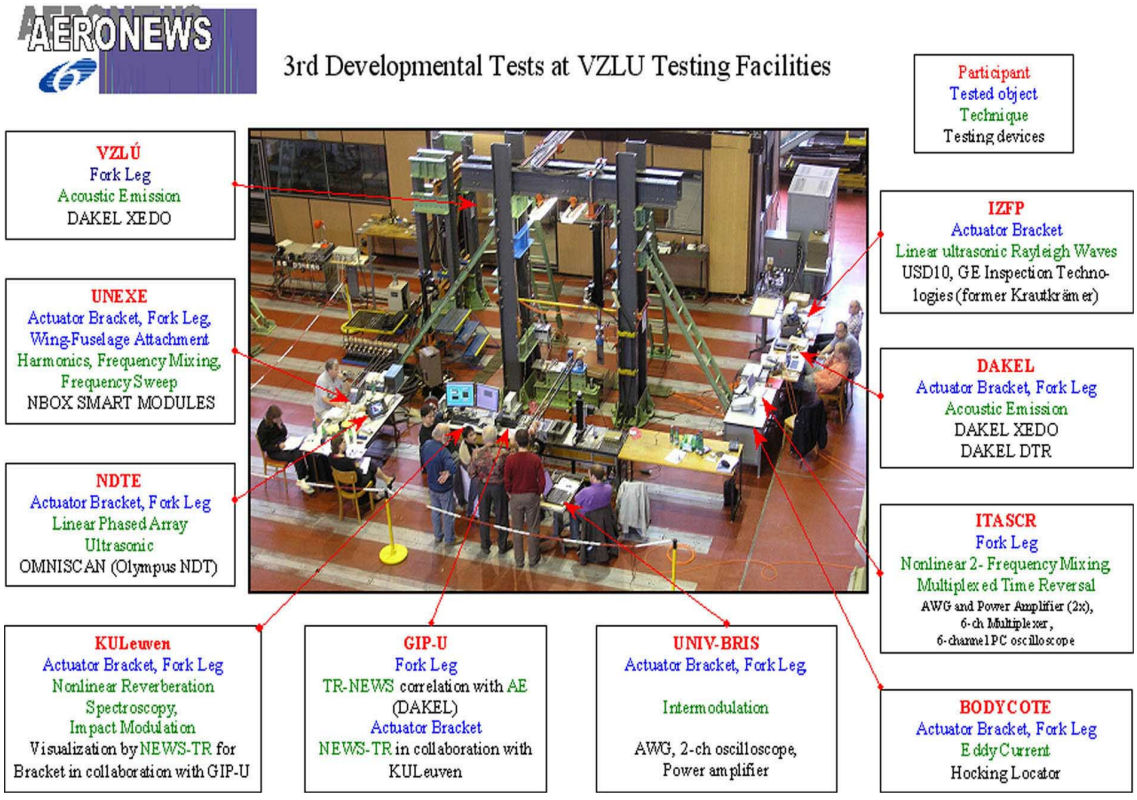

Included in this thesis is other work performed during the period of this PhD research program both prior to and after the Aeronews work program. This has been funded from other sources principally Theta Technologies Ltd and is concerned with non-linear acoustic testing of railway track and concrete structures.

1 INTRODUCTION

The testing of modern composite materials and structures has posed many problems since conventional ultrasonic pulse echo methods have often been difficult to apply since they cause multiple reflections and non-direct ray paths. This thesis gives details of research carried out by the author involving the use of non-linear acoustic methods and identifies how these techniques can overcome many of the obstacles found in conventional ultrasonic testing. This section starts with the overall aims and objectives then outlines some general information on acoustics that are needed in understanding the subsequent chapters of this thesis.

1.1 Aims and objectives of this research

The aim of the research detailed in this thesis is to investigate the non-linear acoustic properties of materials with the objective of developing a methodology by which these properties can be used to provide a measure of progressive degradation in a material. The research investigated various non-linear acoustic measurement techniques. One of these methods examines an acoustic waveform as it traverses through or over a complex structure and material. Examination of this ultrasonic waveform and how it changes in shape, or distorts, enables the degree of damage to be ascertained and quantified. The specific objective of this method of testing is not to locate a single defect but to determine the overall mechanical properties within a defined region. The changes in the waveform are directly related to the stress-strain relationship and the hysteretic properties of the material and not unduly effected by the ray path. In damaged materials, particularly ones that have micro-cracking, the stress-strain relationship does not obey Hooke's Law of elasticity, stress is not proportional to strain (i.e., not linear), resulting in the distortions to a single frequency ultrasonic stress waveform traversing through it. The degree of this distortion is determined by examining the spectral content of the waveform; second, third and higher harmonics will be present and the relative amplitude of these are related to the amount of damage. Other variants of this method that are detailed in this thesis utilise waveforms with greater complexity such a frequency sweeps and the sum of two sine waves. These were investigated to determination if they provide any additional advantages.

Other non-linear techniques investigated involved comparing the impulse response of a material to a compressional pulse to that of a tensile pulse, this being particularly suited for materials that are de-laminated or have de-bonding, where the stress-strain relationship is non-symmetric. In a damaged material the responses will be different, and one of the objectives of this research was to find methods by which this can be quantified. The variation of resonant frequency with amplitude is a known non-linear phenomenon and another objective within this research was to determine a practical method by which this variation can be measured.

1.2 Composite materials and structures

The range of modern composite materials and structures that are produced using them is vast. In recent times some of the most important composite materials are based on glass or carbon fibres imbedded within an epoxy. This type of composite will exhibit anisotropic behaviour; acoustic properties such as velocity and attenuation will be dependent upon the direction of fibres. Cross-weave layers bonded together will introduce acoustic interfaces that give rise to reflections or deviated wave paths, making testing by conventional ultrasonic methods difficult. Figure 1 shows a schematic of typical stacked and bonded fibre-reinforced sheets.

Figure 1 Stacked and bonded fibre-reinforced sheets

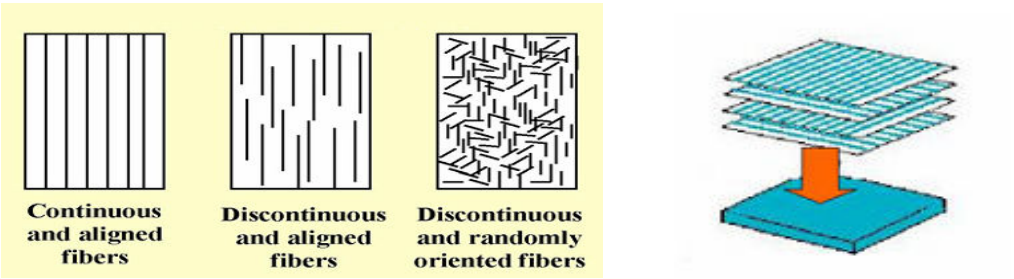

The types of defect that are of concern to manufactures and users of this type of composite material are principally micro-cracking and de-laminations. Non-linear acoustic testing methods although unable to locate the position of such defects precisely do have the ability to detect them within a specified region with considerable

sensitivity; a sensitivity far in excess of that provided by conventional ultrasonic methods.

Concrete is one of the most widely used composite materials, this has been used extensively in Civil engineering applications from ancient Roman times to the present day. Conventional ultrasonic testing has proved to be very difficult with this material due to scattering of the acoustic waves and has been limited mainly to just velocity measurements. The author has prior to this research project had some success in extending this to reflection and time of flight ultrasonic methods for the detection of defects and voids. Armitage[1] and [2]. Figure 2 shows a cross section of a sample of concrete, the high density aggregates reflect and scatter any acoustic energy transmitted into the material. The sample shown in this figure has a defect known as micro-cracking, which can be observed as lines radiating out from and between the aggregates.

Figure 2 Concrete with micro cracking

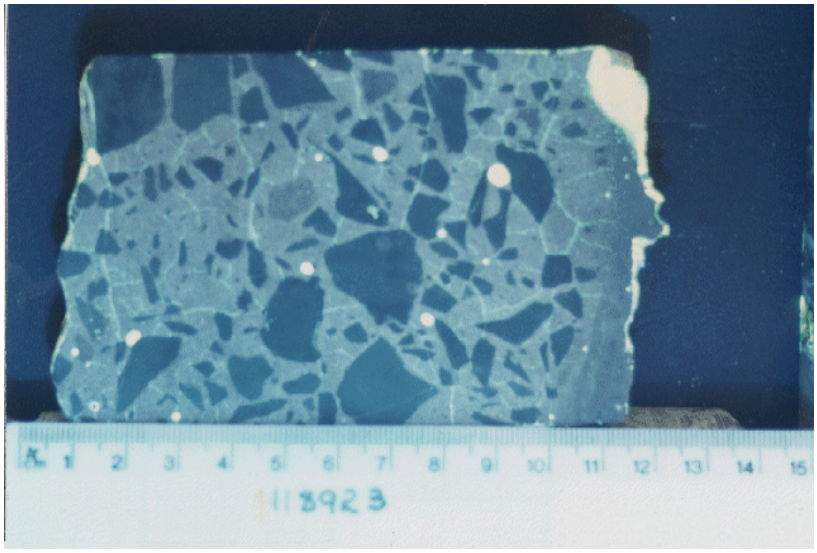

In the aircraft and other similar industries one of the important building materials is based on a structure consisting of honeycombed panels so conventional acoustic testing methods based on transmission or reflection of ultrasonic waves through the material will be subject to multiple paths, scattering and multiple reflections. The structural voids in honeycombed panels will indicate as defects. Figure 3 shows an example from Fosham Youchaoshi Ltd of a basic sandwich panel with honeycomb core.

Figure 3 Sandwich panels with honeycomb core

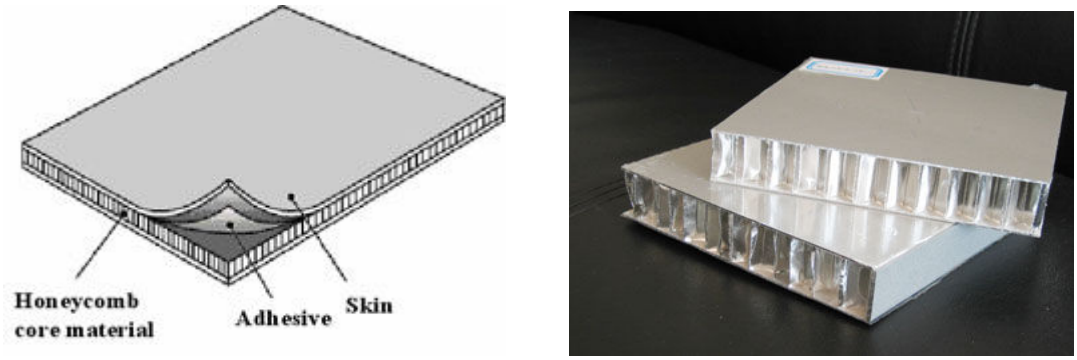

The main advantage of non-linear acoustic techniques, detailed in this thesis, is that it is a frequency domain method, unlike conventional ultrasonic methods which are time domain methods, these methods are concerned with spectral content, the path taken by the ultrasonic wave is not critical. It is only dependent upon the mechanical properties that the wave encounters while travelling over or through a structure.

Aircraft composite materials

Military aircraft composites account for up to 80% of the structure, for example the Harrier GR5 is composed of 32% composites and the Euro Fighter 70%. Figure 4, shows an example of the typical construction of a fighter jet from Composite Horizons inc, USA.

Figure 4 Military aircraft composite structure

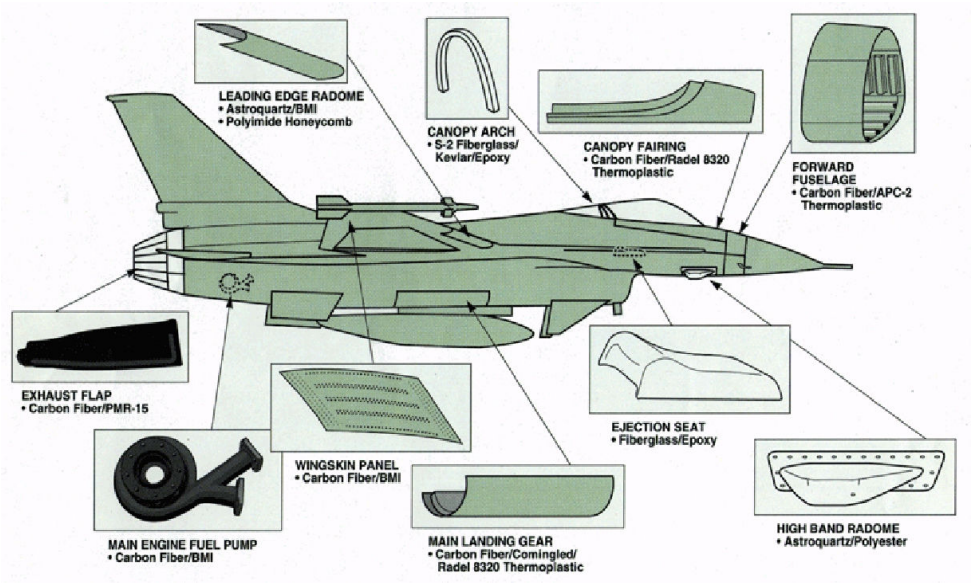

Approximately 20% of the structure of modern civil airlines is constructed from composite materials for example MD11 is 30% and the Airbus A320 is 16%. An example is shown in Figure 5 from Firenet International.

Figure 5 Civil aircraft composite structure

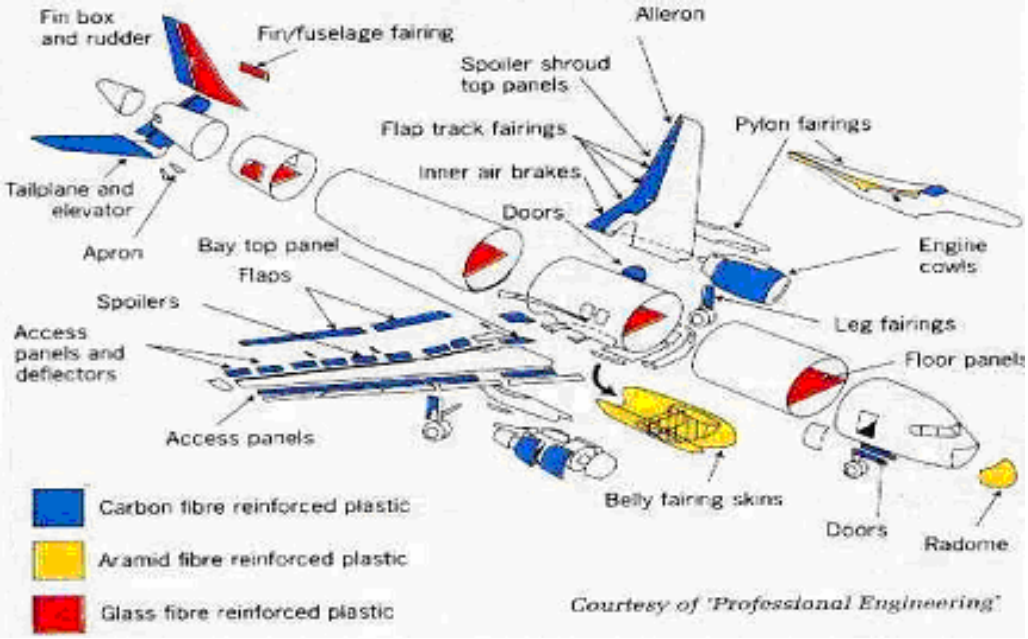

1.3 Acoustic impedance

Acoustic impedance is an important parameter and is used in evaluating acoustic transmission and reflection at the boundary of two materials having different composition. It is also of considerable use in the design of ultrasonic transducers and in analysing the ray paths of sound in a medium. The acoustic impedance Z is a frequency dependent parameter. Mathematically, it is the sound pressure P divided by the particle velocity V and the surface area A, through which an acoustic wave of a specified frequency propagates.

$$\text{Acoustic impedance } Z = \frac{\text{sound pressure}(P)}{\text{particle velocity}(V) * \text{surface area}(A)} \quad [\text{Pa}\cdot\text{s}\cdot\text{m}^{-3}]$$

The product of particle velocity and the surface area is sometimes called the volume velocity.

Specific acoustic impedance

The specific acoustic impedance *z* is the ratio of sound pressure P to the particle velocity V at a single frequency, therefore:-

$$\text{Specific acoustic impedance, } z = \frac{\text{sound pressure(P)}}{\text{particle velocity(V)}} \qquad [\text{Pa}\cdot\text{s}\cdot\text{m}^{-1}]$$

$$= \text{acoustic impedance(Z)} * \text{surface area(A)}$$

Characteristic acoustic impedance

The characteristic acoustic impedance Z_o of a material is defined as the product of its density ρ [$\text{kg}\cdot\text{m}^{-3}$] and its longitudinal acoustic velocity C_L [$\text{m}\cdot\text{s}^{-1}$].

$$Z_o = \rho.C_L \quad [\text{kg}\cdot\text{m}^{-2}\cdot\text{s}^{-1}]$$

The Rayl

The Rayl is a unit that can represent both specific acoustic impedance and the characteristic acoustic impedance. One Rayl represents the acoustic impedance when a sound pressure of 1 Pa produces a linear velocity of 1 m/s. In MKS units, 1 Rayl equals 1 Pascal-second per metre [$\text{Pa}\cdot\text{s}\cdot\text{m}^{-1}$], or equivalently 1 Newton-second per cubic metre [$\text{N}\cdot\text{s}\cdot\text{m}^{-3}$]. In SI base units this is [$\text{kg}\cdot\text{m}^{-2}\cdot\text{s}^{-1}$]. In practice when working with metals and composite solids the working unit is called the MRayl. (10^6 * Rayl). For example in Aluminium the longitudinal sound wave velocity C_L is 6374 $\text{m}\cdot\text{s}^{-1}$ and the density is 2700 $\text{kg}\cdot\text{m}^{-3}$. The characteristic acoustic impedance is then Z_o = 6370 * 2700 = 17.2 * 10^6 * Rayl = 17.2 MRayls. Figure 6 was compiled by the author from various manufacturers data sheets give the characteristic acoustic impedance of some common composite materials.

Figure 6 Acoustic impedance of common composite materials

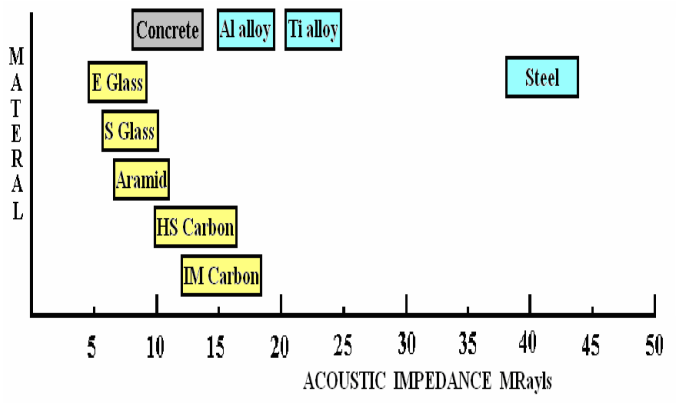

HS: (high strength) carbon fibre
IM: (intermediate modulus) carbon fibre
E: (electrical-low alkali) glass fibre
S: (strong) glass fibre
Aramid: (polyamide-kevlar) fibre
Al alloy: Aluminium alloy
Ti alloy: Titanium alloy
Steel: Iron alloy
Concrete: Sand / cement / stone aggregate

The materials shown in yellow are based on discontinuous randomly oriented fibres. Aligned fibres will exhibit different acoustic impedances in different directions (anisotropic acoustic impedance). Structural composites will in addition to anisotropy have an abrupt change in acoustic impedance at the boundary layers.

1.4 Ultrasonic wave propagation

The characteristics of sound wave motion depend upon the mechanical properties of the medium in which they propagate. The elastic behaviour of an isotropic solid can be completely defined in terms of two constants, known as Lame's constants. For convenience four elastic constants are normally used, these are Young's modulus, Poisson's ratio, the Bulk modulus and the Rigidity modulus. Details of these constants and their relationship to each other are given in Appendix A.
Three types of sound wave motion can be produced in an isotropic infinitely extended solid medium these are:-

Longitudinal Waves:- These are waves are also known as compressional waves, p-waves or irrotational waves (Figure 7a). The velocity of these waves is given by $C_L = [E(1-\upsilon) / (\rho(1-2\upsilon) (1+\upsilon))]^{1/2}$ where E = Young's modulus, , υ = Poisson's ratio and ρ = density.

Transverse Waves:- These waves are also known as shear waves or s-waves. These are rotational waves, having a plane of polarisation. The energy is at right angles to the direction of travel (Figure 7b). The velocity of these waves is given by $C_S = [E / (2\rho(1+\upsilon))]^{1/2}$ where E = Young's modulus, υ = Poisson's ratio and ρ = density.

Rayleigh Waves:- These waves are also known as surface waves, They are confined to the surface of an extended medium. The wave energy decreases rapidly with depth and its particle motion has an elliptical form (Figure 7c). To an approximation Harker[3] gives the velocity of these waves, C_R to be equal to $C_S(0.862 + 1.14\upsilon) / (1+\upsilon)$ where C_S= shear wave velocity and υ = Poisson's ratio.

In an isotropic bounded medium the waves are constrained in some way, either by the physical dimensions of the material in which they are propagating or by the interface between two or more dissimilar materials. When a sound wave is constrained in this manner, the wave is guided along its path (a guided wave) and can have various modes of propagation. In addition the velocity of propagation is found to depend on the frequency, this phenomenon is called dispersion. A detailed analysis is provided in Kolsky[4]. If a pulse or wave packet is transmitted into such a medium, since it is composed of many frequency components, each of these components will propagate with different velocities. This causes the pulse or wave packet to change shape, "spread out" or disperse. Two quantities are used to define this "spreading" the phase velocity $V_p = \omega / \gamma$ and the group velocity $V_g = \delta\omega / \delta\gamma$.

Longitudinal Rod Waves (cylindrical bars):- These are compressional waves that propagate within a solid rod. If the wavelength is long compared to the dimensions of the rod then the velocity is given by $C_E = (E/\rho)^{1/2}$.
If the wavelength is smaller than the dimensions of the rod; the rod wave group velocity C_{Eg} and the phase velocity C_{Ep} is given by:-

$$C_{Eg} = (E/\rho)^{1/2} [1 - 3\upsilon^2 \pi^2 (a / \Lambda)^2]$$
$$C_{Ep} = (E/\rho)^{1/2} [1 - \upsilon^2 \pi^2 (a / \Lambda)^2]$$

where E = Young's modulus, υ = Poisson's ratio, Λ = wavelength, ρ = density, a = diameter of the rod.

Torsional Waves:- These are "twisting" waves that propagate along a rod. According to Mason [5] the velocity of a torsional wave in a cylindrical bar is given $C_T = (\mu / \rho)^{1/2}$ where μ = shear modulus and ρ = density.

Lamb Wave (thin plate wave):- These are plane waves that propagate in an infinite plate, normally with a wavelength comparable with the plate thickness. Lamb waves are dispersive waves. Figure 7f, from Mircea[6], shows a plot of the group and phase velocities of a Lamb wave versus frequency for a thin carbon fibre plate. The attenuation versus frequency for this material is given in Figure 10.

According to Harker[7] a Lamb wave is composed of both compressional and shear waves. In one set of modes, the motion is symmetrical about the mid thickness plane. In the other set it is anti-symmetric, illustrated in Figures 7d and 7e.

Sezawa waves:- These waves are higher order Rayleigh waves and have been investigated by Grewal[8] for applications in detecting defects just below the surface of a railway track.

Stoneley Wave (boundary wave):- These waves consist of a motion that is confined to the interface between two solids or a fluid and a solid, illustrated in Figure 7g.

Love Wave:- According to Dobrin[9], these waves are horizontally polarized shear waves (SH waves) guided by an elastic layer, which is "welded" to an elastic half space on one side while bordering a vacuum on the other side. They are mainly of concern to the geophysics industry and have importance in earthquake damage prediction, however they are starting to be of interest in material testing. Love waves travel with a slower velocity than P- or S- waves, but faster than Rayleigh waves, they are illustrated in Figure 7h.

Floquet waves: Potel[10] describes the methodology to analyse acoustic waves passing through layered materials of carbon or other fibre composites. Though the Floquet waves are not plane waves, they play the role of plane waves for the infinite periodically multilayered medium.

Summary of principal wave motions

Figure 7a Compressional

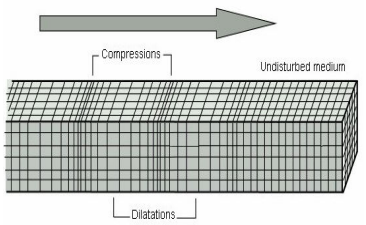

Figure 7b Shear

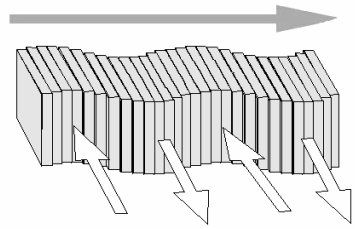

Figure 7c Rayleigh

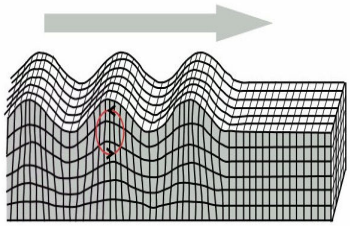

Figure 7d
Anti-symmetric Lamb wave

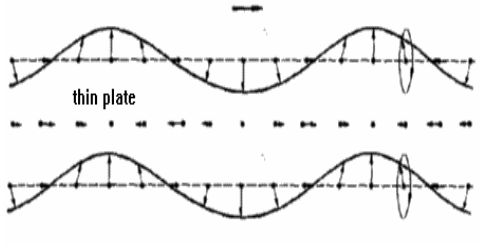

Figure 7e
e) Symmetric Lamb wave

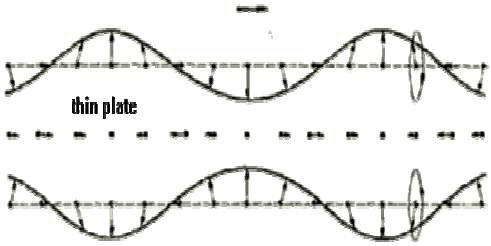

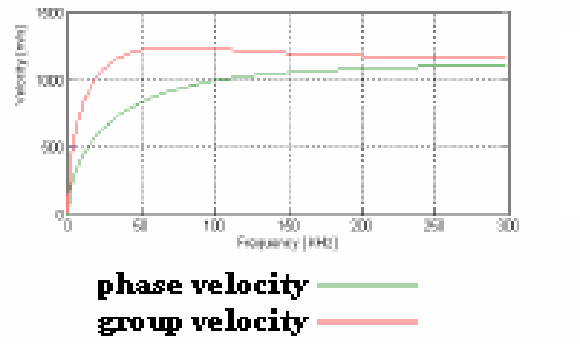

Figure 7f
Group and Phase velocity for Lamb waves in carbon fibre plate

Figure 7g Stoneley Wave motion

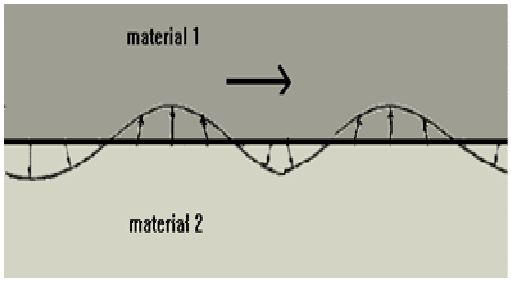

Figure 7h Love wave motion

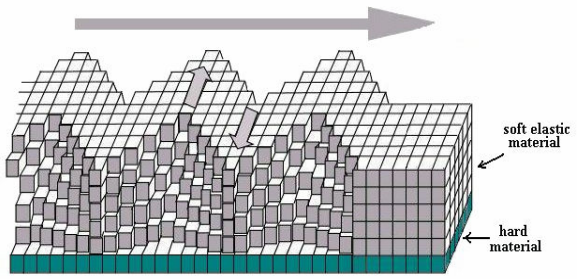

Acoustic reflection and transmission

Ultrasonic waves are reflected at boundaries where there is a difference in acoustic impedances (Z) of the materials on each side of the boundary. This difference in Z is commonly referred to as the impedance mismatch. The greater the impedance mismatch, the greater the percentage of energy that will be reflected at the interface or boundary between one medium and another, this is illustrated in Figure 8 below.

Figure 8 acoustic reflection and transmission

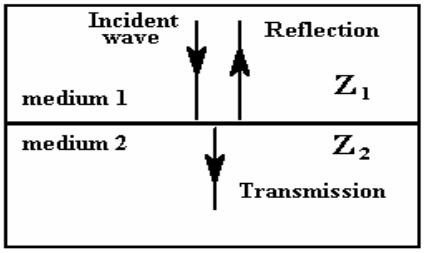

Reflection coefficient, $R = \frac{Z_2 - Z_1}{Z_1 + Z_2}$

Transmission coefficient, $T = \frac{2.Z_2}{Z_1 + Z_2}$

The coefficients R and T above refer to proportions of the amplitudes of the stress (pressure) waves that are either reflected or transmitted. A negative sign indicates a phase reversal at the boundary, that is if the incident wave is compressive then the reflected wave is tensile and vice-versa. R will also represent the proportion of the strains, however T does not. The power is related to amplitude and wave velocity (time rate of flow of energy), and the power per unit area is the intensity. The ratio of reflected intensity to the incident intensity is R^2 and the ratio of the transmitted intensity to the incident intensity is $4Z_1Z_2 / (Z_1 + Z_2)^2$

Both the acoustic transmission and reflection coefficients are important in determining the efficiency with which ultrasound can be injected into a material, and the choice of a coupling material to optimise the transfer of ultrasound between the transducer and test specimen. The optimum transfer is obtained when the transducer's (source) acoustic impedance is the same as the test material (load).

Acoustic refraction

Refraction takes place at an interface due to the different velocities of the acoustic waves within the two materials. Figure 9 shows the general angular relationship between incident p-waves and s-waves with their corresponding reflections and transmissions.

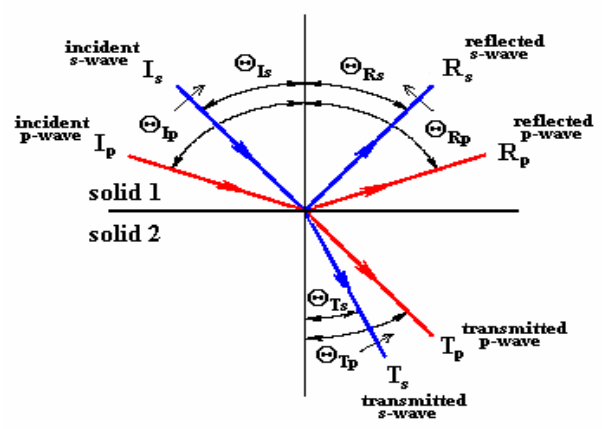

Figure 9 acoustic refraction

Solid 1:-
p-wave velocity = C_{L1}
s-wave velocity = C_{S1}

Solid 2:-
p-wave velocity = C_{L2}
s-wave velocity = C_{S2}

$C_{L2} < C_{L1}$
$C_{S2} < C_{S1}$

This relationship is subject to Snell's Law:-

$$\frac{\sin\Theta_{Ip}}{C_{L1}} = \frac{\sin\Theta_{Is}}{C_{S1}} = \frac{\sin\Theta_{Rp}}{C_{L1}} = \frac{\sin\Theta_{Rs}}{C_{S1}} = \frac{\sin\Theta_{Tp}}{C_{L2}} = \frac{\sin\Theta_{Ts}}{C_{S2}}$$

When the solid 2 has a slower velocity of sound than solid 1 the refracted wave (transmitted wave Ts or Tp) is bent or steered toward the normal (which is the case illustrated). When solid 2 has a higher velocity than solid 1 the refracted waves are bent toward the surface.

When a longitudinal wave moves from a slower to a faster material, there is an incident angle that makes the angle of refraction for the wave 90°. This is known as the first critical angle. At this critical angle of incidence, much of the acoustic energy is in the form of an inhomogeneous compression wave, which travels along the interface and decays exponentially with depth from the interface. For any angle beyond the critical angle, total reflection of the incident wave occurs.

Attenuation of ultrasonic waves

When sound travels through a medium, its intensity diminishes with distance. In idealized materials, sound pressure (signal amplitude) is only reduced by the spreading of the wave. Natural materials, however, all produce an effect which further weakens the sound. This further weakening results from scattering and absorption. Scattering is the reflection of the sound in directions other than its original direction of propagation. Absorption is the conversion of the sound energy to other forms of energy. The combined effect of scattering and absorption is called attenuation. Ultrasonic attenuation is the decay rate of the wave as it propagates through material.

The amplitude change of a decaying plane wave can be expressed as:-

$$A = A_0 e^{-\alpha z}$$

In this expression $\mathbf{A_0}$ is the un-attenuated amplitude of the propagating wave at some location. The amplitude **A** is the reduced amplitude after the wave has travelled a distance **Z** from that initial location. The quantity $\boldsymbol{\alpha}$ is the attenuation coefficient of the wave travelling in the z-direction. The dimensions of α are Nepers / length, where a Neper is a dimensionless quantity. The units of the attenuation value in Nepers per meter (Np/m) can be converted to decibels/length by dividing by 0.1151. Attenuation is generally proportional to the square of sound frequency, however in many cases graphical plots of attenuation versus frequency for a particular material are provided. Figure 10 shows a plot of attenuation (Nepers / mm) against the frequency (kHz) for a Lamb wave travelling in a unidirectional carbon fibre laminate.

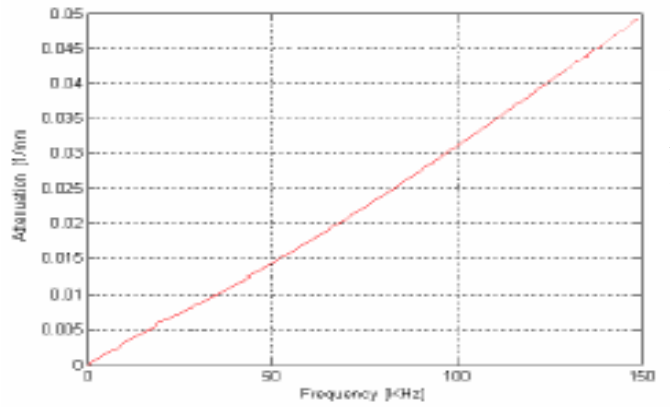

Figure 10
Attenuation versus frequency for Lamb wave in carbon fibre composite.

Wave conversion

According to Harker [11], when an acoustic wave undergoes reflection or refraction at a boundary three processes can occur, changes in amplitude, changes in wave mode and changes in phase. This is illustrated in Figure 11.

Figure 11 Mode conversions on reflection and refraction

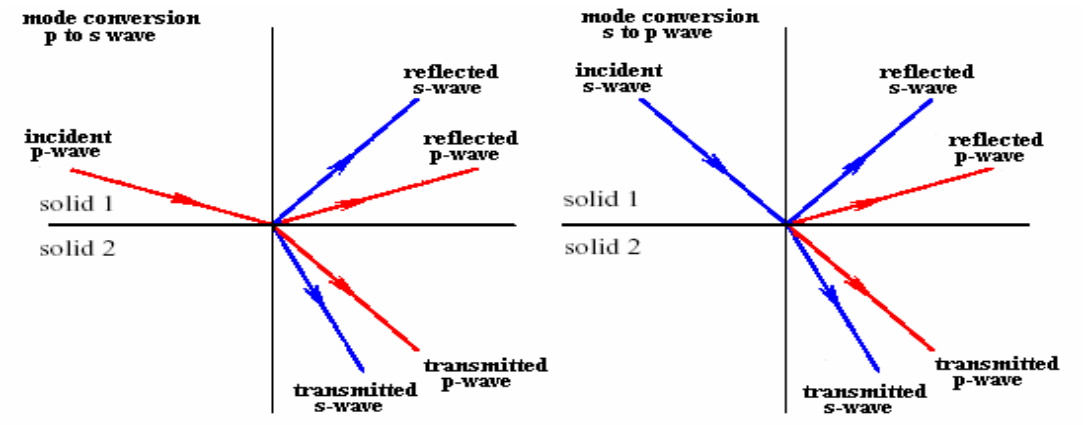

When sound travels in a solid material, one form of wave energy can be transformed into another form. For example, when a longitudinal wave hits an interface at an angle, some of the energy can cause particle movement in the transverse direction to start a shear (transverse) wave. Mode conversion occurs when a wave encounters an interface between materials of different acoustic impedances and the incident angle is not normal to the interface.

The mode conversion is zero for normal incidence and for glancing incidence. For angles of incidence in the region of 60 to 70 degrees there is substantial loss of compression wave (p-wave) amplitude into shear waves (s-waves). This is illustrated in Figure 12, from Harker[11] page 28.

Figure 12

Amplitudes of reflected p and s waves
for incident p waves and two values of Poisson's ratio.

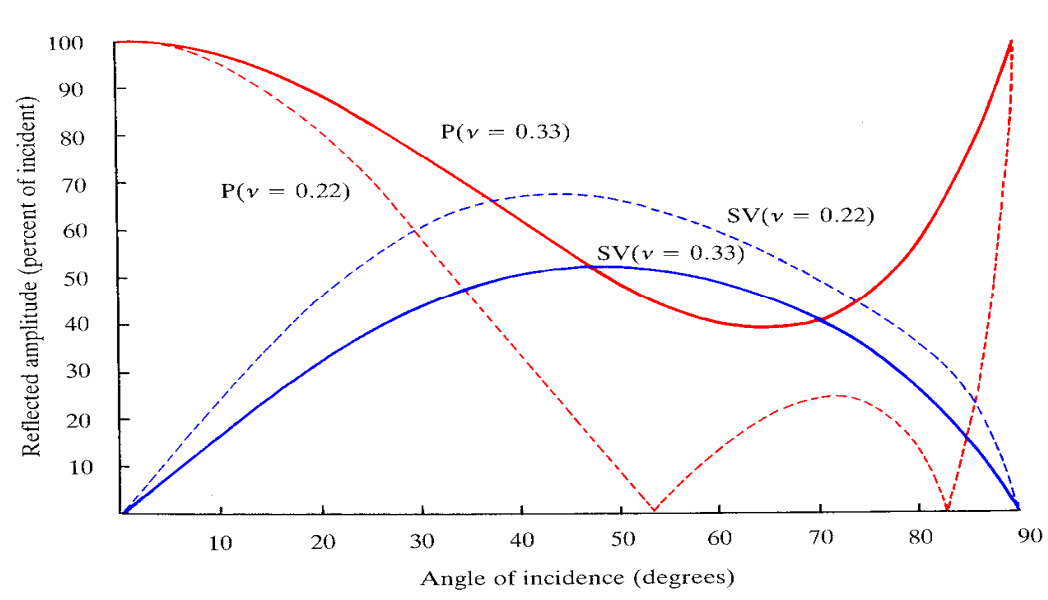

2 NON-LINEAR ACOUSTIC METHODS

The author's researches, presented in this thesis, are concerned with the measurement of harmonic and inter-modulation product generation, resonant frequency variation with amplitude, pulse and inverted pulse response, frequency sweep response and spectral filtering resulting from defects in a wide range of materials. The first part of this chapter outlines the basic principles behind the non-linear acoustic testing method and how the measurements are made. The final part of this chapter includes a brief overview of the time reversal non-linear acoustic method. The author was not directly involved with the time reversal theoretical and experimental work, however the system hardware designed and developed during this research period will enable these techniques to be performed and for this reason has been included here.

2.1 Mechanical non-linearity

The well established linear acoustic method to detect defects measures reverberation, reflection, scattering, transmission and absorption of acoustic energy. The presence of a defect changes the phase or amplitude of a signal while the frequencies remain unchanged. The non-linear technique correlates the presence and characteristics of a defect with acoustic signals that have changed in frequency or frequency content. This change is due to the non-linear transform of the acoustic energy by a defect.
Materials containing cracks, fractures, de-laminations and de-bonding have a relatively large non-linear response to acoustic signals. Non-linear fault detection methods provide much higher sensitivity than conventional linear methods, particularly in non-homogeneous materials such as concrete and other composites. The physical mechanism involves the fact that when a sinusoidal acoustic wave traverses a defective region, or is incident upon a defect, the wave changes the contact area, increasing in compression, decreasing in tension. The cracks close under compression and open out under tension. This non-linearity gives rise to three important phenomena these are;
1) Acoustic waveform distortion; that is the generation of harmonics, overtones and inter-modulation products. 2) A change of velocity or dampening with acoustic wave amplitude. 3) An ability to store energy and then release this at a later time (Hysteresis).

Figure 13 Stress versus Strain for Linear and Non-Linear materials.

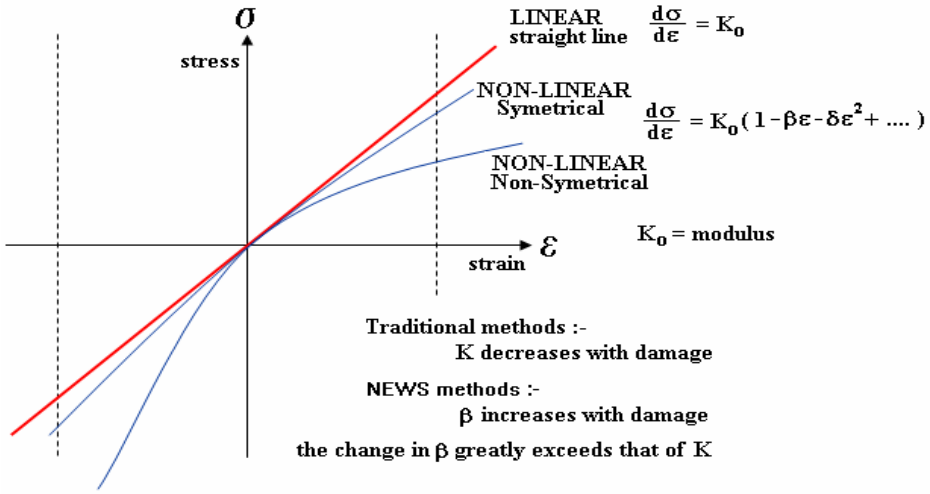

Referring to Figure 13 above, the red straight line represents the well known Stress-Strain relationship for a material obeying Hooke's Law of elasticity. The two curved blue lines show the Stress-Strain relationship for two types of non-linearity. One is symmetrical about the zero point. This implies that the stress-strain relationship is the same for both compression and tension. The second lacks symmetry about the zero point. This implies that there is a significant difference in the Stress-Strain relationship when the material is under compression from that when it is under tension. Typically this will be found in materials that have micro-cracks. Under compression the cracks close up, under tension they open out, giving rise to different elastic properties.
Both these non-linear effects will cause distortion to an elastic wave as it passes through the material, giving rise to changes in its frequency content, this is illustrated in the Figure 14. In the case of a pure sine stress-wave, harmonics and overtones will be generated.

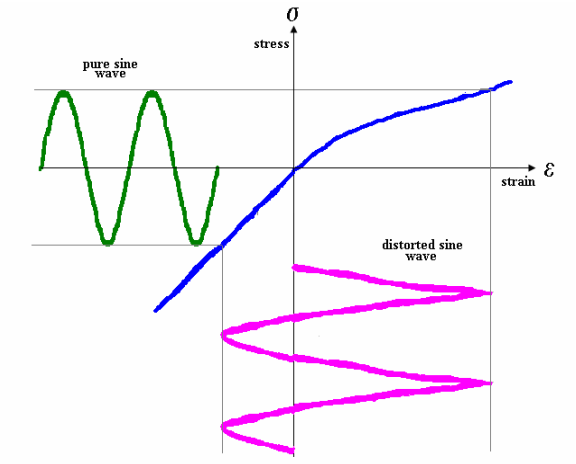

Figure 14 Harmonic generation

In a material with non-linear stress-strain properties an applied sinusoidal stress will produce a non sinusoidal strain.

For elastic waves consisting of two sine waves harmonics, overtones and inter-modulation product frequencies will be generated. The practical methods by which these frequency measurements are made are detailed in sections 2.2 and 2.3.
Figure 15 illustrates how the velocity of an elastic wave can change as a function of its amplitude in a non-linear material. The plot on the left shown in green is the non-linear, non - symmetrical, Stress - Strain relationship for the material. The modulus of elasticity (stress/strain) will depend upon the strain that is applied at any one point. The velocity of an elastic wave depends upon the materials density and its elastic modulus. Large positive amplitudes, corresponding to large compressive strains, will have a high modulus of elasticity and consequently a faster velocity. Large negative amplitudes, corresponding to large tensile strains will have a low modulus and therefore a low velocity.

FIGURE 15 wave velocity variation with amplitude

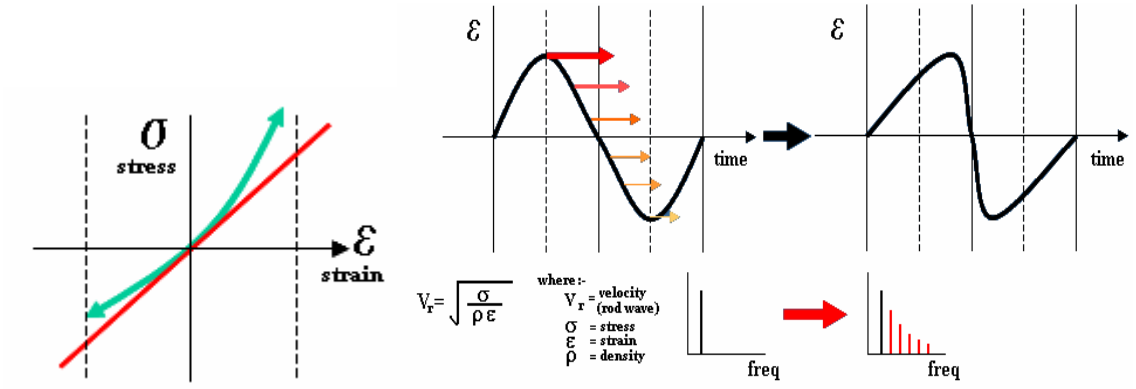

The effect illustrated right in the above Figure 15 shows the elastic waveform is "re-shaped" and "bunched up", its frequency content is increased and the peak to peak distance between cycles reduced. Practical methods by which these changes are measured are detailed in section 2.4.
The Figure 16 below shows the Stress – Strain relationship for a material that exhibits Hysteresis. Under cyclic loading energy is stored within the material and then suddenly released. The elastic modulus changes in "steps" over time and causes a sinusoidal elastic wave to re-form in to a triangular shape. The consequence of this is the generation of odd harmonics.

FIGURE 16 Stress-strain in hysteretic materials

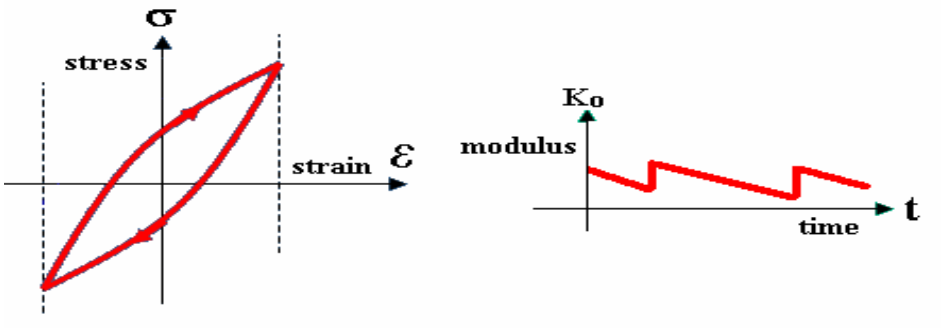

According to Van Den Abeele [12] the one dimensional relation between the stress σ and the strain ε in models of the dynamic behaviour of solids can be expressed as:-

$$\sigma = \int K\left(\varepsilon, \frac{d\varepsilon}{dt}\right) d\varepsilon$$

where:-

K = the non-linear and hysteretic modulus
σ = the stress
ε = the strain
dε/dt = the strain rate

K the non-linear and hysteretic modulus is given by:-

$$K\left(\varepsilon, \frac{d\varepsilon}{dt}\right) = K_0 \left\{ 1 - \beta\varepsilon - \delta\varepsilon^2 - \alpha\left[\Delta\varepsilon + \varepsilon(t)\, \mathrm{sign}\left(\frac{d\varepsilon}{dt}\right)\right] + \cdots \right\}$$

where:-

Ko = the linear modulus
β and **δ** = classical non-linear perturbation coefficients
α = a measure of the material hysteresis
Δε = the local strain amplitude over previous period
[Δε = (εmax - εmin) / 2] for continuous sine excitation
sign (dε/dt) = +1 when dε/dt > 0
sign (dε/dt) = -1 when dε/dt < 0

The Figure 17 illustrates the effects of non-linearity and hysteresis on the modulus-strain and stress-strain relation, the deformation of the elastic wave, the harmonic spectra and the amplitude dependence of the second and third harmonics.

FIGURE 17 Overview of Non-Linear effects on waveform propagation.

	Linear	Nonlinear Classic 1st order pertubation β	Nonlinear Classic 2nd order pertubation δ	Nonlinear Hysteretic α
Modulus - Strain	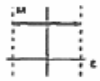			
Stress - Strain	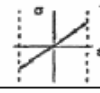		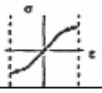	
Modulus - Time	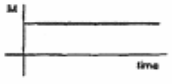	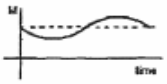	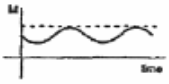	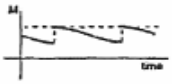
Strain - Time	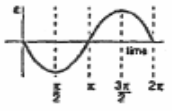	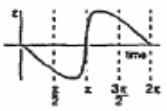	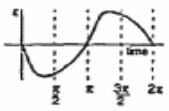	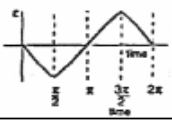
Strain Amplitude Frequency Spectrum	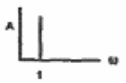		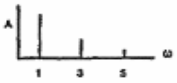	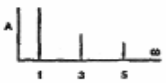
Harmonic Amplitude Dependence	No Harmonics	All Harmonics	Odd Harmonics	Odd Harmonics

For materials with linear properties the modulus is constant under all strain conditions, and throughout all time. The stress versus strain curve is a straight line function. An acoustic wave will apply a strain to the material at specific times. The result is no waveform distortion, no harmonic generation.

For materials with non-linear properties the modulus varies with the strain and is time dependent. The stress versus strain curve is not a straight line, it changes in some specific way depending on the type of non-linearity. An acoustic wave will become distorted, harmonics are generated. According to Frouin [13] the non-linear ultrasonic parameter β that represents this departure from linearity is given by A_2 / A_1^2 where A_1 is the amplitude of the fundamental and A_2 is the amplitude of the second harmonic.

2.2 Harmonic and overtone generation

The simplest method in a practical system that measures non-linear effects in a material using acoustic waves is to measure the harmonics generated when a pure tone (pure sinusoidal wave) becomes distorted as it is transmitted through or over the surface of a material. This is illustrated below in Figure 18.

Figure 18 Harmonic generation (single sine wave)

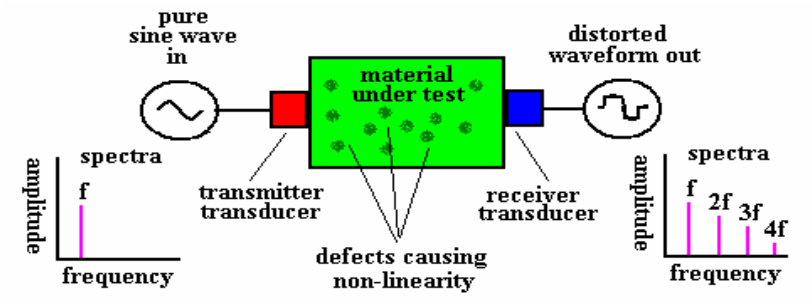

The harmonics are measured by examining the power spectra of the received signal. The transmitted frequencies (fundamental) magnitude is compared to that of the magnitude of each of the harmonic frequencies. These harmonics are expressed in terms of decibels (dB's) below the fundamental level's amplitude. These values can be converted to a distortion factor that is expressed as a percentage. For details on these measurements see section 3.3. Other non-harmonically related frequencies may also be generated by the sound wave, particularly in the presence of severe defects, these are called overtones and noise which result from acoustic emissions, hyteresis and other effects.

2.3 Inter-modulation product generation

A method that provides greater sensitivity over that of measuring the harmonics generated by a single pure tone is a technique that involves measuring the frequencies generated by the inter-modulation of two frequencies. This is illustrated generally from Johnson[14] and is shown below in the Figure 19.

Figure 19 Inter-modulation of two sine waves

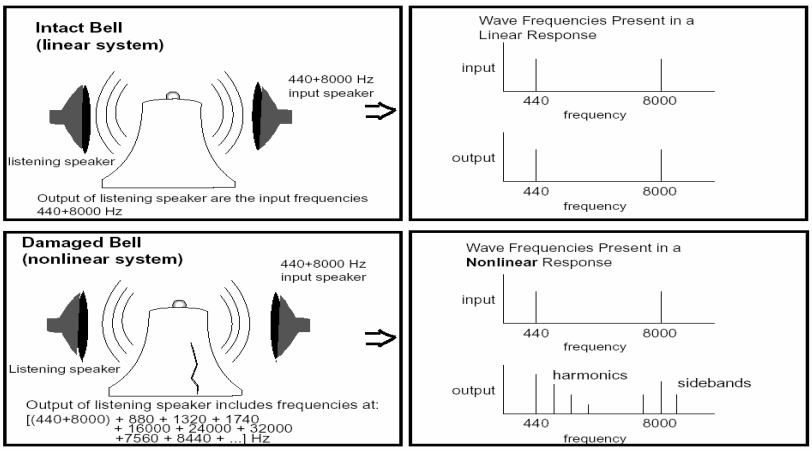

When two sine waveforms of equal amplitude are added together the result is a waveform shown green in Figure 20a. The corresponding spectra are shown in Figure 20b. The result of this addition process is to produce an amplitude varying waveform that has two spectral peaks at the original frequencies.

Figure 20a Two sine waves added together Figure 20b spectra (sum)

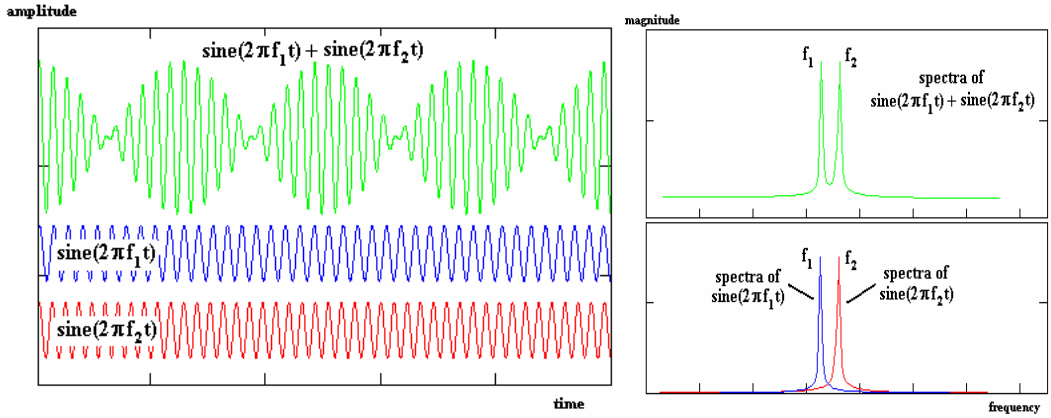

When two sine waves of equal amplitude are multiplied together the result is shown in Figures 21a and 21b.

Figure 21a Two sine wave multiplied together Figure 21b Spectra (product)

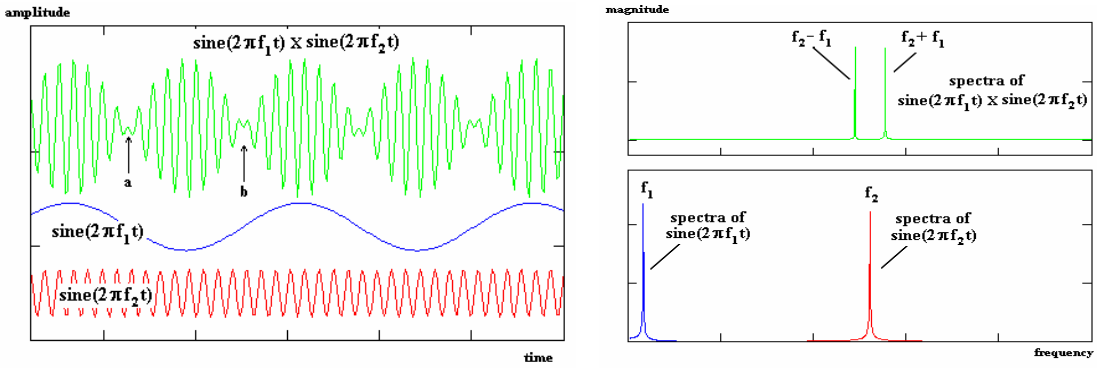

The resulting waveform is different from that of summing two frequencies, there is a phase change between adjacent troughs shown at points **a** and **b** in Figure 21a, the spectra no longer contains f_1 and f_2 components, instead there is only f_2-f_1 and f_2+f_1 frequencies. This process can be expressed mathematically as:-

$$\sin(\omega_2.t) * \sin(\omega_1.t) = \tfrac{1}{2} [\cos(\omega_2.t - \omega_1.t) - \cos(\omega_2.t + \omega_1.t)]$$

where:- $\omega_1 = 2*\pi*f_1$ and $\omega_2 = 2*\pi*f_2$

The equation shows that in the frequency spectra the magnitude of f_2-f_1 and f_2+f_1 is half that of the original individual components f_1 and f_2. If the two frequencies are the same then $\omega_1.t = \omega_2.t = \omega$ the result of the multiplication is:-

$$\mathbf{\sin(\omega.t) * \sin(\omega.t) = \tfrac{1}{2} [\cos(\omega.t - \omega.t) - \cos(\omega.t + \omega.t)]}$$

then $\mathbf{\sin(\omega.t) * \sin(\omega.t) = \tfrac{1}{2} [1 - \cos(2\omega.t)]}$

since; $\cos(\omega t - \omega t) = \cos(0) = 1$

The resulting waveform shows a constant of magnitude ½ together with a single cosine wave of half the magnitude and twice the original frequency.

When an ultrasonic sound wave composed of the sum of two sine waveforms of equal amplitude $[\sin(\omega_2.t) + \sin(\omega_1.t)]$ is passed through a material that exhibits a square law stress-strain relationship, the resultant wave forms can be expressed as:-

$$\mathbf{A(t) = [\sin(\omega_2.t) + \sin(\omega_1.t)]^2}$$

by expansion this gives

$$\mathbf{A(t) = \sin^2(\omega_2.t) + 2\sin(\omega_2.t)\,\mathrm{sine}(\omega_1.t) + \sin^2(\omega_1.t)}$$

$$\mathbf{A(t) = \tfrac{1}{2}[1 - \cos(2\omega_2.t)] + [\cos(\omega_2.t - \omega_1.t) - \cos(\omega_2.t + \omega_1.t)] + \tfrac{1}{2}[1 - \cos(2\omega_1.t)]}$$

re-arranging :-

$$\mathbf{A(t) = 1 + \cos(\omega_2.t - \omega_1.t) - \cos(\omega_2.t + \omega_1.t) - \tfrac{1}{2}\cos(2\omega_2.t) - \tfrac{1}{2}\cos(2\omega_1.t)}$$

The following Figures 22a and 22b show a graphical representation of this process.

Figure 22a Sine sum squared

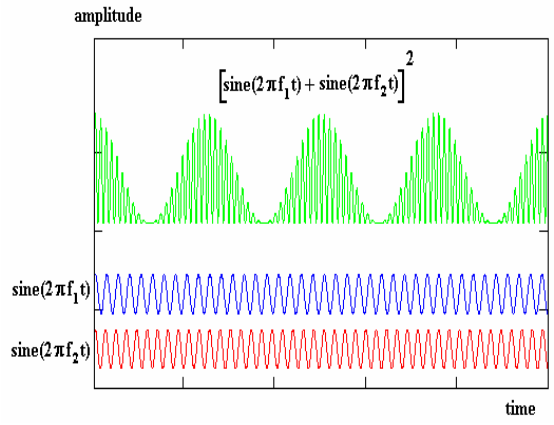

Figure 22b Spectra of sine sum squared

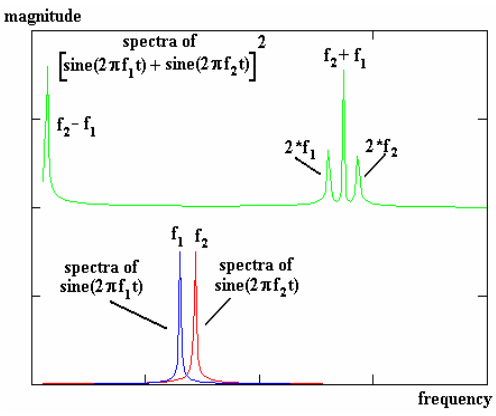

Four distinct frequencies and one DC term are generated by this process, the frequencies are; the second harmonics of f_1 and f_2 that is (2* f_1) and (2* f_2). The sum and difference frequencies of f_1 and f_2, that is ($f_1 + f_2$) and ($f_1 - f_2$). The second harmonics are half the amplitude of the sum and difference frequencies. As there is a larger variation in the generation of the sum and difference frequencies these provide a greater sensitive indication of any non-linearity.

If an object such as a large aircraft wing is slowly subject to cyclic load, while a high frequency acoustic wave is transmitted through or over its surface, defects will cause the amplitude of the acoustic wave to be varied (modulated) in sympathy with this cyclic loading. This results from the effect of cracks opening or closing under the load causing variations in the attenuation of the high frequency acoustic wave.

If the high frequency acoustic wave transmitted through the material (carrier wave) is represented by:-

$$\upsilon_c = V_c \sin(\omega_c t)$$

where υ_c is the amplitude at any instant, V_c is the maximum amplitude and $\omega_c t$ is the carrier frequency. If the cyclic loading applied (modulating wave) is of a sine wave form represented by:-

$$\upsilon_m = V_m \sin(\omega_m t)$$

Where υ_m is the amplitude at any instant, V_m is the maximum amplitude and $\omega_m t$ is the modulating (cyclic loading) frequency. Then the amplitude of the carrier wave received after traversing the material (υ_R) will be modulated by the cyclic loading and varies as a sinusoid between the values of ($V_c + V_m$) and ($V_c - V_m$), shown from Connor[15] in the Figure 23 below.

Figure 23 Amplitude modulation

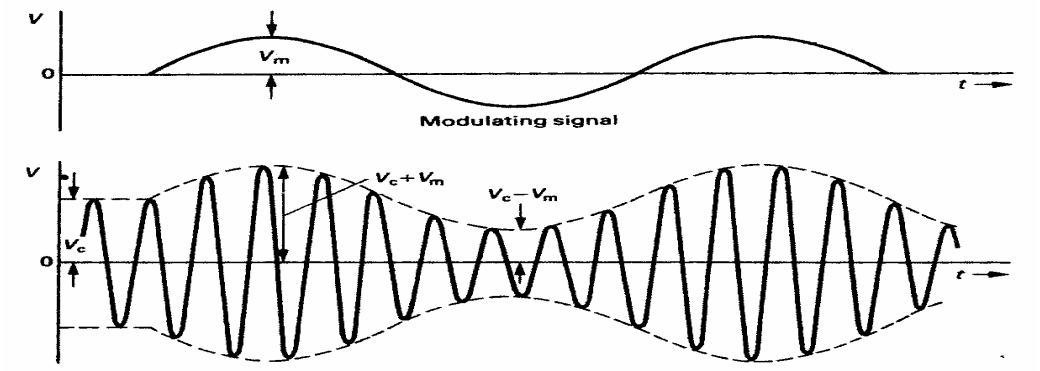

The instantaneous amplitude is given by:-

$$\upsilon_R = [\, V_c + V_m \sin(\omega_m t) \,] \sin(\omega_c t)$$

expanding:-

$$\upsilon_R = V_c \sin(\omega_c t) + V_m \sin(\omega_m t).\sin(\omega_c t)$$

$$\upsilon_R = V_c \sin(\omega_c t) + \tfrac{1}{2} V_m [\, \cos(\omega_c t - \omega_m t) - \cos(\omega_c t + \omega_m t)]$$

$$\upsilon_R = V_c \sin(\omega_c t) + \frac{V_m}{2} \cos(\omega_c t - \omega_m t) - \frac{V_m}{2} \cos(\omega_c t + \omega_m t)]$$

This can be re-written as:-

$$\upsilon_R = V_c \sin(\omega_c t) + \frac{mV_c}{2} \cos(\omega_c t - \omega_m t) - \frac{mV_c}{2} \cos(\omega_c t + \omega_m t)]$$

Where **m** is called the depth of modulation and will depend upon the relative values of V_c and V_m. ($\mathbf{V_m = mV_c}$)

This waveform is composed of the original carrier plus two side bands, the upper side band, at the carrier plus the modulation frequency, and the lower side band at the carrier frequency minus the modulation frequency. The power spectrum for this amplitude modulated waveform shown in the Figure 24. The amplitude of these side bands is dependent on the depth of modulation m, and is m times half the value of the amplitude of the carrier.

Figure 24 Spectra of amplitude modulated signal

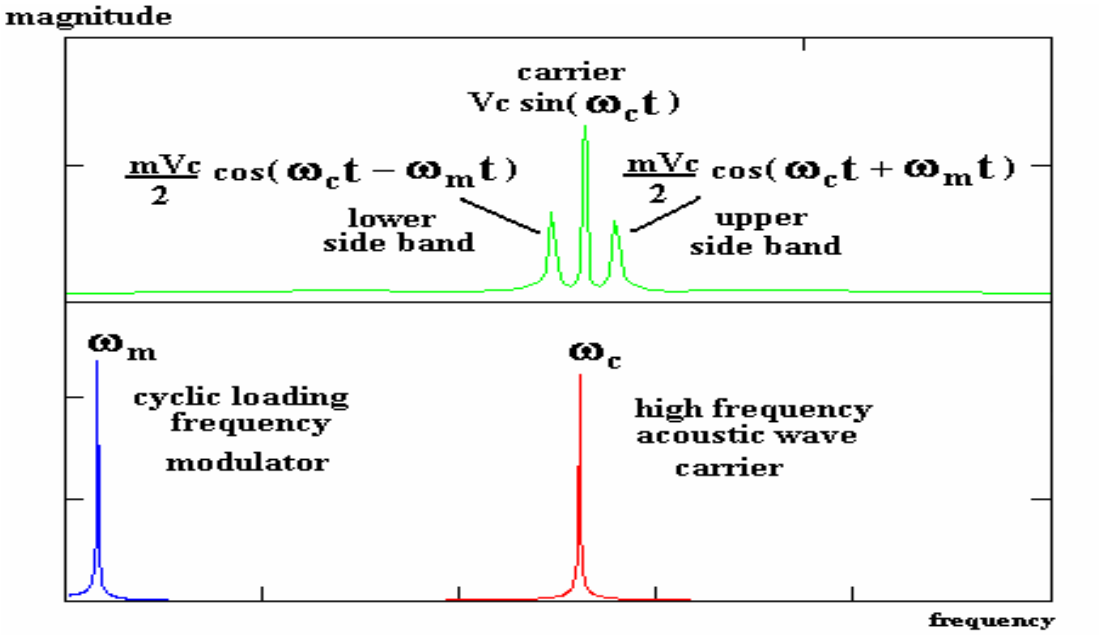

An alternative to the application of a low frequency cyclic load is to apply an impact. This method is detailed in Van Den Abeele [16]. A high frequency wave, for this example 382 kHz, is made to travel through a test sample and an impact is produced by a hammer. If the sample is micro damaged (and thus non-linear) the impact will produce a modulation of the high frequency by the lower frequency resonance modes (in range 0-20 kHz) of the vibrating test object. This is observed by following the inter-modulation spectrum as function of the decaying reverberation of the hammer impact. The 'hits' are performed at different positions, to allow all modes to develop. This technique, called impact modulation spectroscopy and is illustrated in Figure 25.

Figure 25 Impact modulation

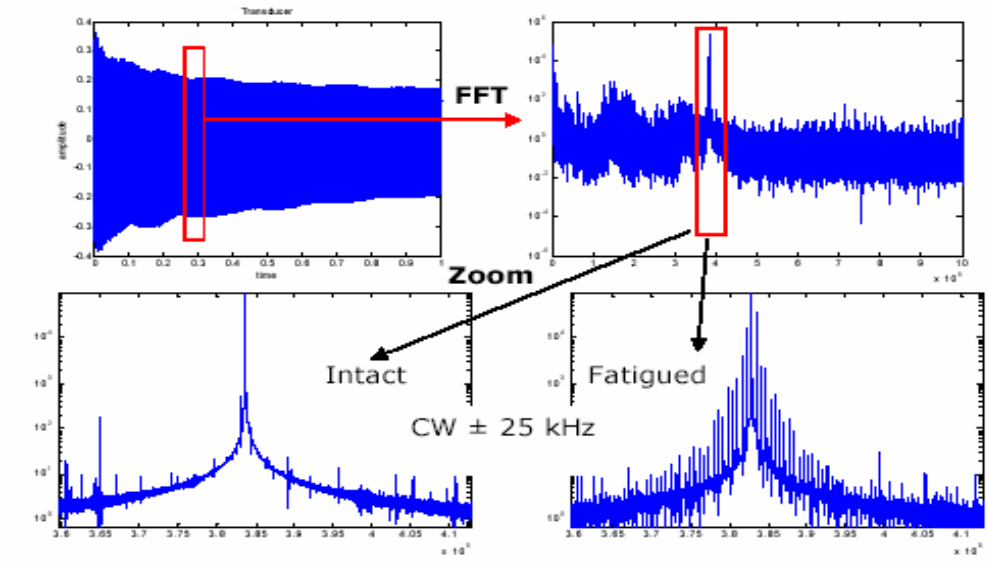

Referring to Figure 25, top left shows the received signal from one impact. Top right is the spectra of the windowed section. Bottom left is the zoomed spectra for intact sample around the high frequency component. Bottom right is the zoomed spectra for cracked sample around the high frequency component. This clearly shows the overtones produced by a defect around a particular high frequency inter-modulation component.

2.4 Resonant frequency shift

Another non-linear method is to apply a mechanical impact (impulse) to the material and measure precisely its acoustic frequency response. When the impulse is applied the material will start to "ring" or resonate with a particular set of natural frequencies of

vibration, these frequency components are called modes or overtones. The frequency and amplitude of these modes are dependent upon the materials state, composition and geometry. If the material has no defects the amplitude of the initial impact will have no effect upon the frequency components produced. The same modes are present regardless of whether the impact was hard or soft, only their amplitude changes. If the material contains defects, the non-linear properties will give rise to different frequency components being generated with different magnitudes of impact.
This is illustrated generally from Johnson[14] for a bell in Figure 26.

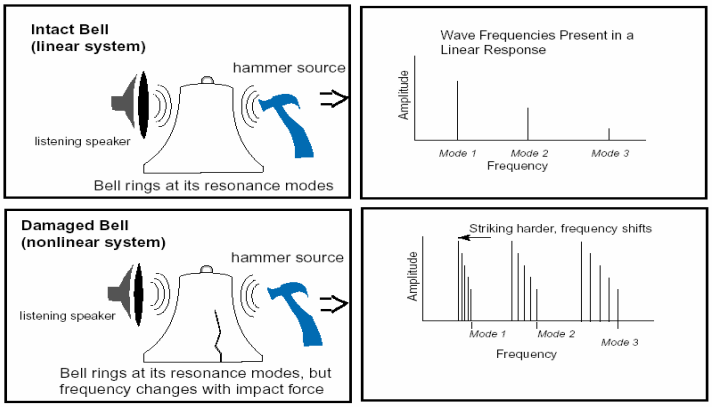

Figure 26

General frequency shift with amplitude

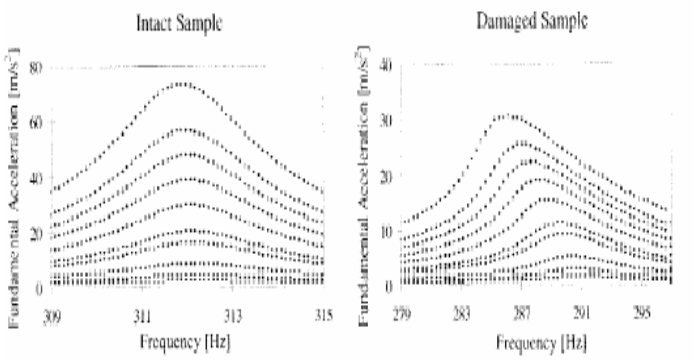

Figure 27

Resonant frequency peak shift with amplitude

The damaged bell provides a non-linear system. An impact will produce extra frequency components (overtones) around the natural modes. The greater the impact the more overtones are produced. In addition to the overtones generated the dominant frequency of the modes shift very slightly in value as the amplitude increases.
Figure 27 from Van Den Abeele K et al [17] shows an example of this frequency shift (plotted on x-axis) with amplitude (plotted on y-axis) of the dominant resonance peak in a damaged sample. There is no frequency shift in these peaks in the undamaged (intact) sample. If the material has a high degree of damping the impact method may not be

practical as the resonant modes die away too quickly to be measured, or the initial impulse causes the measuring apparatus insufficient time to recover from the high input hammer strike, in this case an alternative method is used. The test material is brought to a state of resonance slowly by the application of a sound source, for example an air coupled loud speaker, transmitting at a frequency equal to that of one of the materials resonant modes. The frequency is then measured precisely just after removal of this sound source. This frequency is continuously monitored as the amplitude decays. If the material is damaged this resonant frequency will slowly change as the amplitude decays. This technique is detailed in the experimental work given in section 6.2.4.

2.5 Pulse inversion response

Two pulse inversion methods were investigated during the period of this research. Mattei [18] previously investigated a method that involved transmitting two pulses, one after the other, with a short time delay between them. The pulses are high frequency (5 MHz) of Gaussian form, one ordinary and the other phase shifted by 180 degrees (inverted). The outputs from these two pulses are summed together as illustrated in the Figure 28 below.

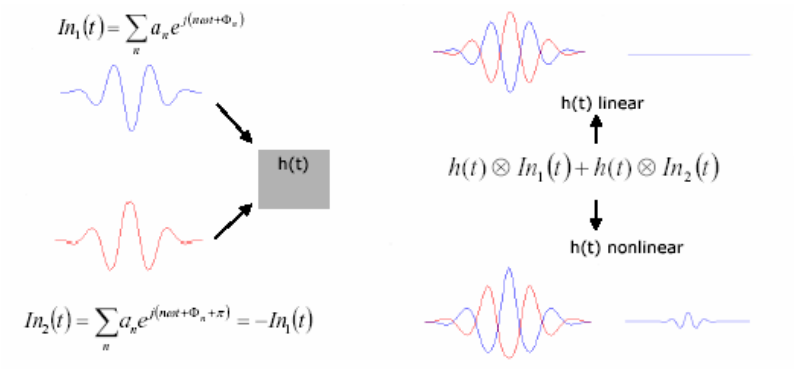

Figure 28

Pulse inversion method 1

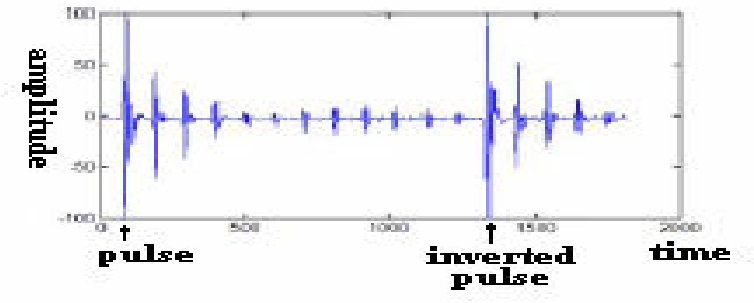

Figure 29

Pulse inversion example

Figure 29 shows the received signals resulting from the transmission of the two pulses. The signals relating to the pulse and inverted pulse are then separated as shown in Figure 30. Then added together shown in Figure 31. The non-linear defect is then observed as a clear signal.

Figure 30 pulse separation

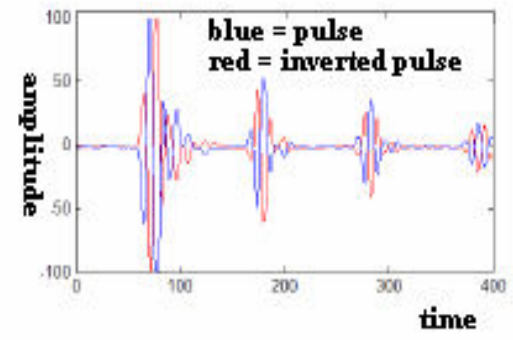

Figure 31 pulse summation

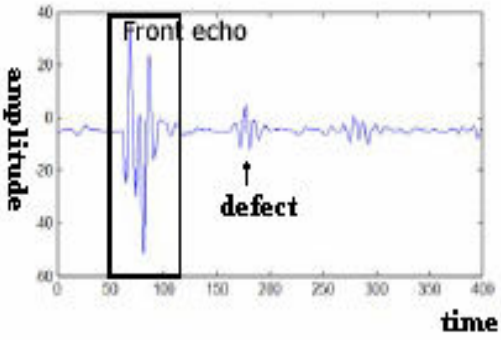

This method has the advantage of being able to detect and localise a region of non-linearity and is particularly good a detecting de-bonding in thin and laminated structures. These experiments performed by Mattei used water coupling (water bath).

An alternative method was investigated by the author in the work of this thesis. This method involved direct transducer contact coupling and two relatively low frequency pulses sent into the test material, one positive going (compressional) and one negative going (tensile). In the absence of defects (symmetrical stress-strain characteristics) the summation of the effects of these two signals produces a zero level, since the response of the material to these pulses are the same but have opposite polarity. In the presence of defects (non-symmetrical stress-strain) the summation of the signal produces a non-zero result, as the two waveforms will be unequal. With this method it is important to ensure that the receiver and transmitter transducers are securely fixed to the test sample when the two pulses are applied, so that no changes have occurred between the two recordings. The Figures 32, 33 and 34 show the results of using this technique. For each of these examples a positive pulse of 1 microsecond is transmitted into the material and the resulting received signal recorded to a single data file, then a negative pulse of 1 microsecond transmitted into the material and the resulting received signal recorded to a second file. The data from these two files are then added together to produce the summed data plot.

Figure 32 Pulse inversion method on good steel sample

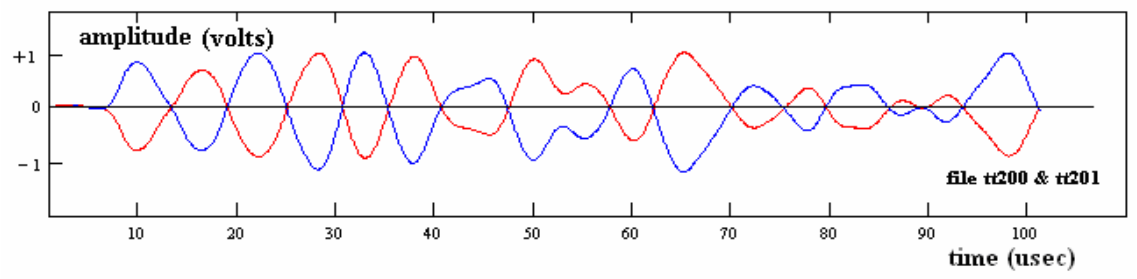

Summing the two signals:-

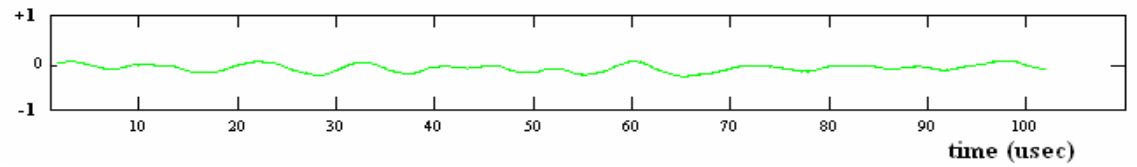

Figure 32 shows the signals received through a good quality steel block (31*25*16 mm), the signal being transmitted across its smallest dimension (16 mm).

The blue plot is the result from a positive going pulse, the red plot is the result from the inverse, negative going pulse. The green plot shows the summation of the two received signals over their entire recording time. In this example the summation produces a near null or void result, the plot is fairly flat.

It should be noted that the received signals are the response of both the material and the transducers to a single impulse in either the positive or negative direction. The reflections from the larger dimension boundaries of the block become superimposed and form a complex waveform, however as this example shows this complex waveform sums to near zero values throughout all of the recording period.

Figure 33 pulse inversion method on undamaged carbon fibre sample

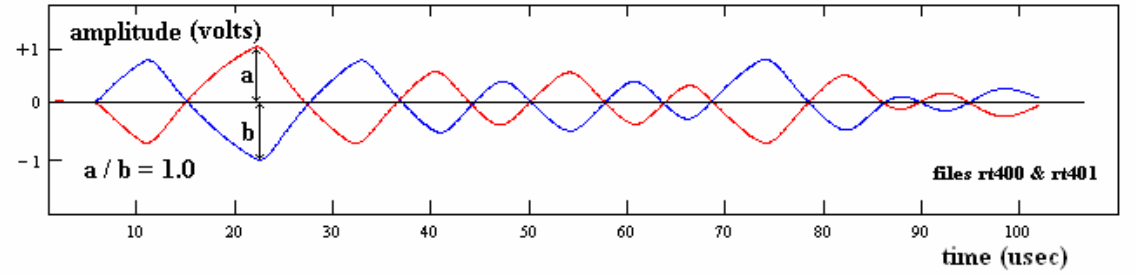

Summing the two signals:-

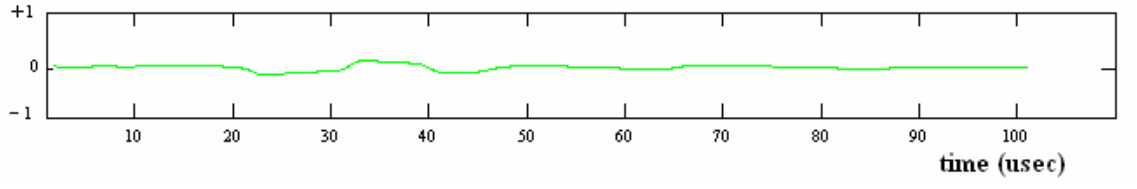

Figure 33 shows an example of the signals received for an undamaged carbon fibre composite wing material (278*22*4.2 mm). Transmission is a p-wave, through the thickness (4.2 mm) of the sample.

The slight "slewing" or triangular wave shape in the first cycle of the recorded signals have been observed in a number of tests on undamaged carbon composites. It is not certain what causes this, however it seems not to effect the ability of the pulse inversion method to detect faults. The maximum (a) and minimum (b) amplitudes were measured and the ratio a/b was found to be 1.0. The summation produces a flat plot.

Figure 34 pulse inversion method on damaged carbon fibre sample

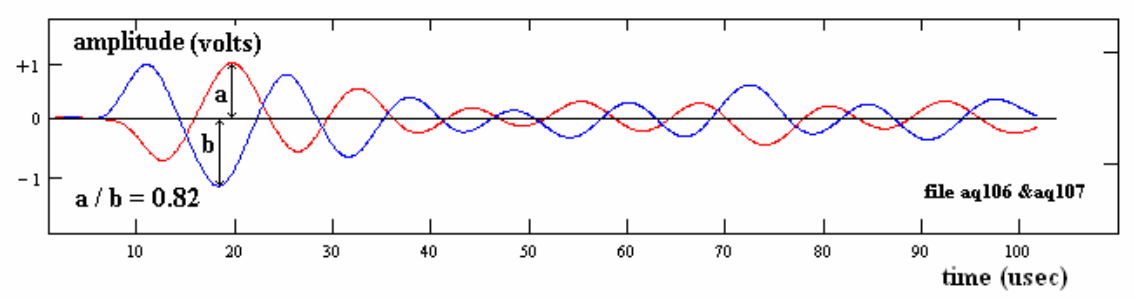

Summing the two signals:-

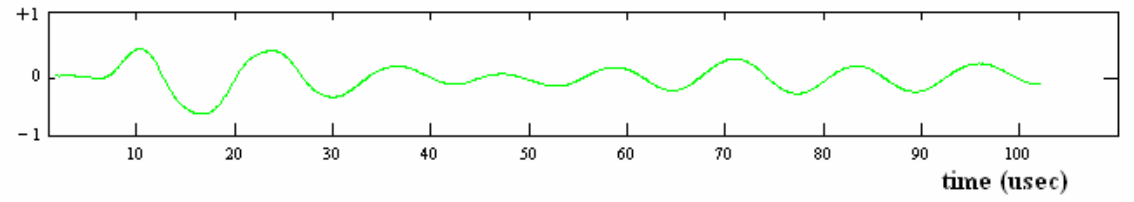

Figure 34 shows an example for a damaged carbon fibre composite wing material (278*22*4.2 mm).Transmission is a p-wave through the thickness (4.2 mm) of the sample. Adding the two signals together produces a non-zero result. The minimum to maximum amplitude ratio (a/b) is measured to be 0.82.

These results suggest it may be possible to quantify this testing method. The amplitude of the largest compressional (+ve) pulse is compared with the corresponding largest tensile (-ve) pulse, and the ratio of the smallest to the largest calculated. This will produce a number between 0 and 1 indicative of the degree of non-linearity. A value of 1 would indicate that there is no difference between a compressional and tensile pulse, and the material is linear. From the results above and other experiments (see sections 6.2.1 and 6.2.5) values below 0.95 indicate some damage and values below 0.8 suggest significant damage.

2.6 Spectral notch filtering

This method had previously been investigated by the author (Armitage [19]) and at a later date by others in relation to the detection of gauge corner cracked railway tracks. The method employed by the author used a single cycle of a sine wave transmitted over the surface of a material as a Rayleigh wave. Subsequent investigations used a sine wave frequency sweep. Transmitting a single cycle has similarities to sending an impulse or frequency sweep, they all produce broad bandwidth frequency spectra. A single cycle produces a broad sinc function shaped spectrum centred on the cycle period. If the pulse width is very narrow an impulse produces a spectrum shaped like a rectangle over a large bandwidth. The frequency sweep produces spectra that is similar in shape and has a bandwidth approximately equal to the range of the sweep. Transmitting a broad band acoustic wave into a material, any frequency filtering effects can be readily observed by observing “notches” or dips in the received spectra. Experiments have shown that cracks within and on the surface of a material will act as a filter and produce characteristic “notches” or dips in the spectra of a wave that has travelled through or passed over them. For further details see section 6.2.6. Figure 35 shows the results of an experiment performed by Dixon [20] that involved transmitting a Rayleigh wave pulse over the surface of samples of aluminium that had slots cut into them at various depths. It shows that deep slots attenuate higher frequencies more strongly relative to shallower slots.

Figure 35

Relative frequency content of Rayleigh wave after passing over slots of various depths

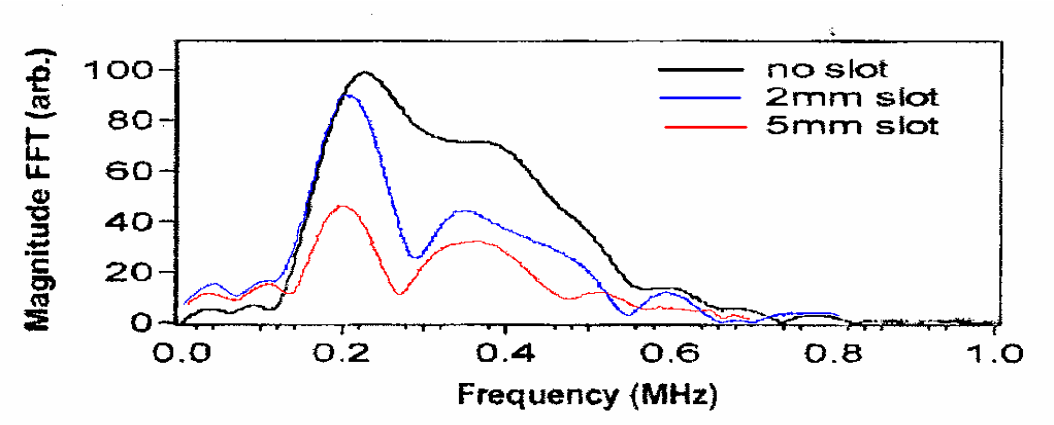

2.7 Frequency sweep response

This technique was only investigated briefly by the author during the work of this thesis. The method involves sending a frequency sweep (or chirp) into the material and examining the resulting harmonic spectra. The principle is illustrated in the Figure 36

Figure 36 frequency sweep response

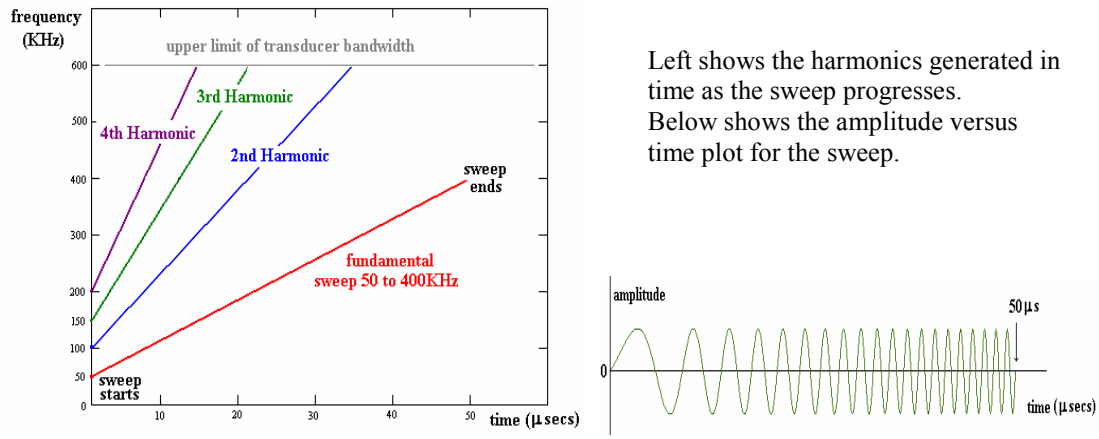

Referring to the frequency versus time plot of Figure 36 at the commencement of the sweep any harmonics generated will be multiples of 50 kHz. As the sweep progresses in time, harmonics will be generated that will be multiples of the fundamental frequency at any particular instant. In the absence of harmonics the spectra of a sweep would be composed of a flat response over the range 50 to 400 kHz. In the presence of harmonics it would be expected that the spectra would be modified and contain a greater magnitude at the high end of the frequency spectra (a high frequency "lift").

In practice it was found that this method was not very reliable at detecting defects. There are two factors which effect the magnitude of the harmonics first the non-linearity that is generating them and secondly the filtering effect that cracks have on the frequency content, this causes "notches" in the spectra and can also reduce the high frequency content, as outlined in the previous section 2.6.

An example of a frequency lift is shown in Figure 37. However depending upon the size and nature of the cracks it is also possible to have a reduction in the high frequencies as shown in other experimental work, see sections 6.2.3 and 6.2.5 for details.

In addition it was found that sweeping up (low to high frequency) or sweeping down (high to low frequency) makes no significant difference to the spectra.

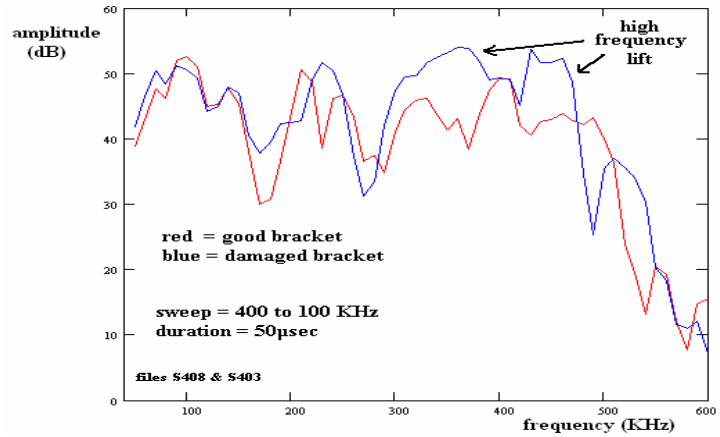

Figure 37

High frequency lift due to defects in a steel actuator bracket.

2.8 Time reversal techniques

This technique is being investigated principally by Dos Santos and Van Den Abeele [21] . It involves effectively reversing the direction of propagation of an elastic wave and returning the energy back to its point of origin. The principle is illustrated in the Figures 38a to 38d .

Figure 38a time reversal-initial stage

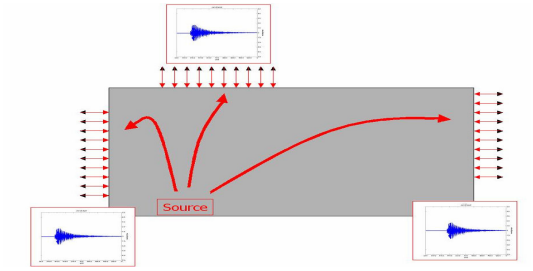

A source transmits acoustic wave.
Signal received and recorded at the outer regions of the material

Figure 38b time reversal-second stage

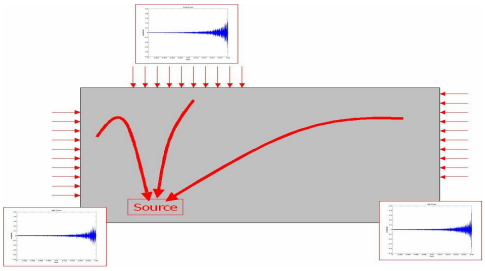

The receive positions now become transmit positions.
The recorded signals at each point is reversed in time order and transmitted back into the material.
The sound wave path traces back along its original path.
The energy is finally returned to the source position

Figure 38c time reversal-third stage

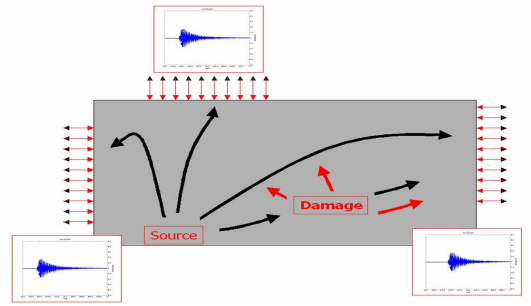

In a material that contains a non-linear defect a source will cause the generation of harmonics at the damage site.

Figure 46d time reversal-final stage

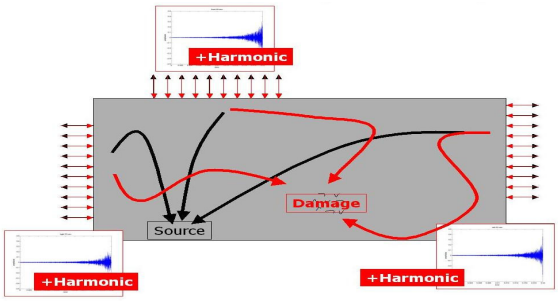

Transmitting back the time reversed signals will result in two concentrations of sound energy, one at the originating source and the other at the defect.

This method provides a mechanism for the location of defects. It will function in all types of composite materials, since the sound ray path is always traced back to its point of origin regardless of the route. The process is often referred to as phase conjugation. The method can be used to provide an acoustic energy concentration at a specific point (the damaged region) or a method to "illuminate" a damaged region.

If the harmonics only are time reversed and transmitted back into the material then the return energy is concentrated only at the defect (point of origin of the harmonics). The method relies primarily on phase information and therefore can be transmitted back at higher amplitudes as this has no effect the wave path.

An example of this is shown in Figure 39a to 39c and is from the simulation work of Koen Van Den Abeele[22].

Figure 39a

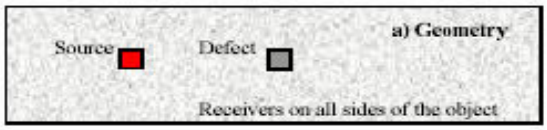

Simulated two dimensional object (200 x 50 mm) with acoustic source (5 cycles at 250 kHz Gaussian window and defect (non-linear region 10 x 10 mm)

Figure 39b

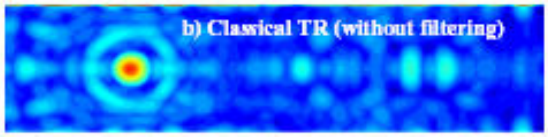

Time reversal whole signal
(energy re-focused to source)

Figure 39c

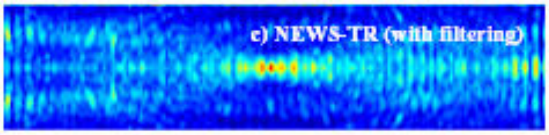

Time reversal filtered (high pass 400 kHz) removes fundamental but passes the 2nd harmonics and above. filtered signal returns to source which is the defective region.

The following chapters presented in this thesis concentrates on the transducers, instrumentation and experimentation used to detect departures from the linear stress-strain relationship when a material undergoes progressive damage and involves the measurement of harmonics produced when a single frequency acoustic wave is transmitted through or over a test object. Additional instruments were developed and experimental investigations made to include the use of dual frequency acoustic waves detecting both the harmonics and inter-modulation products, the use of a frequency sweeps to detect harmonic “lift” and “notches” in the spectra, pulse inversion techniques to detect the difference between the resonant properties of a test object when subject to a compressional and a tensile pulse and the changes in the resonant frequency of a test object as the amplitude decays.

3 TRANSDUCERS FOR NON-LINEAR ACOUSTIC TESTING

At the start of this research project the author undertook a detailed technical survey of commercially available ultrasonic transducers (both actuators and sensors) that would be suitable for non-linear acoustic testing applications and in particular transducers that are brought in to physical contact with the material under test.
This section provides a brief summary of the survey made of the current transducer technology that is only relevant to the research detailed in this thesis. This summary includes the identification of relevant properties such as acoustic impedance, operating frequency, efficiency, coupling and other factors significant for their application that is considered important when applied to non-linear acoustic testing methods. A more detailed version was submitted to the E.U. commission as Aeronews deliverable 11 titled; Description, critical evaluation and adoption of available transducers on the market.

3.1 Technical survey of suitable transducers

The first part of the survey consisted of establishing the transducers currently being used by researchers within the Aeronews project consortium. These included those used in linear and non-linear acoustic testing of materials. A graphical summary of the type and operating frequency ranges are given in Figure 48.

Figure 48 Consortium transducer frequency range

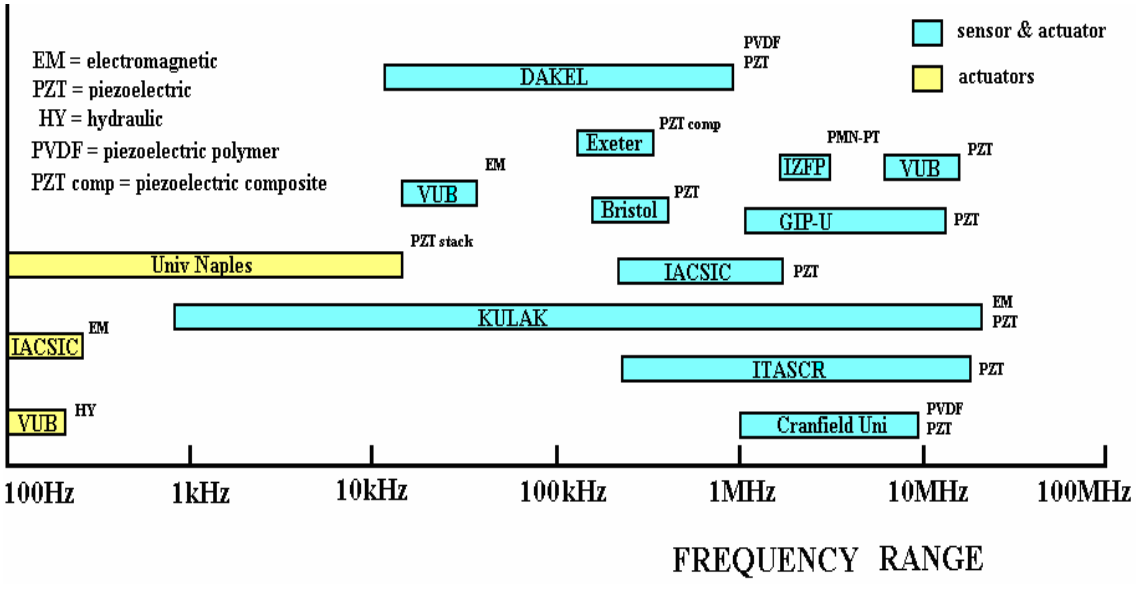

The second part of the survey extended this work beyond the consortium and investigated emerging technologies that could find applications in non-linear ultrasonic techniques. The survey examined in detail the following types of transducer technology; piezoelectric, electrostrictive, magnetostrictive, electromagnetic, capacitive, inductive, resistive, optical and quantum. Details of the piezoresistive sensors and the electromagnetic transducers, in particular Elecro-Mechanical Acoustic transducers (EMAT's) were investigated by the author but are not included in this thesis since they were not used in this particular research program; details on piezoresistive sensors can be found in Arnold[23] and for EMAT's in Lingenberg[24].

The survey found that transducers based on Electrostrictive materials would not be suitable as sensors in non-linear acoustic applications due to their inherent non-linear characteristics; strain is proportional to the square of the applied electric field.

Magnetostrictive materials comprise a wide range of material types. Those based on Iron and Nickel have been used for some time in conventional linear ultrasonic testing, other types based on Giant Magnetostrictive Materials (GMM), such as Terfenol-D, and those based on Magnetic Shape Memory (MSM), such as Ni-Mn-Ga allows are of future interest. These materials in most cases do not have sufficient linear performance characteristics, and were rejected for use as sensors in this research program.

It was determined that piezoelectric / epoxy composite based transducers would be of the greatest significance for the research carried out and detailed in this thesis.

Piezoelectric composites consist of an array of piezoelectric ceramic rods (illustrated in Figure 40) or fibres aligned in one direction within a polymer matrix. They can also be fabricated by mixing a powdered ceramic with a polymer, and aligned by electrical poling.

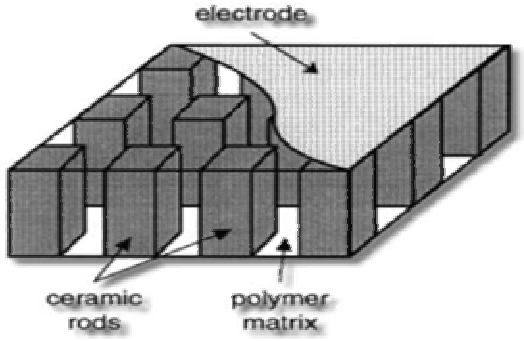

Figure 40

Piezoelectric composite

The main advantage of these composites over a pure ceramic is that the lower density gives lower acoustic impedance, thereby allowing acoustic matching to low density materials. By varying the ceramic / polymer ratio it is possible to optimise acoustic

impedance to match exactly to that of the material under test, this being an important factor when making measurements of non-linear acoustic properties. A good acoustic match between the transducer and the material under test will ensure efficient transfer of energy from the transducer to the material under test, little or no reflections occurring at the point of contact will reduce the likelihood of non-linear effects due to localised stress concentrations.

The technical survey examined and compared some properties of piezoelectric, electrostrictive and magnetostrictive transducer materials. Day [25] provides a comparison between piezoelectric and electrostrictive materials. Figure 41 was compiled by the author from many sources and gives a summary of important properties of a wide range of piezoelectric, electrostrictive, piezoelectric polymer and magnetostrictive materials.

Figure 41a Transducer active element versus acoustic impedance

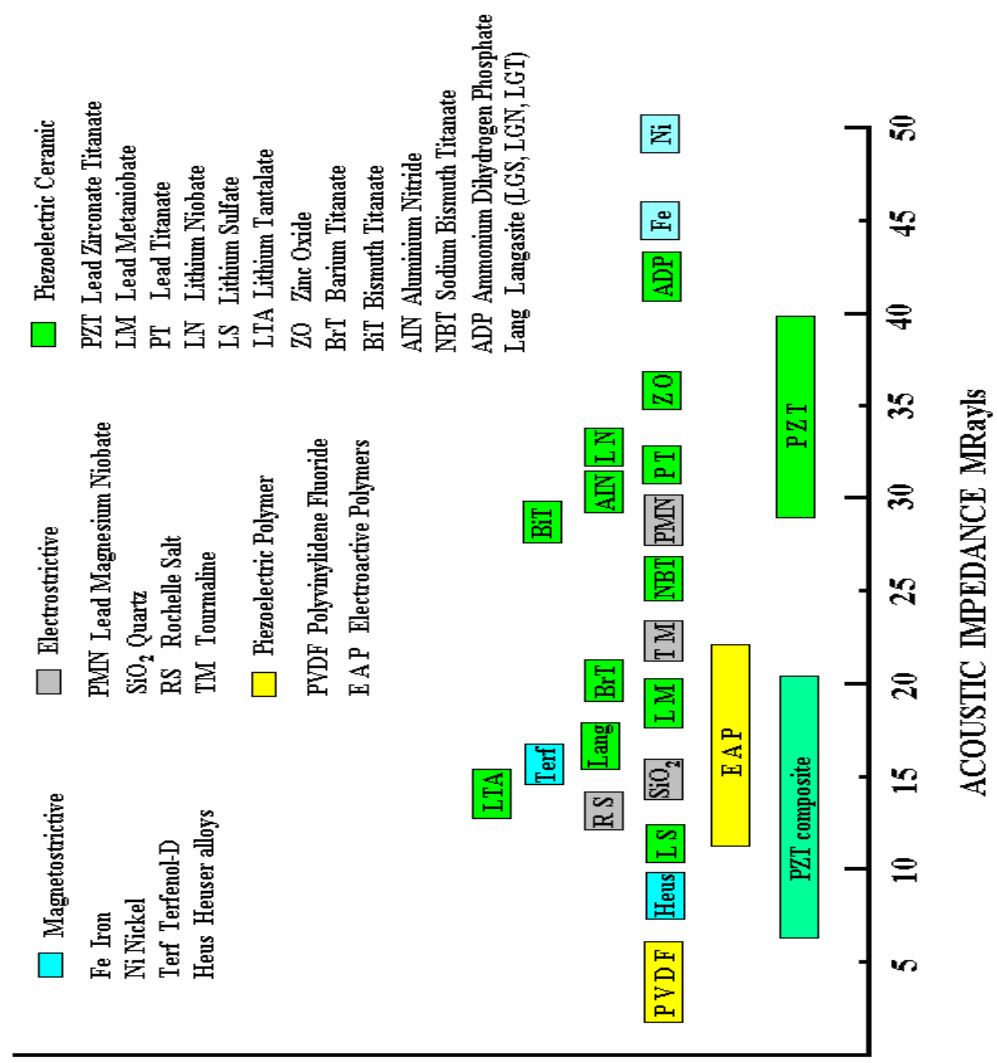

Figure 41b Transducer active element versus coupling coefficient

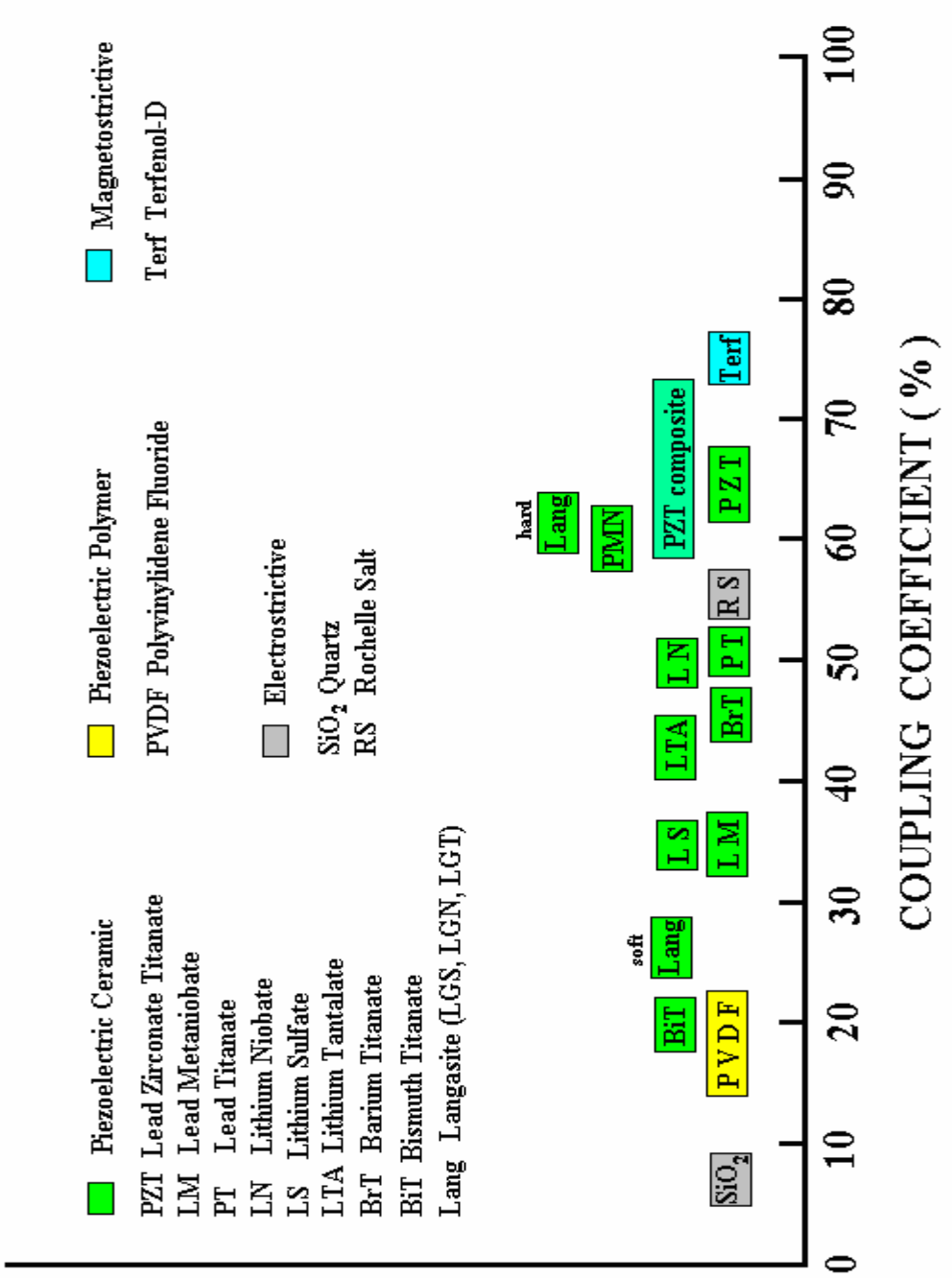

3.2 Transducer acoustic impedance matching

Figure 42 shows a plot, compiled by the author, of the acoustic impedance of various composite materials together with the acoustic impedance of various sensor materials. The ideal transducer arrangement is to ensure that the sensor (or actuator) has the same acoustic impedance as the material under test.

Figure 42 Acoustic impedance of composite materials

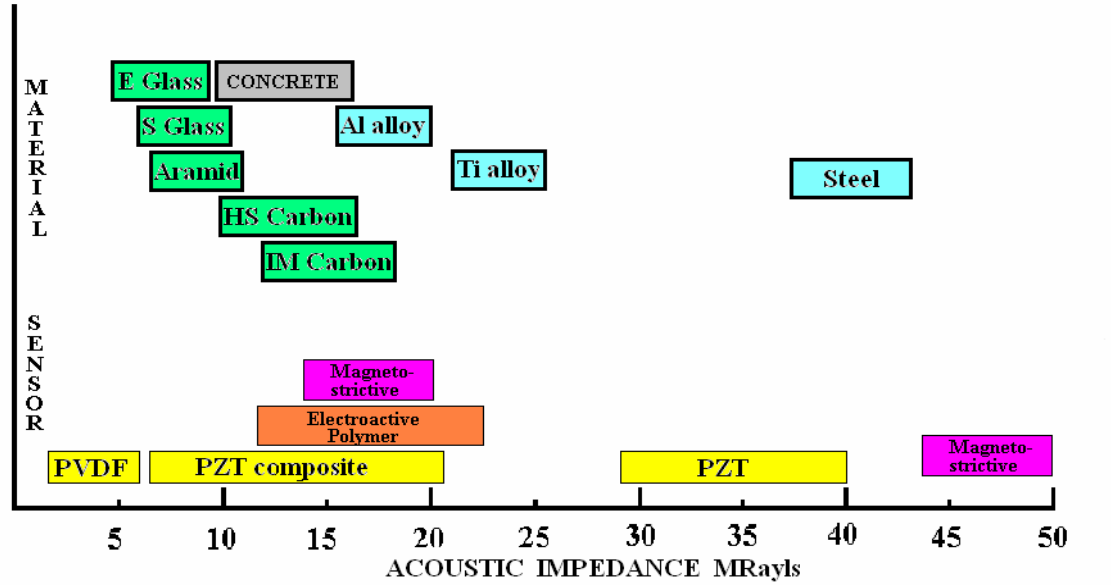

Details about the various materials composition and the definitions of acoustic impedance can be found in section 1.3.

In practice it is not always possible to exactly match the transducer to the test material, in conventional ultrasonic testing procedures this is not so important, in non-linear acoustic measurements it is a factor that must be considered.

Within this research project much consideration was given to the development of a prototype transducer that had an active element of the same acoustic impedance as that of the material under test, this is detailed in section 4. Various methods have been used over the years to match the transducer's active element to the material under test, some are based on having one or more intermediate material layers between the transducer and the test material. Other methods use a single shaped intermediate material. Clark[26] gives details by which acoustic matching by shape is achieved. Figure 43 shows a horn shaped material that acts as an acoustic impedance transformer. If the small area S1 is connected to a piezoelectric ceramic of acoustic impedance Z_{pzt} then the acoustic impedance will be transformed and reduced to Z_{pzt}*S1/S2 at the large area S2, but over a limited band of frequencies.

Figure 44 shows the frequency versus relative output power for air filled horns of various shapes. It can be seen from these plots that the frequency range is limited. For low frequencies the power output drops to zero. The most efficient shape of horn is an exponential this has the flattest response over a wide bandwidth.

Figure 43 Acoustic matching by shape

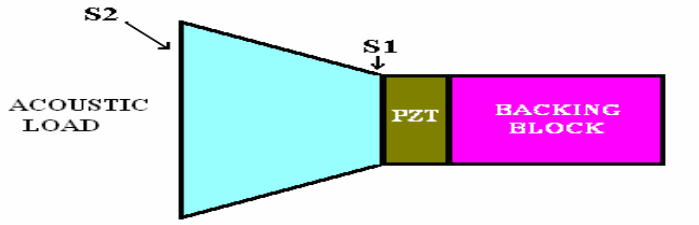

Figure 44 frequency range versus shape

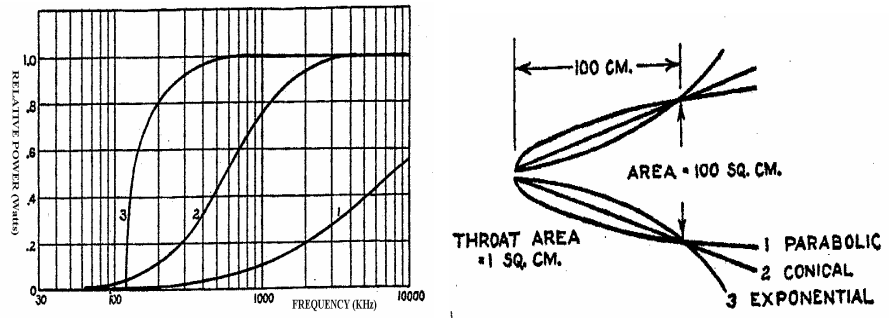

The Figure 45a shows a method by which acoustic impedance matching can be achieved by using one or more layers of different materials.

Figure 45a Acoustic matching by layers

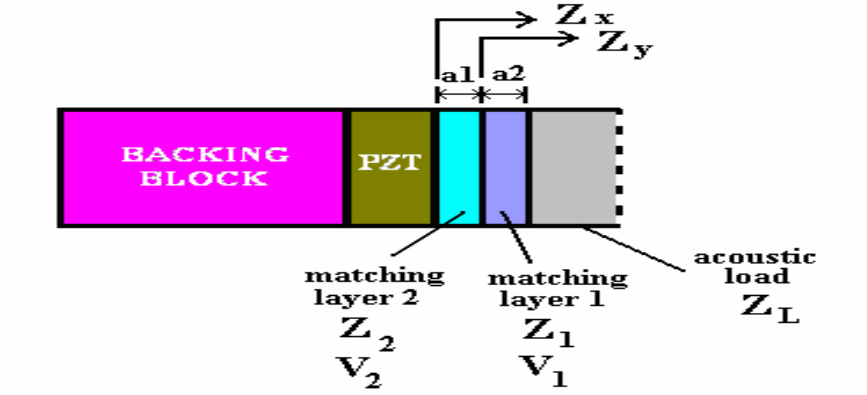

Figure 45b impedance versus frequency

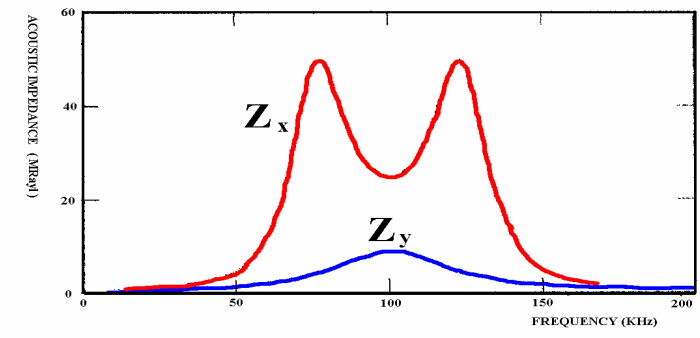

This matching method is outlined in Goll [27] and gives the acoustic impedance as a function of frequency (f) looking towards the load at Z_x and Z_y.

$$Zy = \frac{Z_1.(Z_L.\cos(X1)) + j.(Z_1.\sin(X1)}{Z_1.\cos(X1) + j.(Z_L.\sin(X1)}$$

$$Z_x = \frac{Z_2.(Z_y.\cos(X2)) + j.(Z_2.\sin(X2)}{Z_2.\cos(X2) + j.(Z_y.\sin(X2)}$$

Z_L = acoustic impedance of load
Z_1 = acoustic impedance of layer 1
Z_2 = acoustic impedance of layer 2
$a1$ = thickness of layer 1
$a2$ = thickness of layer 2
V_1 = sound phase velocity in layer 1
V_2 = sound phase velocity in layer 2
$X1 = 2\pi.a1.f / V1$
$X2 = 2\pi.a2.f / V2$

Figure 45b shows an example plot made by the author of the frequency versus acoustic impedance at positions Z_x and Z_y. These were calculated for the matching layer thicknesses a1 and a2 equal to 5mm. The acoustic impedance of layer 1 (Z_1) is 3 MRayls, the acoustic impedance of layer 2 (Z_2) is 15 MRayls, the sound velocity of layer 1 (V_1) is 2000 m/sec and that for layer 2 (V_2) is also 2000 m/sec. In this analysis the acoustic impedance is represented as a complex quantity, only the real part is plotted. It can be seen from this plot that acoustic impedance is very dependent upon frequency, it peaks at 10 MRayls at Z_y and twice at 50 MRayls at Z_x. For ideal matching it is required that the acoustic impedance be 40 MRayls (equal to the PZT) over all frequency ranges at position Z_x. If many layers are used of the right combinations of acoustic impedance and thickness it is possible to approach this ideal matching characteristic.

3.3 Transducer linearity

Since the non-linear acoustic testing system measures the effect of non-linearity in materials it is very important to ensure that the transducers themselves do not introduce any non-linear effects. The measurements made of the linearity of a prototype transducer are given in section 4.6.

There are many factors that produce non-linearity and hysteresis in piezoelectric transducers and various ways to improve linearity, some examples are; reversible and irreversible domain wall motion, an effect that can be remedied by using single crystal materials. Dielectric displacement saturation, this can be prevented by limiting the applied voltage. Residual charge which is charge left on surface and depends on the

prior applied electric field, using low impedance drivers and limiting fields to below 100 Volts per millimetre will reduce this effect. There is also some dependence of the piezoelectric constants on the applied electric field and the applied compressional stress, these effects can be limited by applying a DC bias or to keep constant static pressure low (typically below 10MPa) ensuring that the material is working in a linear region of its characteristic curve. One particular problem encountered with all piezoelectric materials is aging and pre-aging must be applied to gain the stability and linearity required. Power dissipation can cause thermal run away effects that will destabilise the piezoelectric material if insufficient heat sinks are not provided. Within the structural components of the transducer, both at the back and front ends, non-linear stress-strain relationships can occur, it is important to maintain all forces within the elastic limits of all the components. Non-linearity can result if resonant modes different from the fundamental mode of oscillation start to occur, mechanical damping may reduce or prevent these modes being generated. In practical the coupling of the transducer to the test material is potentially the greatest source of non-linearity, so acoustic coupling should be kept as thin as possible, the accelerations low and the use of linear couplants, either solid, gel or liquid is preferred. Acoustic mismatch will produce reflected waves and localised high stresses, the transducers impedance must be as close in value to the material under test.

Linearity measurement

A measure of the linearity of a transducer is the Total Harmonic Distortion (THD) that it produces when driven with a single frequency pure sine wave. This is usually expressed in decibels (dB) or as a distortion factor (%). The definition of THD is given below:-

$$\mathrm{THD} = \frac{\sum \text{harmonic powers}}{\text{fundamental frequency power}} = \frac{P_2 + P_3 + P_4 + P_N}{P_1}$$

P_1 is the fundamental's power, P_2 the second harmonic's power, P_3 the third harmonic's power, and P_N the Nth harmonic's power. For this project the power from each harmonic is measured from the power spectrum plots directly and expressed as decibels

(dB) down from the fundamental, or as a percentage distortion figure. Tables that convert decibels to distortion figures are provided in Appendix B.
In terms of direct voltage measurements, THD can be expressed in dB by the relationship:-

$$\text{THD (dB)} = 20 \log_{10} \sqrt{\frac{V_2^2 + V_3^2 + \cdots V_N^2}{V_1}}$$

V_1 is the fundamental's peak voltage, V_2 the second harmonic's peak voltage, V_3 the third harmonic's peak voltage, and V_N the Nth harmonic's peak voltage.
The distortion factor is given by:-

$$\text{DISTORTION FACTOR (\%)} = 100 \sqrt{\frac{V_2^2 + V_3^2 + \cdots V_N^2}{V_1^2 + V_2^2 + V_3^2 + \cdots V_N^2}}$$

3.4 Transducer coupling to test materials

The research conducted by the author concentrated on the development of transducers that are in temporary physical contact, some non-contact types were developed for the resonant frequency deviation measurements, these involved two air coupled and one optical coupled device. See NBOX's 7, 8 and 10 in section 5.2. Air coupling is very inefficient due to the large acoustic impedance mismatch between the air and the material under test, however despite these losses in some cases non contact methods are essential, particularly if large areas have to be tested in a short period of time, or contact will disturb the measuring process. Optical coupling has many advantages as there is no requirement to consider the problems of acoustic matching, however the cost of such equipment is very high. An alternative to contacting methods is to have the transducers already embedded within or permanently fixed to the materials under test. Investigative research by the author was made into the types of embedded sensors and actuators currently used in the aircraft industry. A very brief outline from this survey is given below as there is some interest in adapting these transducers for non- linear acoustic testing techniques.

Embedded transducers, smart materials and structures

Embedded transducers are in permanent bonded contact, and are considered as part of the composite material making up the aircraft structure.

Smart materials have the characteristics of both sensor and actuator. These materials are capable of reversibly changing their mechanical properties (viscosity, stiffness, shape) due to the influence of temperature change or an electric or magnetic field. With some of these materials the reverse effect can be used for sensor tasks that is a mechanical load generates an electrical or magnetic field.

A smart structure involves a structural material, distributed actuators and sensors which may also be comprised of the structural material itself, a control strategy, and power electronics. A smart structure has the capability to respond to changing environmental and operational conditions (such as vibrations and shape change).

A non-linear acoustic measurement system can be realized by having transducers permanently embedded within the composite material making up the aircraft structure, techniques involving this principle are outlined Mook et al [28] and are illustrated in Figure 46:-

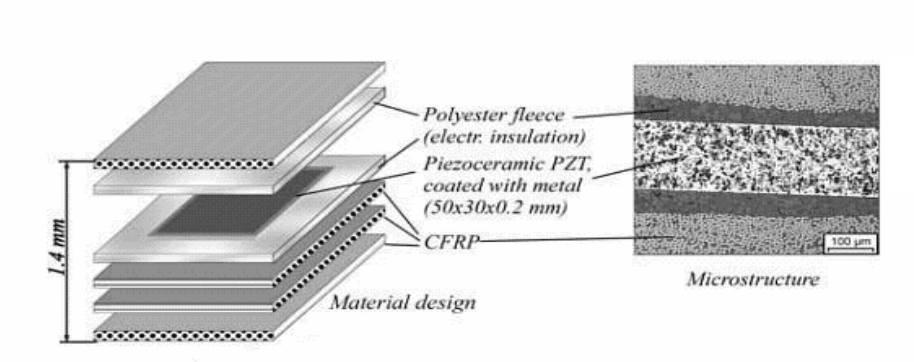

Figure 46 smart active material

Other active structural components have been investigated by Torben [29]. The diagram Figure 47 shows embedded piezoelectric fibres as part of an aircraft structural material

Figure 47 embedded piezoelectric fibres

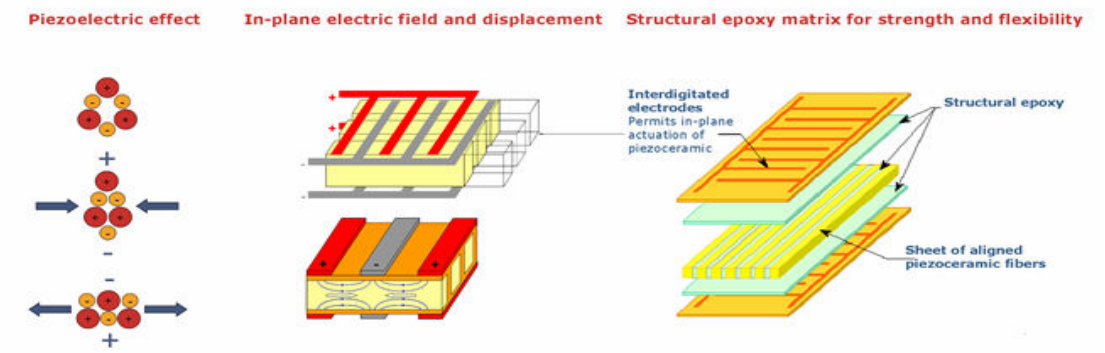

The Figure 48 from Moses [30] shows a piezoelectric actuator arrangement on an aircraft flexible tail. Figure 49 from NASA smart materials corporation shows a macro fibre composite (MFC) actuator.

Figure 48 piezoelectric actuator on aircraft tail

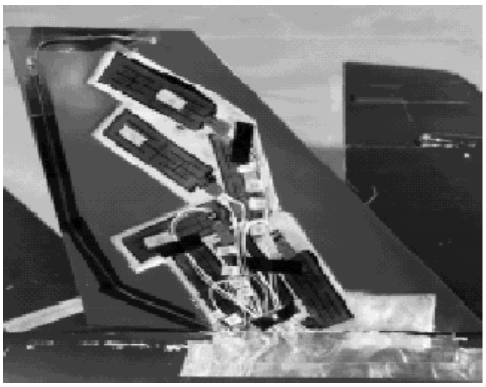

Figure 49 macro fiber actuator

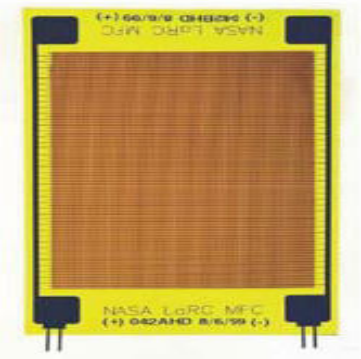

Kessler [31] describes how piezoelectric materials embedded into aircraft structural component can generate Lamb waves; these waves are used to test the material, as illustrated in Figure 50. Chang[32] describes how transducers can be embedded into panels, shown in Figure 51.

Figure 50 Embedded Lamb wave generator

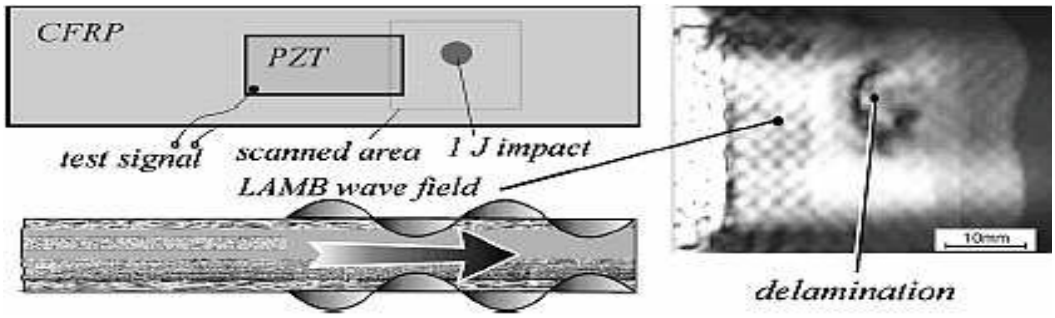

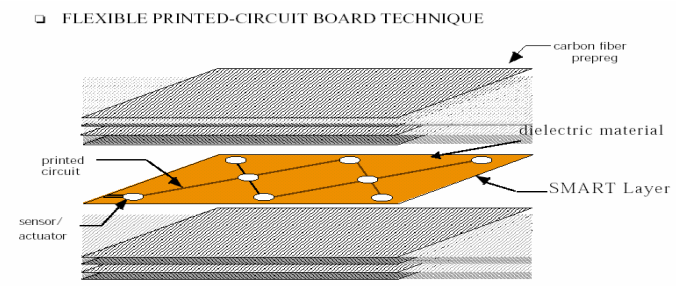

Figure 51
SMART components

Examples of commercial smart devices incorporated in to aircraft components are illustrated below in Figure 52a from TenXsys Inc and Figure 52b from Krantz[33].

Figure 52a Sensor washer

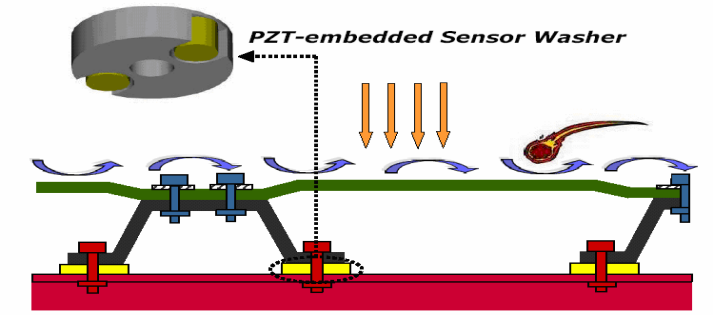

Figure 52b induction loop powered sensor

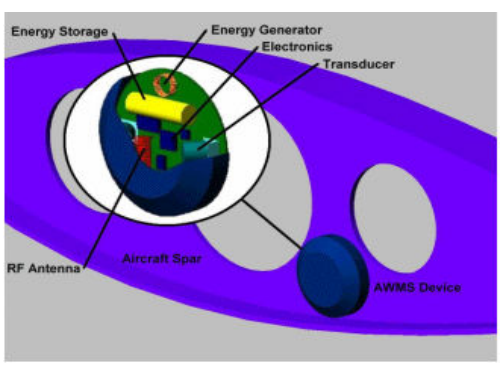

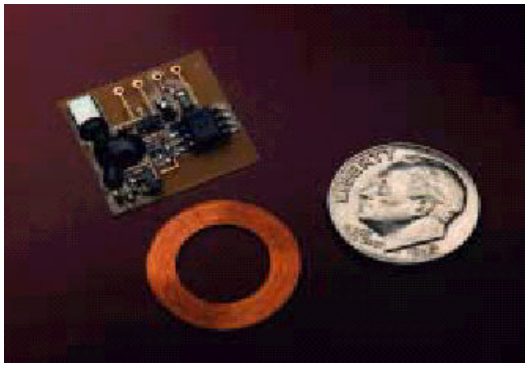

The transducer development, detailed in the next chapter, forms a very important part of the research program with the main emphasis being on providing transducers based on piezoelectric composite materials that are acoustically matched to the material under test.

4 PROTOTYPE TRANSDUCER DESIGN

A prototype transducer was designed and built by the author for surface contact application in non-linear acoustic testing. This chapter initially provides an overview of the design techniques for piezoelectric based narrow and wide band transducers, secondly the chapter describes the development and testing of a prototype wide band transducer intended for use on materials such as carbon and glass fiber composites, concrete and low density metals such as Aluminum and Titanium. Finally a simple mathematical model is given that was used to aid in the design of the driving and receiving electronic circuits.

4.1 Design of narrow band and broad band transducers

Narrow band transducers

These tend to be high Q devices and the selection of the backing material demands careful consideration of parameters such as operating frequency, bandwidth, insertion loss, and operational environment. These devices can provide high efficiency and high power, however they are narrow band and any acoustic mismatch between the load and piezoelectric element, at high power, may result in low energy transfer, “ringing” and crystal damage. Figure 53 shows the design of a typical piezoelectric narrow band transducer. When alternating electrical power at a particular frequency is supplied to the piezoelectric element it expands and contracts, this acoustic energy is transmitted forward into the load and backwards into the backing block. Acoustic energy is reflected from the rear end of the backing block and returns to the piezoelectric element. If the frequency, backing block material and dimensions are designed correctly this energy reinforces that being transmitted into the load in the forward direction.

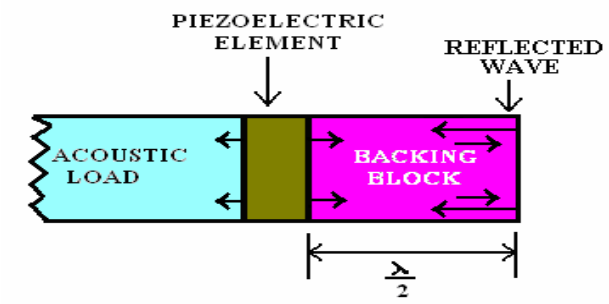

Figure 53

Narrow Band Transducer

A summary of design considerations is listed below:-

(i) The front face of the piezoelectric is often matched to the material under test (the load) by the use of one or more intermediate matching layers that have an acoustic impedance value between the piezoelectric crystal and the test material. The thickness and shape of these matching layers are also important, and particularly designed for a single working frequency. This matching will avoid reflections back into the transducer from the piezoelectric / load interface, as this would cause "ringing" of the transducer.

(ii) The acoustic impedance of the backing material is critical, if used. Usually the backing is made from brass which has the same acoustic impedance value as that of PZT. Sometimes no backing is used and the piezoelectric element is its own reaction mass.

(iii) The dimensions of piezoelectric and backing material are very critical in determining the frequency of operation.

(iv) The backing must have low attenuation to allow back wall reflections.

(v) Phase shifts at piezoelectric/backing/air interfaces must be taken into consideration. A low to high acoustic impedance interface resonate in $\lambda/4$ thickness mode due to the 180 deg phase shift. Whereas a high to low interface resonate in $\lambda/2$ mode)

Broad band transducers

By choosing a highly attenuating backing material of appropriate acoustic impedance, the Q factor can be lowered, thereby producing a wide band transducer. However this wider bandwidth is obtained at the cost of power efficiency. Figure 54 shows the design of a piezoelectric wide band transducer. When alternating electrical power is supplied to the piezoelectric element it expands and contracts, this acoustic energy is transmitted forward into the load and backwards into the backing block. The acoustic energy is absorbed by the backing material and the energy supplied to the load is only that which was generated in the forward direction.

Figure 54

Wide band Transducer

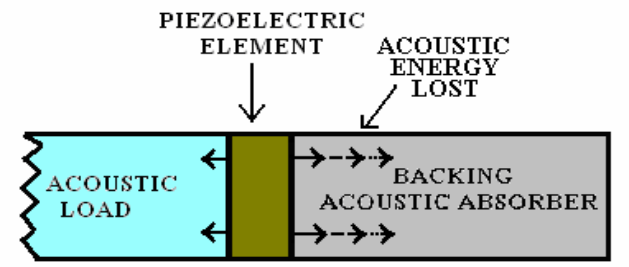

A summary of design considerations is listed below:-

(i) For maximum efficiency the front face of the piezoelectric must be matched to the material under test. This matching must be independent of frequency. Any mismatch at the load will cause reflections back into the transducer, however unlike the narrow band transducer this reflected wave will be absorbed in the backing, so no 'ringing' occurs.

(ii) The backing must have a value of acoustic impedance that is close to that of the piezoelectric element. For most pure PZT elements this is 35 to 40 MRayl. For PZT Epoxy composite this is usually between 8 and 15 MRalys.

(iii) The backing must have sufficient acoustic attenuation to prevent unwanted acoustic reverberations at all frequencies, i.e. no back wall reflections. Ideally the backing reflected acoustic signal should be at least 90 dB down from transmitted signal level).

(iv) The backing must be able to bond to the piezoelectric material, either directly or via a very thin film of glue, if the backing material is an electrical insulator this bonding glue must be conductive to allow electrical connections.

(v) The structural bonding layer thickness between transducer elements should be less than $1/200^{th}$ of the acoustic wavelength, to be transparent to the waves. For a sound velocity of 5000m/sec, at 100kHz this is 0.25mm, and at 1MHz this is 0.025mm.

4.2 Transducer composite piezoelectric element

The piezoelectric composite selected for the prototype transducer was provided by Sensor Technologies Ltd. A detailed specification of its material properties are given in Appendix C. Figure 55 below shows the structure of a 1-3 piezoelectric / polymer composite material.

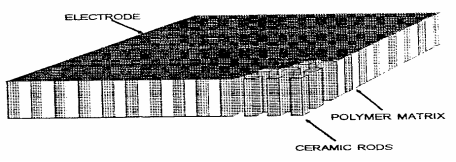

Figure 55

Piezoelectric / polymer composite structure

Figure 56

Impedance v frequency for PZT / Epoxy composite

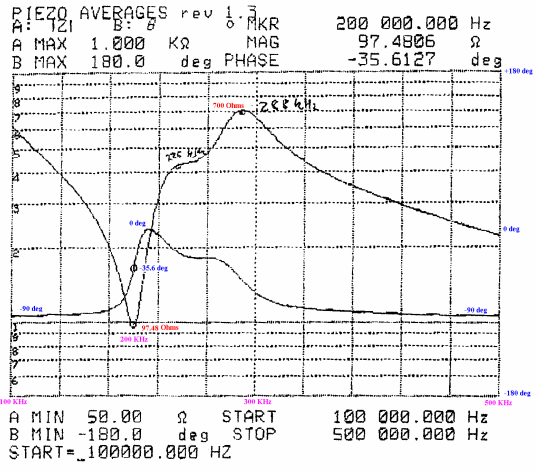

Figure 57

Impedance v frequency for PZT

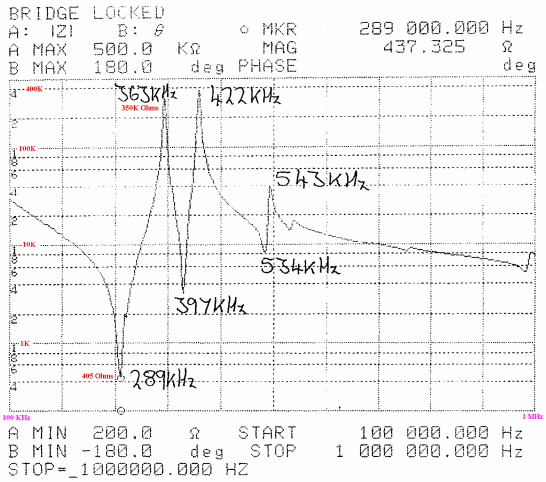

A similar composite is also available from Morgan Matroc Ltd. Figure 56 shows an industry standard impedance and phase versus frequency plot for a large (35 x 35 x 5 mm) 1-3 piezoelectric / polymer composite material, from this company. From this plot it is noted that there is only one peak and one trough, the impedance varies from 700 to 97 Ohms and the phase variation is from -90 to 0 degrees over the full bandwidth. In the bandwidth 200kHz to 288kHz it varies between 0 and -35.6 degrees. Figure 57 shows the impedance versus frequency plot for a pure piezoelectric material of similar size and thickness (5mm). There are two peaks and one trough in the band 100kHz to 500kHz. The impedance has a large variation, from 350K ohms to 405 Ohms. The phase will change rapidly from -90 degrees to +90 degrees as the frequency passes from 288 to 290 kHz (crosses the series resonance of 289 kHz). When the frequency reaches 363

kHz, the parallel resonance value, the phase will change rapidly from +90 to -90 degrees. At the two resonant frequencies, 289 and 363 kHz the phase is 0 degrees.
If V is the applied voltage and I the current following into the piezoelectric material the power dissipated in this material will be given by:- Power = VI cos(Φ)
where Φ is the phase angle between the current and voltage.
When the phase angle is 0 degrees then cos(Φ) is equal to its maximum value of 1. The power dissipated is a maximum.
If the phase angle is +90 or -90 degrees then cos(Φ) is equal to zero, no power is dissipated in the material. In the example of the pure piezoelectric, power is only dissipated at the resonant frequencies of 289 and 363 kHz since the phase angle is 0 degrees only at these values. At other frequencies the phase angle is +/-90 degrees.
The impedance has its lowest value (405 Ohms) at the series resonant frequency 289 kHz. This will dissipate the most power. At the parallel resonance (363 kHz) the impedance is 350K Ohms, for a given voltage less power will be dissipated due to this higher impedance. For the piezoelectric / polymer composite between the frequency range 200 to 288 kHz the phase changes from 0 to -35.6 degrees. The power dissipated will vary from its maximum at 0 degrees to 81% of full power at -35.6 degrees (cos(-35.6 deg) = 0.81). The use of composite piezoelectric materials has the advantage that it smoothes out the peaks and troughs in the frequency versus impedance characteristic and provides a lower variation in power dissipation. The following section shows that by providing suitable backing materials addition improvements in transducer performance can be achieved.

4.3 Transducer backing materials

The backing material for a wide band transducer should have the same acoustic impedance as the active element, for the prototype piezoelectric / polymer composite this is 12 MRayls. The backing must be highly absorbent to acoustic waves over a wide range of frequencies, to obtain this high absorption the acoustic wave is scattered and the energy being ultimately converted to heat. This is achieved by using a mixture of two materials one of a very high acoustic impedance, Tungsten of 105 MRayls and the other of a very low impedance, epoxy resin of 3 MRayls. For this to be effective, over a wide frequency range, particles of various sizes of Tungsten are mixed with an epoxy

resin and in a ratio such that the composite has a resultant acoustic impedance of 12 MRayls. The acoustic impedance of a Tungsten epoxy mixture Z_m is given by:-

$$Z_m = (\text{elastic bulk modulus of mixture} * \text{density})^{0.5}$$

To calculate the elastic bulk modulus of this mixture three models are considered:

Reuss model

Constant STRESS throughout the composite solid

$$\frac{1}{Kc} = \frac{V1}{K1} + \frac{V2}{K2}$$

where :-
Kc = Bulk modulus of composite
K1 = Bulk modulus of material 1
K2 = Bulk modulus of material 2
V1 = Volume fraction material 1
V2 = Volume fraction material 2

Voigt model

Constant STRAIN in the composite solid

$$Kc = V1 * K1 + V2 * K2$$

Logarithmic model

This is an empirical model that falls between the two extremes above.

$$Ln(Kc) = V1 * Ln(K1) + V2 * Ln(K2)$$ where Ln = natural logarithm

Figures 58 and 59 from Wang [34], show values of acoustic impedance and attenuation against volume fraction of Tungsten. The experimental values are shown in red. The tests were performed at 30Mhz, using Epoxy EPO-TEK301 and a Tungsten particle size 5 μm. The Logarithmic model is seen to be a close fit to experimental values.

Figure 58

Acoustic impedance versus volume fraction of Tungsten

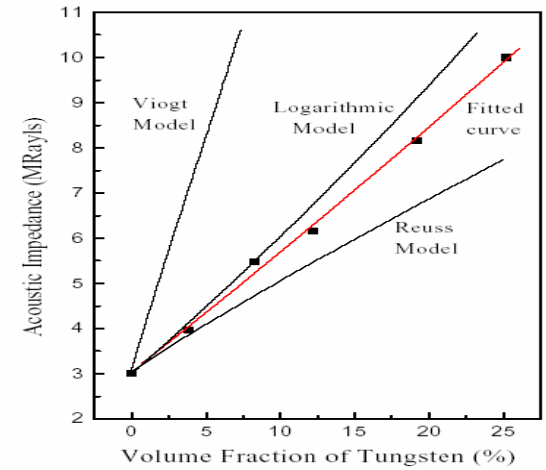

Figure 59

Attenuation versus volume fraction of Tungsten

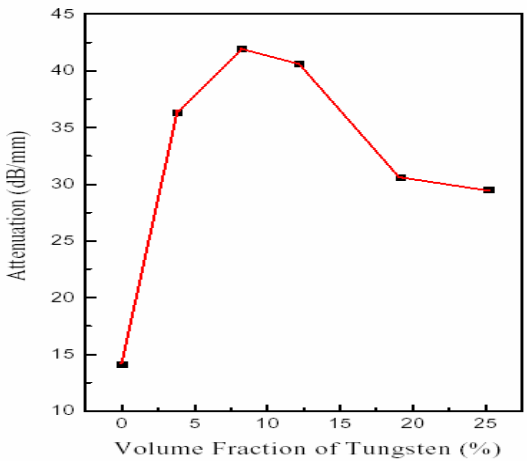

The experimental results given in Wang's paper follow very closely to those found in an earlier paper by Grewe[35], these are summarized in Figures 60 and 61 below, the tests performed at 5 mHz, using epoxy EPO-TEK301 with various Tungsten particle sizes. The data for Alumina particles is also included.

Figure 60 Acoustic impedance versus volume fraction of Tungsten (Grewe)

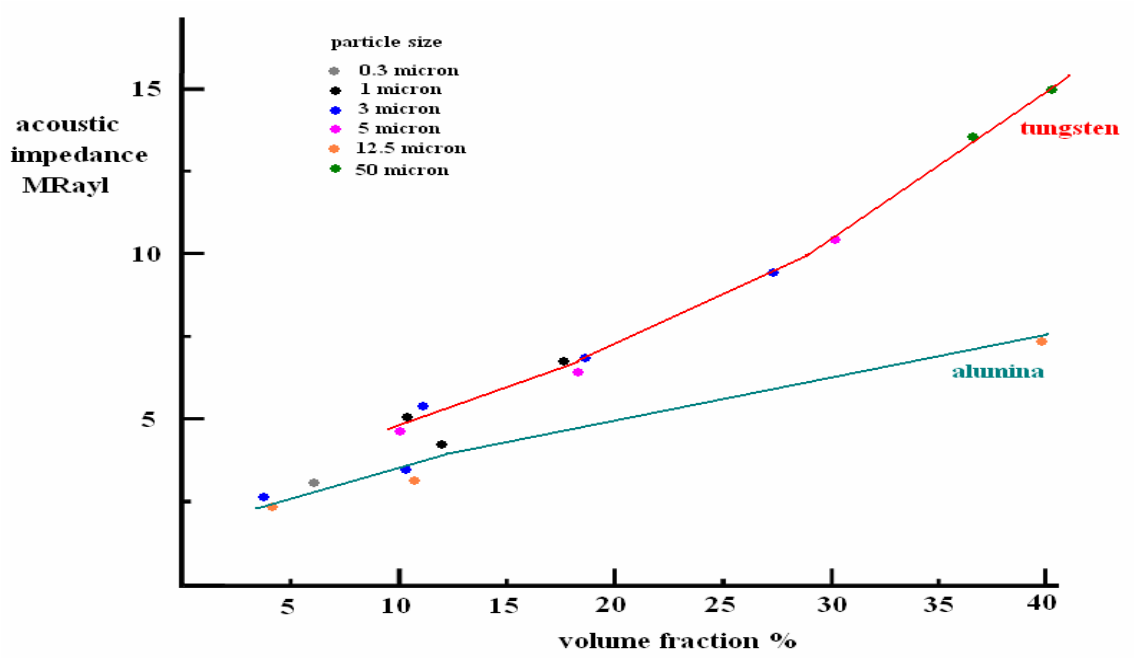

Figure 61 Attenuation versus volume fraction of Tungsten (Grewe)

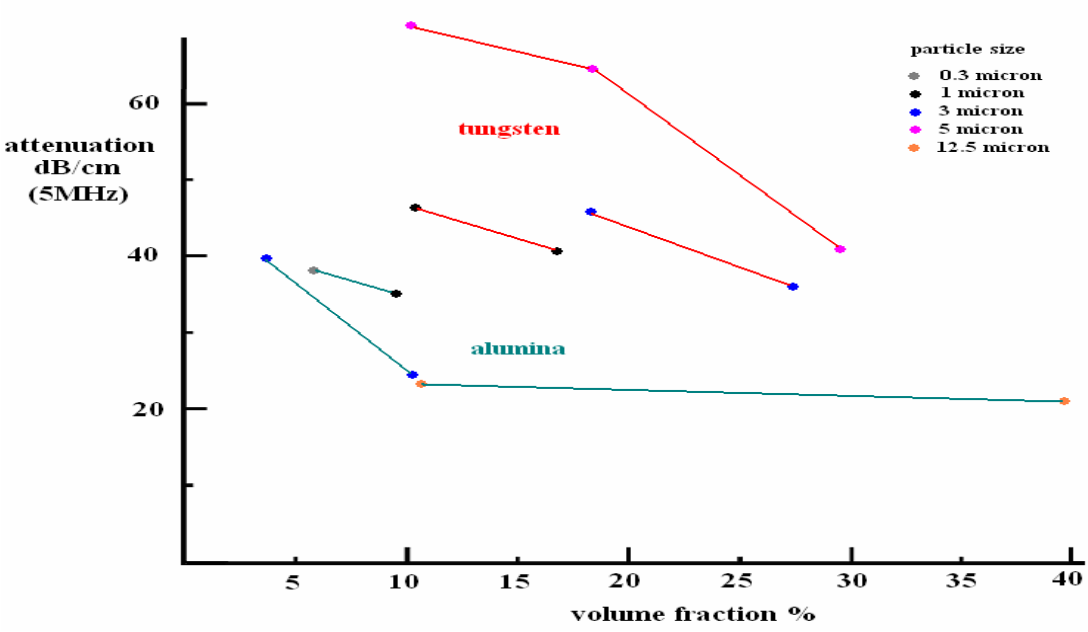

The backing material design

The piezoelectric composite element has an acoustic impedance of 12 MRayls.
The required backing material should have the same value. Unfortunately there is an upper limit to the acoustic impedance that can be achieved using a mixture of a metal particles and an epoxy, this is due to the interstitial packing limit. For spheres in normal stack this is 52.4%, for body-centered cubic packing it is 68% and for face-centered cubic packing it is 74%. In practice these limits are seldom reached. For the composite to be manufactured with any useful mechanical properties the upper limit is about 40%. From the graph of Figure 60 the volume fraction of 35% Tungsten in epoxy will produce an acoustic impedance of 12 MRayls. The Tungsten particle sizes (50μm, 5μm and 3μm) seem not to have a great effect on the impedance value, as shown in this Figure. From the Figure 61, the attenuation is plotted as a function of the volume fraction of Tungsten. It is observed that particle size is an important factor in attenuation at low volume fractions of Tungsten. The larger particles provide a greater attenuation. Extrapolating all the particle size curves there is a tendency for them to converge at a volume fraction of 40% Tungsten, giving an attenuation of about 25 dB/cm.
At 35% volume fraction the 5 micron particles provide an attenuation of about 30dB/cm at 5 mHz frequency. For the prototype broad band transducer the backing material is 2.5 cms long, this gives a two way (reflected from the back) distance of 5 cms. This corresponds to an attenuation of 150 dB at 5 MHz. No information has been found for attenuation at lower frequencies or larger particle sizes. For the prototype transducer a mixture containing a range of Tungsten particle sizes was used (250, 50, 25, 5 and below 1 μm). This was found to give acceptable attenuation down to 10 kHz, for details see section 4.5 which gives transducer frequency performance.

4.4 Prototype transducer construction

Figure 62 shows the inner transducer assembly, the PZT / epoxy composite is glued to a macor plate this provides mechanical protection to the piezoelectric element and it has an acoustic impedance of 12 MRayls matching that of the load and element. The Tungsten / epoxy backing material is glued to the other side of the element using silver loaded epoxy. The connecting wires have a break down voltage of 4kV. With a margin

of safety the transducer should be able to operate up to 1.5kV (the PZT / epoxy element has a breakdown of about 2.5kV).

Figure 62 Inner transducer assembly

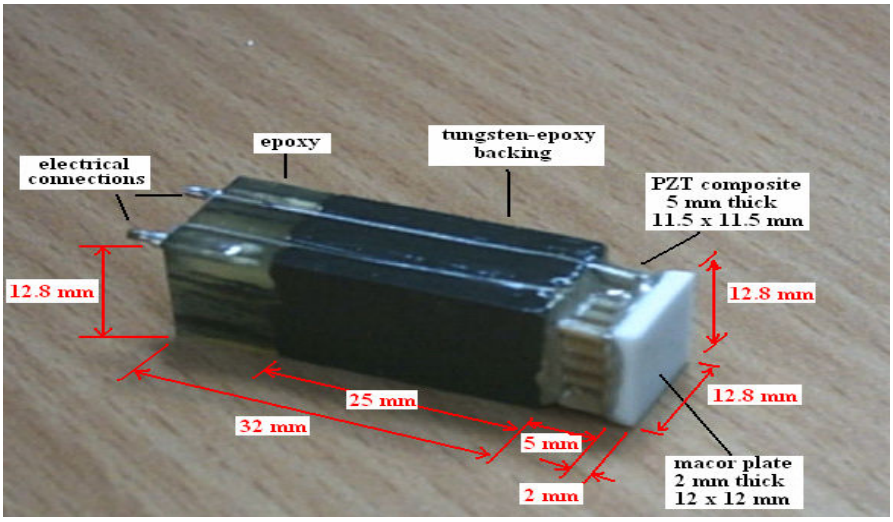

Figure 63 electrical screen layer

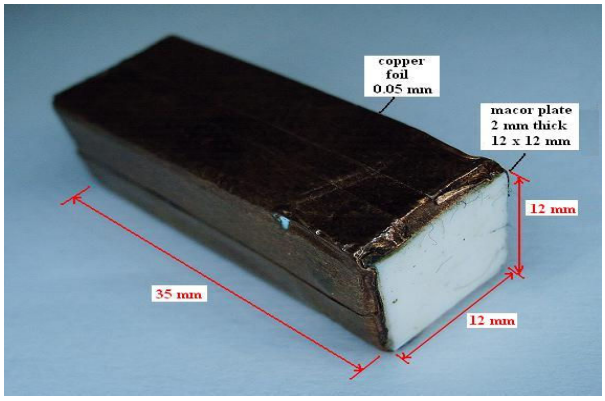

Figure 63 shows the electrical screening layer. First a plastic insulation layer (heat shrink) covering the outside of the backing and PZT / epoxy element goes over the whole length of the transducer, and is shrunk down to fit. The copper foil is then wrapped around this. The foil acts as an electrical shielding and is connected to earth Figures 64a and 64b shows the front and back views of the transducer assembly placed in a plastic carrier. The foiled assembly is slotted into this carrier and glued in place with epoxy resin. Two holes are drilled (about 4 mm deep, 1.5 mm dia) and two pins (1 mm dia, 8 mm long) are glued into these holes. These form the electrical connections. Two wires from the PZT /epoxy element are soldered to these pins. One pin, the pin that connects to the outer face of the PZT/epoxy element, is also connected to the copper foil, so the whole transducer is surrounded by an earth shield. Another hole (4 mm deep,

5 mm dia) is drilled in the centre, and a nylon threaded rod is glued into this hole, with 25 mm protruding from the end of the transducer assembly. Figure 65 shows the final transducer with its spring in place.

Figure 64a Transducer assembly

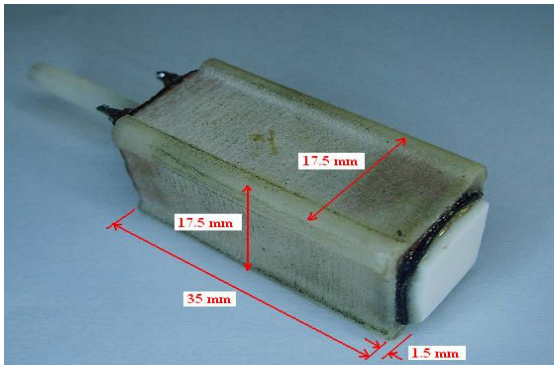

Figure 64b Transducer assembly

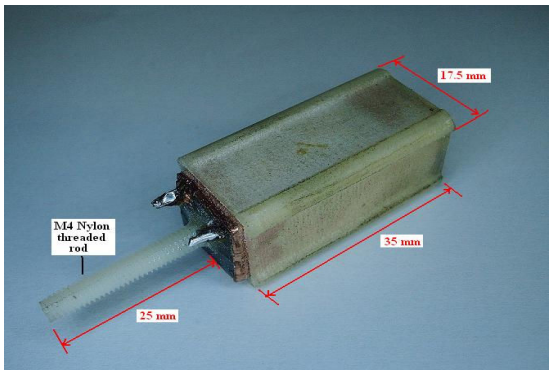

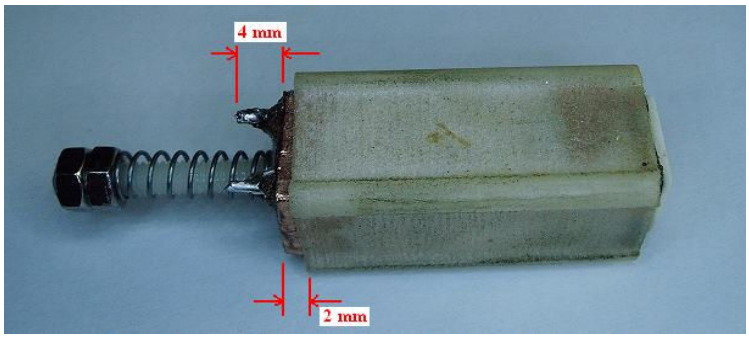

Figure 65

Complete transducer assembly with spring

4.5 Frequency response tests

Figure 66 shows the measured impedance versus the frequency for three types of backing; 1) no backing, 2) backing with a Tungsten volume fraction of 25% (8 MRayls) and 3) backing with a volume fraction of 35% (12 MRayls). The effect of introducing the backing can be clearly observed. With no backing (shown in blue) there is a large peak at 425 kHz and a low trough at 293 kHz. With a backing of 25% volume fraction Tungsten (shown in red) the peaks and troughs start to flatten out, with a backing of 35% Tungsten (shown in green) the peaks and troughs have almost been removed by being dampened out.

Figure 66 Acoustic impedance v frequency for different backing materials

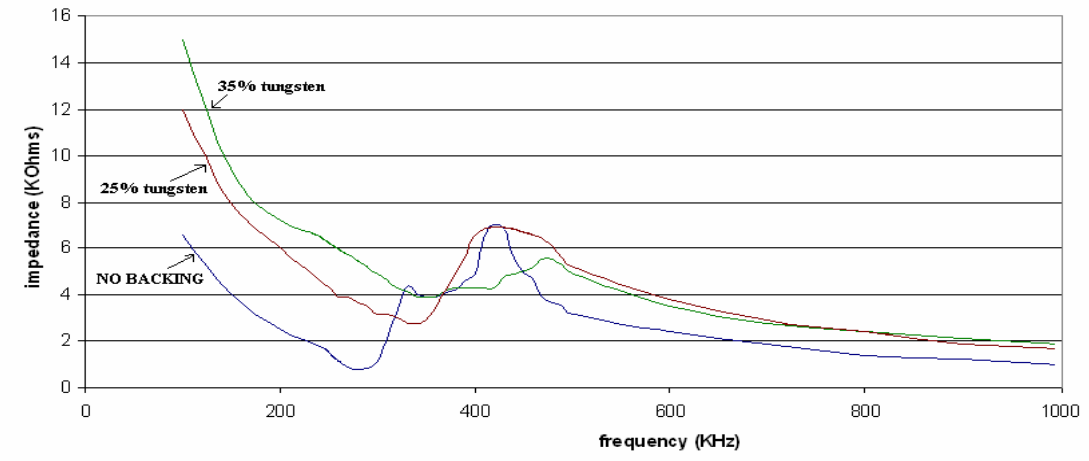

Figure 67 shows the phase relationship between the voltage applied to the transducer and the current flowing through it at various frequencies. With no backing at the low frequency the transducer is capacitive, as the frequency increases the phase angle increases and becomes zero at 293 kHz, corresponding to the series resonant condition then goes inductive, (for details about piezoelectric resonance see section 4.7).
At 335 kHz it returns to zero and then goes capacitive at higher frequencies. The effect of the backing is to keep the transducer capacitive. With 35% Tungsten backing the phase angle is maintained between -60 and -80 degrees (capacitive).

Figure 67 Phase angle v frequency for different backing materials

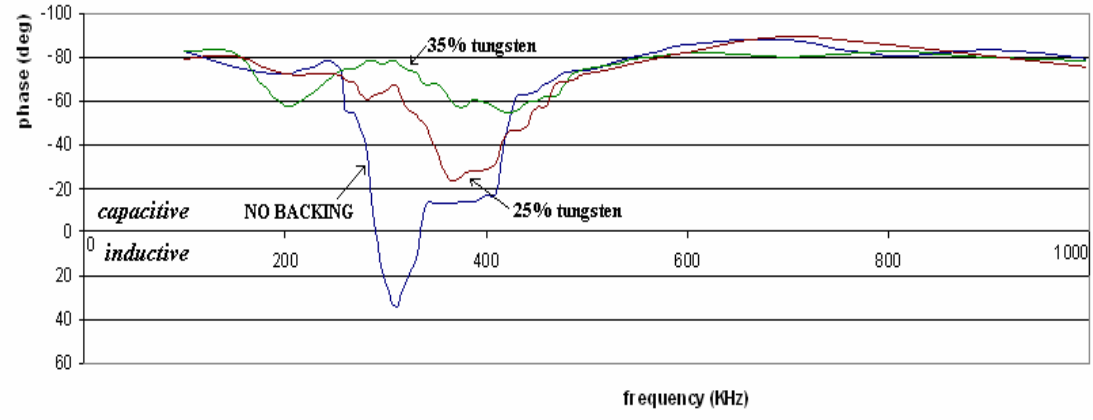

Figure 68 shows the transducer power dissipation with no backing, with 25% and 35% Tungsten backing. The power dissipation is given by VI.cos(Φ), where V is the applied voltage, I is the current flowing and Φ is the phase angle between current and voltage.

Figure 68 Power dissipation v frequency for different backing materials

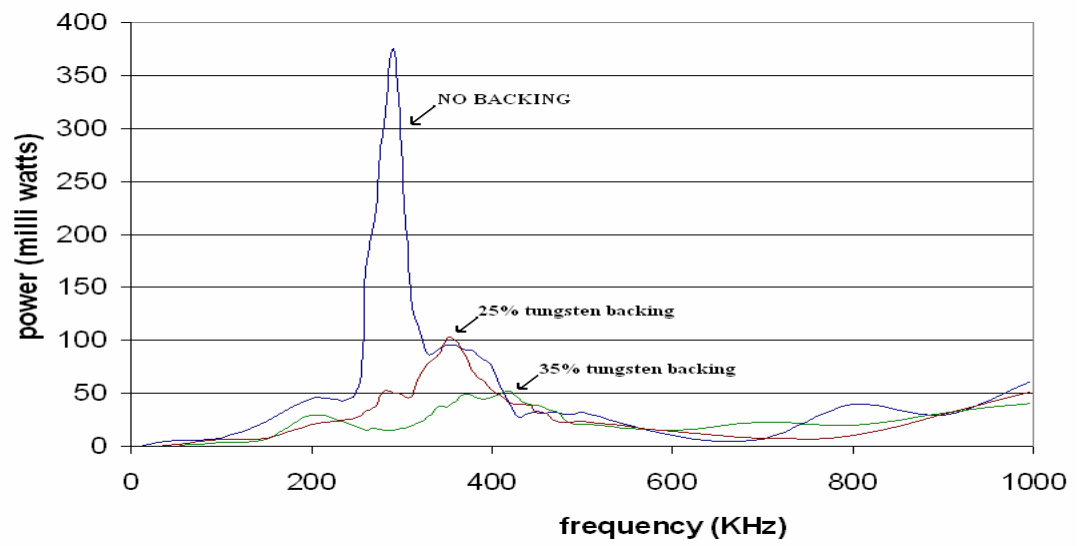

This power dissipation graph shows clearly the effect of the backing material on the transducer Q, with no backing the piezoelectric element is free to oscillate, peaking at its series resonant frequency (293 kHz), with phase angle zero. The dissipation in the band between 300 kHz and 400 kHz is likely due to the properties of the PZT/epoxy composite from losses and lateral vibrations. With 25% Tungsten (8 MRayls) the peak at 293 kHz is reduced and shifted in frequency. With 35% Tungsten (12 MRayls) the dissipation starts to even out across the frequency range 200 to 1000 kHz, bandwidth is gained at the expense of power dissipation.

Transmission and reception

Two transducers (35% tungsten backing) were coupled together, face to face, as shown in Figure 69. One is used to transmit a signal driven from a 10 Volts peak sine wave generator. The other is used to receive the signal. The relative amplitudes of the received signal, at various frequencies were measured and plotted in the graph of Figure 70, using different coupling media.

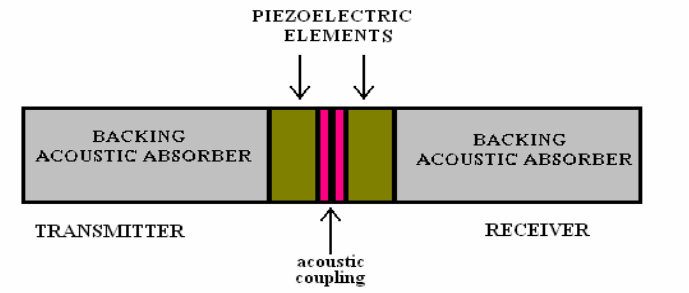

Figure 69

Transducers face to face for response test.

Figure 70 Signal level v frequency
Transducers face to face with different coupling medium

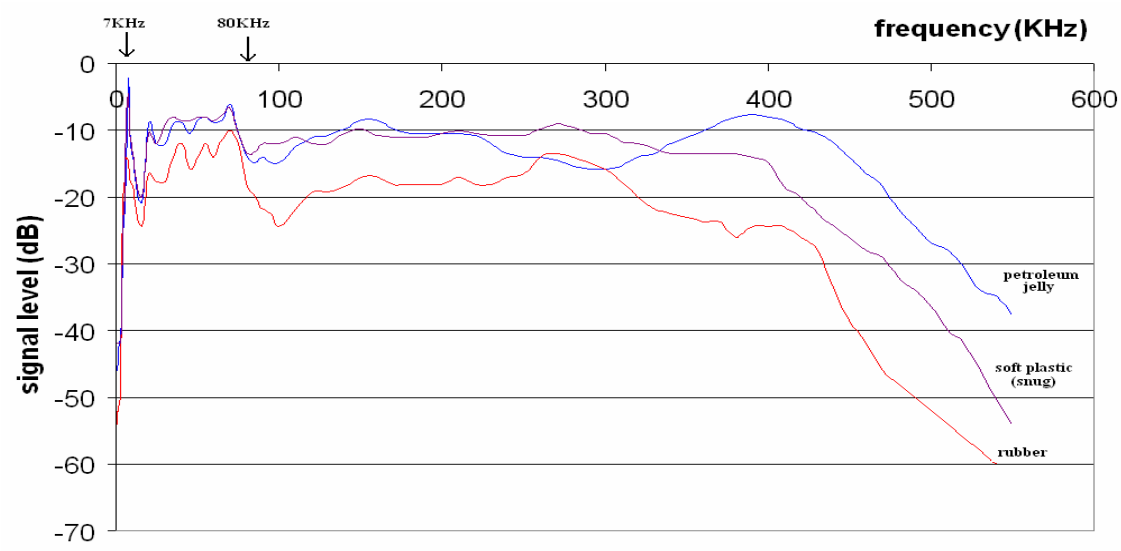

The graph shows that using petroleum jelly (vaseline) the frequency response between 80 kHz to 450 kHz is within +/- 4dB. For Soft plastic (snug) the frequency response between 80 kHz to 400 kHz is within +/- 2.5dB and for rubber the frequency response between 80 kHz to 350 kHz is within +/- 5dB.

The Figure 70 shows that the transducer has a reasonably flat response in the band 80 kHz to 450 kHz. There are some ripples in the amplitude at frequencies lower than 80 kHz, this may be due to the backing material not attenuating sufficiently at these low frequencies and reflections from the back end of the backing material causing interference. At 7 kHz there is a strong resonant peak, this may be due to lateral movements of the piezoelectric composite and front ceramic (macor) plate.

4.6 Linearity tests

Two transducers were coupled face to face, using a soft plastic (snug). One of the transducers transmitted a continuous pure sine wave acoustic signal, the other received this signal. The spectral content and the levels of each harmonic were examined at set frequencies using a spectrum analyzer. A plot of frequency versus Total Harmonic Distortion (THD) is given in the Figure 71.

Figure 71 Measured distortion at various frequencies

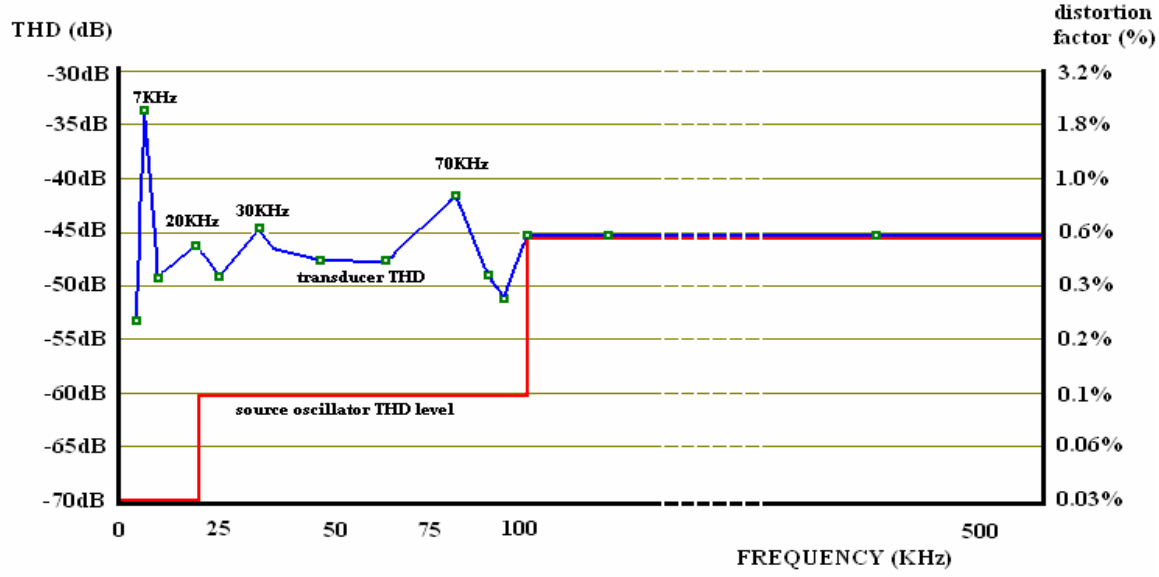

For this test the oscillator drive voltage was 20 volts peak to peak. Only the 2nd and 3rd harmonics were used in the calculation, as the other harmonics were negligible. less than –65dB (0.06%), with the exception of measurements taken at 7 kHz. The total harmonic distortion for the transducer is below 0.6%, with exceptions at 7 kHz and 70 kHz. It was not possible to determine transducer THD values at frequencies above 100 kHz, since the driving oscillator introduces its own distortion (shown in red). However we can say with certainty that the transducers distortion is less than 0.6%.

4.7 Modeling of prototype transducer

A simple mathematical model for the transducer was developed as an aid to the designs of the electronic driver and receiver circuits. This model is based on the well known Van Dyke model [36], shown in the Figure 72

Figure 72 VAN DYKE MODEL

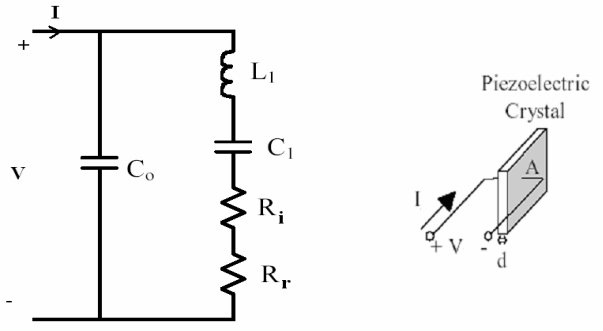

C_o = static capacitance of the piezoelectric plate
L_1 = motional analogue of the piezoelectric mass
C_1 = motional analogue of the piezoelectric compliance
R_i = motional analogue of damping, due to internal losses
R_r = motional analogue of damping, due to radiation losses

R_r is proportional to the acoustic impedance of the mechanical load applied to the piezoelectric crystal, and represents the acoustic power dissipated into the load.
R_i represents the internal power losses within the piezoelectric material. With no mechanical load R_r is neglected. (R_r = 0 ohms) and only the internal losses are considered. C_o represents the static capacitance due to the plate electrodes either side of the piezoelectric material and is considered constant in this model.
The values C_1 and L_1 represent motional analogues of the compliance and mass of the piezoelectric. They are considered constant for a given size and piezoelectric material.
Two resonant frequency conditions will occur in this model. The first is called series resonance (F_S) this occurs at a frequency such that C_1 and L_1 form a series resonant combination, in this state all the power will be dissipated in R_i and R_r since C_1 and L_1 provide no restrictions to the mechanical movements. The second resonance is called the parallel resonance condition (F_P) and occurs when the frequency is such that C_o and C_1 in series form a parallel combination with L_1, in this state very little power will be dissipated in R_i and R_r as restrictions to mechanical movement will occur.
As the frequency applied to the piezoelectric increased, the impedance of the transducer changes from capacitive to inductive and back to capacitive, around the two resonant conditions. Before and after these resonant regions the crystal behaves as a capacitance in series with a resistance. This is illustrated in Figure 73.

Figure 73 Capacitive and Inductive reactance changes with frequency

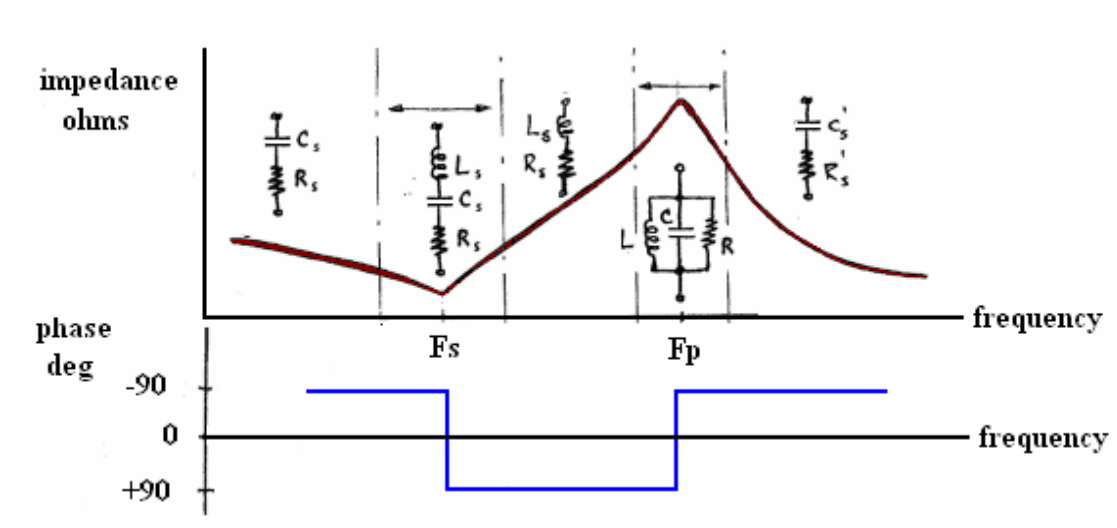

For the piezoelectric composite material used in the transducer design the values of C_o, C_1 and L_1 can be derived from the material's dimensions and properties. This is illustrated below:-

Dimensions of PZT/epoxy composite, area A = 11.5 * 11.1 mm^2, thickness d = 5mm

Permittivity of PZT/epoxy composite $\varepsilon_{pzt} = 890 * 8.85*10^{-12}$ farads/m

Zero phase resonance (taken from frequency verses phase plot Figure 67) :-

F_s = 293kHz (series resonance), impedance = 852 ohms

F_p = 335kHz (parallel resonance)

and:-

$$Co := \frac{\varepsilon_{pzt} \cdot A}{d} = 201pF$$

$$C1 := \left(\frac{Fp^2}{Fs^2} - 1\right) \cdot Co = 62pF$$

$$L1 := \frac{1}{4 \cdot \pi^2 \cdot Fs^2 \cdot C1} = 5mH$$

$$Q = 2\pi * \frac{\text{Energy Stored during a cycle}}{\text{Energy dissipated per cycle}} = \frac{2 \cdot \pi \cdot Fs \cdot L1}{Ri} = 10.3$$

The Van Dyke model is used extensively to design the driver circuitry for narrow band resonant transducers, and precision crystal controlled oscillators. The model is mainly intended for Quartz or PZT ceramic crystals. It is only considered accurate around the resonant frequency. The Figure 74 below compares the Van Dyke model for impedance values at certain frequencies with the prototype transducer using a piezoelectric / epoxy composite with no load or backing, oscillating freely in air.

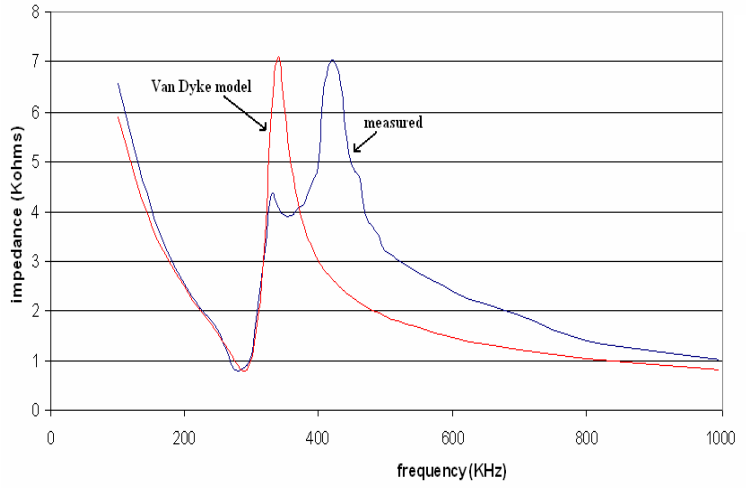

Figure 74

Comparison of Van Dyke model to measured values for PZT/Epoxy composite

In the composite the zero phase condition occurs as predicted by the model at 293 and 335 kHz, however there is an additional peak in the impedance value formed at 425 kHz, the phase at this point is non zero and capacitive. This may be due to other modes of oscillation, and losses in the PZT / epoxy composite. Applying a mechanical load to the piezoelectric will reduce the Q. If the Q can be lowered substantially then resonance can be prevented, under these conditions the transducer can be modeled as a resistor – capacitor series combination.

The Figure 75 below shows the electrical impedance verses frequency for the 35% Tungsten transducer. This is compared with the impedance from that of a 100 pF capacitor in series with a 1500 ohm resistor.

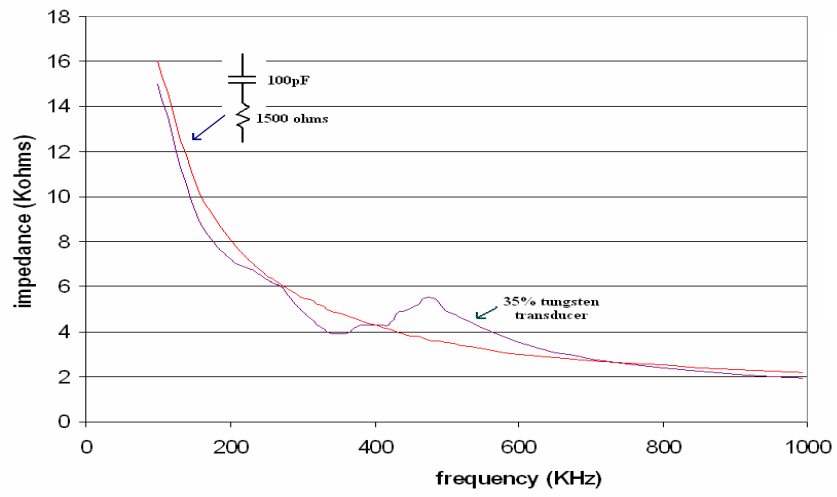

Figure 75

Simple model for piezoelectric / epoxy composite transducer with backing

The experimental data for the transducer shows a curve, asymptotic to 1500 ohms, as the frequency increases. The capacitor value (100 pF) was determined as a value of best fit by trail and error. As the capacitor impedances tends to zero, the resistive part only remains at higher frequencies. This resistive element will increase when the piezoelectric crystal has an applied mechanical load.

This is a very approximate method to model a basic transducer, and is useful in designing a transmitter power amplifier or receiving pre-amplifier.

To calculate the electrical impedance directly from a given acoustic load other models have been shown to be more accurate, particularly for broad band non- resonant applications. The KLM model, Krimholtz[37] is one such example, for details see chapter 7.1. However for our application the resistor capacitor series model was sufficient to design the supporting pre-amplifier and power amplifier circuits detailed in the following chapter.

5 NON-LINEAR ACOUSTIC TESTING SYSTEM

This section describes how a practical non-linear acoustic testing system is applied to various objects in a wide range of situations. In addition the section gives details of the electronic hardware and software developed by the author during the course of this research program and which were finally used in a series of experiments to validate the non-linear acoustic testing technique. The experimental work is given in chapter 6.

5.1 Non-linear acoustic application

The general application methodology for non-linear acoustic testing of components is determined by a series of decisions. The first is to decide on the type of monitoring process required, the main three types being; continuous health monitoring, periodic maintenance and damage assessment. This will define the type of instrumentation, data acquisition methods and display requirements. Continuous health monitoring will require permanently installed transducers and instrumentation and involves recording and analysing substantial amounts of data. The requirements for periodic maintenance will require temporary application of transducers and the instrumentation brought to the object under test, the volume of data required is low, however it needs to be stored long term to assess gradually changing degradation over the operational lifetime of the component. For damage assessment the equipment must be very portable and applied to the test objects in a short time. It must also provide fast analysis of the data.
The second decision is concerned with the test object's size and the detail that is required. In general a small object will require the use of high frequency ultrasound in order to obtain high spatial resolution of defects. Testing a large object that is not required to have a high spatial resolution will allow the use of low frequencies and fewer transducers, this is often the case when a general high speed survey of a large object is required, for example aircraft wings. Other important factors in the decision making process of applying non-linear acoustic testing techniques are; working frequency, resolution, range, recording time, sampling rate, instrument distortion and acoustic wave mode selection. These are detailed in the following sub sections.

Working frequency selection

The selection of the testing frequency is determined by many factors. The well known physical barrier in all ultrasonic testing systems is the trade off between resolution and depth of penetration into a material or distance travelled along it. High frequencies provide greater resolution but are greatly attenuated, so the tests will only cover a short range. Low frequencies are subject to less attenuation and thereby greater ranges can be achieved but at the cost of resolution.

In the non-linear harmonic and inter-modulation product testing method, unlike conventional ultrasonic testing, the resolution is not a critical factor as we are not trying to resolve single defects but determining regional micro-structural damage by introducing frequencies that stimulate non-linear behaviour and cause the generation of harmonic and inter-modulation products, whose frequency may be different, and often lower, than that used in conventional ultrasonic testing.

Figure 76 gives the wavelength and attenuation at various frequencies of a sound wave propagating in an Epoxy solid (DER332, v140,30phr.Ip3,r8) with a compressional wave velocity 2400m/s. From this information we can determine the range over which an ultrasonic wave transmission can be made and the resolution achievable. The methodology by which this is implemented is outlined in the following sections.

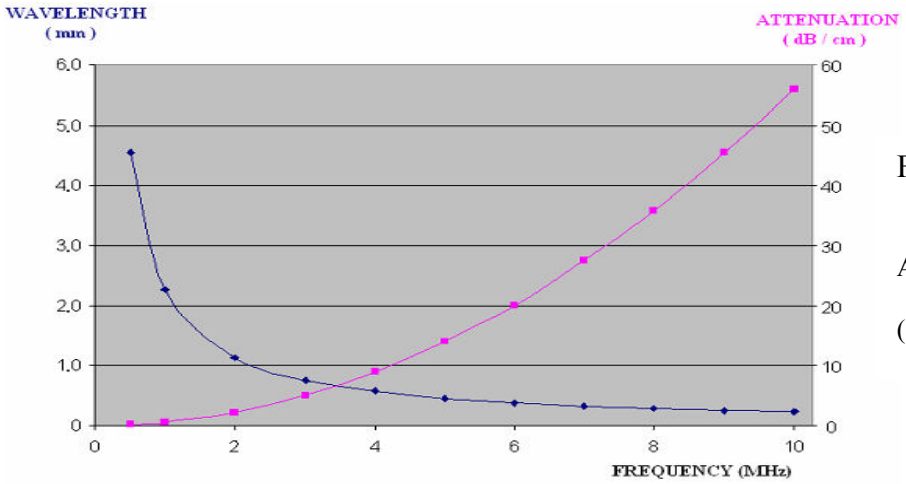

Figure 76

Wavelength & Attenuation versus frequency (for epoxy solid)

Spacial Resolution

In most non-linear acoustic testing applications resolution is not an issue, since we are only interested in defects that occur somewhere in the insonified region, however in time reversal non-linear acoustic methods that involve either defect illumination or re-focussing of the sound wave energy, as with conventional pulse echo ultrasonic testing methods the wave-length becomes a significant factor.

The inline resolution is considered very approximately to equal about half the wavelength. In the example material given in Figure 76, at a frequency of 5 MHz the wavelength is 1.5 mm giving a resolution of about 0.75 mm. This would be the smallest size of defect that can be detected, or the smallest region over which the energy can be re-focussed. In ultrasonic testing systems consideration is given to the problem of spatial aliasing, this sets a limit on the ability while scanning over a surface to resolve a defect along the detection path and is determined by the distance between the transducers or sampling locations. The Nyquist criterion requires the sampling distance to be half the minimum defect size. In practice the sampling distance employed is much smaller than the Nyquist value, typically by five or ten times, particularly in applications where phase information is important.

Range

In all ultrasonic systems the working range becomes an important factor. Referring to Figure 76, at a frequency of 5 MHz the attenuation is 14 dB/cm. To determine the maximum range, first we have to define the dynamic range of the signal that is to be detected. For the recording system developed within this research program a 12 bit A/D converter is used, the smallest detectable signal is 72 dB below the full scale value (the dynamic range, see Appendix H). Therefore the maximum range over which a sound wave can be detected is 5.14 cm (ie., 72/14 cm). When measuring harmonics and inter-modulation products, the attenuation of these frequencies also has to be considered, the 2^{nd} harmonic of 5 MHz is 10 MHz, this has an attenuation of 57 dB/cm giving a range of 1.26 cm (72/57 cm). Appendix H gives details of the dynamic range and signal to noise ratio that can be achieved by various types of analogue to digital converter.
For non-linear acoustic testing that is just required to measure harmonics and inter-modulation products, the working range can be extended if high power is transmitted into the material and the receivers are at a distance such that the signal levels are within the dynamic range of the transducers and the recording system. However an upper limit will be set by the distortion that may occur when driving high power sound waves into materials from a transducer.

Recording time

In pulse transmission ultrasonic systems that measure sound wave velocity the minimum possible recording time is the time it takes for the initial wave front of the

ultrasonic wave to travel from the transmitter to the receiver, sometimes known as the time of the first break. In pulse-echo ultrasonic systems that are used for defect detection and location the recording time is much longer as it must take into account the ultrasonic path times to and from a defect within the material, known as two-way time. However once the reflected acoustic pulse has been detected there is no need to acquire any further data.

In most non-linear acoustic testing the spectrum of a continuously received signal is examined, the travel time of the acoustic wave is not a factor. The method will depend upon the frequency range and resolution required in the spectrum analysis (see below). In pulse reversal non-linear acoustic systems we are interested in measuring the resonant reverberation waveform when subject to both a compressional and a tensile pulse. This will require a recording time that measures a significant number of oscillations, usually just beyond time at which the maximum amplitude occurs. This time will be very dependant upon the transmitted pulse width and the size, shape and material of the test object. The recording time for the time reversal non-linear acoustic method needs to be very long, right up to the point when any signal is no longer detected (zero level), since this whole signal is to be reversed and transmitted back into the material and it is important that an initial state of zero signal is preserved.

Sample rate

The Nyquist criterion states that the sampling rate must be at least twice the maximum frequency of measurement. For example if we are measuring a 100 kHz signal then the minimum sampling frequency is 200 kHz (a sampling interval of 5 micro-seconds). However in the case of the harmonic and inter-modulation product measurement we are interested in measuring the higher frequency components of this signal. If we were to measure the 2^{nd}, 3^{rd} and the 4^{th} harmonic content of this 100 kHz signal then the highest frequency that we need to measure is the fourth harmonic, 400 kHz, requiring to sample at 800 kHz or 1.25 micro-seconds interval. In practice it is generally accepted that for non-linear acoustic applications it is desirable to sample significantly above the Nyquist frequency. In recording systems anti-aliasing filters are used to prevent any possibility of there being any frequency components in the signal above the Nyquist frequency. These filters must have an “roll off” characteristic such that the level of high frequency components at the Nyqiust frequency is at or below the lowest detectable level.

Distortion

From the experimental work (see chapter 6) the lowest (minimum) level of harmonic distortion due to the transducers non-linearity when they are applied to test materials has been observed to be 0.3% for fixed glued transducers, 0.4% for gel coupled transducers and 0.6% for solid plastic film coupling. The maximum recorded distortion was 12.6%, occurring in severely damaged (delaminated) carbon fibre composite.
The electronic components used in most instrumentation systems will have distortion levels significantly less than these minimum values. Typical high quality A/D and D/A converters that sample at 10 million samples per second with 12 bit conversion have a Total Harmonic Distortion (THD) of less than -70dB (0.03%). Commercially available operational amplifiers have typical THD values of below -78dB (0.01%), well below the value introduced by the transducers. For the non-linear acoustic measurement system 12 bit accuracy should be sufficient for most applications, however for more advanced applications, in particular time reversal, 14 or 16 bit conversion may be required in order to provide a higher dynamic range.

Spectral Resolution

In this system the spectral information is obtained by the use of a Fast Fourier Transform program (FFT). This is a convenient software method and for relatively small samples can be performed efficiently and at high speed. However one requirement of this method is that the number of samples taken must be a power of 2.
The prototype developed in this project uses 1024 data samples which full fills this criteria. When a signal is sampled for spectral analysis, the sampling period (h) and the number of samples (N) are chosen so that the sample length is large enough to give adequate frequency resolution in the signal spectrum. In this prototype the sampling period h is 0.1 μsec and the number of samples N is 1024. This gives a sampling time of N*h = 1024 * 0.1 = 102.4 . μsec, which results in a spectral resolution of 1/(N*h) = 1/102.4 μsec = 9.77 kHz. The number of frequency channels is N / 2 = 512,
and the maximum sample frequency is 1/(2*0.1)μsec = 5 MHz.
For the prototype instrument the transmitting frequency is usually between 50 kHz to 300 kHz and the harmonics of interest are the 2^{nd} 3^{rd} and 4^{th}, therefore the maximum frequency to be measured is 4 * 300 kHz = 1.2 MHz. At these frequencies a spectral resolution of 9.77 kHz will be adequate. However at lower frequencies greater

resolution may be required in some applications. This is achievable by either taking a greater number of samples or having a longer sampling period.
Appendix H gives details of typical analogue to digital converter noise, resolutions, distortion and sample rates.

Wave mode selection

After selecting the instrumentation, operating frequency and range a decision is then made for the type of elastic wave propagation mode that is to be used. This will depend upon the material that is to be tested and its geometric construction, this process has been summarized by the author in Figure 77

Figure 77 Wave Mode Selection graph

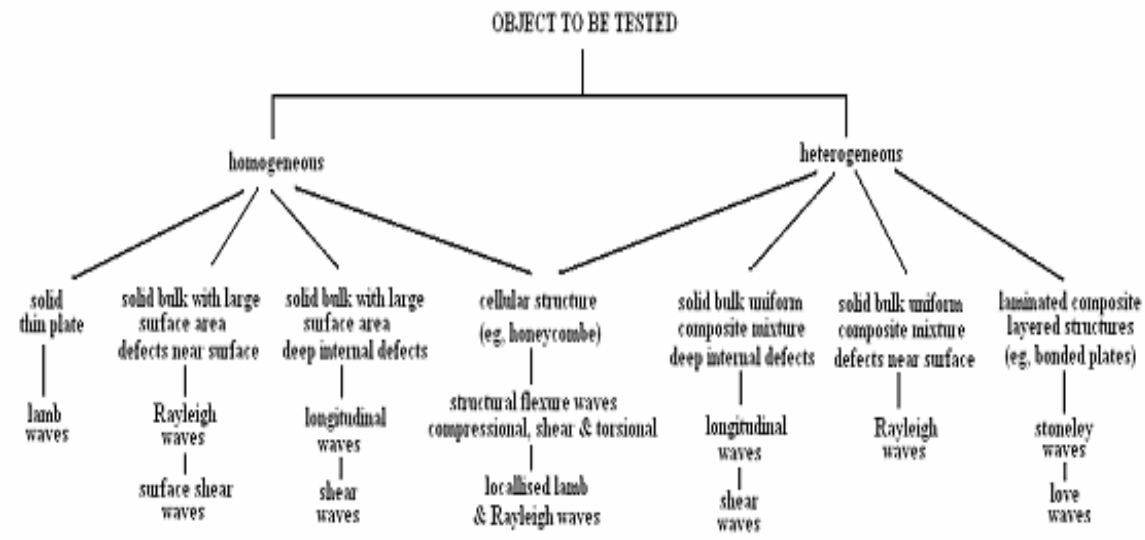

The figure first considers if the material composition is homogeneous, uniform throughout, for example a metal, or heterogeneous, made up of many materials, for example carbon fibre / epoxy or concrete. The second consideration is how the material is structured, for example as a solid block, plate or in a cellular or honeycomb form. This influences the type of waves that are to be generated and made to propagate through the material and this in turn determines the type of transducer that is to be used. For example if a thin metal plate is to be tested then Lamb waves are the most suitable form of wave motion to use and suitable transducers employed. Chapter 1.3 gives details of the principle ultrasonic wave motions.

5.2 Design of SMART modules

A series of SMART modules were developed by the author for various types of non-linear acoustic testing methods called NBOX's. The SMART control box NBOX200 together with the analogue NBOX series 0 to 4 and 6 modules are used for the generation of ultrasonic signals and for the measurement of harmonics, overtones and inter-modulation products. Figure 78 shows the basic operational schematic.

Figure 78 NBOX operation

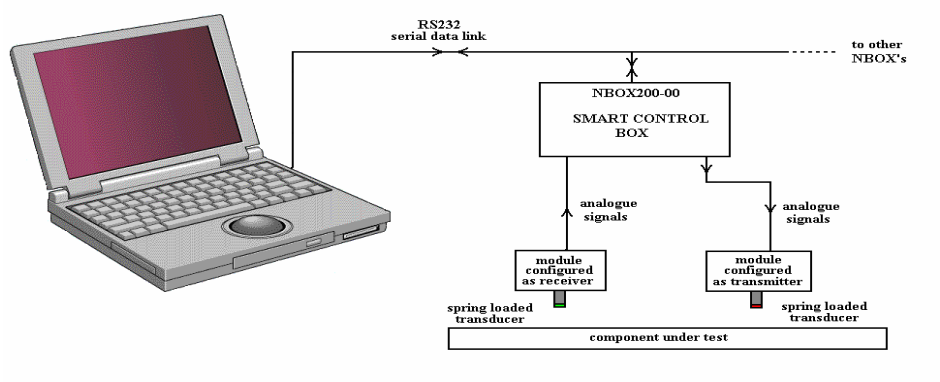

The digital NBOX200 contains one analogue to digital converter (A/D) and one digital to analogue converter (D/A). The module inputs and outputs analogue signals too and from the analogue NBOX's. It provides digital memory for the transmitted and received data. Microprocessors in this module provide a data interface to a PC via an RS232 serial link. A block schematic for this module is shown in Figure 79.

Figure 79 Schematic of NBOX200

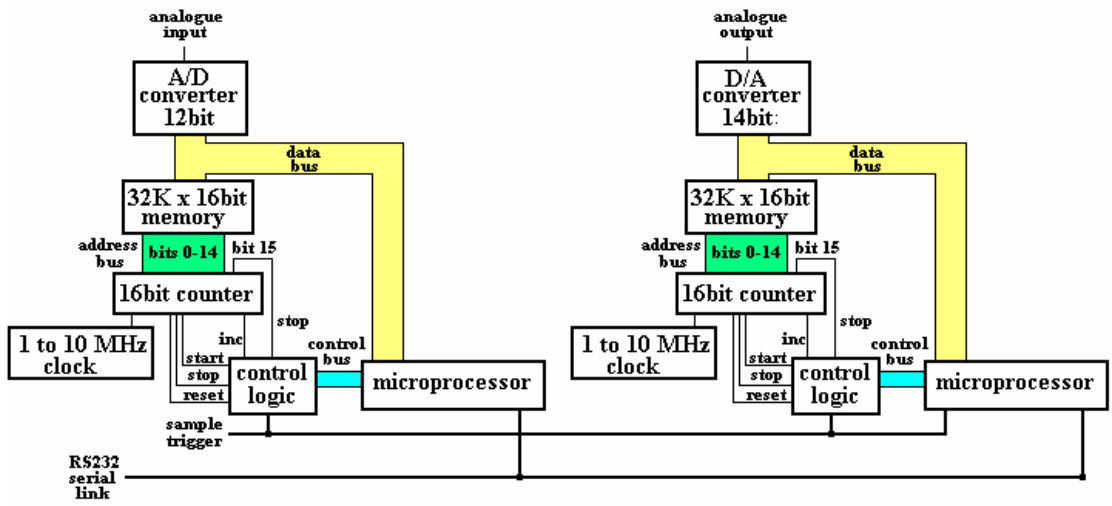

The analogue unit NBOX series 0 to 4 and 6 together with the SMART control box NBOX200 are shown in the photograph Figure 80. The schematics for the analogue units are given in Figure 81.

Figure 80 Photograph of NBOX200 and analogue units

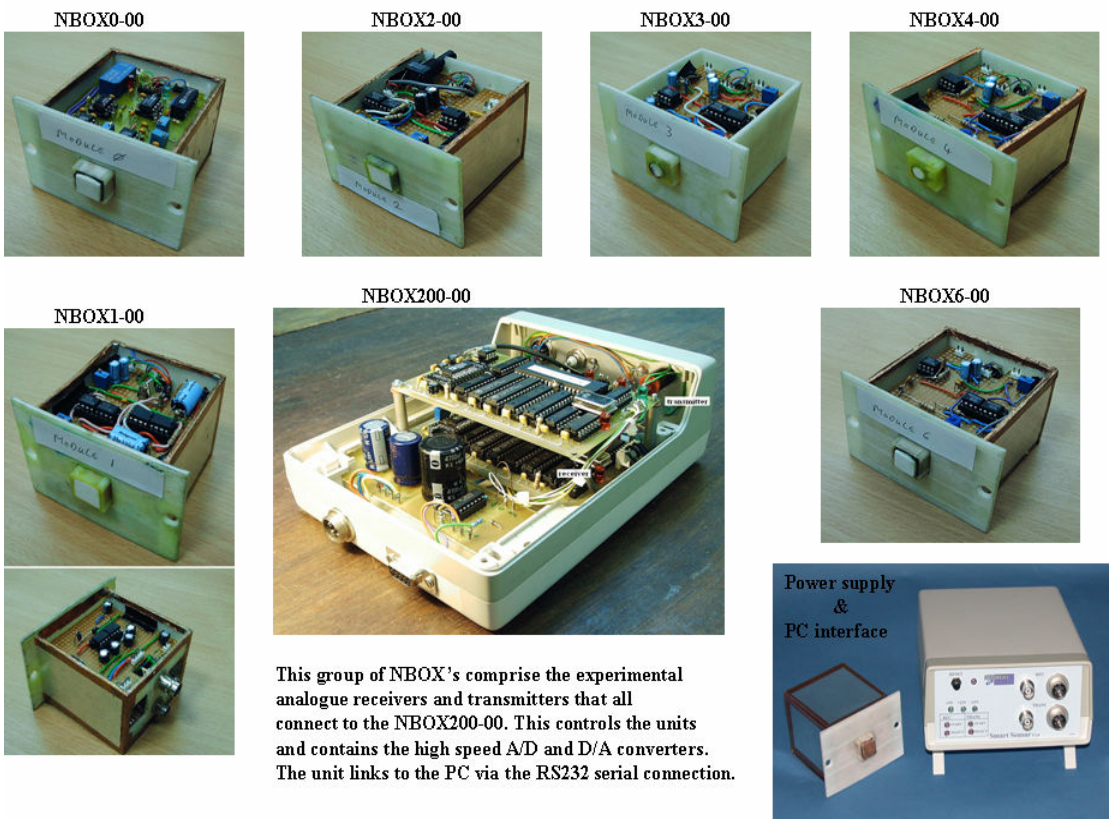

Figure 81 Schematics for NBOX analogue units

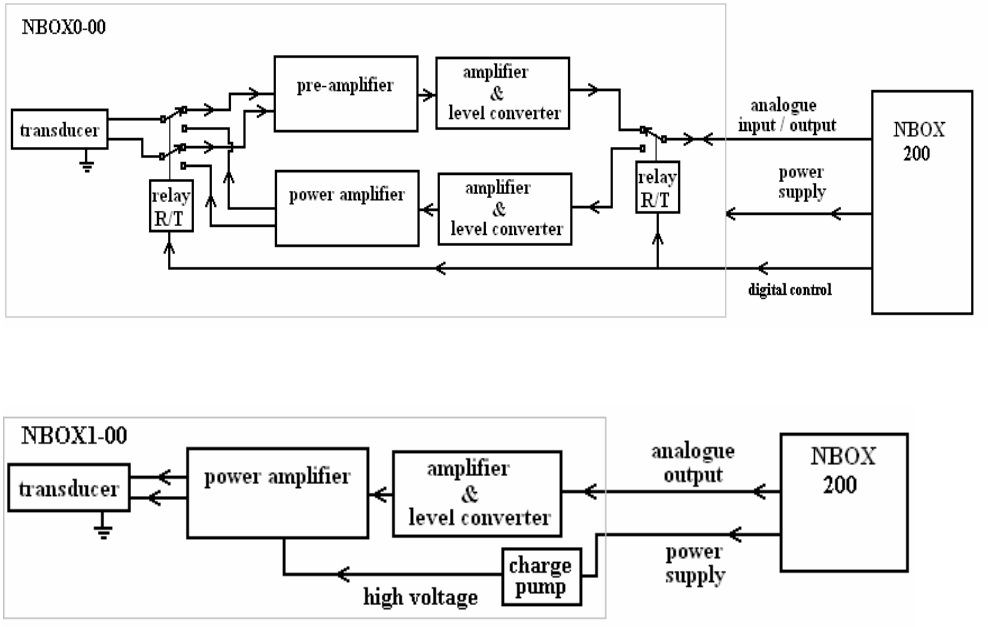

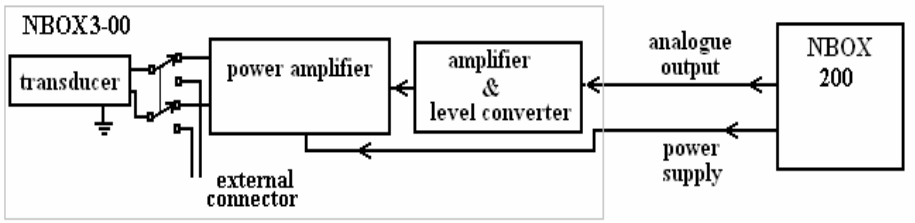

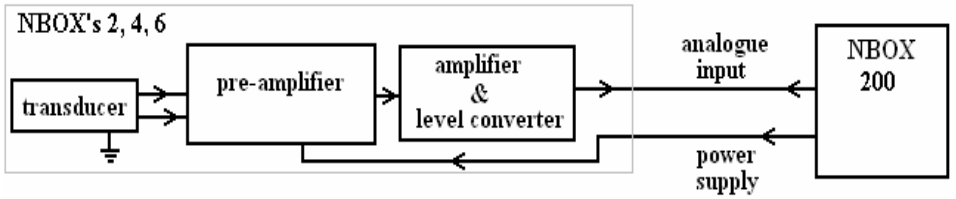

NBOX5-00

This module provides an actuator that transmits the sum of two sine waves ($F_1 + F_2$). In the presence of non-linearity this signal will be distorted and will generate harmonics and inter-modulation products (for details see Section 2.3). The NBOX contains all the analogue circuits plus digital control and communication to any other NBOX unit or to the PC. The photographs Figure 82 shows the unit and a schematic for the NBOX.

Figure 82 NBOX5 sine sum transmitter

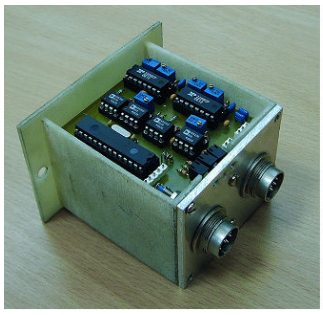

Microprocessor
Digital potentiometers
Waveform generators

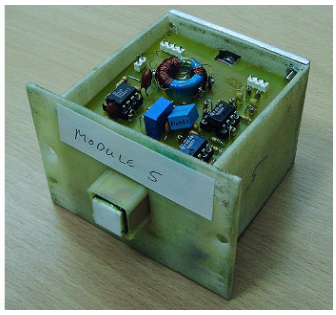

Analogue summer
Harmonic filters
Power amplifier

Power supply (+5V, +12V & -12V)
RS232 interface from NBOX to PC

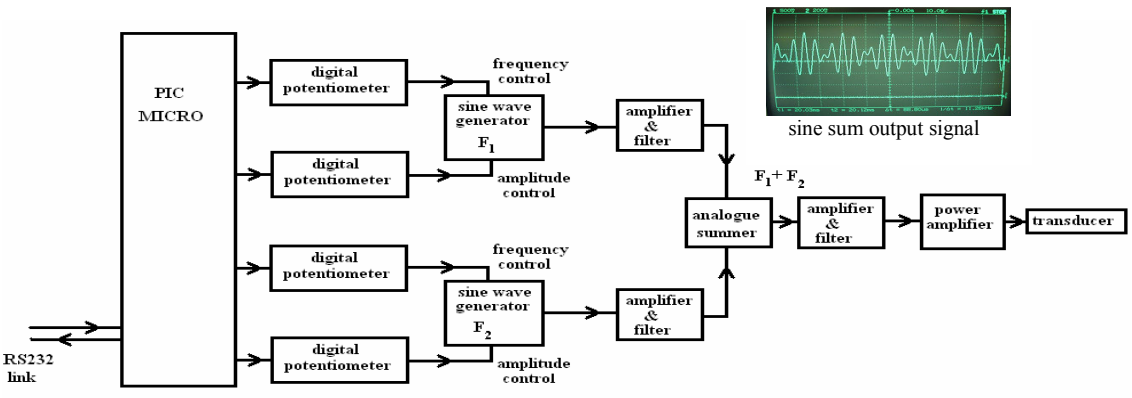

NBOX7-00

This module shown in Figure 83a and 83b provides a method to measure small changes in frequency independently of amplitude, within limits known as lock range. It is used to measure resonant frequency deviation, see chapter 2.4 for details of this method.

Figure 83a Photograph of NBOX7 frequency deviation meter

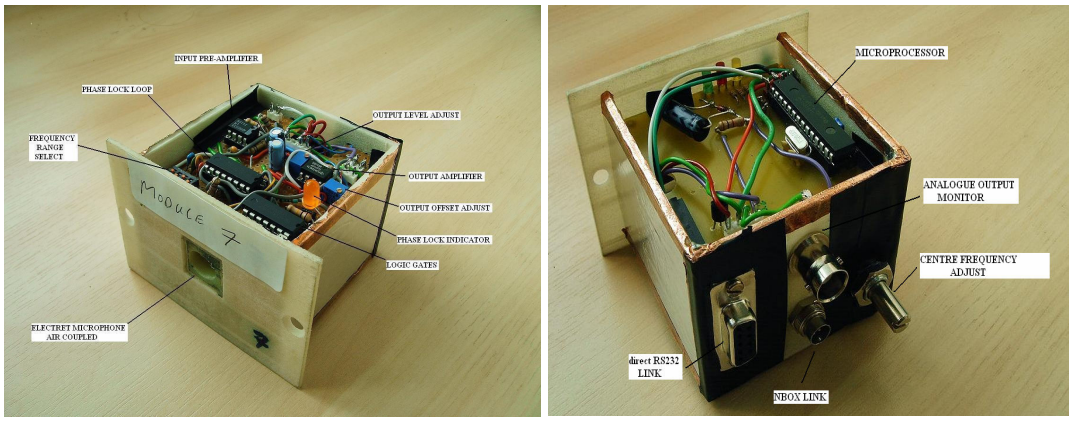

Figure 83a Schematic of NBOX7 frequency deviation meter

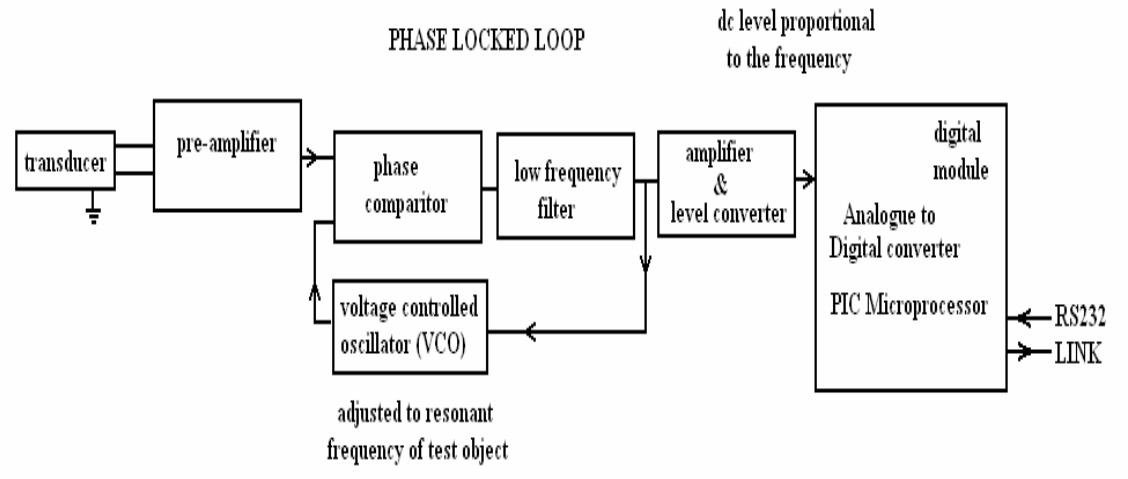

NBOX8-00

This module shown in Figure 84 provides a method to determine when an object is oscillating at its peak resonance using an optical laser interferometer.

Figure 84 NBOX8 Resonant peak detector

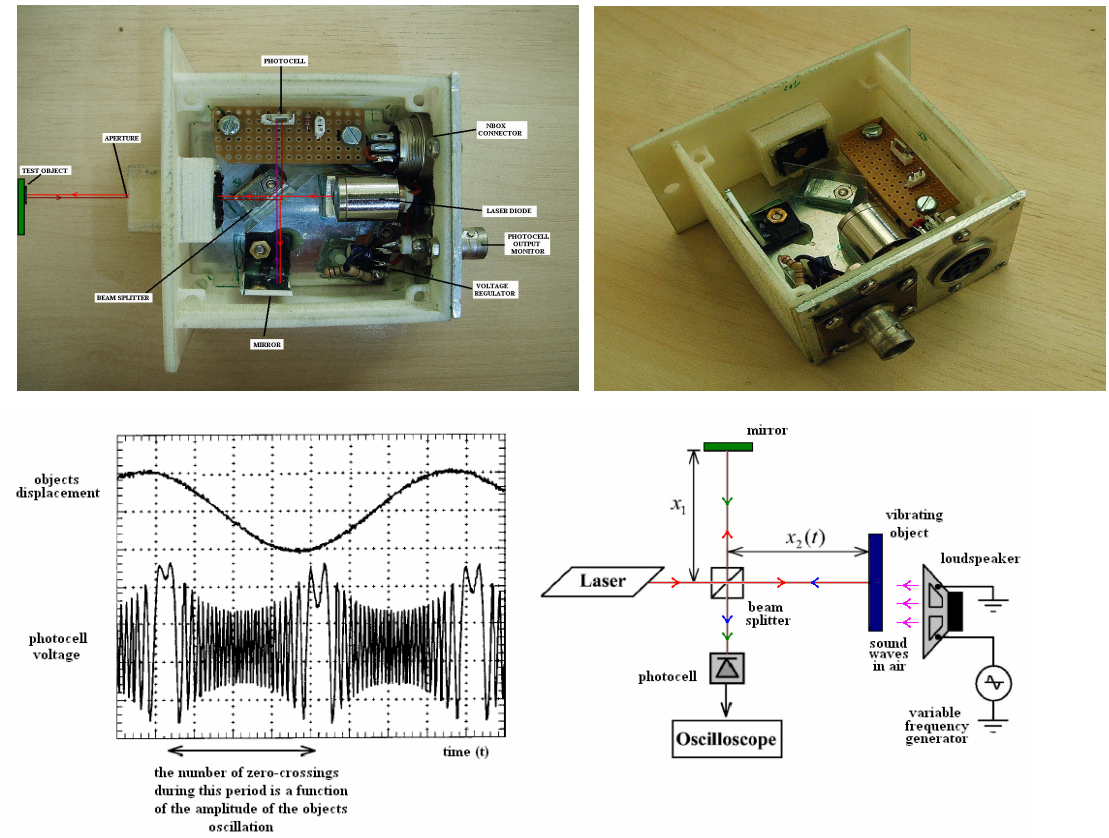

A loudspeaker sends sound waves through the air to the test object, the frequency of these sound waves is varied. The objects maximum amplitude of oscillation will occur at resonance. The point of peak oscillation is determined by counting the number of zero-crossings in the photocells output voltage and looking for a maximum value, this occurs only at the largest amplitude of oscillation. See chapter 2.4 for details of this method.

NBOX9-00

This module shown in Figure 85 provides a standard RS232 communication link to all NBOX's and the PC for command instructions, together with a high speed bi-directional synchronous data link and an event / clock line between all NBOX's and the PC. The module requires additional analogue circuitry to perform specific tasks and power supply converters to provide +/-12 or other application specific voltages

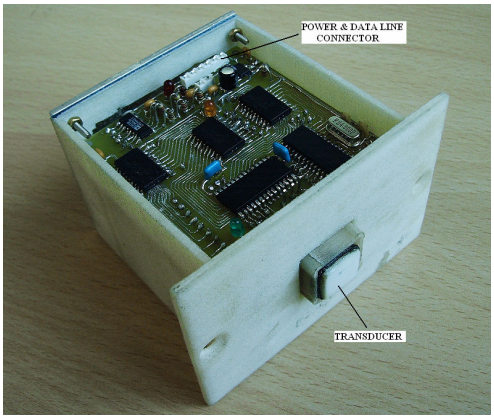

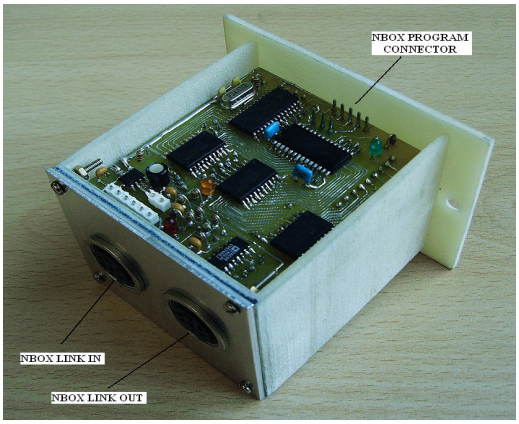

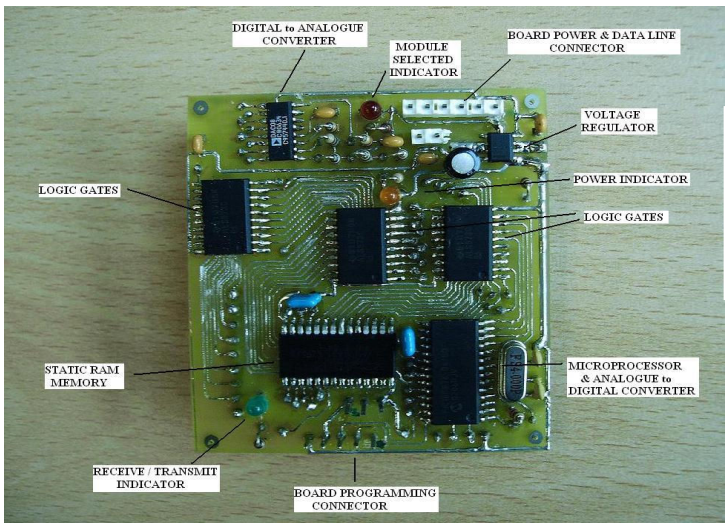

Figure 85

NBOX9

general purpose unit

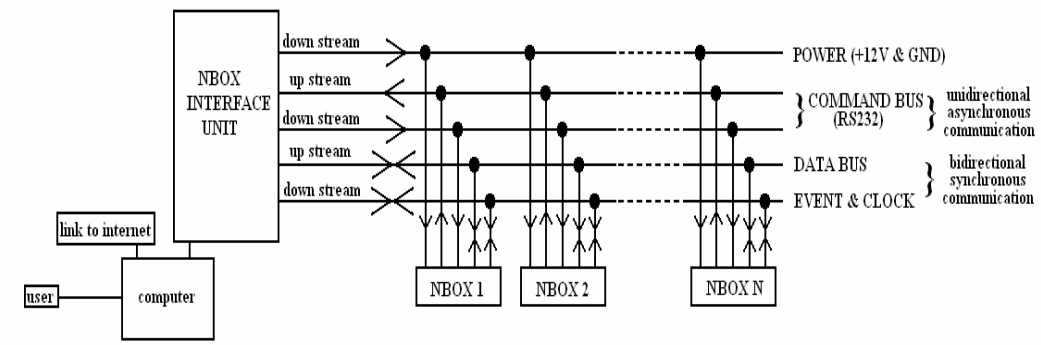

In support of NBOX9 there are two units, shown in Figure 86, one to power and interface the NBOX to a PC and the other a unit that plugs into the NBOX so that the microprocessor can be re-programmed. The interface unit provides bus monitors for RS232 IN, RS232 OUT, event / clock and serial data

Figure 86 NBOX ACCESSORIES

NBOX INTERFACE UNIT

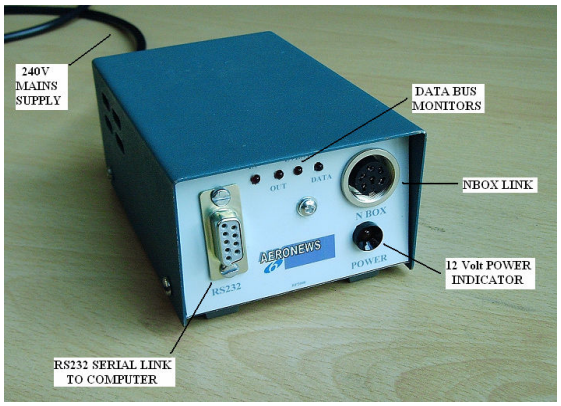

12 Volt 1 amp power supply
RS232 serial command line to PC

NBOX PROGRAMMER

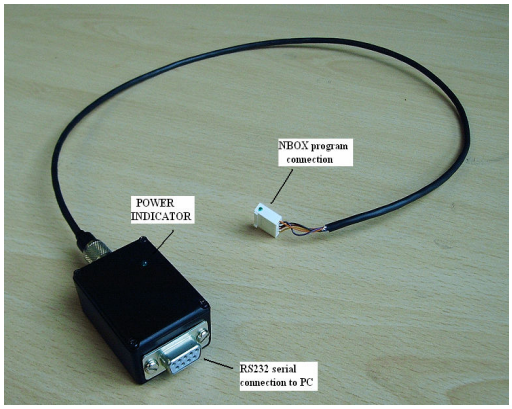

Provides direct access to programming and re-programming of the NBOX's PIC microprocessor.

NBOX10-00

This unit consists of a circuit board which provides an 8 bit analogue frequency variable sine wave signal to a power amplifier. This drives a loudspeaker that has been bolted onto the NBOX module, shown in the photographs of Figure 87. This is used as an actuator for the resonant frequency shift measurements.

Figure 87 Air coupled actuator

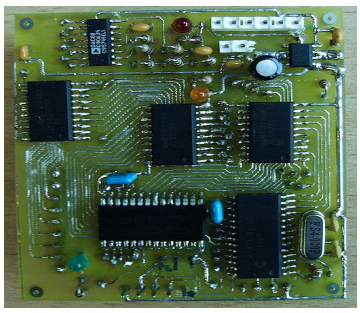

Microprocessor controller

D/A converter = 8 bits

Loudspeaker

Impedance = 8 ohm
Max power = 15 watts (peak)
Frequency range = 130-20KHz (-10dB)
Resonant frequency = 170Hz

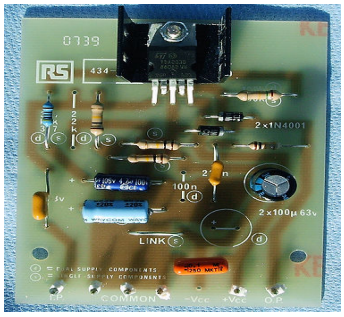

Power Amplifier (RS Components Ltd)

Supply voltage = 12 volts
Output power = 8 watts (8 ohm 40-15KHz)
Distortion (typ) = less than 0.2% (40-15KHz)
Bandwidth = 10 to 140KHz (-3dB)

NBOX100-00

This NBOX, shown in photographs of Figure 88 provides a general purpose unit to control high power actuators. Figure 89 gives the schematic for this unit.

Figure 88 NBOX100 Power controller unit

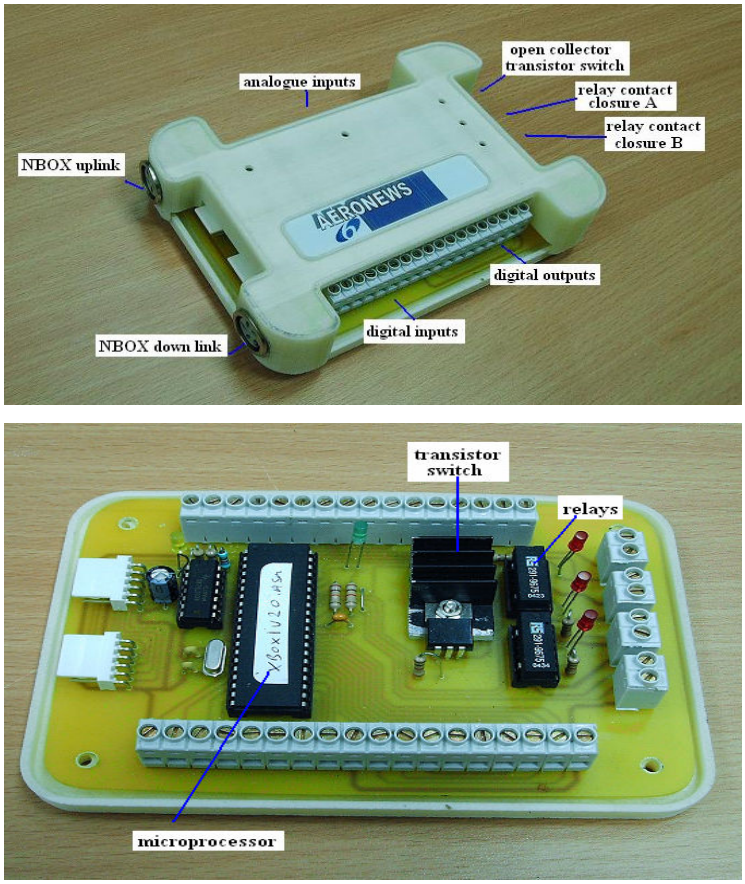

Figure 89 NBOX100 Schematic

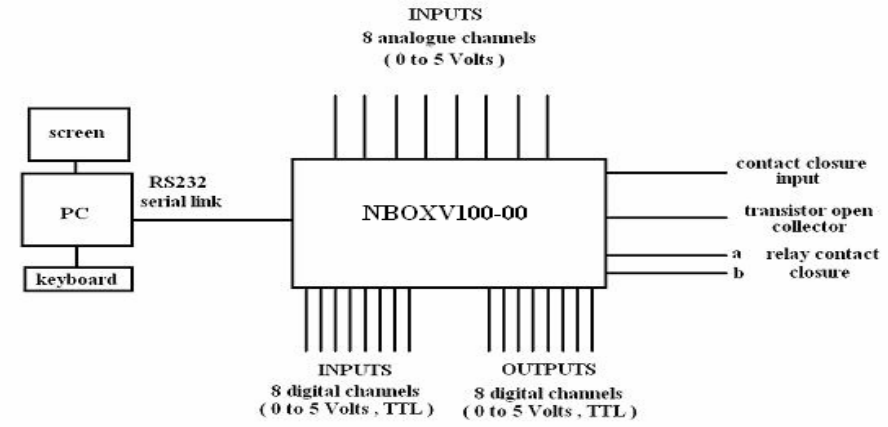

A summary of the roll and function of all the NBOX's designed and constructed as part of the work given in this thesis is given in tables 1 and 2 below.

Table 1 SUMMARY OF BASIC NBOX's

VERSION	FUNCTION	TRANSDUCER	FEATURES
NBOX0-00	Transceiver Suitable for low power harmonics & sidebands, pulse inversion, time reversal and resonant frequency measurement	PZT/epoxy composite Mounted in spring loaded carrier. Solid, liquid or gel coupling	Freq range = 10 to 600kHz Receiver = 4.7Mohm (differential input) Transmitter = +/-15volts switches between receiver and transmitter
NBOX1-00	Transmitter Suitable for medium power harmonics & sidebands and pulse inversion	PZT/epoxy composite Mounted in spring loaded carrier. Solid, liquid or gel coupling	Freq range = 10 to 500kHz Transmitter = +/- 48volts High voltage dual op-amp driver (differential) Charge pump supply voltage multiplier.
NBOX2-00	Receiver Suitable for most NEWS applications, particularly harmonics & sidebands, pulse inversion and resonant frequency measurement	PZT/epoxy composite Mounted in spring loaded carrier. Solid, liquid or gel coupling	Freq range = 10 to 600kHz Receiver = 100Kohms (single ended input) External gain control potentiometer
NBOX3-00	Transmitter Suitable for low power harmonics & sidebands	DAKEL IDK09 Piezoceramic Mounted in spring loaded carrier. Solid, liquid or gel coupling	Freq range = 10 to 600kHz Transmitter = +/- 10volts (op-amp direct drive) Switch for direct external connection to the transducer
NBOX4-00	Receiver Suitable for most NEWS applications, particularly harmonics & sidebands, pulse inversion and resonant frequency measurement	DAKEL IDK09 Piezoceramic Mounted in spring loaded carrier. Solid, liquid or gel coupling	Freq range = 10 to 600kHz Receiver = 10Mohms (single ended input) External gain control potentiometer
NBOX6-00	Receiver Suitable for most NEWS applications, particularly harmonics & sidebands, pulse inversion and resonant frequency measurement	PZT/epoxy composite Mounted in spring loaded carrier. Solid, liquid or gel coupling	Freq range = 10 to 600kHz Receiver = 10Mohms + 2pF (charge amplifier) Internal fixed gain
NBOX200-00	CONTROL UNIT FOR ANALOGUE NBOX's	Any of the NBOX's listed above can be connected to this unit (both receivers and transmitters)	12 bit A/D converter 14 bit D/A converter 32K x 16 bit SRAM memory Sampling to 0.1 microsec Microprocessor control and communication

Table 2 SUMMARY OF ADVANCED NBOX's

VERSION	FUNCTION	TRANSDUCER	FEATURES
NBOX5-00	Transmitter (dual frequency) Suitable for medium power harmonics and sidebands	PZT/epoxy composite Mounted in spring loaded carrier. Solid, liquid or gel coupling	Dual frequency transmitter (sine wave sum, F_1+F_2) Freq range = 40 to 300kHz Default = 184 & 240 kHz Microprocessor control and communication, two frequency generators with remote control of amplitude and frequency. Transmitter = +/- 50volts
NBOX7-00	Receiver (phase locked loop frequency meter) Suitable for resonant frequency shift measurements	Electret microphone Mounted in fixed carrier Air coupled	Freq range = 10Hz to 10kHz Resolution = 0.1 Hz (2kHz) Manual center frequency adjust by potentiometer. Microprocessor control, communication and A/D conversion.
NBOX8-00	Transceiver (laser interferometer) Suitable only for determining the point of resonance of a test object	Laser diode and photocell Spherical aperture in mounted fix carrier No coupling	Freq range = 2kHz Output signal 0 to 5V Zero crossings counted to determine amplitude of oscillation
NBOX9-00	Transceiver circuit board Suitable for low frequency NEWS applications, harmonics & sidebands, time reversal, pulse inversion and resonant frequency measurement	With additional hardware a wide range of sensors and actuators can be used with this module, mounted in spring loaded of fixed carriers. All types of coupling	Features:- 8 bit D/A 10bit A/D (50Ksps) 8 bit digital I/O 64Kx 8bit SRAM memory Microprocessor control and RS232 communications
NBOX10-00	Transmitter	Loudspeaker Mounted to NBOX structure. Air coupled	Freq range = 40 Hz to 14kHz Power = 8 watts Distortion = < 0.2%
NBOX100-00	GENERAL PURPOSE CONTROL UNIT	A wide range of sensors and actuators can be interfaced into this unit	Features :- 8 analogue input channels 8 digital inputs 8 digital outputs 2 relay contact closures 1 transistor switch 1 event input channel Microprocessor control and RS232 communications

5.3 APPLICATION and CONFIGURATION

The application of the NBOX's to a specific non-linear acoustic testing technique is determined by the procedural graphs shown in Figure 90. The actual configurations to perform these tests are given in Figure 91 below.

Figure 90 NBOX application flow chart

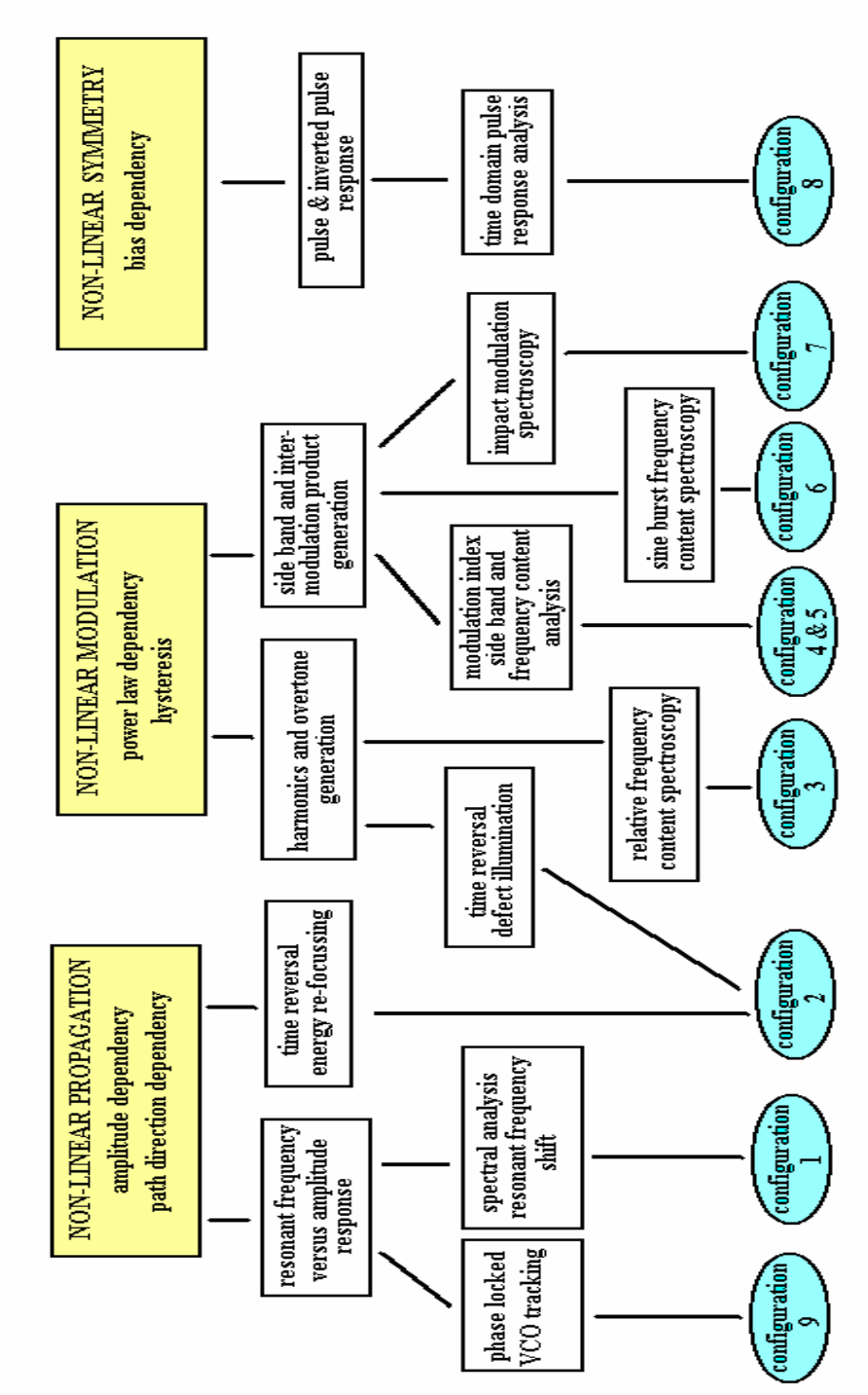

Figure 91 NBOX configuration

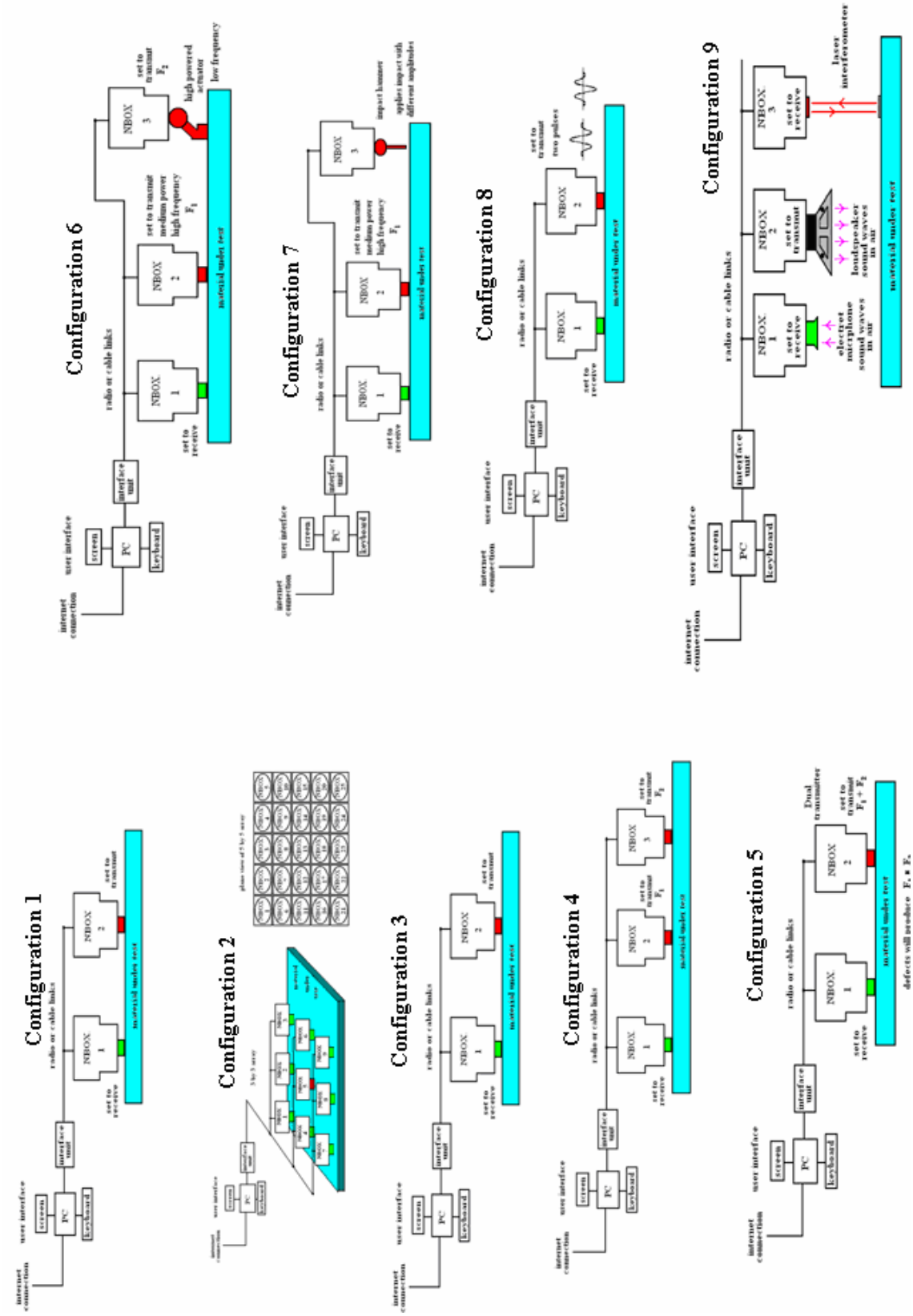

5.4 COMMUNICATION

Having decided upon the non-linear acoustic technique to use in a particular application and determined the NBOX configuration the next stage is to determine the optimum means by which the NBOX's can communicate with each other and to the PC.
This section outlines the communication methods that have been devised by the author and are currently used by the NBOX's. In addition this section provides some examples of communication links used by commercially available SMART transducers.
IEEE 1451 is a standard used by many SMART devices and details of this standard are given in appendix D.

In general there are four common types of data transfer:-

1) Control transfers: Short data packets for device control and configuration.
2) Bulk transfers: Large quantities of data packets
3) Interrupt transfers: Data packets that are polled periodically.
4) Isochronous transfers: These are continuous real time data streams.

The NBOX modules are designed only to take samples of data and use Control transfers, Bulk transfers and Interrupt transfers. For real time continuous monitoring systems Isochronous transfers will be required, but the NBOX's are not designed for this type of operation and such transfers are not included in this thesis. Within this project an investigation was made into the types of data communication that are generally required, for this project these were limited to either wire links or radio. The following section provides details on these two types of medium.

Cable connections

The simplest and most reliable means to connect the NBOX's is via a common bus cable. In all applications that involve low power testing of small detached components in a laboratory or at a test site, short cable length to the PC and the NBOX's will be sufficient. In situations that require testing large component structures such as wing or fuselage sections using roving transducers and high power actuators, such as "shakers" then long cables may still be used but may prove to be difficult and wireless radio links may have an advantage. The following section initially outlines the cable configurations

that have been used or investigated. Figures 92 to 96 show the various cable connections together with their advantages and disadvantages.

Figure 92 Wire link for NBOX's 5, 7, 100 and 200

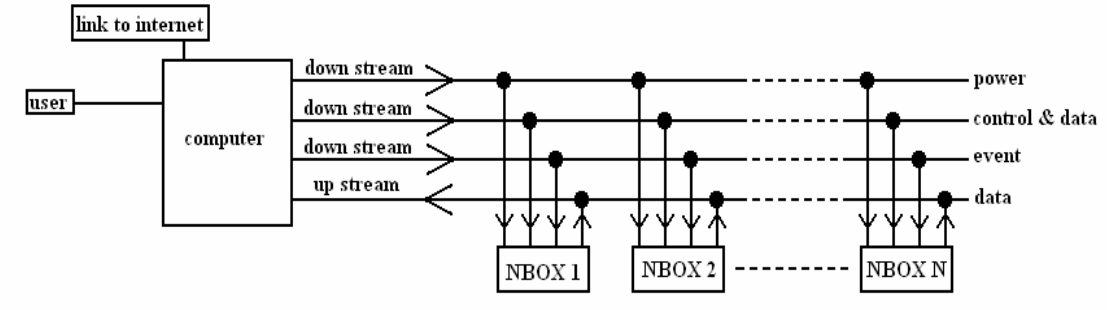

Advantages:- Hardware is simple, little switching is required since lines are either transmitting or receiving data from the single host. Efficiency of data transfer is high, since two lines are used to send and receive data.

Disadvantages:- Having a shared control and data line introduces the probability that data streams may contain a series of digits that can be interpreted as a command instruction, unless suitable precautionary measures are taken, such as ensuring data bit patterns are different from command instructions (for example the most significant bit is zero for all data) or having a lengthy addressing code to access a particular module before a command instruction is sent. Both these techniques will introduce redundancy into the system, reducing the data rates.

Figure 93 Reduced wire version

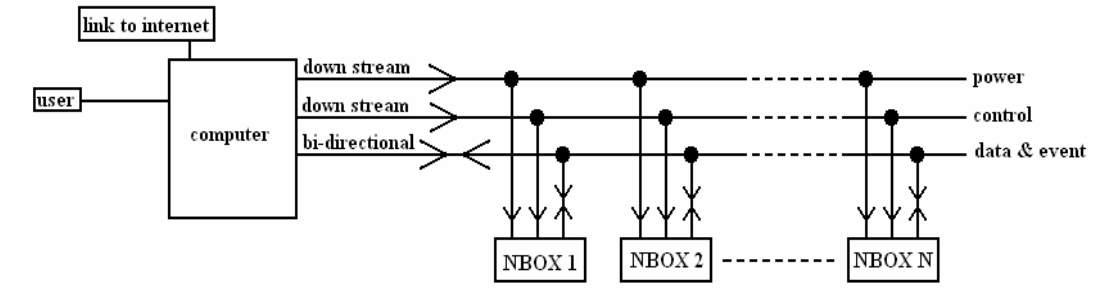

Advantages:- The data is totally separated from the command line, thereby removing the problem of commands being misinterpreted from the data streams.

Disadvantages:-Greater circuit complexity is required in having bi-directional lines.

Figure 94 Single wire SMART transducer linking

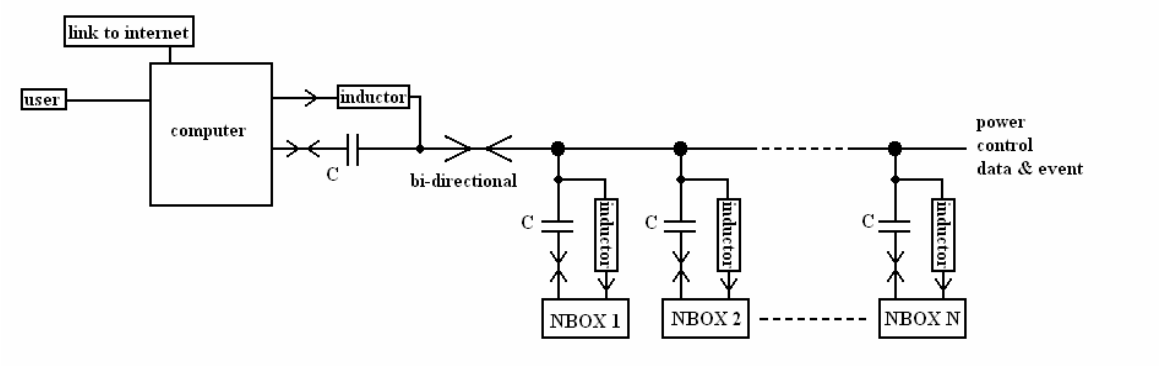

This version of connection is used currently in many SMART sensor applications.

Advantages:- Single wire connectivity ideal for large distributed systems. Much cheaper and simpler to install, ideal for embedded SMART transducers. Readily converted to wireless radio links, however the power would have to be locally sourced at each NBOX.

Disadvantages:- Greater circuit complexity is required in having bi-directional lines and in the separation of the power from the digital information lines.

Figure 95 USB linking

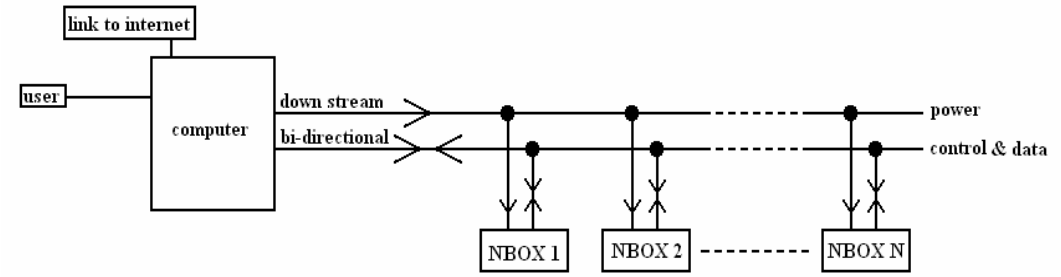

A common method to interconnect devices, four copper wires are used, two for the power (5Volts, 500mA max), and two for the single bi-directional data link (wired as differential pair).

Advantages:- A well established communication standard. Readily converted to wireless radio communication links, as there is substantial commercial development in this area, however power would have to be locally sourced at each NBOX.

Disadvantages:- Single host only. Need to ensure data and commands are not misinterpreted. Limited power supply capability.

Figure 96 Communication links for NBOX9

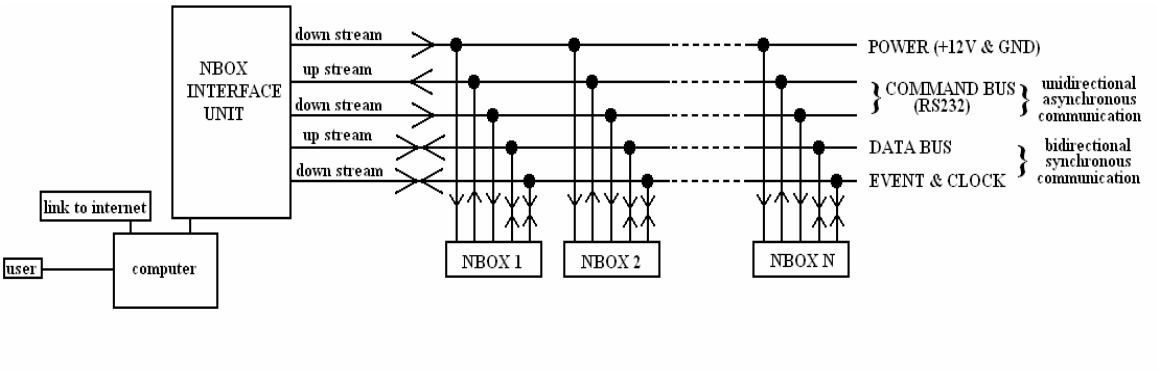

Advantages:- Separate command and data lines, no possibility of data causing command triggers. Efficiency of data transfer is high as multiple lines are used.
Disadvantages:- Greater circuit complexity is required in having bi-directional lines. More wire interconnections are required.

Wireless connections

The photograph of Figure 97 below shows the different wireless communication modules that the author investigated during the research period. Table 3 gives a summary of these radio modules specifications.

Figure 97

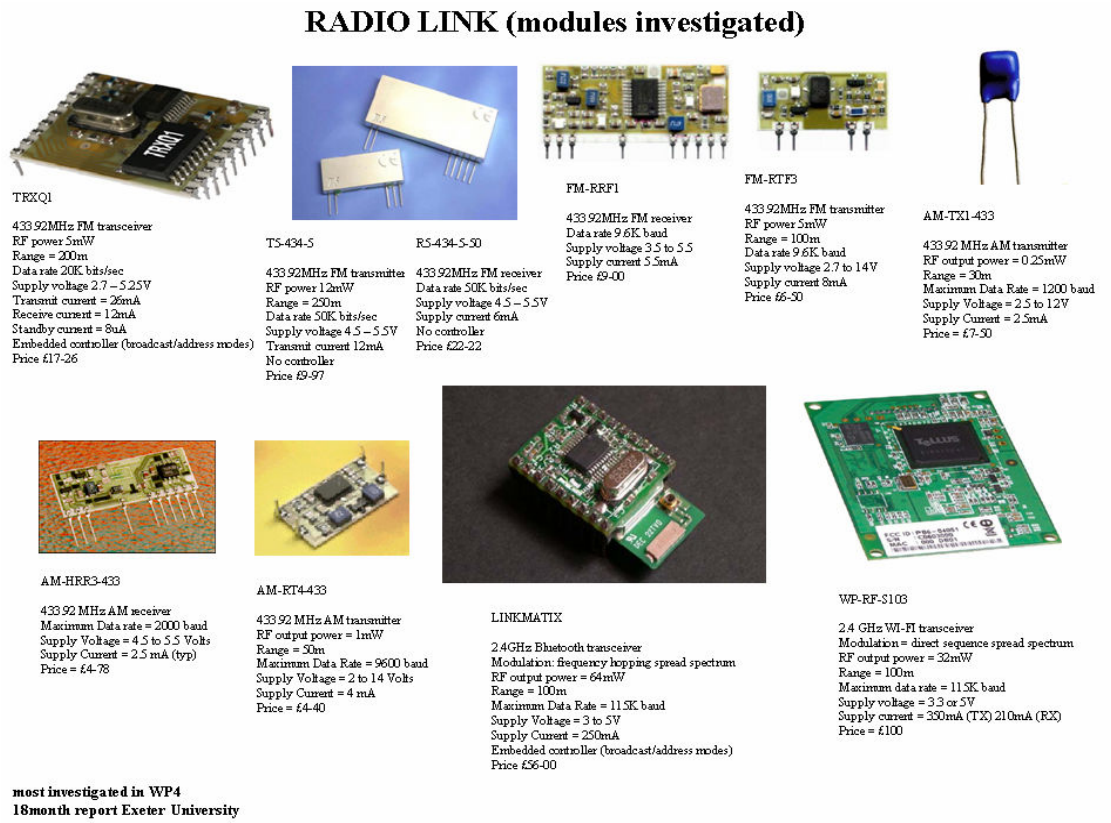

Table 3 A summary of radio module specifications

RADIO MODULE	FREQUENCY (MHz)	(modulation)	MAX DATA RATE (bits/sec)	TRANSMIT POWER (mW)	(range m)*	SUPPLY REQUIREMENTS (volts)	(mA)
TRXQ1 (transceiver)	433	(FM)	20K	5	(250m)*	2.7 to 5.25	26 (TX) 12 (RX)
T5-434-5 (transmitter)	433	(FM)	50K	12	(500m)*	4.5 to 5.5	12 (TX)
R5-434-5-50 (receiver)	433	(FM)	50K	-		4.5 to 5.5	6(RX)
FM-RRF1 (receiver)	433	(FM)	9.6K	-		3.5 to 5.5	5.5 (RX)
FM-RTF3 (transmitter)	433	(FM)	9.6K	5	(250m)*	2.7 to 14	8 (TX)
AM-TX1-433 (transmitter)	433	(AM)	1.2K	0.25	(10m)*	2.5 to 12	2.5 (TX)
AM-HRR3-433 (receiver)	433	(AM)	2.0K	-		4.5 to 5.5	2.5 (RX)
AM-RT4-433 (transmitter)	433	(AM)	9.6K	1.0	(100m) *	2 to 14	4 (TX)
LINKMATIX (transceiver)	2400	(FHSS) Bluetooth	115K	64	(500m)*	3 to 5	250 (TX) 60 (RX)
WP-RF-S103 (transceiver)	2400	(DSSS) WI-FI	115K	32	(200m)*	3.3 or 5	350 (TX) 210 (RX)
EASYBEE (transceiver)	2400	(DSSS) ZIGBEE	250K	1	(50m)*	2.1 to 3.6	18 (TX) 20 (RX)

FHSS = Frequency Hopping Spread Spectrum
DSSS = Direct Sequence Spread Spectrum
FM = Frequency modulation
AM = Amplitude modulation

TX = Transmit
RX = Receive

The range of these devices is difficult to quantify exactly as it depends on the carrier frequency, type of modulation, data rate, receiver sensitivity, antenna and the terrain over which it is operated. The values are quoted as typical ranges for operation in open terrain using a ¼ wave whip antenna. The operating frequencies of the most common low power radio modules for digital or analogue data links were compiled from various national and international radio spectrum standards by the author and are given in Figure 98 below. Birnie [38] gives further details of the operation and functions of low power radio communication systems.

Figure 98 common low power radio band allocations

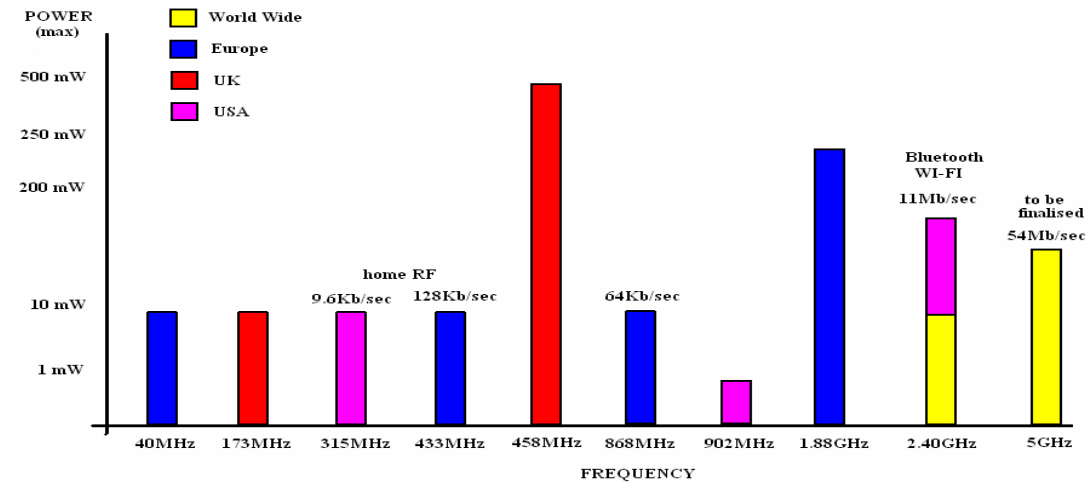

The objective of this investigation within this project was to gain an understanding of the performance and practical limitations of these devices and examine their potential application in non-linear acoustic testing instrumentation. The conclusions drawn by the author are that the only realistic solution for radio wireless links is to use the world wide allocated 2400 MHz radio band, this would involve using WI-FI, Bluetooth or Zigbee devices conforming to the IEEE 802.11 standard (see appendix E). These devices have the additional advantage that they use frequency hopping or spread spectrum modulation which are very robust when used in noisy environments, they also support data whitening, cyclic redundancy checking (CRC), automatic repeat request (ARQ) and forward error correction (FEC) as standard, thereby providing a secure wireless radio link. The findings of the author were that in some applications such as the civil aircraft industry the strict regulations concerning radio transmissions within and near aircraft places limitations on where radio linked equipment can be operated. For example, currently Boeing quote the maximum electromagnetic field strength at these frequencies to be 107dB μV/m, or 1mW at 1m distance, the output power of most modules greatly exceeds this value. Appendix F gives a summary of the relationship between RF power and electromagnetic field strength.

5.5 OPERATIONAL SOFTWARE

A commercial non-linear acoustic testing system will require three levels of operation; a low level for the unskilled operator that wishes to determine a good-bad indication of the condition of a test object. A medium level where a semi-skilled operator wishes to have a clearer indication as to the levels of damage, and a high level where a skilled operator may wish to analyse the data in detail.

Low level:- This requires considerable prior knowledge of the indicators and the types of defects that can occur in different materials. It will require advanced automatic data processing which will have to provide accurate interpretations, utilising for example expert system software and neural networks. The operator will be expected just to record a good / bad condition. In some operational scenarios false indications will result.

Medium level:- This requires some prior knowledge of fault indicators, it will require some data processing. The form of display is important and must be suitable for semi-skilled interpretation, such as spectral plots, frequency deviation plots and pulse inversion plots with fault level indicators. The operator is expected to view and record the raw data files and provide a report on a basic analysis of the data. In some situations the operator may need to refer this data analysis to an expert for greater scrutiny.

High level:- This would require a highly trained expert in the field of non-linear acoustics. Interpretations will be made primarily on the raw data and may require further data processing by specialist software. The operator will be expected to record, view analyse and fully interpret the data.

The software presented in this thesis is aimed at the high level expert operator.
The main data acquisition and display software running on the PC for use with NBOX200 was written by the author in the JAVA computer language. The software running on the NBOX microprocessors was written by the author in assembly language and compiled to machine code.
The main display software window is shown in Figure 99a. On program start up a DOS window is first initiated and displays a series of initial tests applied to the NBOX. If start up is successful the graphic display overlays the DOS window. During operation the DOS window is updated with the current instructions sent to and received from the NBOX, this window can be examined at any time if required to debug should any faults arise.
First a decision is made as to the type of waveform that is to be transmitted. This is selected from a list. When the selection is made a set of drop down list boxes are produced that are particular to the waveform required, such as frequency and duration. The View waveform button is clicked to examine the wave form and further changes may be made if needed. When the desired waveform is selected and displayed it can be loaded in to the NBOX's transmitter memory, this is achieved by clicking on the Load waveform button. After a short while the required transmission wave form is loaded permanently into memory. Transmission of this waveform can be initiated as many times as required. The memory contents can be overwritten at any time by loading a new waveform. To simultaneously transmit and receive data the Sample button is clicked. The synchronisation, or sampling skew, between the transmitted signal and the

received data is within a few nano-seconds; this is insignificant compared to the sampling time of 0.1 micro-seconds and is a factor that gives this system significant advantage over other data acquisition and recording systems. The sampled received data is stored in the receiver NBOX's memory then sent via the serial link to the PC. Here the first 80 micro-seconds of data is displayed and can be saved to a file. The total data length is just over 100 micro-seconds (1024 data samples), the frequency spectrum is also displayed on the screen and the relative amplitude scale is selected by a check box, either linear or logarithmic. Data windowing can also be applied to the data to improve the display of the power spectrum, as outlined in the next section. The Appendix I gives flow chart function and timing diagrams for this operational software.

Figure 99a Main data acquisition and display software

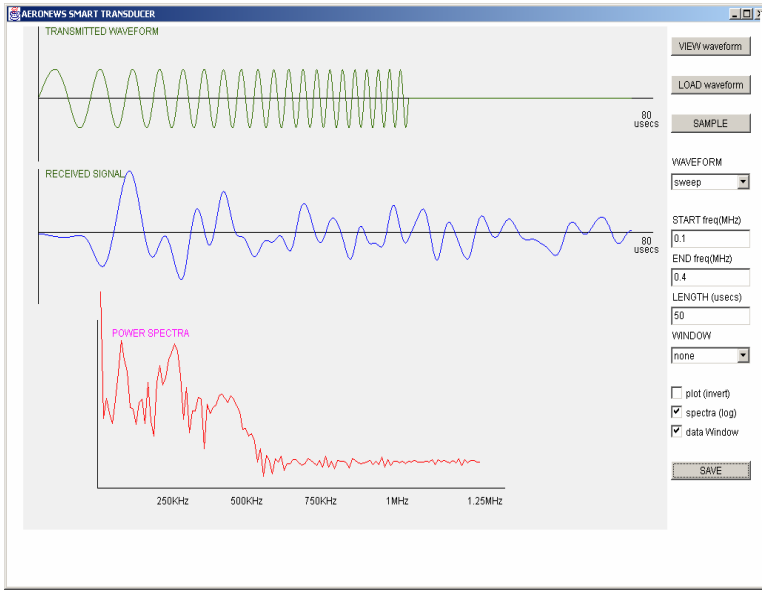

View waveform:- display the selected waveform

Load waveform:- loads the wave form into the NBOX memory

Sample:- triggers and transmission and records the data

waveform selections:-
Continuous (sine wave)
Burst (sine wave)
Sweep (sine chirp)
Sine wave Sum (f_1+f_2)
Pulse inversion
+ve pulse
-ve pulse

Save:- saves the current data to a file

Data windowing for spectral analysis

For the experimental work carried in this research program the spectral analysis consisted of measurements taken from graphical plots of the recorded data using the MathCad software tool. An example of the raw data from one of the experiments is given in Figure 99b and was plotted from a recording of 1024 samples.

Figure 99b Example of raw recorded data

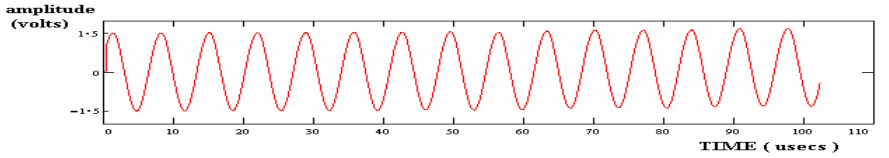

The frequency power spectrum for this data is shown in Figure 99c in black. It has been computed by the use of a Fast Fourier transform (FFT). In practice, and as can be observed in this data the sampled waveform does not contain an exact whole number of waveform cycles. The Fourier transform evaluates this waveform with end point errors and this generates a power spectrum containing false frequency components. The effect of this is to spread out the distinct frequency components (so-called 'leakage').
To overcome this problem a window function was applied to all the data recordings, for all the experiments both in the MathCad programs and in the display software. Figure 99c shows the improvement given when a Bartlett and a Hamming window were applied. The Hamming window was preferred as this produces less "ringing" in the spectral values. The side lobe signal levels generated when using this window are all below -43 dB. This is sufficiently low in comparison with the harmonic levels generated by a damaged material. (Note that the material is considered to be good when the second and third harmonics are below -40 dB (1%) of the value of the fundamental.
The disadvantage of using a window is they will "broaden" the spectral peaks, for a Hamming window this is only 1.5 times the un-windowed spectra and is not considered a problem. See Appendix G for details on the various window functions that can be applied to improve spectral analysis.

Figure 99c Power spectrum with windowing

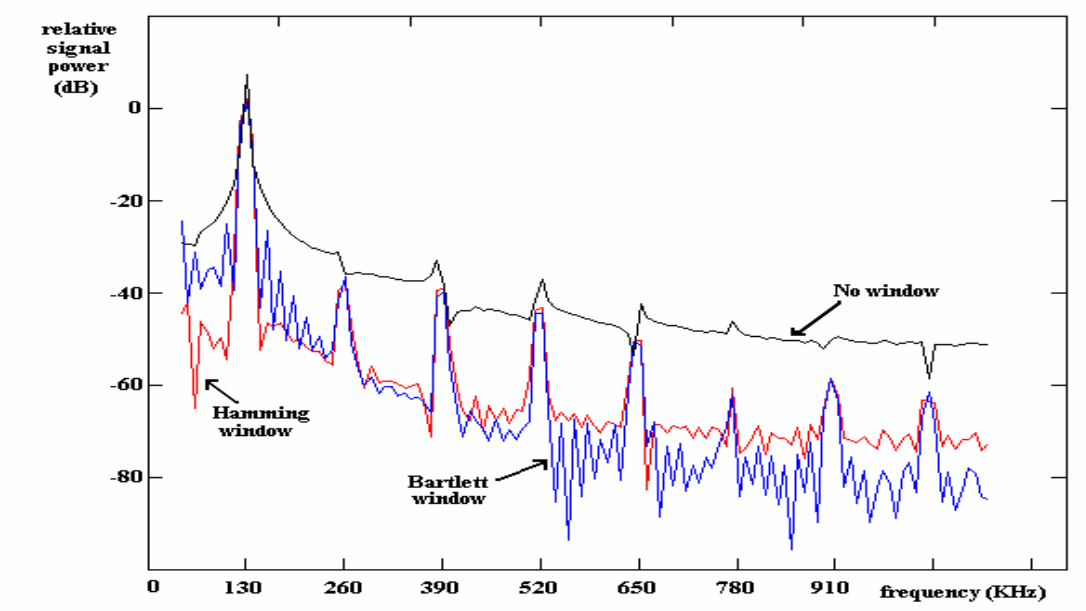

Pulse inversion display software

The main software is used to send both the positive and the negative pulses which are recorded as two separate files. The pulse inversion play back software shown in Figure 100 is used to read back the data files and display them together with the sum of the two waveforms. The software is then able to save this summed waveform for later analysis.

Figure 100 Pulse inversion display software

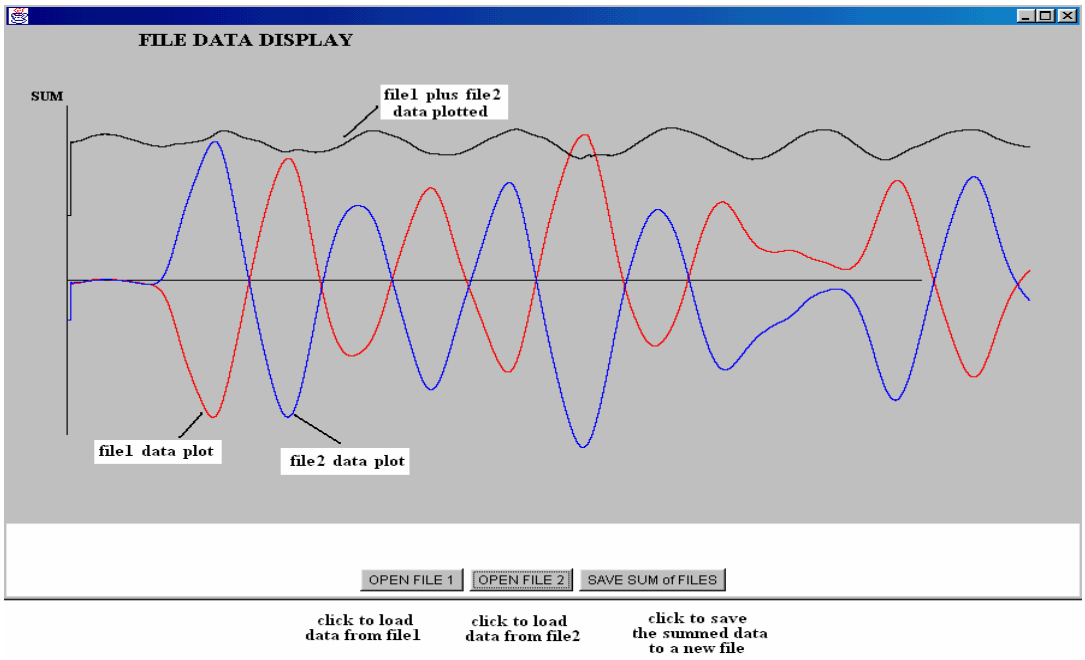

Frequency deviation display software

This software functions in real time, and is used in conjunction with NBOX7.
The object under test is brought to resonant oscillation by application of an external audio source (loudspeaker). The start button is clicked and the display starts slowly plotting in blue. The blue line's position is then adjusted using the control knob on the NBOX unit until it is about centre screen. The red cursor line is then shifted up or down using the on screen slider bar. The red cursor is made level with the blue line being plotted. The audio source is then switched off and the blue line observed as the oscillations decay. Movement of the blue line above or below the fixed red line indicated a very small change in frequency. Figure 101a, shows an example when a frequency generator is applied to the input of the NBOX. A shift up and down of 5 Hz

from a 600 Hz signal is clearly indicated. When the signal level is slowly decreased eventually the device loses lock and the display run's off the screen, as shown at the end of the trace. The SAVE button is used to record the trace and the CLEAR button is used to start another screen plot. Figure 101b shows the actual plot for an object under test. Further details of this experimental technique are given in section 6.2.4.

Figure 101a Frequency deviation display software

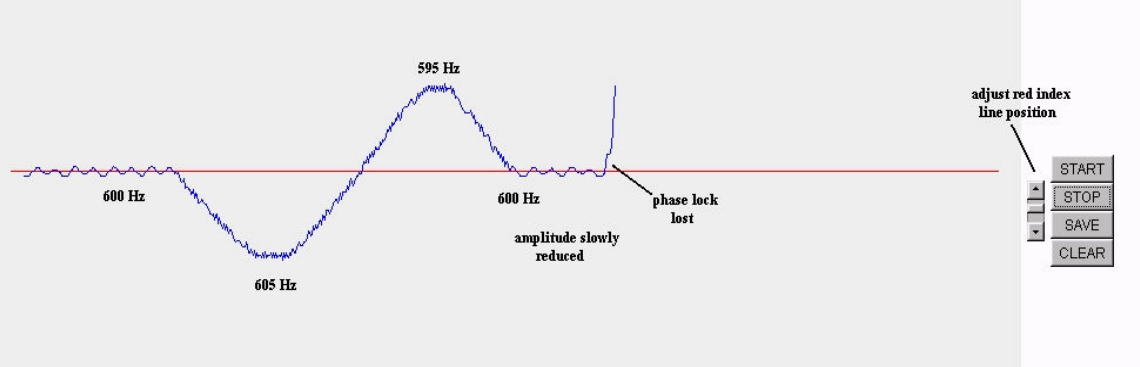

Figure 101b experimental frequency deviation plot

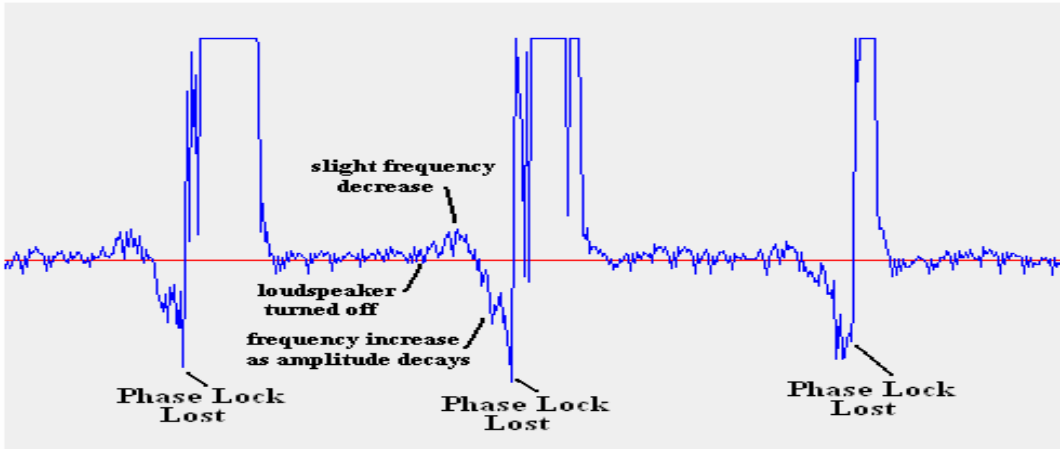

From the development of new instrumentation, outlined in this chapter, it is has been shown that it is possible to assemble a system by selecting an appropriate combination of NBOX's and connecting these together for a particular type of test object and testing methodology. The next chapter details various experiments that were performed to test the operation of both the transducers and instrumentation, and to test the validity of the non-linear acoustic methodology in detecting defects in test samples.

6 EXPERIMENTAL VALIDATION

Three main development tests were conducted by the author as part of a team, one at University of Exeter and the other two at VZLU in Prague, Czech Republic. These tests involved using many different techniques on large scale objects, principally concerned with the aircraft industry. This thesis gives the results of the contribution made by the author to this test development work. A series of smaller scale experimental validation tests were also performed by the author at the University of Exeter and are detailed in this chapter and involved various non-linear ultrasonic testing techniques on a wide range of materials.

6.1 Objectives of the experimental work

The objective of the experimental work was to examine a large variety of non-linear acoustic testing methods, materials and types of damage. The experimental data provided a means to be able to assess the applicability of the non-linear nondestructive acoustic testing techniques. Aspects of the experimental investigation were:-

1) Object to be tested (structure, geometry and composition).
2) Material to be tested (metal, plastic or composite)
3) Nature of the failure to be detected (micro-cracking and de-laminations)
4) Excitation strategy (acoustic waveform type, power and frequency)
5) Threshold of detect ability (base noise and lower limit of measurable distortion)
6) Equipment requirements (oscillators, power amplifiers, computers, NBOX's)
7) Transducer placement (coupling, location, separation)
8) Variables that effect measurement (signal max & min level, frequency, power)
9) Calibration techniques (comparison with good / defective components)
10) Measurement conditions (ambient acoustic and electrical noise)
11) Analysis of results (algorithms, display techniques).

6.2 Tests on selected aircraft components

Within the project a number of test objects and types of damage were investigated. A summary of these defects and the tests that were applied by the author are given in the flow graph plot Figure 102.

FIGURE 102 Objects, types of damage and testing methodology

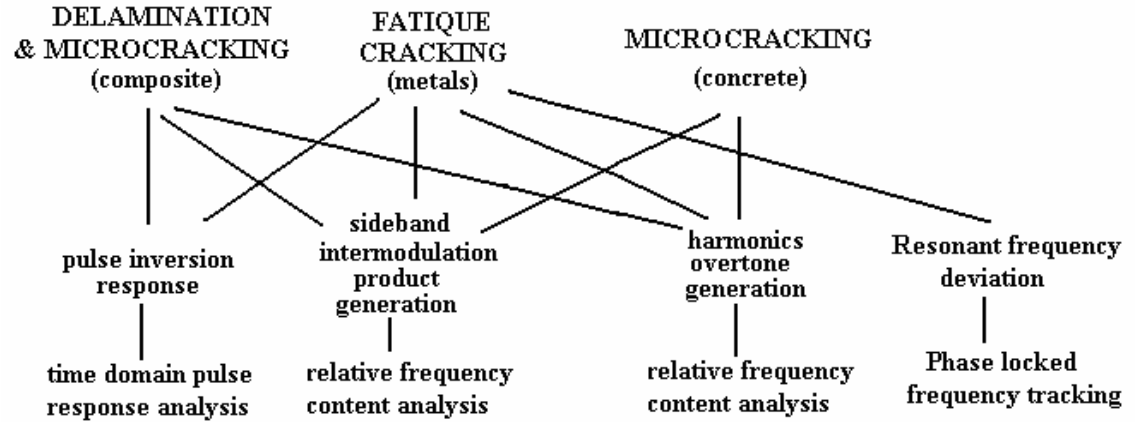

Sections 6.2.1 to 6.2.5 detail the aircraft components that were selected for examination. For each of these components the type of defect, the testing procedure applied and the results are given. Sections 6.2.6 and 6.2.7 detail tests on steel rail and concrete.

6.2.1 Aluminium wing panel

This object was a riveted structure made of Aluminium, simulating part of a real wing and consisted of a skin, five stringers, model of a rib, two doublers with 3 mm diameter rivets, all manufactured by VZLU. An artificial notch, created by spark erosion, was drilled into the panel, in order to initiate the formation of a crack. A photograph and schematic of the test panel is shown in Figure 103.

Figure 103 Aluminium wing test panel

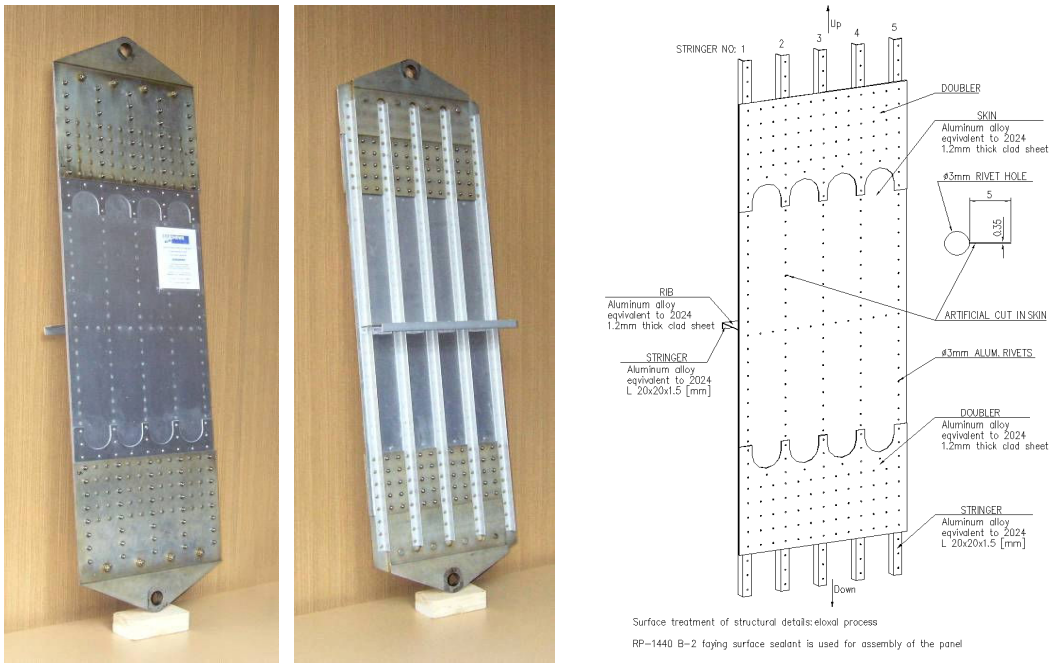

Fatigue testing was performed on the panel using a Schenck 250 kN load frame, shown in Figure 104 below. The wing panel was equipped with steel fittings at both ends. These fittings were joined through spherical hinges as the joints were out of the plane of elasticity of the panel, causing additional bending moments during tensile loading. In this way a real stress distribution on a wing's lower side was simulated. During all cyclic fatigue loading, the applied force was held at 53.7 kN and initially the frequency was 3 Hz, increasing to 3.2 Hz from 10 000 to 26 500 cycles. Strain gauge measurements showed that the loading stress was 71 - 80 MPa in the skin.

The crack length was measured by a visual method and validated by eddy-current testing. Crack activity was also monitored by acoustic emission and hi-frequency ultrasound.

Figure 104 Test panel and Fatigue testing apparatus

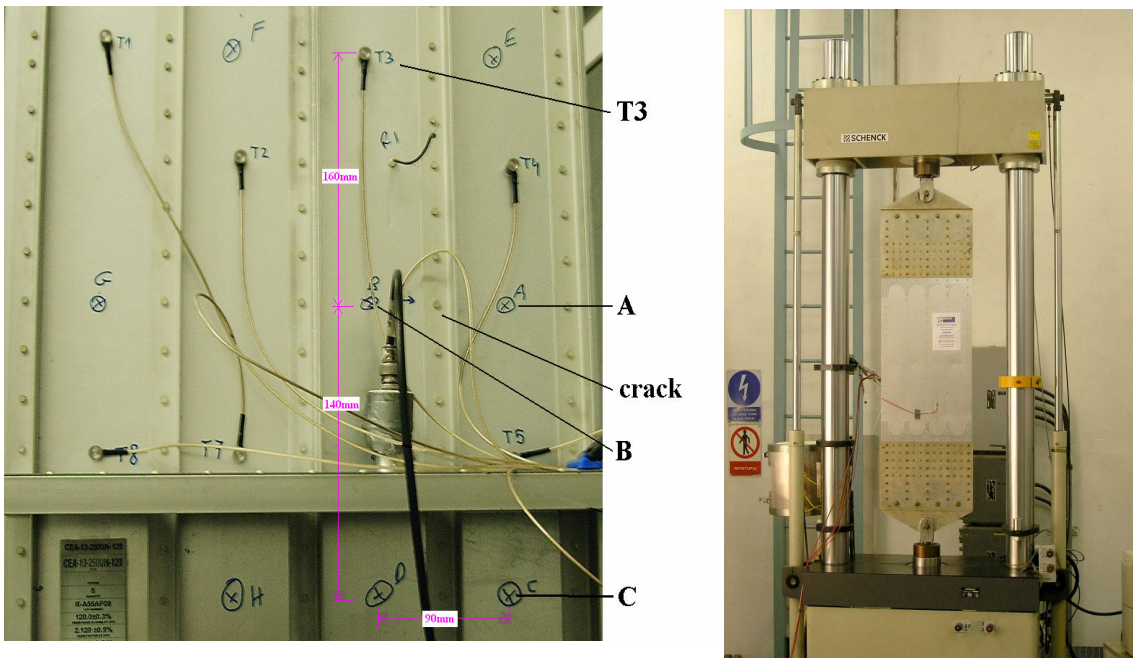

Single frequency harmonic generation test

The wing assembly was fatigue cycled at intervals of 3 hours, and a crack initiated.

An Acoustic transmitting transducer (DAKEL IDK09) was glued at positions T3 shown in the photograph above. This provided a continuous fixed frequency signal of 118 kHz sine wave. The transducer being driven from a power amplifier (Amplifier Research) model 150A 1000B unit and the driving sine wave source from a function generator (Hewlett Packard) model 33120A. At position A an NBOX (module 0), with plastic

film coupling, set to receive was pressed against the wing panel surface and a recording taken. The spectrum of the recorded data at various crack lengths was examined.
The Figure 105 below shows the spectra obtained when the crack was 9 mm and 16 mm in length, at the receiver position A (close to the crack).

Figure 105 Harmonics generated by a crack in aluminium wing panel

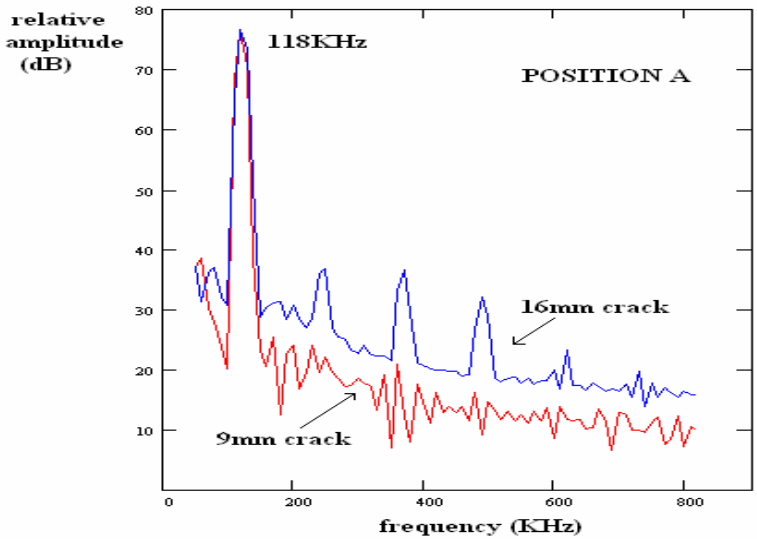

Some harmonics are generated when the crack was 9 mm. The 2nd harmonic (236 kHz) is less than 50 dB below that of the fundamental, or less than 0.3%. This level is about the lowest level of distortion that can confidently be measured, due to the non-linearity of the transducers and coupling, and in this case a defect condition is not certain. When the crack reached 16 mm in length there was generated a high harmonic content. The 2nd and 3rd harmonics were greater than 40 dB below the fundamental, or 1%. This indicates a defect in the wing panel.

6.2.2 Carbon composite aircraft wing

The second test object was made of a Carbon Fibre Reinforced Plastic (CFRP, single skin) used as wing material for a fighter aircraft, provided by Bodycote (CSM). The dimensions of the test sample and the location of the defect is given in Figure 106a.
A Drop Weight Impact Tester, supplied by VZLU, is shown in the photograph Figure 106b. This device was used during a series of tests to provide progressive damage to the composite plate by impacting a set of chosen levels of energy. These levels are given in Table 4:-

Table 4 Impact damage applied to CFRP wing

IMPACT	APPLIED ENERGY	IMPACT RADIUS	TOTAL ENERGY
1	4 Joules	12.5mm	4 Joules
2	5 Joules	12.5mm	9 Joules
3	10 Joules	6.25mm	19 Joules
4	10 Joules	6.25mm	29 Joules
5	10 Joules	6.25mm	39 Joules
6	10 Joules	6.25mm	49 Joules
7	20 Joules	6.25mm	69 Joules

Figure 106a
Sample dimensions with location of defect.

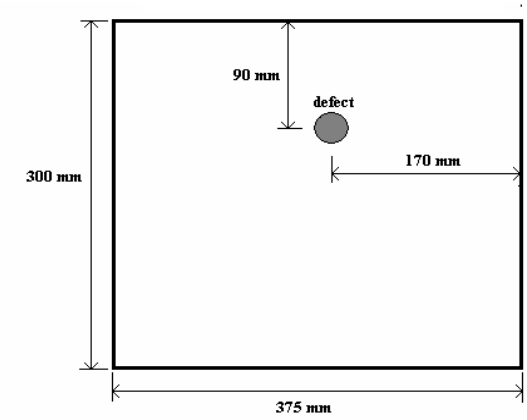

Figure 106b Weight Drop Impact Tester

The photographs of Figure 107 below shows the visual effect of the impact energy on the carbon fibre wing material.

Figure 107 Visual indication of weight drop damage

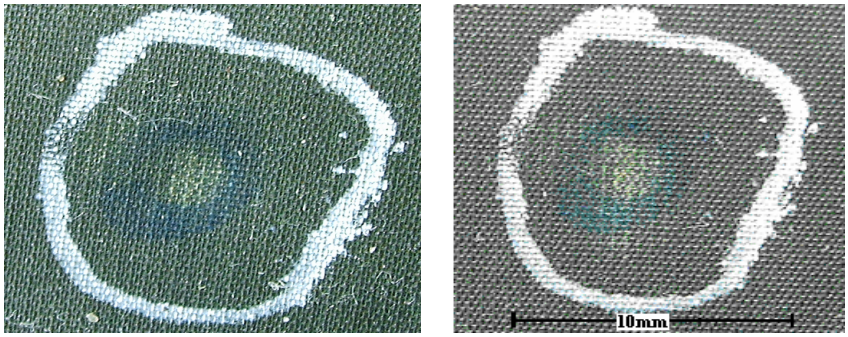

after 39 Joules after 69 Joules

Single frequency harmonic generation.

This method used two NBOX's, both version module 0, one set to receive the other set to transmit, as shown in the schematic of Figure 108. A continuous sine wave of fixed frequency 130 kHz was provided by a Jupiter 2000 function generator, this signal was fed directly to the transmitting NBOX there it was amplified and fed to its internal spring loaded prototype transducer. The receiver NBOX was connected directly to Smart Sensor electronic unit (NBOX200). This unit was set to record data at a data rate of 10 M samples per second, with 12 bit accuracy, a total of 1024 samples taken at any one time. This data was then sent to a lap top PC for display and saving to disk. The Figures 109 and 110 show photographs of the apparatus and transducers being pressed on to the carbon fibre wing panel, with a dry solid plastic coupling.

Figure 108 Schematic of equipment used for harmonic experiments

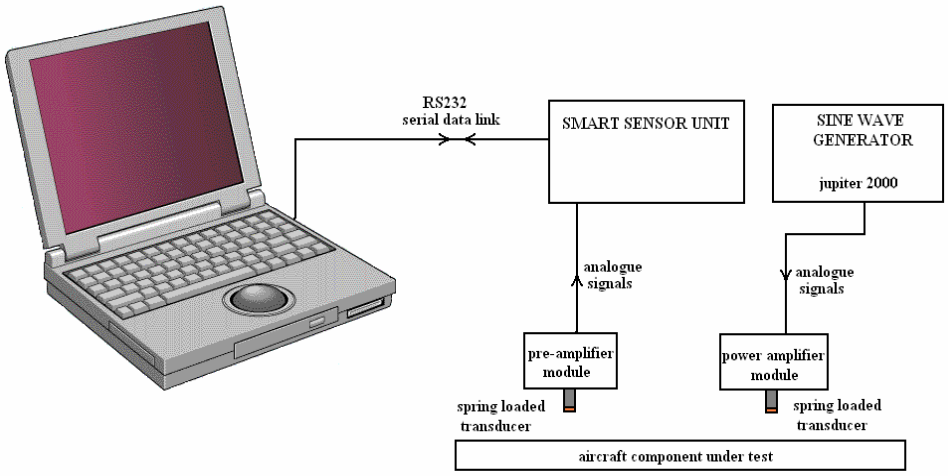

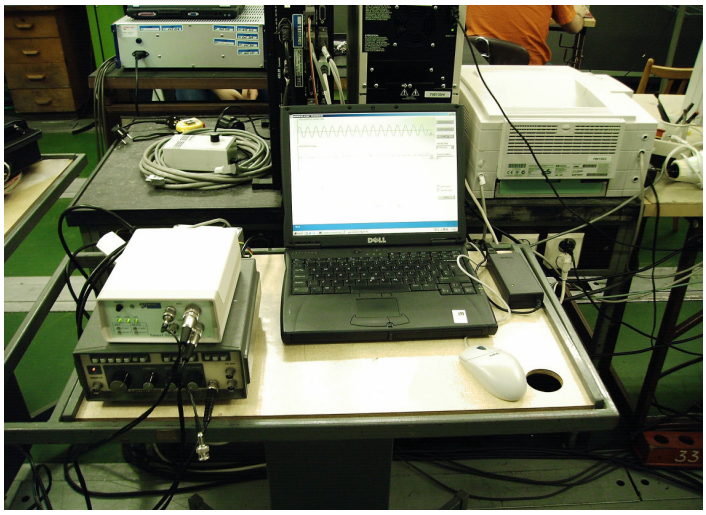

Figure 109

Photograph of harmonic data acquisition apparatus

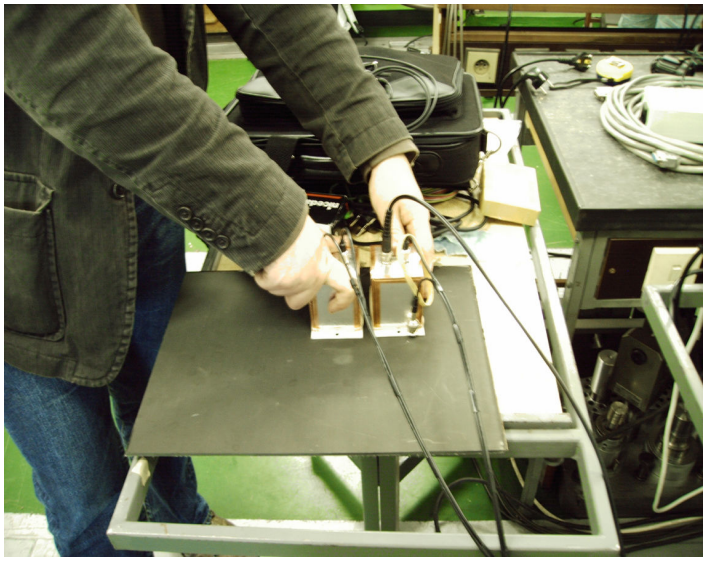

Figure 110

Photograph of two NBOX modules being pressed on to the aircraft wing

Harmonic generation tests with defects between receiver and transmitter (experiment 1)

This involved a series of tests with the transducers placed either side of the defect after each impact, as depicted in Figure 111. The spectrum of the recorded signals was examined and the harmonic content derived and given in Table 5.

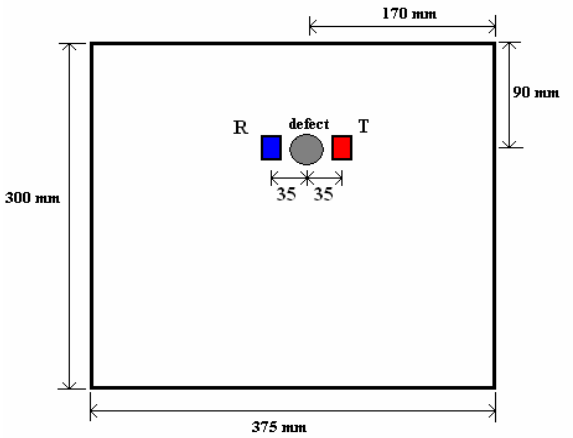

Figure 111

Transducer arrangements for CFRP wing tests.

Defect between transducers
R the receiver position
T the transmitter position

Table 5 Harmonics generated by progressively damaged CFRP wing

Impact energy (Joules)	2nd Harmonic (dB)	(%)	3rd Harmonic (dB)	(%)	4th Harmonic (dB)	(%)
4	-40	1.0	-40	1.0	-45	0.6
9	-37	1.4	-36	1.6	-56	0.2
19	-42	0.8	-40	1.0	-45	0.6
29	-37	1.4	-29	3.6	-43	0.7
39	-30	3.2	-33	2.3	-52	0.3
49	-30	3.2	-33	2.3	-50	0.3
69	-22	7.9	-38	1.3	-44	0.6

Figure 112 Variation of 2nd, 3rd and 4th Harmonics with impact damage (transducers placed either side of damaged region)

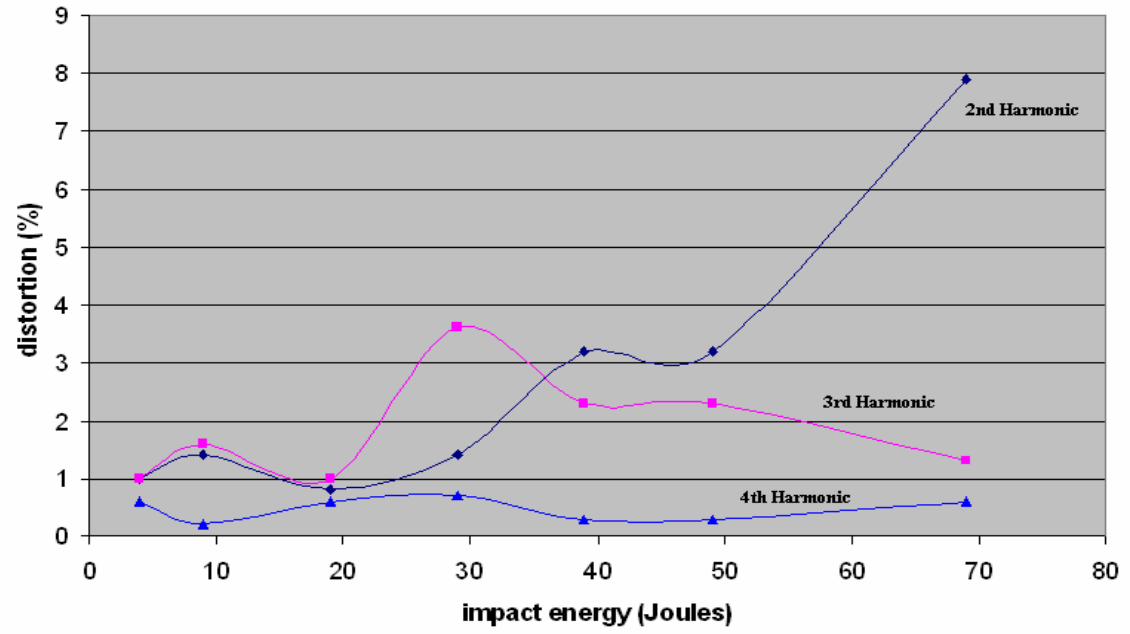

Figure 112 gives a plot of the impact damage versus harmonic content. The 2nd harmonic shows a significant increase with damage, the 4th harmonics are relatively unchanged, and the 3rd harmonic rise's sharply then starts to level off beyond 29 Joules. This suggests that there may be two effects taking place during impact damage, initially one form of damage causes the third harmonic to increase, then as the damage progresses the effect causing the third harmonic is reduced and another damage mechanism takes place that produces a rise in the second harmonic.

Harmonic generation tests with receiver on the defect (experiment 2)

The experimental set up was the same as in experiment 1 with the exception that the receiver was placed directly on top of the defect, as shown in Figure 113.

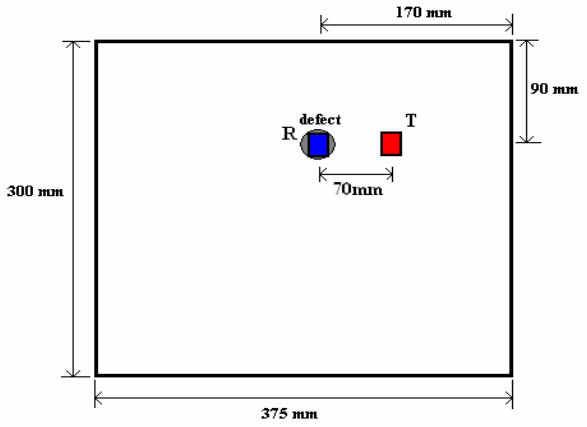

Figure 113
Transducer placed on damage region.

Receiver directly on defect
R the receiver position
T the transmitter position

Figure 114 Variation of 2nd, 3rd and 4th Harmonics with impact damage (with receiver placed on damaged region)

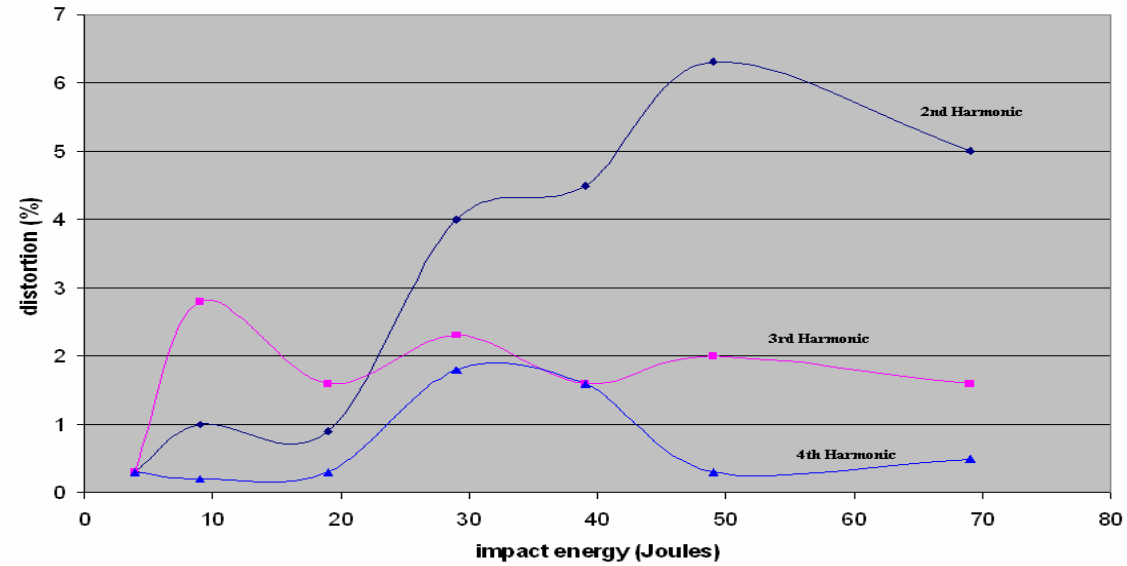

Figure 114 is a plot of the harmonic content versus impact damage. The 2nd harmonic shows a significant increase with damage. The reduction at 69 Joules may be due to surface damage effects near the receiver transducer. Experiments were attempted with the transmitter on the defect but it was found that the signal amplitudes produced were too weak to analyse properly, particularly after high impact damage.

Comparing the variation of the second harmonics in figures 112 and 114, the most sensitive indicator of damage is found when the receiver is placed on the defect, however at high levels of damage the sensitivity decreases and a clearer indication is obtained when the receiver and transmitter are placed between the defect, this is shown in Figure 115.

Figure 115 Variation of 2nd Harmonics with impact damage (transducers on or either side of the defect)

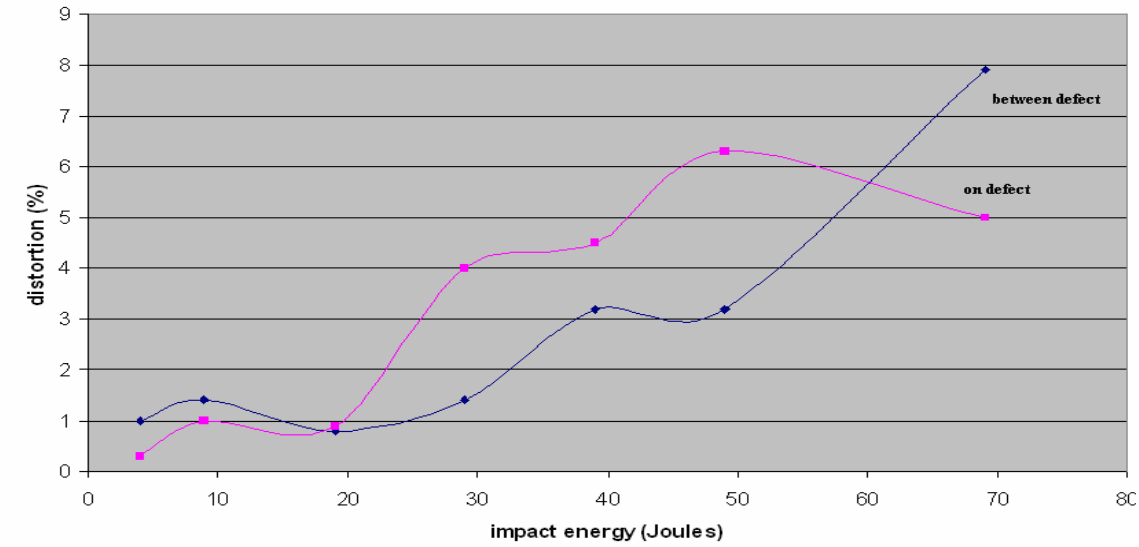

Investigation of transmitter to receiver distance on signal level (experiment 3)

This experiment was to examine the variation of signal amplitude with distance, at various frequencies, this being of importance when designing the required instrument amplifier gains and giving an assessment of the expected range of operation.

The transducer placements for this test are given in Figure 116a.

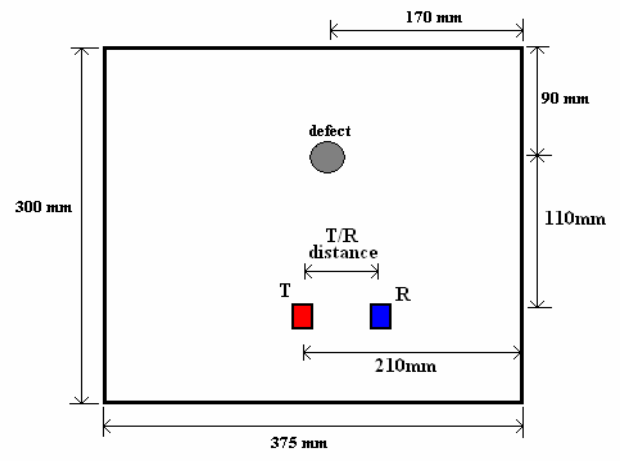

Figure 116a

Signal amplitude versus distance at various frequencies & transducer placement

Figure 116b Plot of signal amplitude versus distance at various frequencies

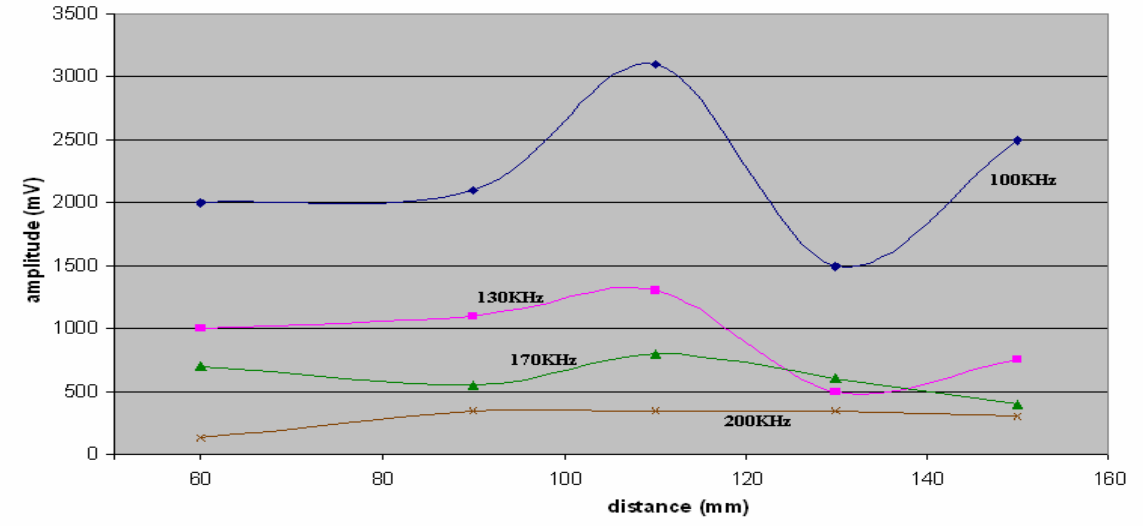

The transmitter was in a fixed position (T), and a signal of constant amplitude transmitted. The receiver was placed at selected distances in a line from the transmitter. The transducers coupling to the wing was a solid plastic. Tests were performed at frequencies 100 kHz, 130 kHz, 170 kHz and 200 kHz

Figure 116b gives a plot of the distance from the transmitter to the receiver versus the amplitude of the signal received for each of the test frequencies.

Referring to Figure 116b; for the frequencies 130, 170 and 200 kHz there is very little change of amplitude with distance. This suggests the material has low attenuation with distance for an acoustic surface wave. The plots show a definite attenuation with frequency, as expected for any material the signal amplitude dropping as the frequency increases. The wide variation in amplitude at 100 kHz is most likely due to the setting up of nodes and anti-nodes over the surface of the wing

Harmonic generation tests with sample subject to tensile stress (experiment 4)

At the developmental tests at Prague (experiment 1), it was observed that during the stages of progressive impact damage there were changes in the relative content of the second and third harmonics. A follow up study was therefore undertaken by the author at the University of Exeter to investigate this in more detail. This study involved applying a tensile load to damage a strip of carbon fibre composite (CFRP).

The sample of CFRP (173 x 22 x 4 mm) was subject to tensile loads of 0,10, 20, 30, 40, and 46 kN. After each loading the sample was removed and the non-linear acoustic properties measured across its surface, at a single frequency of 130 kHz. The sample failed at 52.5 kN, when trying to apply up to 60 kN. The Figure 117 below shows the sample under test. Figure 118 the force – extension curves for each loading.

Figure 117 tensile testing apparatus

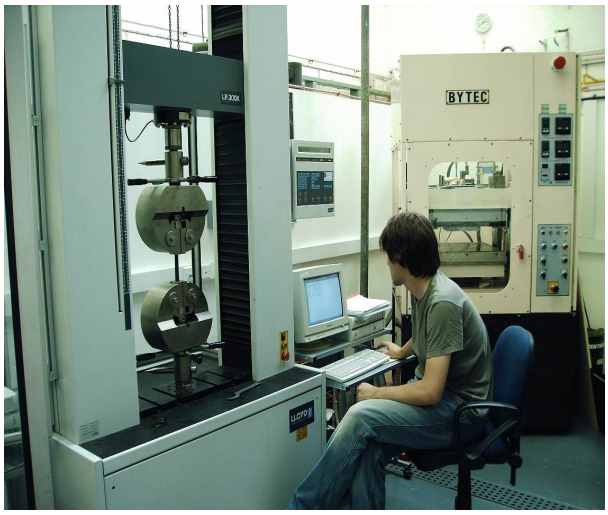

Figure 118 force-extension plots

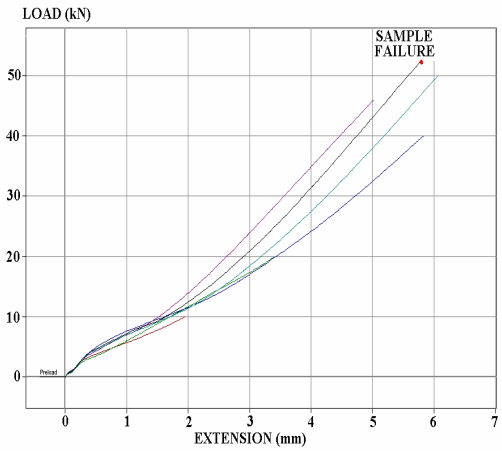

Figure 119 Spectral plots for various tensile loadings

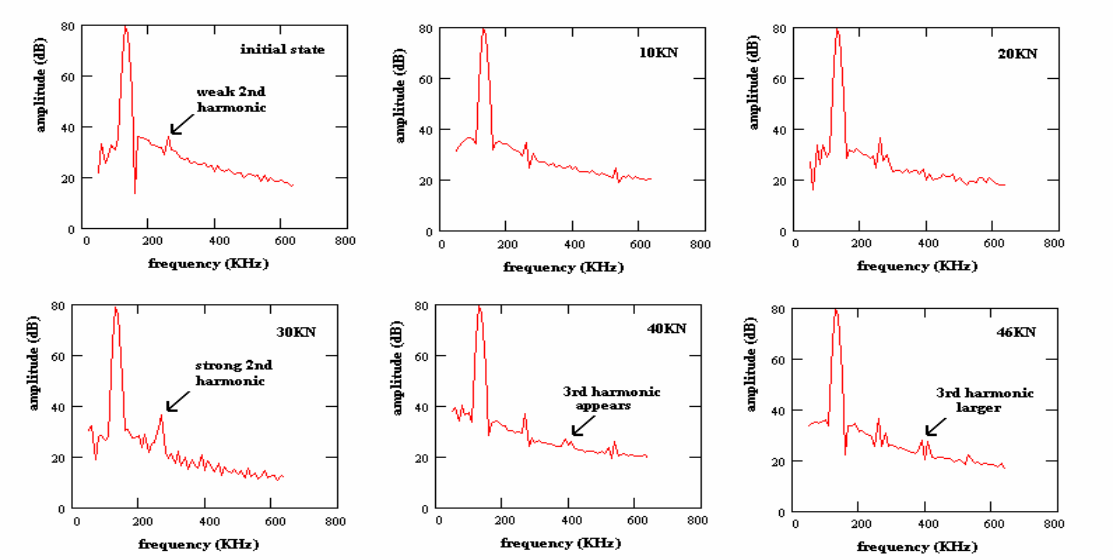

Referring to Figure 119, initially the second harmonic is present at -44 dB (0.6%). After 20 kN has been applied this increases slightly to –42 dB (0.8%). At 30 kN applied force the second harmonic remains at the same level but is more clearly defined. The third harmonic is not visible. On applying up to 40 kN force the sample started to produce a sound burst (high frequency cracking sound), however no visual indication of damage was observed. The acoustic spectrum shows the presence of a weak third harmonic at -54 dB (0.2%). On re-applying the force the sound burst was noted to be more frequent and was stopped at 46 kN. Black powder was found falling from the sample. When the force was released and the sample removed no damage visually observed. The acoustic spectrum was examined and a clear third harmonic was observed at a level of –51 dB (0.3%). The sample was then stressed above 50 kN and finally failed dramatically at 52.5 kN.

It is speculated that when forces between 10 and 40 kN are applied, the carbon composite first undergoes micro-cracking and when stressed above 40 kN it starts to de-laminate. On removal of the force the structure closes back up, thereby not showing any visual damage at the surface. The micro-cracks introduce some acoustic non-linearity (first order perturbation), which gives rise to the initial increase in the second harmonic. Forces greater than 40 kN make the micro-cracks open up and de-lamination starts to occur, this introduces hysteretic non-linearity as material planes move over each other, locking up in places and gives rise to an increase in the third harmonic.

Pulse inversion response over carbon fibre composite surface

This method uses two NBOX's one as a transmitter (module 1) and the other a receiver (module 2). A gel coupling was applied to the NBOX transducers to improve signal quality. The technique involves transmitting an acoustic wave over the surface of the carbon fibre wing, a positive, compressional pulse into the material and recording the response, then transmitting a negative, tensional pulse into the material and recording this response. The two recordings are then compared. If the material response is linear then the two should sum to zero since they should be the same but of different polarity. If there is any non-linearity a non-zero result will occur. To quantify this effect the ratio of the maximum amplitudes of the two recorded waves are measured and the ratio of the smallest to the largest determined.

Figure 120 below shows a photograph of a strip of undamaged carbon fibre composite wing material (300 * 23 * 4.2 mm) placed between the jaws of a tensile testing machine. The pulse transmission and reception is on one side, the distance travelled over the surface is 56 mm by the surface wave.

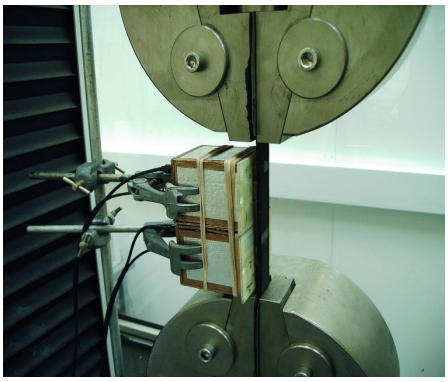

Figure 120

Pulse inversion test on CFRP strip
Photograph of apparatus

The figure 121 shows the recorded data from the compressional, positive (red) pulse and the tensile, negative (blue) pulse, when there is no force applied to the test strip. The ratio of the maximum amplitudes of the compressional and tensile pulses (a/b) is measured to be 0.99.

Figure 121 Pulse tests on undamaged carbon fibre wing strip

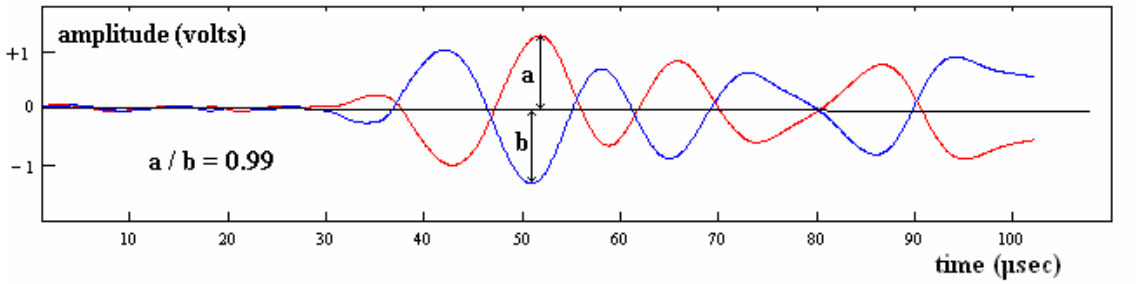

Figure 122 shows the recorded data from the positive (red) and negative (blue) pulses, when there is a force of 55 kN applied to the test strip. There is a significant phase difference between a compressional and a tensile pulse travelling over the surface of the material, suggesting a difference in the velocity of propagation of these two waves. In this experiment it was found that the maximum amplitude of the compressional pulse to the tensile pulse (a/b) was measured to be 0.93.

Figure 122 Pulse tests on damaged carbon fibre wing strip

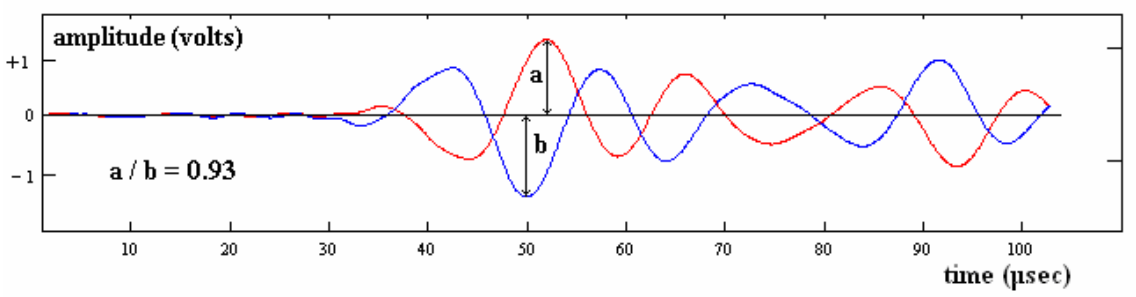

Pulse inversion response through carbon fibre composite

This testing method uses the same NBOX's (modules 1 and 2) as before but instead of sending the compressional and tensile pulses over the surface of the material they are sent through its thickness (4.2 mm) as a longitudinal wave. The sample (278 x 22 x 4.2 mm) was tested first undamaged, then tested after being subject to damage (visual signs of de-lamination). Figure 123a below shows the recorded data from the positive (blue) and negative (red) pulses, when there is no damage to the test strip. The slight "slewing or triangular distortion" in the first few cycles of the recorded signals are observed in many tests on undamaged carbon composites. It is not clear what causes this, however it seems not to effect the ability of the pulse inversion method to detect faults. Summing the two pulses shown in Figure 123b (green) produces a near zero result throughout the whole wave form. The maximum amplitudes of the compressional and tensile waves are the same (ratio a/b = 1).

Figure 123a pulse inversion p-wave for undamaged CFRP strip

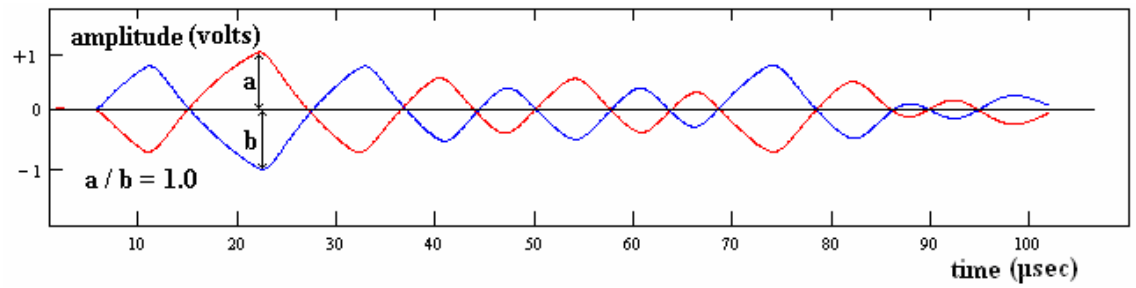

Figure 123b sum of positive and negative pulses for undamaged CFRP strip

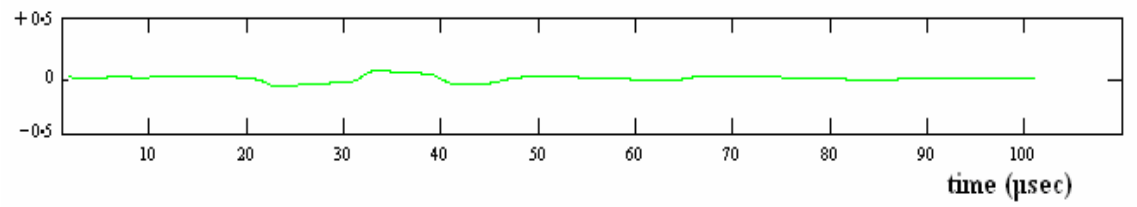

The figure 124a below shows the recorded data from the positive (blue) and negative (red) pulses, when substantial visual de-laminations are observed in the test strip. Summing the two pulses shown in Figure 124b (green) shows a significant non-zero result throughout the 100 micro second recording period. The ratio of the maximum compressional to the tensile waveforms is a/b = 0.82.

Figure 124a pulse inversion p-wave for damaged CFRP strip

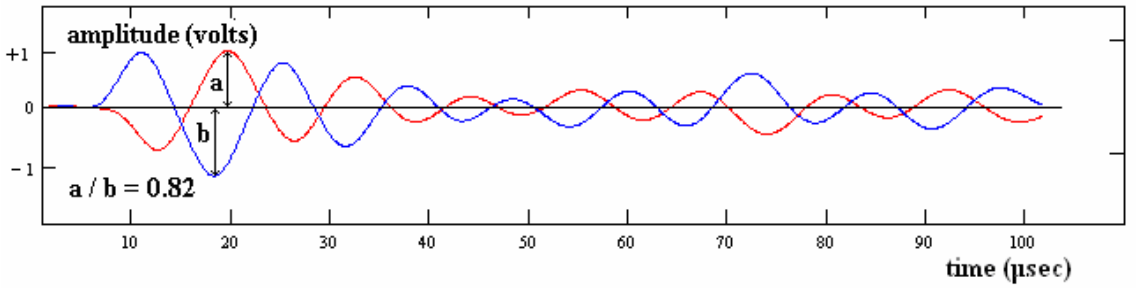

Figure 124b sum of positive and negative pulses for damaged CFRP strip

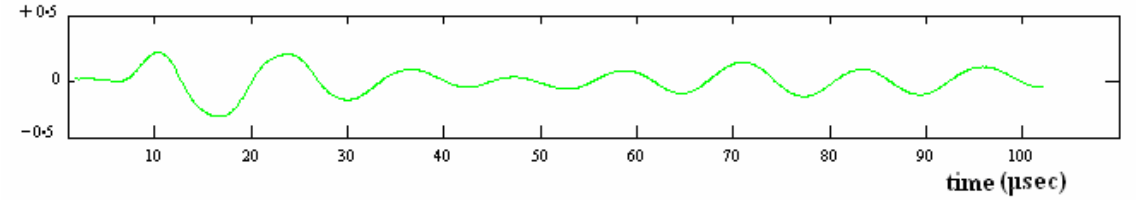

6.2.3 Aluminium wing fuselage attachment

This object tested was one part of an aluminium wing fuselage attachment normally consisting of two parts, the parts being jointed through a hinge pin and bush bearings that are insert into aluminium parts of the lugs and fixed by mating joints. Both parts of the attachment are made of 2124-T851 machined aluminium plate. The fuselage attachment was fixed into grips of a MTS 250 kN load frame, as shown in Figure 125, and loading cycles with constant amplitude of 158.36 kN at stress cycle frequency of 1.7 Hz were applied. The specimen developed a crack at 317312 cycles. Experimental investigations were then carried out on the removed upper section, show in Figure 126.

Figure 125 testing apparatus

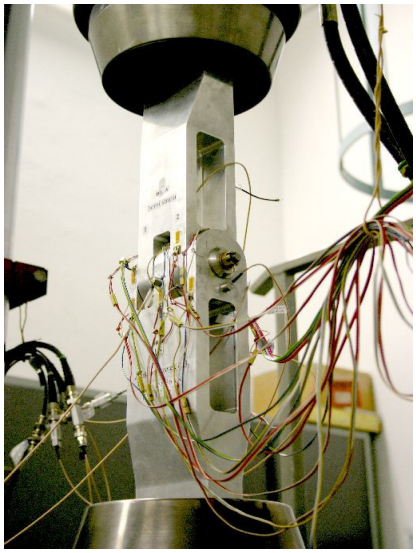

Figure 126 aluminium fuselage attachment

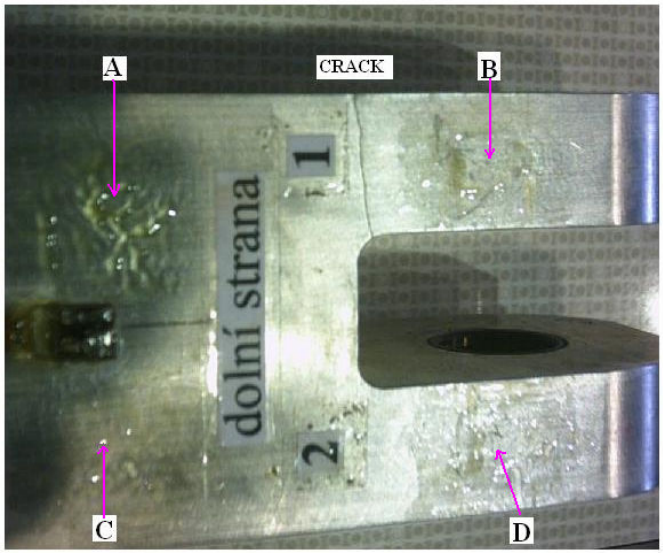

Dual frequency harmonics and inter-modulation generation

The acoustic tests used a dual frequency transmitter NBOX module 5 and an NBOX receiver module 2. The locations for the test on the wing fuselage attachment are shown in Figure 126, the first being across the crack (receiver at location A, transmitter at location B), and the other being over a similar region without any defects (receiver at location C, transmitter at location D). A Gel coupling (Sonatest, sonagel w1) was applied to the NBOX transducers and held in position for the data sampling.

The two frequencies transmitted in this experiment were f_1 = 184 kHz and f_2 = 240 kHz. The harmonics and inter-modulation products generated within the bandwidth of the transducers are; $2*f_1$ = 368 kHz (2nd harmonic of f_1), $2*f_2$ = 480 kHz (2nd harmonic of f_2), $f_1 + f_2$ = 424 kHz (sum of f_1 & f_2) and $f_1 - f_2$ = 56 kHz (difference of f_1 & f_2).

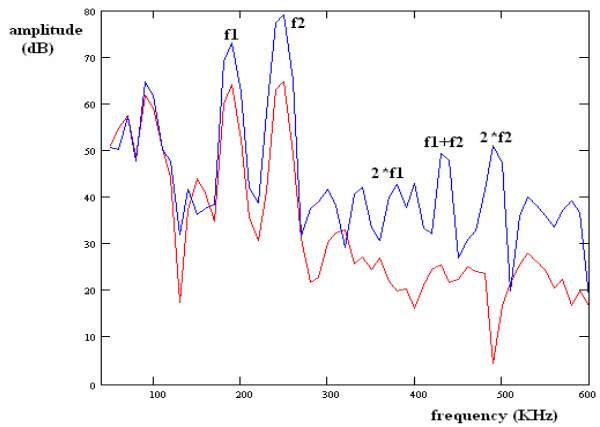

Figure 127
Spectra from fuselage attachment.

Red trace = good region (D > no defect > C)
Blue trace = bad region (B >crack > A)

harmonics	good region	bad region
$2*f_1$	-43dB (0.7%) ref to f_1	-30dB (3%) ref to f_1
$2*f_2$	-55dB (0.2%) ref to f_2	-29dB (3.5%) ref to f_2
f_1+f_2	-40dB (1%) ref to f_2	-30dB (3%) ref f_2

ref = referenced to fundamental signal level

Figure 127 shows there is a significant difference between the good and bad regions. The cracked region produced the generation of f_1+f_2 from 1% to 3% and harmonics $2*f_1$ from 0.7% to 3% and $2*f_2$ from 0.2% to 3.5%.

Spectral analysis of a frequency sweep

This method involves transmitting a sine wave frequency sweep (or chirp) over the surface and through the material, receiving and recording the waveform as it passes from region B to A via a crack, and comparing the spectrum of this when the waveform travels over a similar good region from D to C.

For these experiments NBOX module 1 was used to transmit the sweep from 400 kHz to 100 kHz and NBOX module 4 used to receive the signals.

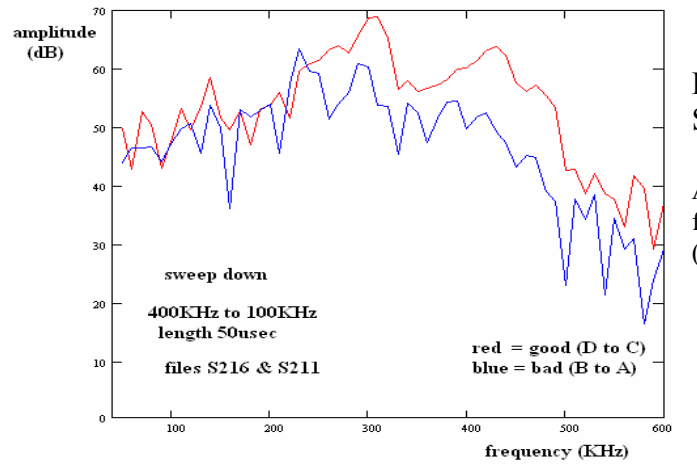

Figure 128
Spectra of frequency sweep

A comparison of the transmission of a frequency sweep between the damaged (B to A) and undamaged (C to D) regions

Figure 128 shows the data from the sweep test. Over the good region (plotted in red) there is a relatively smooth trend in the frequency spectra with some peaks and troughs, more dominant at the lower frequency range. These are probably due to the geometry of the sample forming natural resonances. There are some frequency components outside the sweep band of 100 kHz to 400 kHz these are most likely due to the effects of using a short sweep length and some harmonics generated by the transducers and their coupling. Over the region traversing the crack (plotted in blue) there is a drop in the high frequency components, the peaks and troughs ("notches") are greater in number and distributed more evenly over the whole spectrum. Further experimental testing would be required to determine if this method would be suitable defect detection. However the presence of "notches" in the spectrum has shown to be a method to detect gauge corner cracks in railway lines. See section 6.2.6 for more details.

6.2.4 Steel steering actuator bracket

These objects for testing were steering actuator brackets, an example is shown in the photograph Figure 130, they form part of the nose landing gear of a commuter aircraft shown circled in the photograph Figure 129. The bracket is made of POLDI L –ROL low-alloy Czech steel (Czech standard ČSN 14331).

Figure 129 aircraft steerage

Figure 130 steel steering actuator bracket

Three test specimens were prepared, bracket No.1; damaged with a fatigue crack in a critical point of length of 9 mm and depth 3 mm. This bracket had been subject to 11185 pulsating stress cycles at a 41.7 kN loading force. Bracket No.2; no damage and was used for comparison and bracket No. 3; progressively damaged during the course of experimental investigations. The fatigue loading of the bracket No. 3 was from 0 to 15 000 stress loading cycles using the Instron Schenck 100 kN uniaxial loading machine, shown in Figure 131. The bracket was loaded under pulsating stress cycles and a maximal tensile load level of 41 kN. This level of load caused a maximum tensile stress of about 870 MPa in the critical point of the bracket. The cyclic loading frequency was 1 Hz.

Figure 131 Steering actuator bracket fatigue testing apparatus.
(INSTRON SCHENCK 100 kN testing system. courtesy of VZLU)

From 15 000 cycles on, the loading force was increased to 43 kN with a frequency of 0.5 Hz for loading from 15 000 to 60 000 cycles and 1 Hz from 60 001 cycles till the end of the test at 123,808 cycles when a visual observation of a crack was first noticed, this crack is shown in Figure 132. Acoustic emission monitoring was instigated during this cyclic loading procedure. At 20,000 cycles acoustic emissions indicated the presence of a defect, however no visual indication was observed and conventional ultrasonic and inductive testing methods failed to detect a fault.

Figure 132 Fatigue crack in the critical point of the bracket No. 3
after 123 808 loading cycles (courtesy of VZLU)

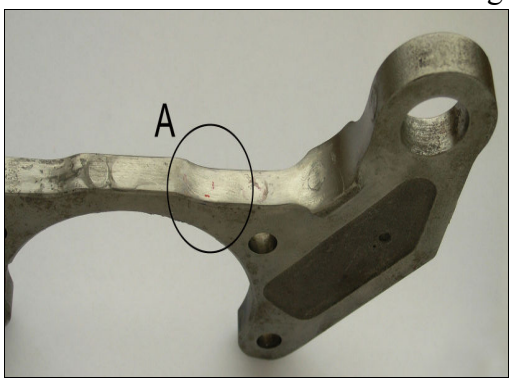

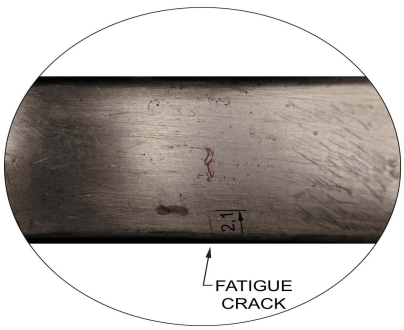

Testing arrangement

The first two testing methods selected for this object involved sending ultrasonic waves or pulses through the thickness of the bracket as shown in the photograph Figure 133.

The transmitter place at the bottom and the receiver on top and held in position by elastic bands. Gel coupling was used on both transducers.

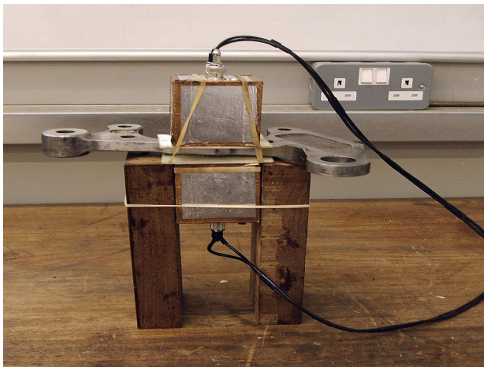

Figure 133

Bracket acoustic testing arrangement

Dual frequency harmonic and inter-modulation product generation

With the bracket place in the testing arrangement, the sum of two frequencies 184 kHz and 240 kHz were transmitted into the bracket. For bracket loadings of 1 to 15000 cycles the harmonics and inter-modulation products were examined and found to be less than -45 dB (0.6%) at three test positions A, B and C. The bracket was further subject to another 5000 cycles. The resulting measured frequency spectra for the bracket is shown in Figure 134. This bracket had been subject to a total of 20,000 cycles of loading, the point at which acoustic emissions were found to occur.

Figure 134
Spectra after 20,000 cycles of loading

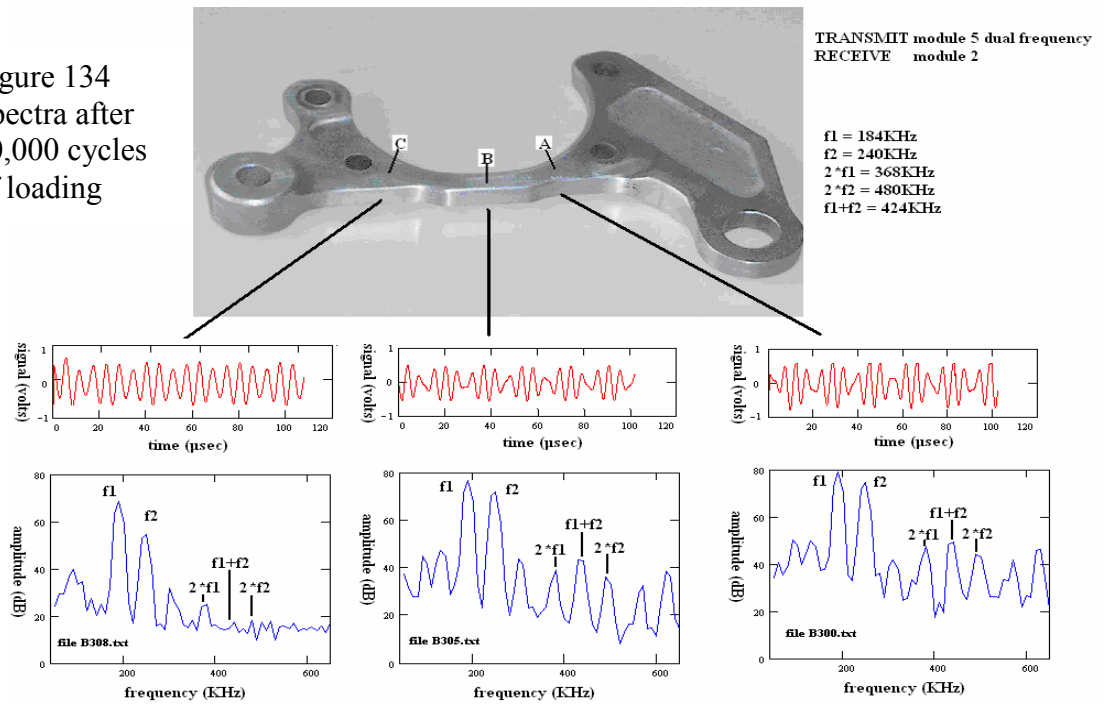

2*f1 below –45dB(0.6%)
2*f2 below –50dB(0.3%)
f1+f2 below -45dB(0.6%)

2*f1 = -39dB(1.1%)
2*f2 = -40dB(1.0%)
f1+f2 = -33dB(2.3%)

2*f1 = 32dB(2.5%)
2*f2 = 35dB(1.8%)
f1+f2 = 30dB(3.2%)

At the 20,000 cycles loading acoustic emission occurred but no fault using conventional methods was detected. From the spectral results shown in Figure 134 a prediction was made that the bracket will start to fail at location A. This is indicated by the high level of the upper side band 3.2 % ($f_1 + f_2$) in this region. The region B also shows some damage (2.3%). Region C shows no damage (0.6%). The bracket was fatigued further until a surface crack formed at 123,808 cycles, the measured spectra shown in Figure 135.

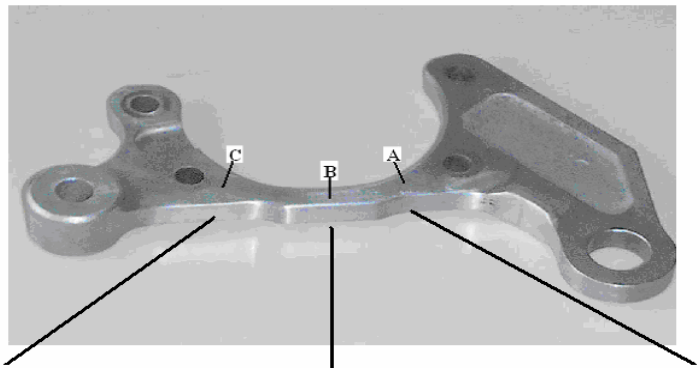

Figure 135

123,808 cycles of damage
fatigue crack 2.1mm long
formed at location A

frequency f1 = 184kHz
frequency f2 = 240kHz
continuous transmission
Transmitter = NBOX module 5
Reciever = NBOX module 2

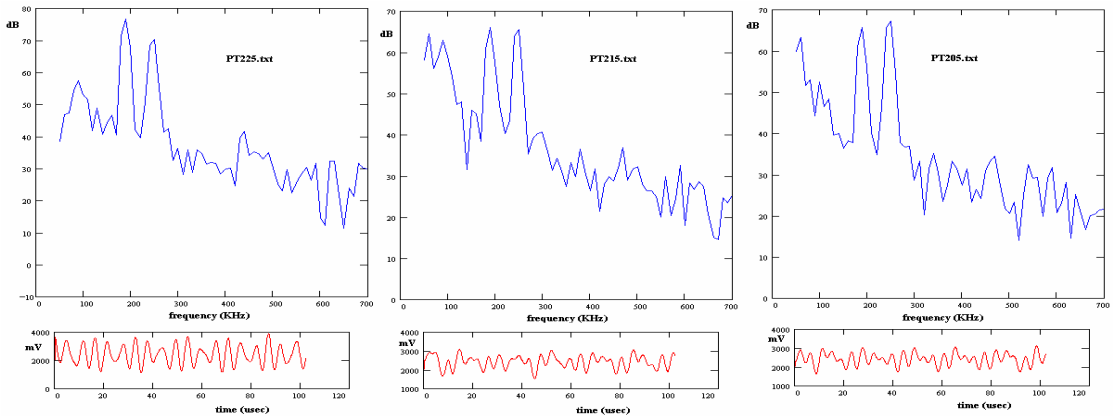

2*f1 = -45dB (0.6%)
2*f2 = -35dB (1.8%)
f1+f2 = -35dB (1.8%)

2*f1 = -29dB (3.6%)
2*f2 = -29dB (3.6%)
f1+f2 = -33dB (2.3%)

2*f1 = -32dB (2.5%)
2*f2 = -33dB (2.8%)
f1+f2 = -33dB (2.3%)

The damage at location A as indicated by the upper sideband (f_1+f_2) has decreased, from 3.3% to 2.3%, however the second harmonic of f_2 ($2*f_2$) has increased from 1.8% to 2.8% indicating a different damage scenario. The region B now shows the potential to failure as the second harmonics of both f_1 and f_2 ($2*f_1$ & $2*f_2$) in this region are now showing high values, changing from 1% to 3.6%. Region C shows slight onset of damage. It is concluded that the method of dual frequency measurement of harmonics and sidebands are a successful way to predict and quantify progressive damage in metals.

Harmonics generated by a sine wave burst

The bracket was tested at 20,000 cycles and at 123,808 cycles of fatiguing using a sine wave burst. Below 15,000 cycles the levels of harmonics measured were less than 2% over the three regions. At 20,000 cycles the region C gave a second harmonic level of -35 dB (1.8%), in regions A and B the levels were both just less than -30 dB (3.2%). The test was repeated after 123,808 fatigue cycles and the result shown in Figure 136.

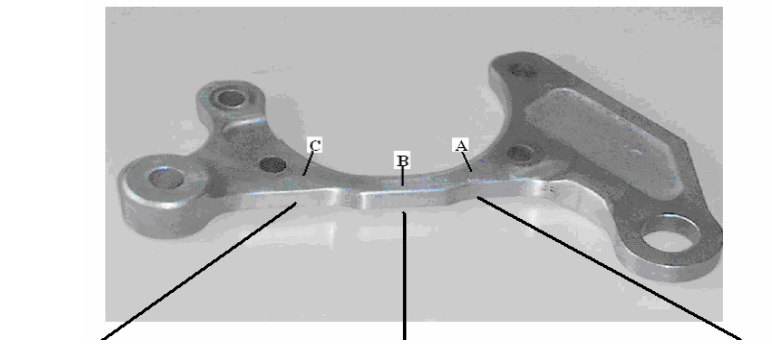

Figure 136

DAMAGE 123,808 cycles
Frequency = 200kHz
Duration = 80microsec
Transmitter = NBOX1-00
Receiver = NBOX2-00

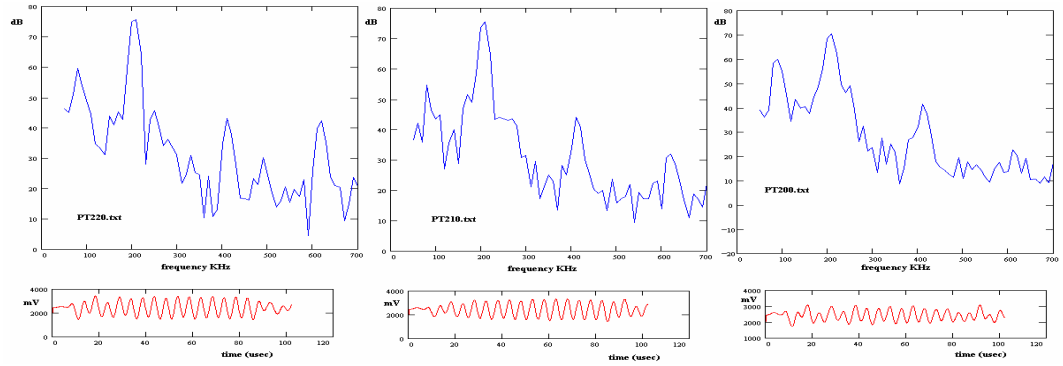

2f = -33dB (2.3%)
3f = -33dB (2.3%)

2f = -32dB (2.5%)
3f = -44dB (0.6%)

2f = -29dB (3.6%)
3f = -48dB (0.4%)

The method indicates that changes have occurred in the level of harmonics generated across all regions, with region A having the greatest change in the 2nd harmonic value, at 15000 cycles less than 2%, at 20000 cycles 3.2% and at 123808 cycles 3.6%. This technique is not as sensitive as the dual frequency method and further experimental testing will be needed to determine if this method is suitable for metal failure prediction.

Pulse inversion test

This test involved sending a positive (compressional) pulse followed by a negative (tensile) pulse into the bracket after it had been subject to 123808 cycles of loading. The impulse responses were recorded and the largest peak values compared in amplitude. Figure 137 below shows the results obtained.

Figure 137 Pulse inversion test on steel bracket

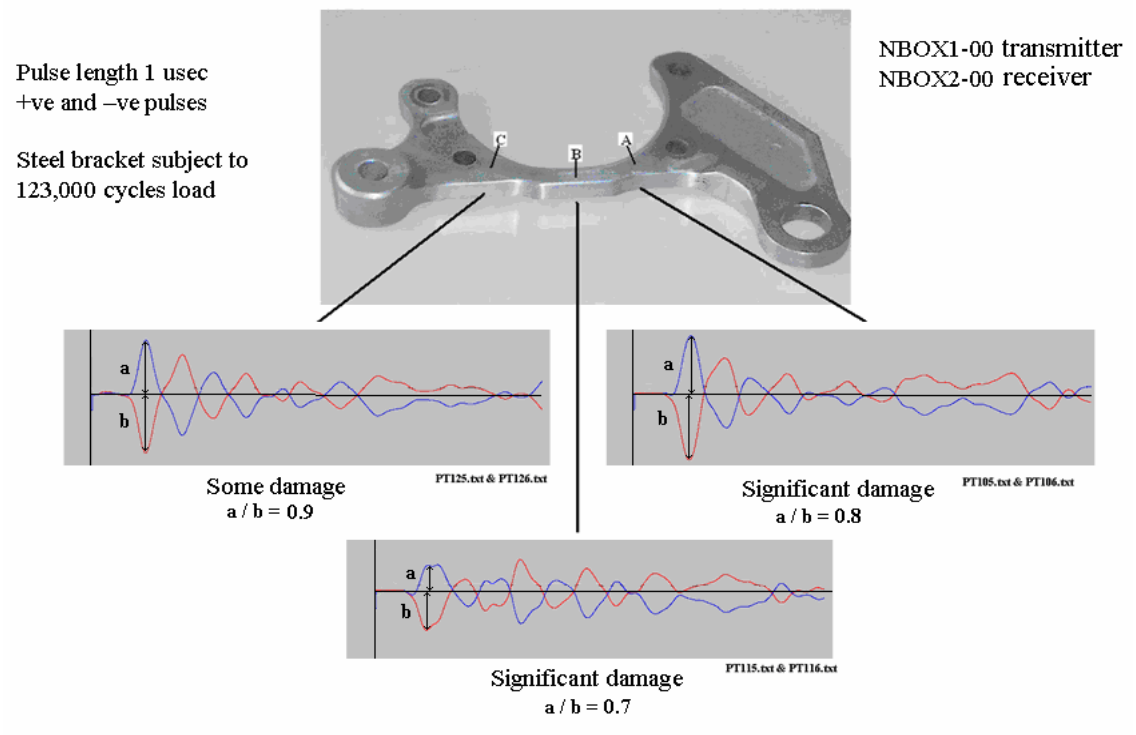

In this case the largest peaks occurred in the first cycle of the waveform received. Region C shows little non-linearity, the amplitudes of the received waveforms **a** and **b** are very nearly equal (a/b = 0.9). Regions A and B shows significant non-linearity indicating damage, since the ratio of amplitudes **a** and **b** at these locations are 0.8 and 0.7 respectively.

Resonant frequency deviation test

The development of this technique was finalised very late in the work program, and this is the only experiment performed on the damaged bracket (No.1) using the phase lock loop NBOX module 7, together with actuator NBOX module 10.

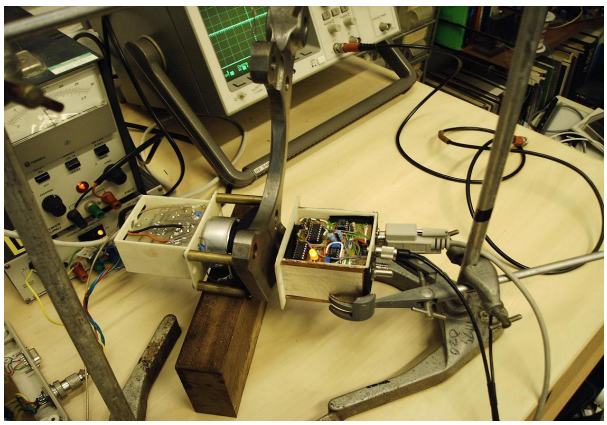

Figure 138
Resonant frequency deviation test

Photograph of the experimental arrangement for measurement of resonant frequency deviation with amplitude.

Referring to Figure 138, the bracket was suspended by a single thin wire. The NBOX10 module consisting of a loudspeaker actuator transmits a sine wave at high power (8 watts) at a frequency that was varied slowly. A small transducer was glued to the bracket and connected to an oscilloscope, displaying the received signal. This signal was used to measure the bracket's amplitude of oscillation. A frequency was determined that produced a maximum amplitude (612 Hz). This was the main resonant mode for the bracket. The transducer was then connected to the input of the phase locked loop of NBOX module 7. This modules output was sent to the PC via a digital link providing a value of the frequency independent of any changes in the amplitude (within limits, known as the lock range). The value of this frequency was displayed graphically in real time on the PC screen. First the bracket is made to resonate then the loudspeaker is turned off. This was repeated three times. Figure 139 shows the display of the change in frequency as the oscillation decays for these three successive tests. Initially just after the loudspeaker is turned off there is a slight decrease in frequency, corresponding to about 1 Hz. This is most likely due to the speaker frequency driving the bracket just slightly off resonance, after this a clear indication of frequency increase is observed (about 6 Hz variation) until phase lock is lost, at which point the frequency can no longer be tracked. This shift in frequency indicates that the bracket is damaged.

Figure 139 Display of resonant frequency deviation (steel bracket)

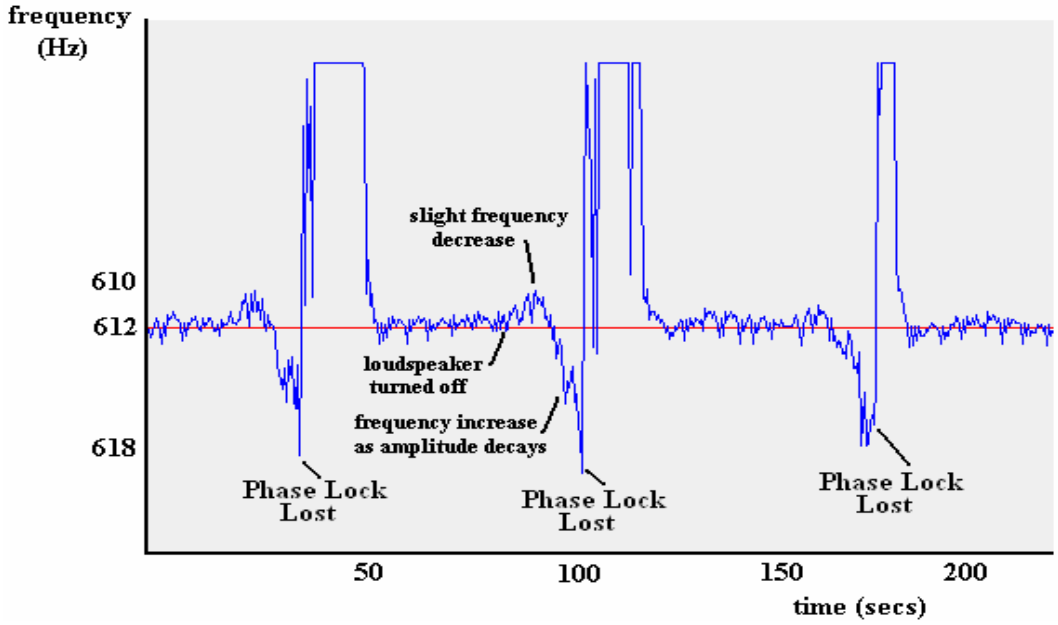

6.2.5 Steel fork leg

This object tested was a steel fork leg shown in the photograph Figure 141 and is part of the nose landing gear of a commuter aircraft, shown in the photograph Figure 140. The fork leg is made from POLDI V - ROL N ultra-high strength low-alloy Czech steel (Czech standard ČSN 16 532).

Figure 140 aircraft landing gear

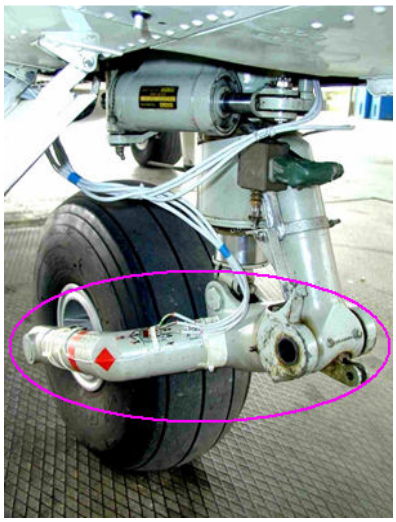

Figure 141 steel fork leg

Two fork legs were prepared. One damaged the other undamaged and used as a reference. The damaged fork leg had accumulated 84520 pulsating stress cycles and developed a 62 mm long crack at its tip, shown in Figure 142

Figure 142 Photograph of fork leg with crack.

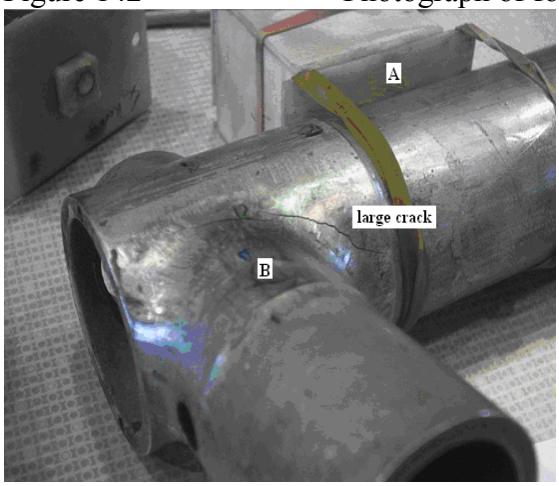

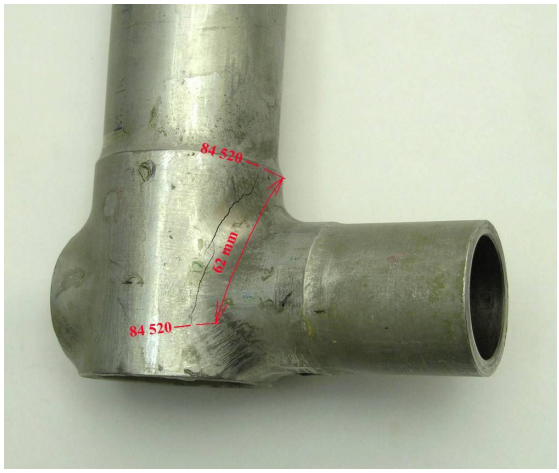

Dual frequency harmonic and inter-modulation product generation

This test involved transmitting a dual frequency into the fork leg and measuring the harmonics and inter-modulation products generated by the crack. Figure 142 left shows the NBOX module placing for the test. The transmitter placed at position A (NBOX module 5) and the receiver at position B (NBOX module 4), on the crack.

The resulting spectrum is shown in the Figure 143

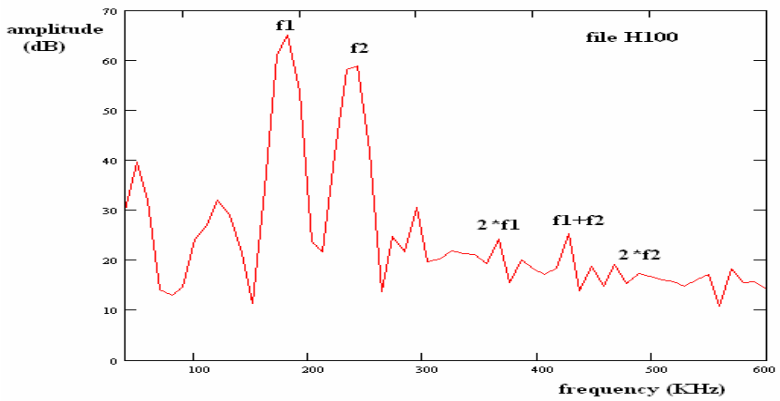

Figure 143

Spectra from fork leg crack

The level of the harmonics and inter-modulation products are all below 1%, indicating little damage. It is concluded that this method is not suitable for the detection of very large cracks of this type.

Frequency sweep test

This test involved sending a frequency sweep into one damaged and one undamaged fork leg and examining the spectra.

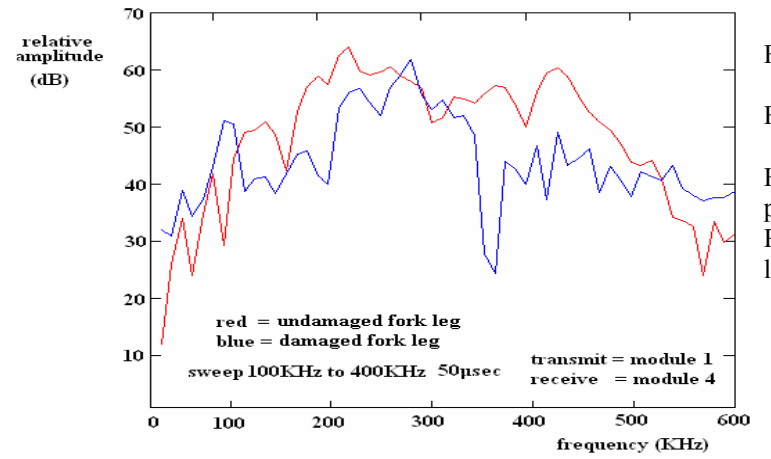

Figure 144

Frequency sweep test

High voltage transmitter module 1 placed at position B (on the crack) Receiver module 4 placed at location A.

The resulting spectrum shown in Figure 144 shows that “notches” form at various frequencies when the ultrasonic wave passes over the cracked material, this effect has been observed before see section 6.2.6 and chapter 2.6. This method may prove successful to detect faults of this type.

6.2.6 Gauge corner cracked rail

The suitability of some of the acoustic techniques previously described was investigated and applied to detect faults in railway tracks. The test objects for these experiments are detailed in the authors paper Armitage [39] and consisted of two samples of rail, one undamaged the other damaged having gauge corner cracking on its surface (rail head). Figure 145 shows a photograph of the top surface of the damaged rail. Figure 146 shows optical and electron microscope photographs of a cut section from this sample.

Figure 145 Gauge corner cracked rail

Figure 146 Optical and scanning electron microscope photographs of a section of gauge corner cracked rail

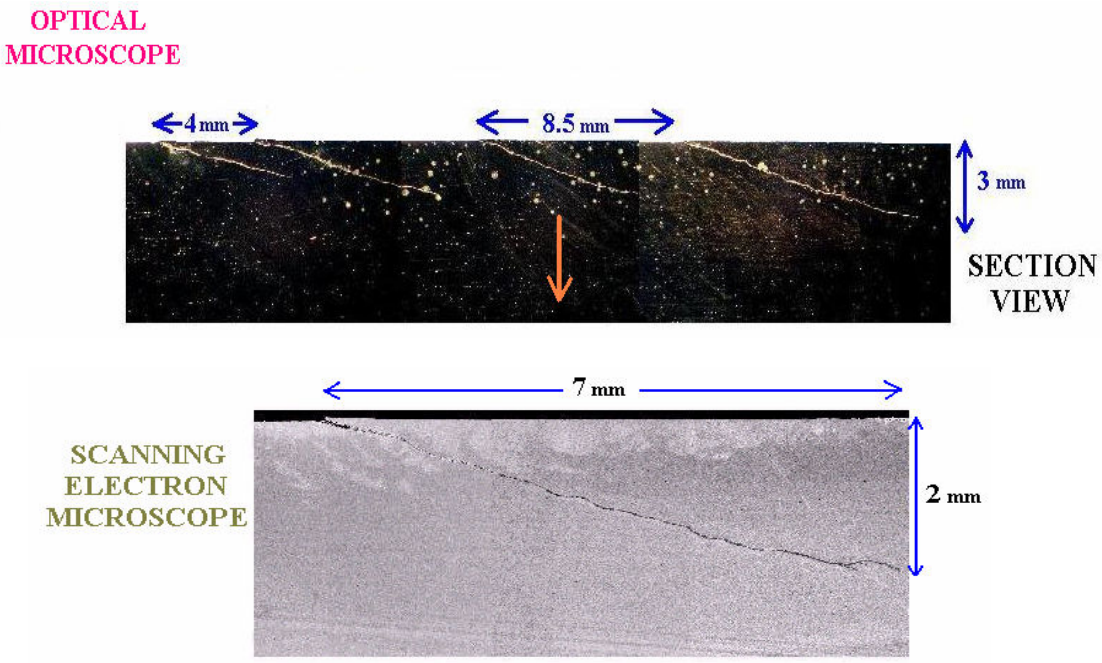

Wide band impulse frequency response

In this method two wideband piezoelectric transducers were first placed on the rail head of a good sample of rail. One transmitted a single cycle (140 kHz) Rayleigh wave and the other received the ultrasonic wave after having travelled over a range of fixed distances along the rails surface. Figure 147 shows the detected signals at various distances from the transmitter together with a schematic of the testing arrangement.

Figure 147 Rayleigh waves over a good rail

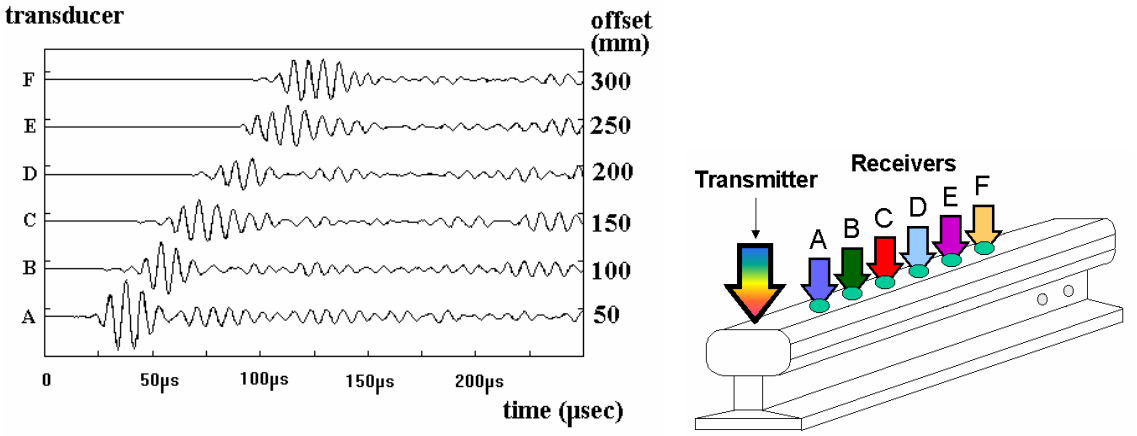

The tests were repeated at the same distances over the rail head of a sample of gauge corner cracked rail, shown in the photograph of Figure 149. The resulting waveforms are shown in Figure 148

Figure 148
Rayleigh wave over bad rail

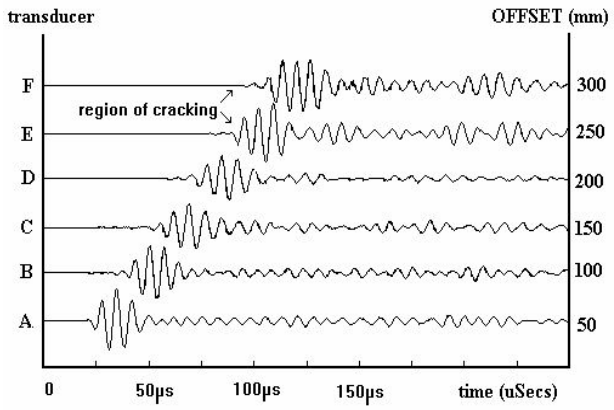

Figure 149
Transducer placements on gauge corner cracked rail

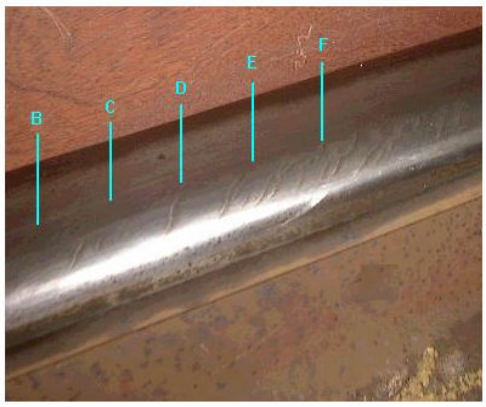

Referring to Figure 148 it is observed that at traces E and F, within a region of gauge corner cracking the signals show signs of modification. Figure 150 shows a comparison of the spectra of the trace F signals recorded for both the good and gauge corner cracked rail. In Figure 150 the good rail shows an approximation to the sinc function distribution for the acoustic Rayleigh wave spectra centered around the transmitted frequency of 140 kHz. This is the expected spectra for a single cycle single frequency transmission. For the gauge corner crack rail there is clearly seen the formation of "notches" within the spectra. Some of the frequency components have been lost within the 100 to 190 kHz band. The reason for the losses is not clear, however the cracks in the rail possibly act as a filter, reinforcing some of the spectral components and removing others.

Figure 150 Spectra of good and damaged rail

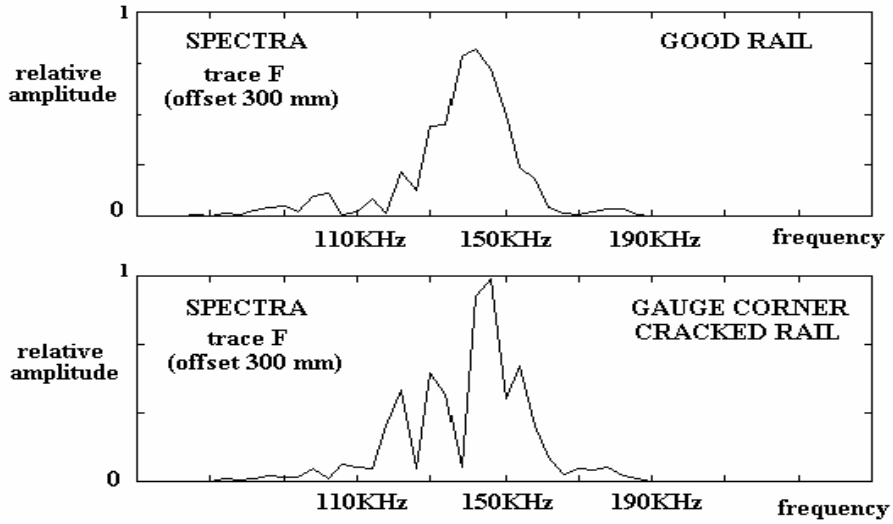

6.2.7 Concrete

Tests were also performed on concrete samples.

Concrete has an acoustic impedance that varies between 8 and 12 MRayls. The density is wide ranging from 1900 to 2500 kg/m^3 depending on porosity.

The p-wave velocities vary from 3500 to 4800 m/sec, the s-wave velocities from 2200 to 3100 m/sec and the Rayleigh wave velocity 1200 to 2900 m/sec. Poisson's ratio is between 0.20 and 0.23. The acoustic attenuation quoted by Chung and Law [40] is 9 to 45 dB/m at 50 kHz, quoted by Gaydecki [41] at 33 to 145 dB/m for 25 to 250 kHz. and determined by Armitage [1] as 17 to 42 dB/m for 50 to 150 kHz in a high density concrete rods. From these physical properties it can be seen that the transducers will

perform well since they are designed to be acoustically matched to materials of around 12 MRayls, a value within the range of most types of concretes. The operational testing frequencies for concrete will have to be lower since the acoustic attenuation in concrete is much greater than metals (steel 4.8 dB/m, at 100 kHz). The attenuation is less than carbon composites (130 dB/m, at 50 kHz), however the sample sizes are expected to be larger than the carbon composite test specimens and therefore a greater range will be required and consequently a lower frequency.

Concrete cube tests

This test object investigated cosisted of a small cube (50 x 50 x 50 mm) of concrete containing a fine aggregate. The two samples tested, one good sample, the other damaged with a crack that runs through the whole length of the sample, are shown in photographs of Figure 151. The transducer placements are shown in Figure 152.

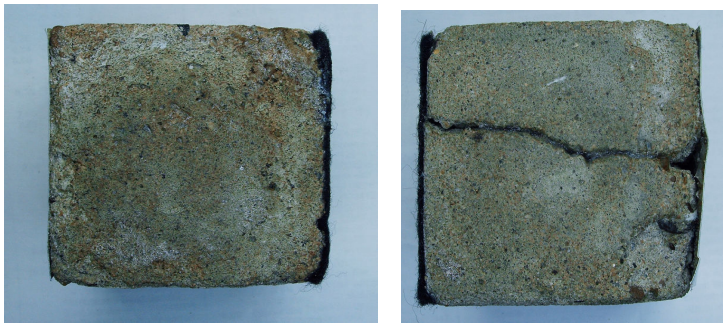

Figure 151
Concrete cube test samples

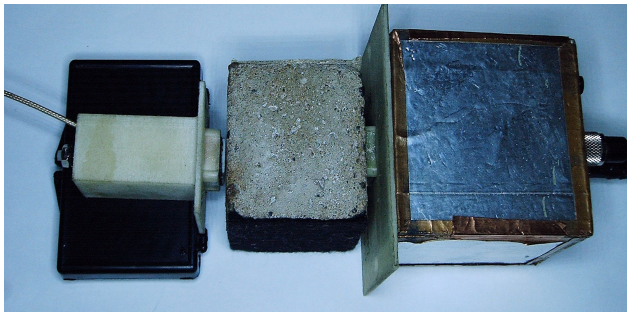

Figure 152 Transducer placements

Left receiver:- prototype transducer
Right transmitter:- NBOX module 5
coupling:- petroleum gel

Dual frequency transmission in good and defective concrete cubes

The sum of two sine waves of frequency 40 kHz and 120 kHz were transmitted continuously through the good and bad sample cubes. In the damaged sample the wave was transmitted along the crack. The time and frequency response is shown in Figure 153.

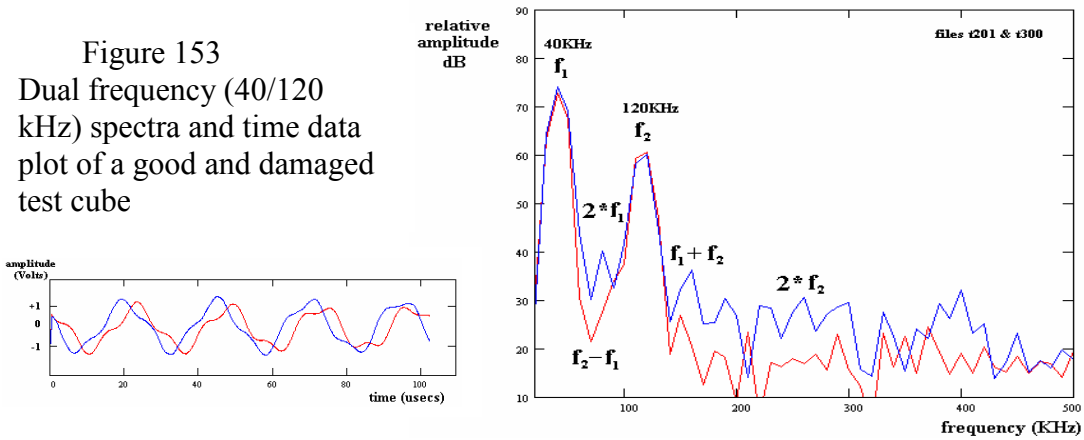

Figure 153
Dual frequency (40/120 kHz) spectra and time data plot of a good and damaged test cube

The data for the damaged sample is shown in blue, and the good sample shown in red. The damaged sample clearly shows that harmonics and inter-modulation products have been generated by the crack. The frequency ($f_1 + f_2$) at 160 kHz is -54 dB (0.2%) for the good sample and rises to -37 dB (1.4%) in the damaged sample. The frequency ($f_2 - f_1$) at 80 kHz also corresponds to the frequency of the second harmonic of f_1 ($2* f_1$), these two combine and produce a level of -46 dB (0.5%) in the good sample and rises to -34 dB (2%) in the bad. The second harmonic of f_2 ($2* f_2$) at 240 kHz has a less significant change, -56 dB (0.16%) in the good sample and rising to -49 dB (0.36%) in the damaged sample. The effect of the combinations of the harmonics and multiples of the inter-modulation products are very noticeable in the frequency range 200 to 350 kHz. For example, $2f_2$ (240 kHz), $2f_1+f_2$ (200 kHz), f_1+2f_2 (280 kHz) and $2f_1+2f_2$ (320 kHz). The result is the formation of peaks and troughs within this range, corresponding to the interaction of their frequencies and phases, this can mask the changes between the good and bad samples. The correct choice of the two frequencies f_2 and f_1 is an important factor.

Figure 154 Dual frequency (40/95 kHz) spectra of a good and damaged test cube.

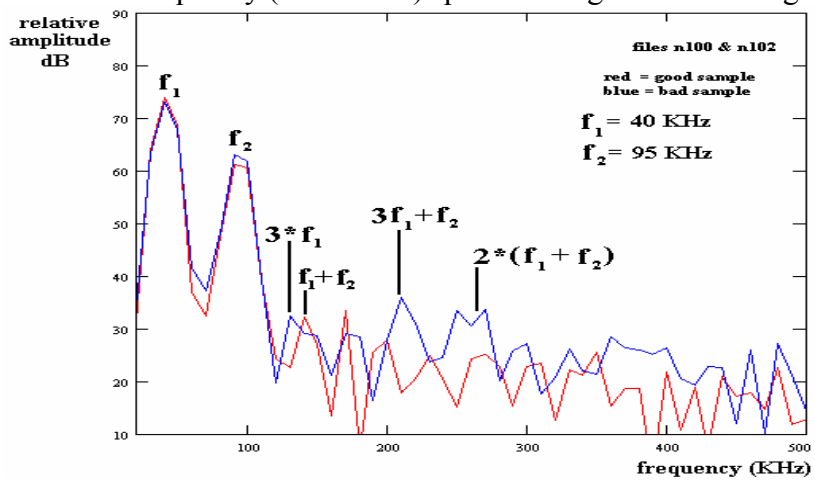

Figure 154 shows the spectra resulting from two different frequency combinations illustrating this effect. The inter-modulation product (f_2-f_1) is masked by f_1. The inter-modulation product (f_1+f_2) is masked by $3f_2$. However the multiples $3f_1$+f_2 and $2(f_1+f_2)$ are clear.

Concrete cylinder tests

This test object consisted of two standard test cylinders of concrete (300 mm long by 150 mm diameter) containing a medium sized aggregate. Two samples were tested, one good sample, the other damaged by being subject to a compressional load to a point where cracks had started to form at the surface. The test samples are shown in photographs of Figure 155a and 155b.

The p-wave velocity measured using a Pundit instrument was found to be 4120 m/sec for the good sample and 2650 m/sec for the cracked sample, this measurement being taken along the cylinders length.

Figure 155a Cracked concrete cylinder

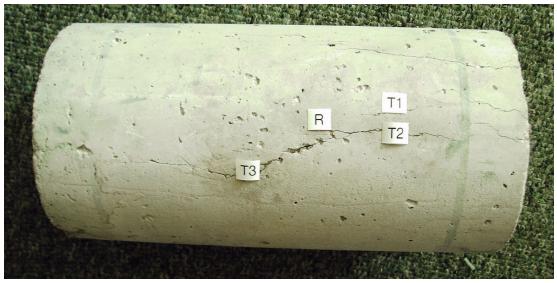

Figure 155b Undamaged cylinder

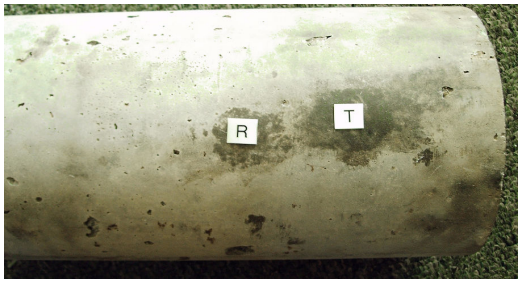

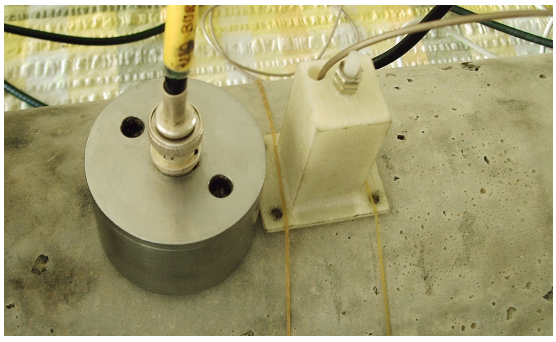

Figure 156

Photograph of transducers on concrete test cylinder

right:- Pundit 50 kHz transducer
left:- Prototype transducer

Single frequency harmonic generation near and on a cracked concrete cylinder

For this test a Pundit fixed frequency (50 kHz) narrow band transducer was used as a transmitter, shown in the photograph of Figure 156 and a prototype wideband transducer used as a receiver.

Various comparisons were made, first a reference for the spectra resulting from a good sample (the undamaged cylinder) was recorded with the transmitter placed at location T and the receiver placed at location R (see Figure 155b).
A set of measurements were then taken on the cracked cylinder, with the transmitter located at T1 and the receiver at R, and then again with the transmitter located at T3 (see Figure 155a). The resulting spectra for these two series of measurements are given in Figures 157 and 158.

Figure 157 spectra mild crack

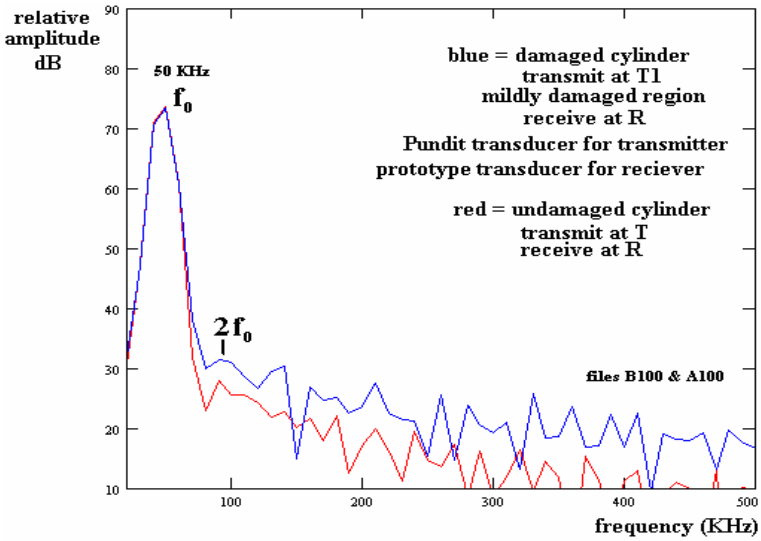

Figure 158 spectra severe crack

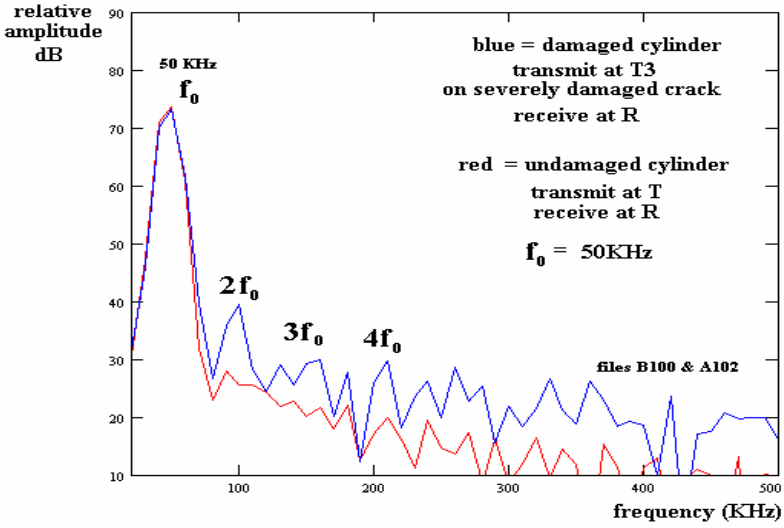

With the transmitter in a mildly cracked region (Figure 157) there is a general increase in the level of frequency components but nothing particularly significant. The second harmonic rises from -45 dB (0.6%) to -43 dB (0.7%), which is not a clear indicator of

damage. With the transmitter on a crack (Figure 158) there is a significant change, the second harmonic rises from -45 dB (0.6%) to -34 dB (2%), the third harmonic rises from -50 dB (0.3%) to -43 dB (0.7%), and the fourth harmonic from -54 dB (0.2%) to – 45 dB (0.6%).

Dual frequency harmonic and inter-modulation product generation on large cracked concrete cylinder

For this test the dual frequency transmitter NBOX module 5 was used to make measurements on both test cylinders. The transmitter placed on a large crack at location T3 (see Figure 155a). The receiver (prototype transducer) positioned at R on the damaged cylinder. For the undamaged cylinder, transmit and receive positions were T and R (see Figure 155b). The resulting spectra are shown in Figure 159.
It can be seen from this figure that the most significant changes are in $2(f_1+f_2)$ rising from -46 dB (0.5%) to -40 dB (1%)and in f_1+2f_2 which rises from -51 dB (0.3%) to – 39 dB (1.1%) in the damaged cylinder.

Figure 159 Dual frequency (40/70 kHz) response of a surface crack in concrete test cylinder.

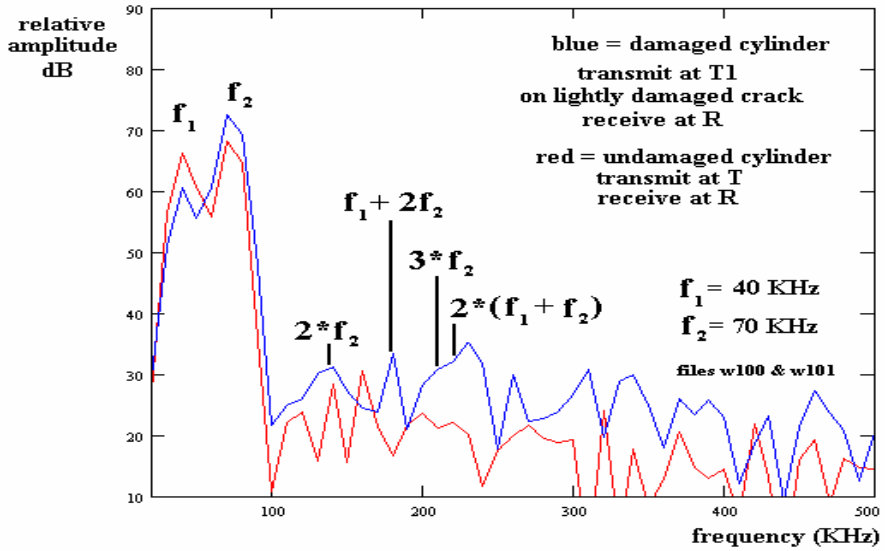

Harmonic generation on an undamaged multi-aggregate block

This experiment was to determine the linearity of an undamaged concrete block containing multi-sized aggregates using the harmonics generated by a 50 kHz, 20 Volt peak signal. The test block is shown left in Figure 160, the transmitter being placed at T (red) and the receiver in the centre R (green). Figure 161 shows the frequency spectra.

All harmonics are below -40 dB (1%). It is concluded that it should be possible to use harmonic generation as a means to test concrete of variable aggregate size as there is a low base level of harmonic generation and we can use both gel and plastic film coupling. 50 kHz provided a sufficient test level of signal but frequencies above 70 kHz showed a very high degree of attenuation.

Figure 160

Multi-aggregate test block

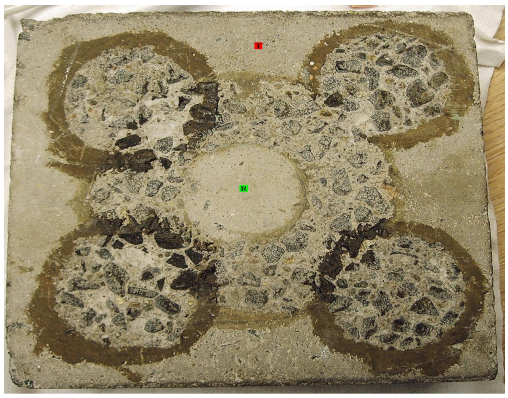

Figure 161

Spectra of mulit-aggregate test block

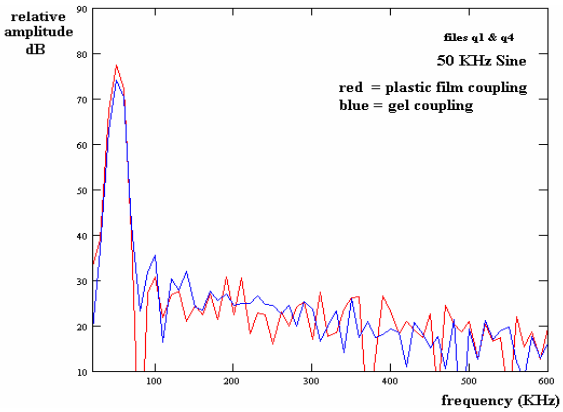

Harmonics and inter-modulation products generation from a drilled core with known micro-crackingn (transmitting through the sample).

For this test a drilled core sample of concrete with known micro-cracking was used, the sample is shown in the photograph of Figure 162a. In addition the sample had a large crack which extended throughout its whole length. A dual frequency transmitter NBOX module 5 was place on one side of the test core and the receiver placed on the other side, as shown in this photograph.

Figure 162a Drilled concrete test core with micro-cracking

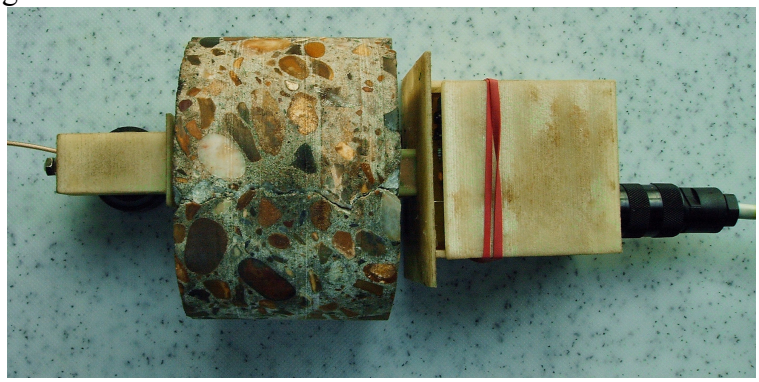

Figure 162b shows high magnification photographs of a section through the core sample, provided by Geomaterials Research Services Ltd and taken using epifluorescence illumination with a Zeiss Axioskop polarizing photomicroscope.

Figure 162b High magnification photographs of the core sample,

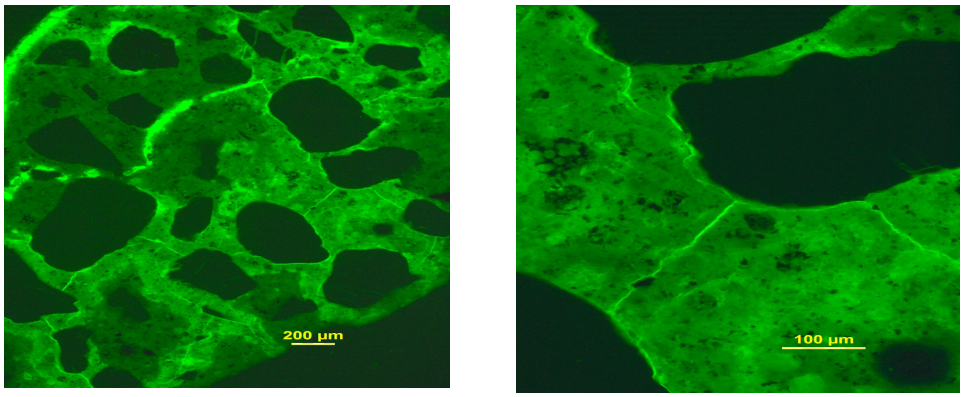

Drilled core micro-cracked concrete test sample (dual frequency)

Two frequency spectra were examined and are given in Figure 163, one with the transmitter and receiver located near to the crack (blue), the other was made with the transmitter and receiver located near an edge furthest away from the crack (red).

Figure 163 Dual frequency spectra of micro cracked test core

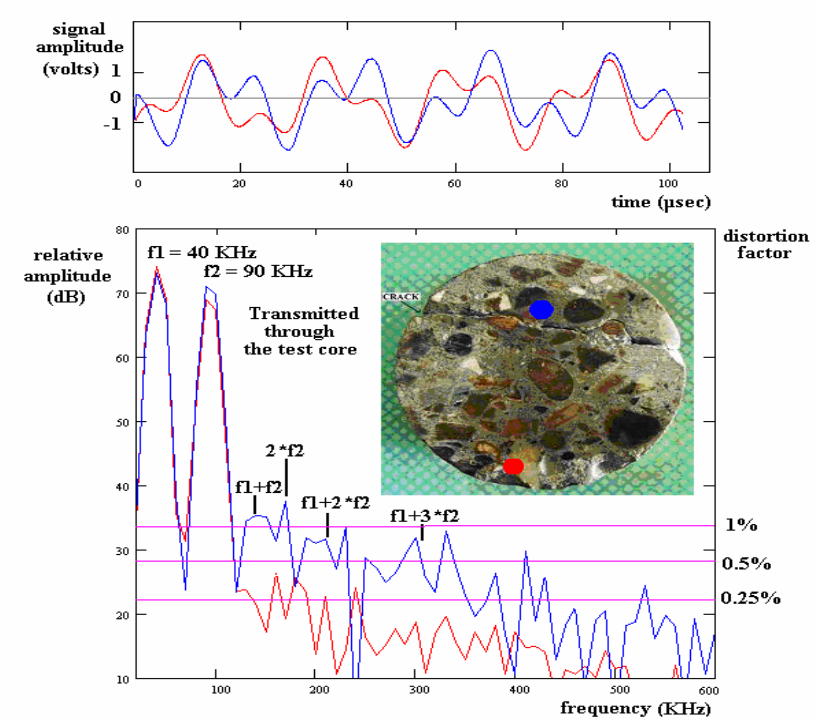

The most significant changes are in f_1+f_2 which rises from -52 dB (0.25%) to -39 dB (1.1%) and in the second harmonic of f_2 ($2*f_2$) which rises from -50 dB (0.3%) to -36 dB (1.6%) There is also a considerable rise in the frequency band 200 to 350 kHz, this corresponds to the sidebands, harmonics and inter-modulation products $2(f_1+f_2)$, f_1+2*f_2 and f_1+3*f_2,

Harmonic generation from a drilled core with known micro-cracking transmitting through the sample (single frequency)

This experiment involved sending a single frequency (40 kHz) through the sample core at two locations, shown in red and blue in the photograph of Figure 164. This Figure also shows the spectra resulting at these two locations. The cracked (blue) region shows significant generation of a range of harmonics. In this region the 2nd, 3rd and 4th harmonics are all above -42 dB (0.8%). Away from the crack, in the red region, the 2nd harmonic is below -46 dB (0.5%) and the other harmonics below -50 dB (0.3%).

Figure 164 Drilled core micro-cracked concrete test sample (single frequency)

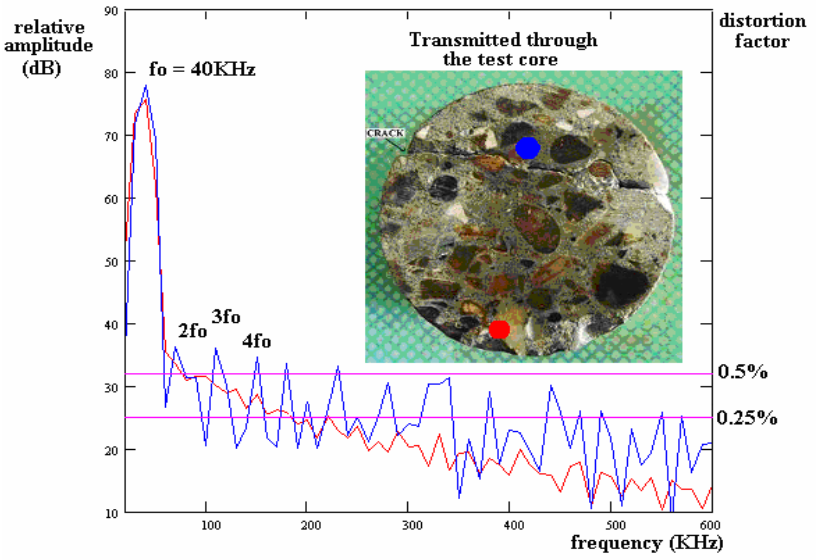

Harmonic generation from a drilled core with known micro-cracking, transmitting over the surface of the sample (single frequency).

In this experiment a sine wave of 40 kHz frequency was transmitted and received on same side of the test sample as shown in the photograph of Figure 165.

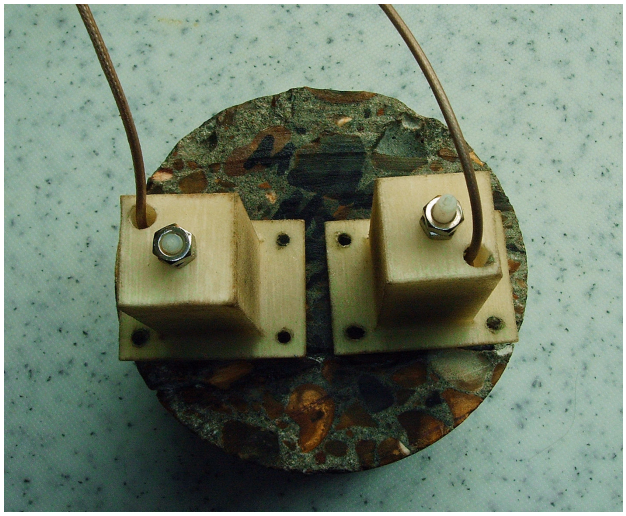

Figure 165

Single side testing of drilled concrete test core

Figure 166 shows the spectra received over two regions of the surface indicated by T (transmission) and R (reception), blue for the region near the crack and red for the region away from the crack.

Figure 166 Spectra of drilled test core (single frequency, over surface)

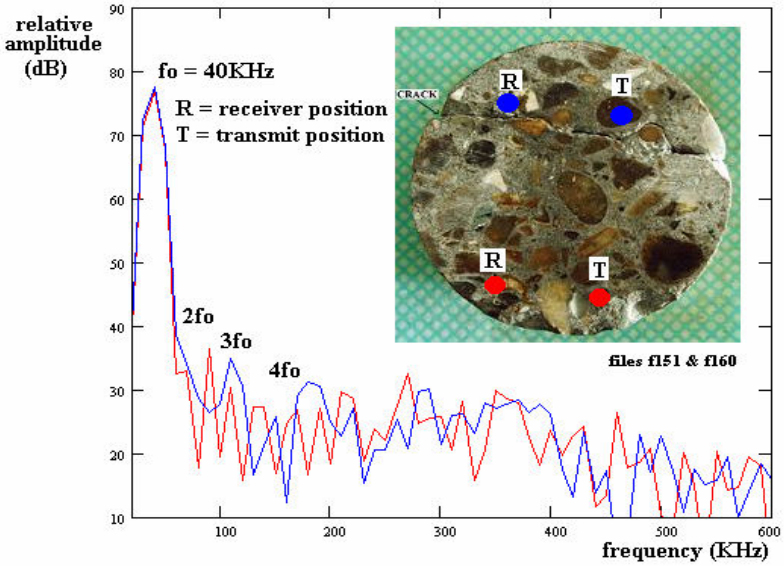

Both regions show poor signs of the generation of harmonics, the region near the crack (blue) shows a distinct 3rd harmonic at -43 dB (0.7%) below the fundamental, whereas in the region away from the crack (red) it is weaker at -48 dB (0.4%). Considerable amounts of noise are generated in both regions. The results from this test suggest it is not possible to discriminate a good and bad region over such a short surface distance. The use of a higher frequency sine wave may resolve this problem as the insonified region will be more localized.

Harmonic and inter-modulation product generation from a drilled core with known micro-cracking, transmitting over the surface of the sample (dual frequency).

In this experiment a dual frequency transmitter (NBOX module 5) was used to transmit two frequencies over the surface of the test sample. Again two regions for recording were selected, one near the crack, the other far from the crack, shown in Figure 167

Figure 167 Spectra of drilled test core (dual frequency, over surface)

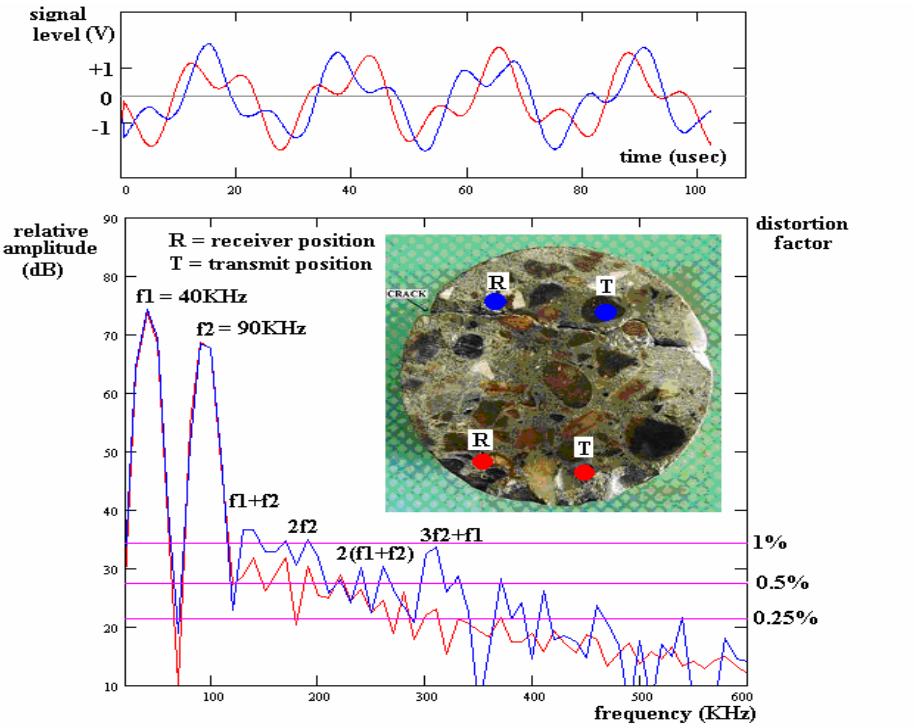

In the region away from the crack (red) there is observed the generation of noise but at a level only slightly less than that present in the region near to the crack (blue), which shows some harmonics and inter-modulation products. It is concluded that over the surface of the sample, with the transducers separated by a large distance the micro cracks have a great influence on the transmitted and received signals and produce high levels of noise.

The following and final chapter gives the conclusions of the research work carried out and presented in this thesis together with suggestions for further investigations and commercial exploitation.

7 CONCLUSIONS AND FUTURE WORK

7.1 Conclusions

The research detailed in this thesis has shown that the measurement of the non-linear acoustic properties of a material can provide a very sensitive method by which to detect the onset of progressive mechanical damage, particularly at the early stages before other conventional testing method start to register defects. This ability was illustrated dramatically in the experiment given in chapter 6.2.4 involving an aircraft steel steering actuator bracket, after 20,000 cycles of loading no defects were detected in any regions of the bracket using conventional ultrasonic and magnetic induction testing methods. The non-linear technique indicated a defective region and a prediction made of failure to occur in this region. At 128,000 cycles of loading this region developed an observable crack.

The research has shown that the lowest level of non-linearity using harmonic and inter-modulation spectra analysis that can practically be measured using contacting piezoelectric sensors and actuators on metals, carbon composite and concrete materials glued to the surface with cyanoacrylate adhesive is 0.3% (-50dB), with a gel coupling 0.4% (-48dB) and with a solid plastic coupling 0.6% (-44dB).

For the materials investigated by the author within this research program it has been shown that measurement of non-linearity below 1.0% (-40dB) indicates that the material is good. Values above this up to 1.8% (-35dB) indicate the onset of degradation, values between 1.8% and 3.2% (-32dB) indicate damage and values above 3.2% indicate serious damage.

Measurements of non-linearity based on using the pulse inversion method, detailed in chapters 2.5, 6.2.1 and 6.2.4 indicate that if the ratio of the maximum compressional wave amplitude to the maximum tensile wave amplitude has a value between 1.0 and 0.95 the material is considered to be good, values between 0.95 and 0.8 indicate damage and values below 0.8 indicate serious damage.

Further experimental research will be required to identify the limits over which a material is considered usable (its design life range) and at which level the material is considered likely to fail and needs to be removed from service.

The research has highlighted that for non-linear measurements it is important to ensure good acoustic contact between the transducers and the material under test and careful monitoring of the acoustic signal level will be required, too large signals may cause non-linear effects at the transducer coupling and over drive the electronics. Too low acoustic signal levels will not provide a clear spectrum as noise and electrical pickup may be detected. Spectral resolution considerations have also been shown to be an important factor to consider particularly if at a later date automatic determination of the levels of the harmonics is to be performed by software programs and provide to the operator a numeric evaluation.

From a practical point of view the research has shown that determination of the condition of a material will ideally be determined by a combination of tests using spectral, pulse inversion and frequency deviation since this would provide a greater certainty of defect detection, however in reality the tests applied depend upon the size and composition of the test object. For large objects made of metals the resonant frequency deviation method is most suitable, providing a cheap rapid testing procedure. For small objects made of carbon fibre composite materials that have undergone micro-cracking the frequency deviation method may not be possible as sufficient resonant amplitude will not be generated due to the acoustic attenuation. In these situations the harmonic and inter-modulation spectra or pulse inversion techniques provide a more suitable testing methodology.

The investigations carried out by the author have shown that there are some limitations to this technique. Non-linear harmonic and inter-modulation product spectral analysis will not be able to measure large metal objects that have undergone severe damage, chapter 6.2.5 gives details of tests performed on a steel fork leg having a large crack defect, the technique being unable to detect the fault. Other ultrasonic techniques and visual inspection methods will be more suitable in these situations, however for early stage material degeneration and testing of composite materials the non-linear ultrasonic technique has shown to be very successful and provides great potential in applications requiring the long term health monitoring of materials.

Within the research program, undertaken by the author and presented within this thesis, there was conducted concurrently with the experimental investigations of the non-linear properties of progressively damaged materials the development of instrumentation and a system by which the non-linear acoustic method could be commercially exploited. This development anticipated the requirement to extend the capabilities of this technique to a very wide range of objects of differing materials and sizes. The design philosophy adopted was that of an iterative process involving the use of inter-connecting SMART modules, a selection of these modules being made and assembled to perform a specific testing task. This research highlighted the types and limitations of various interconnecting methods of SMART modules and these are detailed in sections 5.3 and 5.4. It is the conclusion of the author that this "pick and mix" method is the best approach to take when implementing the non-linear testing methodology.

Two of these instrument developments by the author are completely original the first is a direct contact transducer to detect the impulse response of a compressional and a tensile acoustic pulse. By comparing these responses non-symmetric non-linear properties of the material can be measured and quantified. The second method is an instrument that provides real time measurement of the frequency shift that occurs when a defective material that has been made to oscillate at its resonant frequency starts to decay in amplitude.

In conclusion this research has extended our knowledge of the measurement of non-linear acoustic properties of materials by introducing new instruments and techniques that detect departures from the linear stress-strain relationship that occur when materials undergo micro-cracking or de-lamination. The experimental work utilising these new instruments have provided evidence that the non-linear acoustic method is a practical and viable technique that can be applied to a wide variety of materials.

7.2 Hardware development

The Hardware development can be split into two parts, the first being transducer development and the second being the instrumentation development.

Transducer development

The development of the transducers will play a very significant role as the non-linear acoustic testing method is introduced into a wide range of industries. Different frequency ranges, sizes, coupling and application, use on a wider range of materials. As an example concrete will require lower frequency range but more power. Scanning large aircraft wings may require "rolling" wheel transducers. We may need to test materials that are covered in cloth, requiring transducers with pins to provide contact through the cloth.

The mathematical models developed for the transducer design given in this thesis may need to be extended and improved to provide greater performance prediction. One such model that provides a greater accuracy is called the KLM model, this is illustrated in Figure 168.

Figure 168 The KLM model

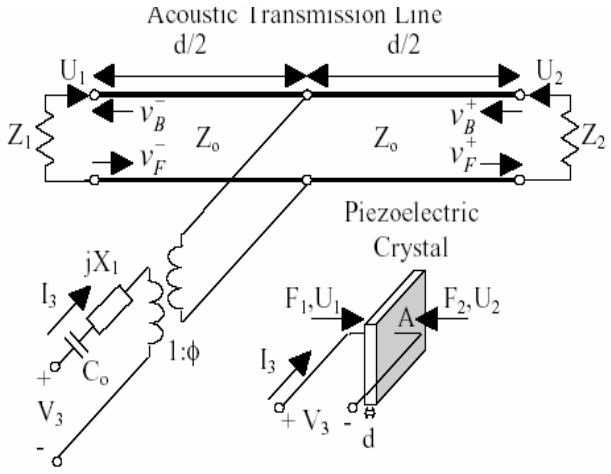

Where; X1 is a electrical reactance resulting from the dynamic behaviour of the charges released in the piezoelectric crystal. Co the static capacitance of the piezoelectric plate. Zo the acoustic impedance of the piezoelectric crystal. Z1 and Z2 are the mechanical acoustic impedances of the load applied to the two faces of the piezoelectric crystal.

In this model the electrical and mechanical parts are separated and clearly distinguished, it also allows for the calculation of the electrical impedance for a given acoustic load. The model has been used with some successes by the author previously and is described in Krimholtz[37]. For advanced work various computer aided design packages are currently available to aid detailed transducer design, one such example is TransCAD which is mainly used for marine applications such as SONAR and underwater communications, see Maguire[42].
For unusual transducer applications that may require shaped contact to a material, for example pin point contacts, various models exist to aid design. One of the most useful guides to shaped acoustic components is given in Gal'perina[43].

Instrumentation development

Some factors relating to the hardware development found during the research were that it is important to ensure good transducer contact to the test material, the monitoring of signal levels was important, ensuring the acoustic signal levels are not too large (avoid over-driving amplifiers) or acoustic signal levels are not too small (noise and electrical pickup) and if possible use a combination of tests (spectral, pulse inversion, freq dev). These factors will influence future instrument design, there will be a requirement to use Automatic Gain Control (AGC) circuitry to maintain signal levels to within acceptable limits and to provide an indication if they are outside these limits, this also provides a simple indication to the operator that a good contact has been made between the transducer and the material under test.. The hardware will also be required to have advanced programming in order to perform automatically a sequence of tests, thereby improving the confidence of the detection of a fault.
Currently various development programs of the NBOX and non-linear acoustic technology are being undertaken by the author. The most recent is that of its application to concrete structures, some of this work has been included in this thesis, and is currently ongoing with further experimental testing being carried out. It is apparent that for concrete structures the working frequencies will be lower, typically 20 to 60 kHz, since the attenuation of ultrasound in this material is high particularly above 50 kHz. Higher levels of transmitted power will also be required and will depend upon the type of the aggregates used. Testing at these lower frequencies will require a higher spectra resolution, this being achieved by longer recording times or a reduced sampling rate. The requirements of the civil engineering industry are that instrumentation must be

totally portable, easy to use, light weight and internally powered by batteries. Facilities must include a link to lap top PC for more detailed investigations. The instrument software must be able to be updated via a serial link connection to the unit.
Other applications in a wide range of industries are in negotiation which will involve additional hardware instrumentation development at a later date.

7.3 Software development

Software advances will progress on two fronts, the first being the development of methods and algorithms by which the defects can be automatically assessed and analysed. This may include expert systems and the use Neural Networks. However advances in these fields can only be undertaken with the necessary experimental data, which will involve considerable expense and time.
The second area of progression which can be implemented immediately and at relatively low cost is to examine cost savings in the PC and NBOX operational software. Considerable savings could be made by shifting some or most of the signal processing functions, fault identification or analysis, from the Java programming running on the PC to the assembly program running on the NBOX microprocessors. In this way less information will be required to be sent along the serial communications link, for example sending the spectra information only will result in considerable savings in bandwidth and transmission time. Recent advances in development of PIC microprocessors have produced a new family of devices the PIC24 series which include on chip hardware multipliers which perform high speed FFT and other signal processing functions. These would be particularly suited in reducing the bandwidth requirements for time reversal NEWS methods.

7.4 Closing discussions

Further developments of this interesting technology are now underway, with patents being filed and the technology starting to be applied to wide range of commercial markets. This technology is now being spun out from the primary activity in the Aviation industry into the Railway, Civil Engineering, Marine and the oil / gas production industries. In the rail industry it is expected to provide alternative testing methods and health monitoring procedures for railway tracks and other rail critical components such as switches and signalling. In the Marine industry modern boat constructors and operators are particularly interested in monitoring the state of ship hulls which are now composed of a wide range of materials such as epoxy-fibre composites, steel or concrete. Currently the ultrasonic pulse echo method is used but is unsatisfactory when trying to measuring the thickness and damage of thin hulled vessels. This is because the transmission time to the first return received signal is very short and does not provide sufficient depth resolution. Non-linear techniques rely only on spectral information, the transit time is of no importance. The oil and gas production industries will greatly benefit from this technology, particularly in testing oil and gas pipelines. One of the most serious problems today is the scouring of the inside of gas pipes due to rock particles within the gas flow, in order to minimise and monitor this damage flow rates are reduced and pipe thicknesses periodically measured. The non-linear acoustic technique will supplement this testing procedure to include the detection of micro-scale damage that could eventually leads to catastrophic pipe failures.
Manufacturing industries may also benefit from this technology by incorporating it into quality control during and after manufacture. Some interest has already been shown in manufactures of drain covers and ceramic tiles.
In the Civil engineering sector buildings, bridges and other large concrete structures need to be monitored for micro-cracking, this type of defect being a precursor for water ingestion which ultimately leads to frost damage and re-bar oxidation.
A major manufacturer of conventional ultrasonic testing equipment for this industrial sector has expressed interest in the technology for testing and evaluating concrete structures and currently a pre-production instrument is being developed for this application. In addition a paper has been written detailing some of the experiments from this thesis and has just been peer reviewed and accepted for publication. It will be presented in July at the third international conference on concrete repair (Concrete

Solutions) in Venice, Italy. Additional interest within the aviation industry has recently been expressed for its application to testing rotary wing aircraft. A presentation will be given on this technology to the 7th International Helitune Conference in Viterbo in a few days time.

The advances in non-linear acoustic detection of damage made in this thesis may well lead to widespread adoption and application of this powerful new technique.

APPENDIX A

Relationship between the elastic constants

A table of the relationship between the elastic constants from Hartsuijker[44] is given in table 6.

Table 6 The relationship between the elastic constants

	λ, μ	E, μ	B, λ	B, μ	λ, v	μ, v	E, v	B, v	B, E	M, μ
B	$\lambda + \frac{2\mu}{3}$	$\frac{E\mu}{3(3\mu-E)}$			$\frac{\lambda(1+v)}{3v}$	$\frac{2\mu(1+v)}{3(1-2v)}$	$\frac{E}{3(1-2v)}$			$M-\frac{8\mu}{3}$
E	$\frac{\mu(3\lambda+2\mu)}{\lambda+\mu}$		$\frac{9B(B-\lambda)}{(3B-\lambda)}$	$\frac{9B\mu}{3B+\mu}$	$\frac{\lambda(1+v)(1-2v)}{v}$	$2\mu(1+v)$		$3B(1-2v)$		$\frac{\mu(3M-4\mu)}{M-\mu}$
λ		$\frac{\mu(E-2\mu)}{3\mu-E}$		$B-\frac{2\mu}{3}$		$\frac{2\mu v}{1-2v}$	$\frac{Ev}{(1+v)(1-2v)}$	$\frac{3Bv}{1+v}$	$\frac{3B(3B-E)}{9B-E}$	$M-2\mu$
μ			$\frac{3(B-\lambda)}{2}$		$\frac{\lambda(1-2v)}{2v}$		$\frac{E}{2+2v}$	$\frac{3B(1-2v)}{(2+2v)}$	$\frac{3BE}{9B-E}$	
v	$\frac{\lambda}{2(\lambda+\mu)}$	$\frac{E}{2\mu} - 1$	$\frac{\lambda}{3B-\lambda}$	$\frac{3B-2\mu}{2(3B+\mu)}$					$\frac{3B-E}{6B}$	$\frac{M-2\mu}{2M-3\mu}$
M	$\lambda+2\mu$	$\frac{\mu(4\mu-E)}{(3\mu-E)}$	$3B-2\lambda$	$B+\frac{4\mu}{3}$	$\frac{\lambda(1-v)}{v}$	$\frac{\mu(2-2v)}{(1-2v)}$	$\frac{E(1-v)}{(1+v)(1-2v)}$	$\frac{3B(1-v)}{(1+v)}$	$\frac{3B(3B+E)}{9B-E}$	

where:- B = Bulk modulus E = Youngs modulus

λ = Lame's first constant μ = Lame's second constant (shear modulus)

v = Poisson's ratio M = p-wave modulus

APPENDIX B

Table 7 is a conversion table from Sengpielaudio[45] that gives the relationship between the distortion factor expressed as –dB from the fundamentals magnitude to the distortion factor expressed as a percentage of the fundaments magnitude. This reference, which is an internet site, also contains many other conversion tables related to audio and electronics.

Table 7 Conversion table :- Distortion dB to factor %

Distortion Factor (dB)	(%)	Distortion Factor (dB)	(%)	Distortion Factor (dB)	(%)	Distortion Factor (dB)	(%)	Distortion Factor (dB)	(%)	Distortion Factor (dB)	(%)
-10	31.6	-20	10	-30	3.2	-40	1.0	-50	0.32	-60	0.100
-11	28.2	-21	8.9	-31	2.8	-41	0.89	-51	0.28	-61	0.089
-12	25.1	-22	7.9	-32	2.5	-42	0.79	-52	0.25	-62	0.079
-13	22.4	-23	7.1	-33	2.3	-43	0.71	-53	0.22	-63	0.071
-14	19.9	-24	6.3	-34	2.0	-44	0.63	-54	0.20	-64	0.063
-15	17.8	-25	5.6	-35	1.8	-45	0.56	-55	0.18	-65	0.056
-16	15.8	-26	5.0	-36	1.6	-46	0.50	-56	0.16	-66	0.050
-17	14.1	-27	4.5	-37	1.4	-47	0.45	-57	0.14	-67	0.045
-18	12.6	-28	4.0	-38	1.3	-48	0.40	-58	0.13	-68	0.040
-19	11.2	-29	3.6	-39	1.1	-49	0.36	-59	0.11	-69	0.036

Distortion (-dB) = 20 log10 [Factor(%) / 100]

Factor (%) = 100 * $10^{\text{Distortion(-dB) / 20}}$

if using a calculator:-

Factor (%) = 100 * (inv $\log_{10}$ [Distortion(-dB) / 20])

APPENDIX C

Piezoelectric material specification

Data supplied Sensor Technology Ltd [46].

PZT / epoxy composite specification:-

Acoustic Impedance = 12 MRayls

Composite element piezoelectric BM532

Supplied sample size = 35 * 35 * 5 mm

1-3 connecting pattern

Relative Dielectric Constant KT_{33} = 890 +/- 20%

Dissipation factor = 0.03

Frequency Constant (N3) = 1475 +/- 5%

Coupling factor K_{ε} = 0.62

Mechanical Quality factor Q (unloaded) = 5

Ceramic volume = 25-30%

Operating frequency range = 150kHz to 1.5MHz

Specification for pure BM532:-

Operating frequency range = 150kHz to 1.5MHz

Relative Dielectric constant KT_{33} = 3250

Dissipation factor = 2.0%

Coupling factor K_p = 0.56, K31 = 0.34, K33 = 0.68

Charge constant $d_{31} = -250*10^{-12}$ C/N, $d_{33} = 630*10^{-12}$ C/N

Voltage constant $g_{31} = -7.5*10^{-3}$ Vm/N, $g_{33} = 20*10$ V^{-3}m/N

Mechanical Quality factor Qm = 70

Frequency constants Np = 2100 Hz.m, N1 = 1425 Hz.m, N3 = 1850 Hz.m

Elastic Modulus Compliance $SE_{11} = 14.0*10^{-12}$ m^2/N, $SE_{33} = 20.0*10^{-12}$ m^2/N

Density 7.65 gms/cc

Curie temperature T_c = 210 deg C

Ageing characteristics:- coupling factor K_p = -1.0

Dielectric constant KT_{33} = -1.0

Frequency constant N_p = 1.0 Hz.m

Definition of piezoelectric constants from Morgan[47]:-

direct effect:- reverse effect:-

$d = \frac{\text{short circuit charge density}}{\text{applied mechanical stress}}$ $[C\ N^{-1}]$ $d = \frac{\text{strain developed}}{\text{applied field}}$ $[m\ V^{-1}]$

$g = \frac{\text{open circuit electric field}}{\text{applied mechanical stress}}$ $[V\ m\ N^{-1}]$ $g = \frac{\text{strain developed}}{\text{applied charge density}}$ $[m^2\ C^{-1}]$

Superscripts are used to describe external factors such as physical mounting, electrical conditions that effect the piezoelectric property. D indicates that electrodes are open circuit, E electrodes are short circuit, T no external forces applied, piezoelectric is free to move, S piezoelectric constrained preventing deformation in any direction. Subscripts describe the relationship of the property to the poling axis. 1 is the x-axis, 2 the y-axis and 3 the z-axis. Higher numbers are used to represent sheer around a particular axis, 4 represents sheer around axis 1, 5 represents sheer around axis 2 and 6 represents sheer around axis 3. In general the first subscript refers to the electrical connections (electrodes) and the second to the direction of the mechanical forces. For example, constant g_{31}, first subscript (3) indicates that the electrodes are perpendicular to the z-axis, the second subscript (1) indicates that the applied stress or piezo-electrically induced strain is in the x-axis.

The coupling coefficient relates the amount of energy that can be changed from the electrical form to the mechanical form or visa versa.

The coupling coefficient:-

electrically stressed component:- mechanically stressed component:-

$k^2 = \frac{\text{stored mechanical energy}}{\text{electrical energy applied}}$ $k^2 = \frac{\text{stored electrical energy}}{\text{mechanical energy applied}}$.

The efficiency of a transducer depends on the mechanical and dielectric loss as well as the coupling coefficient. The dielectric loss (or dissipation factor) is usually most significant and is given by:-

$$\text{dielectric loss} = \text{Tan}(\delta) = \frac{\text{series resistance}}{\text{series reactance}}$$

Quality factor, Q = (2π*energy stored during a cycle/ energy dissipated per cycle)

Frequency constant N = Controlling dimension x Resonant frequency [Hz m]

APPENDIX D

IEEE 1451 Standard

Information from this standard was obtained from IEEE[48]

IEEE 1451.2 is an open standard that gives sensor makers a way to interface to different types of field buses. A standard transducer interface module (STIM) described by the standard includes the sensor interface, signal conditioning and conversion, calibration, linearization and basic communication. The main goals for this standard are 1) to develop network independent and vendor independent transducer interfaces, 2) to allow transducers to be replaced and / or moved with minimum effort, 3) eliminate error prone, manual system configuration steps, 4) support a general transducer data, control, timing, configuration and calibration model, 5) develop Transducer Electronic Data Sheets (TEDS) that remain with the transducer during normal operation. The schematics below summarise the implementation of this standard.

Figure 169 Implementation of IEEE 1451

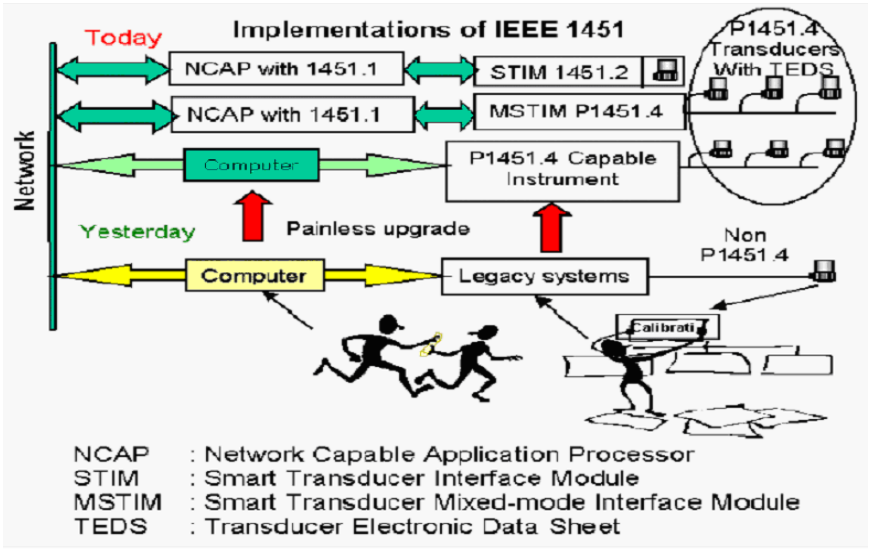

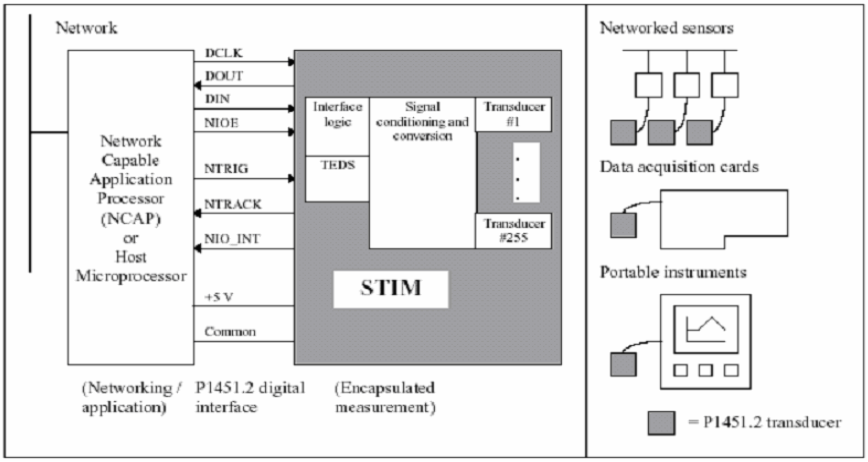

APPENDIX E

IEEE 802.11 Standard

Information from this standard was obtained from IEEE[48]

The IEEE 802.11 standard is the family of specifications created by the Institute of Electrical and Electronics Engineers Inc. for wireless and Ethernet local area networks. The scope of this standard is to develop a specification for wireless connectivity for fixed, portable, and moving stations within a local area, and to provide wireless connectivity to automatic machinery and equipment or stations that require rapid deployment, which may be portable, handheld, or which may be mounted on moving vehicles within a local area. Because radio waves are used, the communication does not have to be line of site, and even links through brick walls are possible over a limited range.

The RF transmission standards in the standard are Frequency Hopping Spread Spectrum (FHSS) and Direct Sequence Spread Spectrum (DSSS).

Both these are defined for operation in the 2.4GHz frequency band typically occupying the 83 MHz of bandwidth from 2.400 GHz to 2.483 GHz. Differential BPSK (DBPSK) and DQPSK is the modulation for the direct sequence. Frequency hopping uses 2-4 level Gaussian FSK as the modulation signalling method. The radiated RF power at the antenna is set by the rules governed by FCC part 15 for operation in the United States and ETSI in Europe. Antenna gain is also limited to 6 dBi maximum. The radiated power is limited to 1W for the United States, 10mW per 1MHz in Europe and 10-100 mW for Japan. There are different frequencies approved for use in Japan, United States and Europe and any WLAN product must meet the
requirements for the country where it is sold. The physical layer data rate for FHSS system is 1 and 2 Mbps. For DSSS both 1 Mbps and 2 Mbps data rates are also supported. In case of DSSS, High Data Rate, the Access Point must be capable of servicing 1, 2, 5.5 and 11 Mbps devices. The choice between FHSS and DSSS will depend on a number of factors related to the user's application and the environment that the system will be operating.

IEEE 802.11a = 5.7 GHz with data rates up to 54 Mb/s
IEEE 802.11b = 2.4 GHz (WI-FI) with data rates up to 11 Mb/s
IEEE 802.11g = 2.4 GHz with data rates up to 22 Mb/s

APPENDIX F

RF power conversion tables

The information in this section of the appendix was obtained from Balanis[49].

for a short dipole antenna:-

$$\text{Field Strength, E [volts / meter]} = \frac{\sqrt{49.2 * \text{Transmitter Power [watts]}}}{\text{distance [meters]}}$$

Voltage, V [dBμV / meter] = 20 $\log_{10}$ (E * 10^6)

Power measurement in [decibel meters] dBm = 10 $\log_{10}$ [power in milliwatts]

Power measurement in milliwatts = 10 (dBm /10)

Table 8 Power to field strength conversion for short dipole antenna

Power (watts)	Field Strength (volts / meter)	Volts (dBμV / meter)
100 W	70	157
10W	22	147
1W	7	137
100 mW	2.2	127
10 mW	0.7	117
1 mW	0.22	107
100 μW	0.07	97
10 μW	0.022	87
1 μW	0.007	77

APPENDIX G

Window Functions (Wikipedia[50]) Figure 170

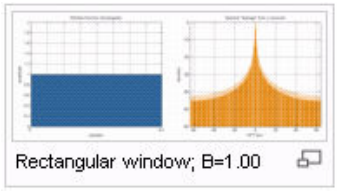

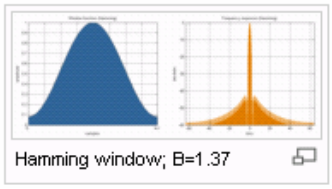

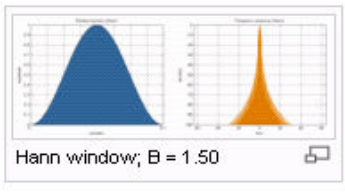

$$w(n) = 1$$

$$w(n) = 0.53836 - 0.46164\cos\left(\frac{2\pi n}{N-1}\right)$$

$$w(n) = 0.5\left(1 - \cos\left(\frac{2\pi n}{N-1}\right)\right)$$

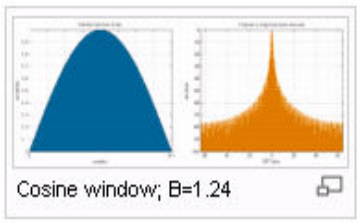

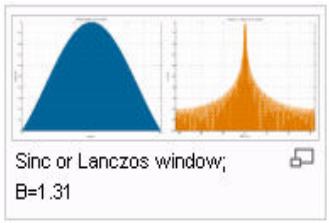

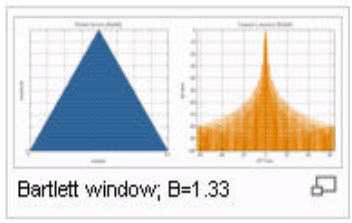

$$w(n) = \cos\left(\frac{\pi n}{N-1} - \frac{\pi}{2}\right) = \sin\left(\frac{\pi n}{N-1}\right)$$

$$w(n) = \operatorname{sinc}\left(\frac{2n}{N-1} - 1\right)$$

$$w(n) = \frac{2}{N-1}\cdot\left(\frac{N-1}{2} - \left|n - \frac{N-1}{2}\right|\right)$$

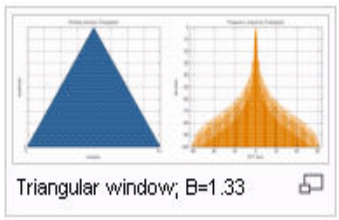

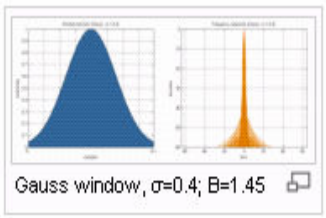

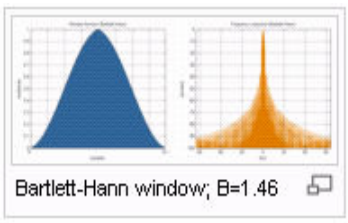

$$w(n) = \frac{2}{N}\cdot\left(\frac{N}{2} - \left|n - \frac{N-1}{2}\right|\right)$$

$$w(n) = e^{-\frac{1}{2}\left(\frac{n-(N-1)/2}{\sigma(N-1)/2}\right)^2}$$
$$\sigma \leq 0.5$$

$$w(n) = a_0 - a_1\left|\frac{n}{N-1} - \frac{1}{2}\right| - a_2\cos\left(\frac{2\pi n}{N-1}\right)$$
$$a_0 = 0.62;\quad a_1 = 0.48;\quad a_2 = 0.38$$

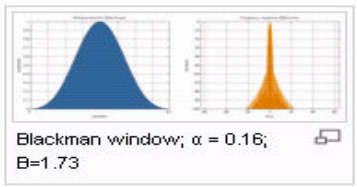

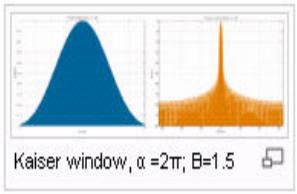

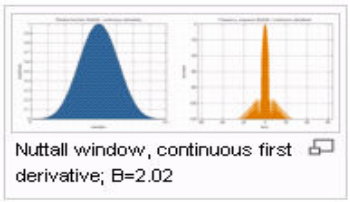

$$w(n) = a_0 - a_1\cos\left(\frac{2\pi n}{N-1}\right) + a_2\cos\left(\frac{4\pi n}{N-1}\right)$$
$$a_0 = \frac{1-\alpha}{2};\quad a_1 = \frac{1}{2};\quad a_2 = \frac{\alpha}{2}$$
unqualified term *Blackman window* refers to α=0.16.

$$w(n) = \frac{I_0\left(\alpha\sqrt{1-\left(\frac{2n}{N-1}-1\right)^2}\right)}{I_0(\alpha)}$$

$$w(n) = a_0 - a_1\cos\left(\frac{2\pi n}{N-1}\right) + a_2\cos\left(\frac{4\pi n}{N-1}\right) - a_3\cos\left(\frac{6\pi n}{N-1}\right)$$
$$a_0 = 0.355768;\quad a_1 = 0.487396;\quad a_2 = 0.144232;\quad a_3 = 0.012604$$

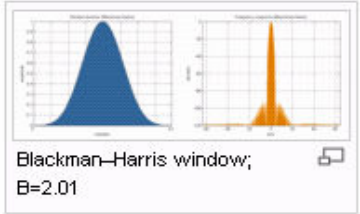

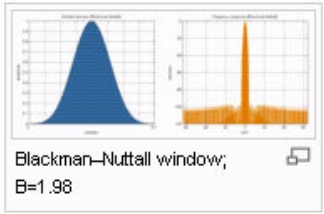

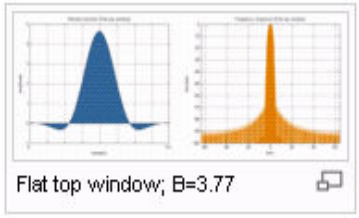

$$w(n) = a_0 - a_1\cos\left(\frac{2\pi n}{N-1}\right) + a_2\cos\left(\frac{4\pi n}{N-1}\right) - a_3\cos\left(\frac{6\pi n}{N-1}\right)$$
$$a_0 = 0.35875;\quad a_1 = 0.48829;\quad a_2 = 0.14128;\quad a_3 = 0.01168$$

$$w(n) = a_0 - a_1\cos\left(\frac{2\pi n}{N-1}\right) + a_2\cos\left(\frac{4\pi n}{N-1}\right) - a_3\cos\left(\frac{6\pi n}{N-1}\right)$$
$$a_0 = 0.3635819;\quad a_1 = 0.4891775;\quad a_2 = 0.1365995;\quad a_3 = 0.0106411$$

$$w(n) = a_0 - a_1\cos\left(\frac{2\pi n}{N-1}\right) + a_2\cos\left(\frac{4\pi n}{N-1}\right) - a_3\cos\left(\frac{6\pi n}{N-1}\right) + a_4\cos\left(\frac{8\pi n}{N-1}\right)$$
$$a_0 = 1;\quad a_1 = 1.93;\quad a_2 = 1.29;\quad a_3 = 0.388;\quad a_4 = 0.032$$

Summary of Window function properties Figure 171

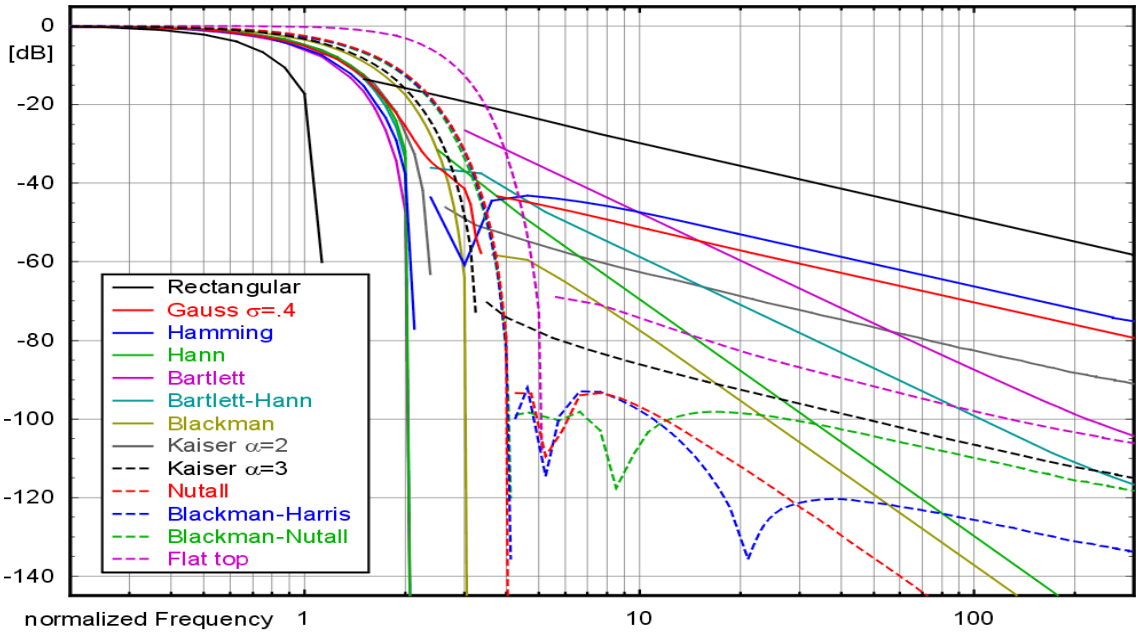

Table 9 Summary of window function design parameters (Bores [51])

Window function	Sidelobe level (dB)	Fall off (dB per octave)	Coherent gain	Equivalent noise bandwidth (bins)	6 dB bandwidth (bins)	Worst case processing loss (dB)
Rectangular	-13	-6	1.00	1.00	1.21	3.92
Triangular	-27	-12	0.50	1.33	1.78	3.07
Hanning	-32	-18	0.50	1.50	2.00	3.18
Hamming	-43	-6	0.54	1.36	1.81	3.10
Poisson (3.0)	-24	-6	0.32	1.65	2.08	3.64
Poisson (4.0)	-31	-6	0.25	2.08	2.58	4.21
Cauchy (4.0)	-35	-6	0.33	1.76	2.20	3.83
Cauchy (5.0)	-30	-6	0.28	2.06	2.53	4.28
Gaussian (3.0)	-55	-6	0.43	1.64	2.18	3.40
Kaiser-Bessel (3.0)	-69	-6	0.40	1.80	2.39	3.56
Kaiser-Bessel (3.5)	-82	-6	0.37	1.93	2.57	3.74

Sidelobe level = The attenuation to the top of the highest side lobe
Fall off = The asymptotic rate of fall off to the side lobe
Coherent gain = The normalised DC gain
Equivalent noise bandwidth = The bandwidth of a rectangular filter which would let pass the same amount of broadband noise.
6 dB bandwidth = The bandwidth in which the window function falls by 6dB
Worst case processing loss = The ratio of input signal to noise to output signal to noise, including scalloping loss for worst case frequency.

APPENDIX H

A/D conversion range and noise

Melkonian [52] views the analogue to digital process as the signal plus the noise introduced by the digitization process. From this application note, quantization of an analogue signal produces noise which is added to the signal entering an A/D converter. For large amplitude, complex signals, the quantization error from sample to sample will be statistically independent and uniformly distributed over the quantizing interval. The probability density P(v) for the quantization error v will be given by:-

$$P(v) = \begin{cases} \frac{1}{q}, & |v| < \frac{q}{2} \\ 0, & |v| > \frac{q}{2} \end{cases}$$

where q = the size of the quantizing interval

The rms noise V_{noise} is then :-

$$v_{noise} = \left[\int_{-\infty}^{\infty} v^2 P(v)\, dv \right]^{1/2}$$

$$= \left[\int_{-q/2}^{q/2} v^2 \frac{1}{q}\, dv \right]^{1/2} = \left[\frac{q^2}{12} \right]^{1/2}$$

For an n-bit ADC, the largest sinusoidal signal that can be converted without clipping has a peak-to-peak amplitude of $2^n q$ this corresponds to an rms level of :-

$$v_{signal} = \frac{2^{n-1} q}{\sqrt{2}}$$

The signal to noise ratio is then :-

$$\frac{S}{N} = 20 \log \left\{ \frac{v_{signal}}{v_{noise}} \right\} = 20 \log \left\{ \frac{2^{n-1}\, q/\sqrt{2}}{q/\sqrt{12}} \right\}$$

$$= 1.76 + 6.02\, n$$

The quantization noise is independent of the quantizing interval and only depends upon the number of bits n in the conversion. Table 10 gives the gives the signal to noise ratio calculated from the above formula together with some values quoted from the manufactures data sheets for some typical A/D converters that are suitable for this prototype application.

TABLE 10. Signal to Noise ratio and distortion for various A/D converters

converter	Number of bits	Sampling Rate(MSPS)	SNR (dB) manufacturers	THD (dB) Manufactures	S/N (db) Calculated
AD9280	8	32	-48	-58	-50
AD9200	10	20	-56	-58	-62
AD9220	12	10	-70	-84	-74
AD9240	14	10	-78	-77	-86
AD9446	16	10	-80	-78	-98

APPENDIX I

System Flow diagrams

This appendix gives an analysis of the time taken for each process in the NEWS system. The NBOX's are designed to be "reactive" they are sent an instruction, they perform the required task and then send a reply. This reply may be an acknowledgement of an instruction or it may be to send up a series of data values. The following analysis gives flow charts which name the instruction and give a function for the time it takes to implement these instructions.

Figure 172 Non-linear harmonic generation process time requirements

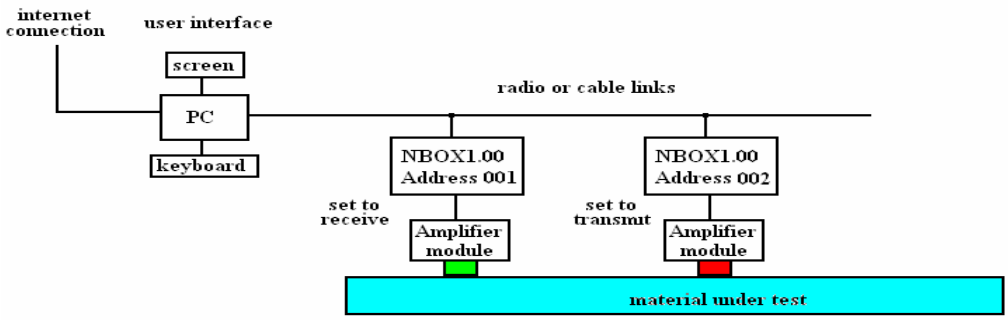

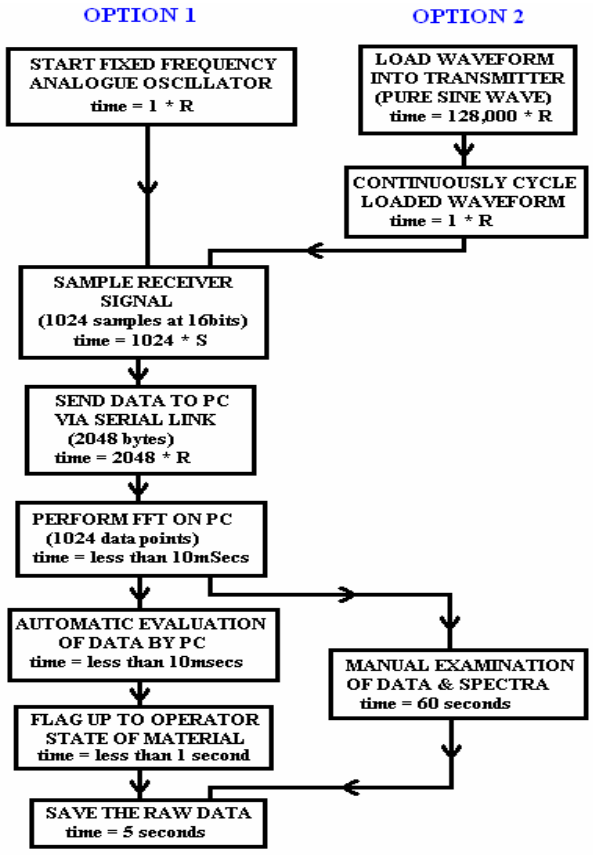

R = Data transmission period; time taken to send one word of data over a serial link.
Note; A command instruction sent to the NBOX consists of one word.
10 bits are needed to send one word of data, 8bits of data, 1 start bit and 1 stop bit.
for example a data rate of 20K baud R = 0.5mSec. for 1Mbaud R = 10usecs.
(If parity is used then an additional bit will be needed).

S = A/D or D/A sampling rate, this is dependent upon the clock oscillator frequency.
16 bits are sampled simultaneously, on each clock cycle.
for example a clock speed of 10MHz S = 100nsecs, for 40MHz S = 25nsecs

N = number of NBOX units

Referring to Figure 172; Option 1 requires only to start an oscillator, take a sample and then to send this data up to the PC. Option 2 requires the transmitted waveform to be loaded into a memory, take a sample and then send this data up to the PC. In most cases the waveform need only be loaded once since it is retained in memory and used for subsequent sampling. For this system the time taken to load this memory is the main bottleneck (point at which data flow and system operation slows to a minimum). For a 20K baud data rate this time will be 64 seconds (that is to load 64K 16 bit data values), for 1 M baud the time is greatly reduced to 1.28 seconds.
Option 1 eliminates this bottleneck as it uses an internal analogue oscillator, removing the need to load a waveform to memory.

The sampling of only 1024 data values will reduce the system overhead very significantly. The sampling time with a 10 MHz clock is only 0.102 seconds
Sending the data via the serial link to the PC is 1.02 seconds (20K baud)

The current system using NBOX200 takes the full 64K samples but only sends 1024 data values along the RS232 link to the PC. There may be a necessity to take more samples particularly when operating at higher frequencies or if higher spectral resolution is required, this would increasing the amount of data to be transfer across the serial link. The computer calculation of the spectra involves using a FFT program, this has a requirement that the number of samples must be a power of two. PC computation of the FFT is very fast and is considered insignificant for most practical sample sizes for this harmonic analysis.
Once the data is in the PC and displayed on the screen the manual examination of the data is the second bottleneck, estimated to be up to 60 seconds. Automatic evaluation will reduce this time, but may be less effective in determining the state of the aircraft structure.

Figure 173 Non-linear modulation process time requirements

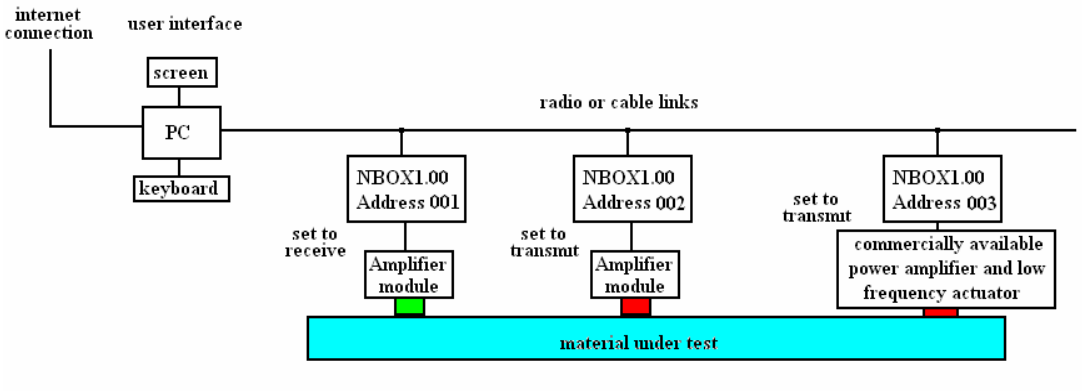

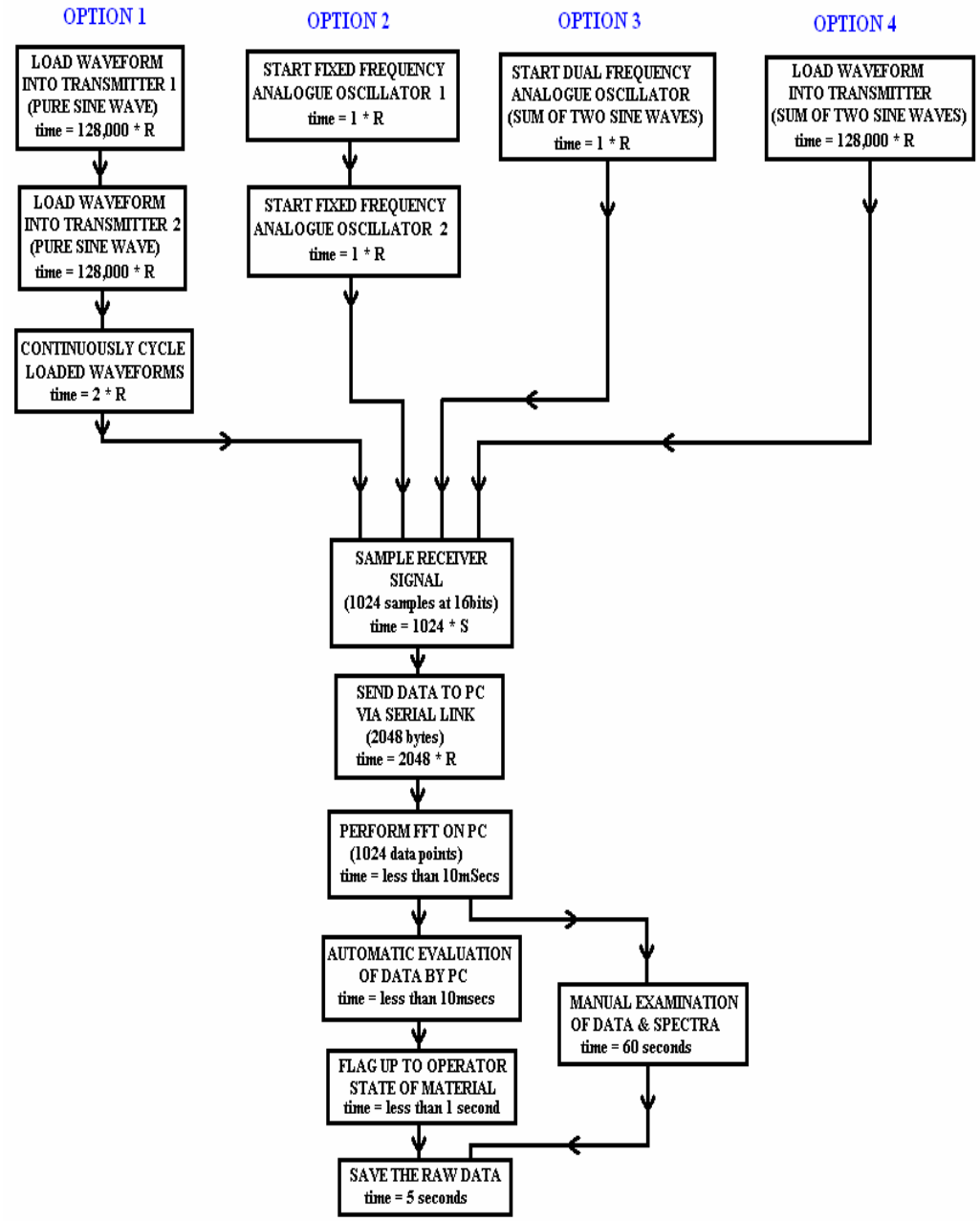

Referring to Figure 173. Option 1 will take the longest time, since we have to load two waveforms in to two separate units. Option 4 reduces this time by only loading one unit with a waveform that is the sum of two sine waves. Options 2 and 3 take the least time since they are required only to switch on analogue oscillators.

Figure 174 Non-linear pulse inversion process time requirements

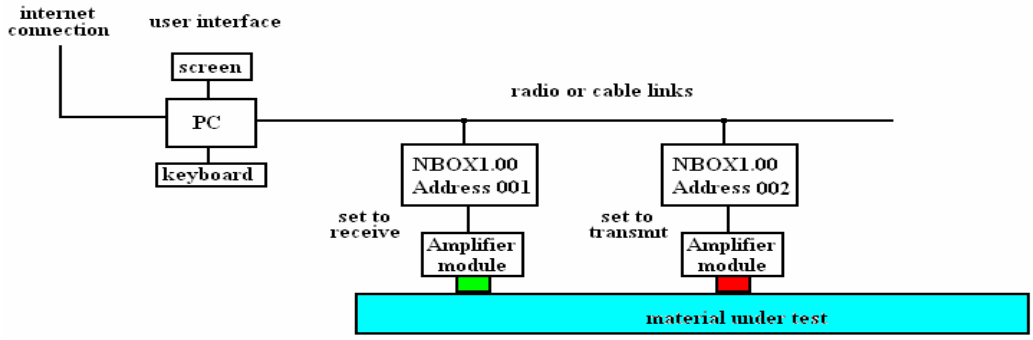

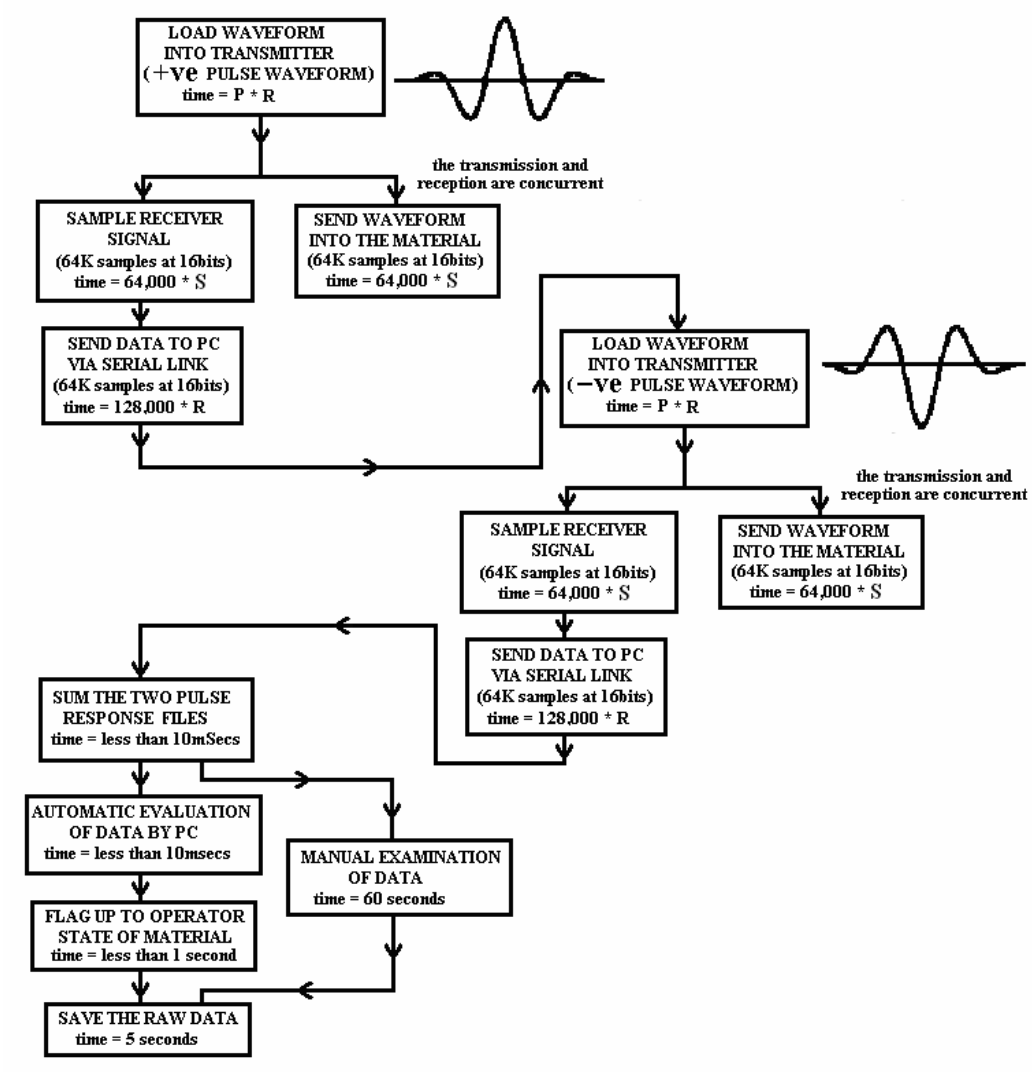

Referring to Figure 174. The two main overheads with this method are, loading of the two wave forms and sending up the received data to the PC. In order to reduce the first overhead, the pulse waveform that is to be transmitted (time P*R) can be made as short as possible. In this figure P is the number of data words representing the pulse and R is the data transmission period.

In the experimental work the pulse waveform loaded consisted of just a square wave (either positive or negative) of duration 1 microsecond. (P = 10 data values).

The sampling time is negligible in comparison, for 10 MHz clock and 64K samples the total sampling time is 6.4 milliseconds.

To reduce the second overhead the data transfer rate could be increased for example from 20K baud to 1M baud then the total time reduces from 128 seconds to 2.624 seconds. This time can be further reduced if less data is recorded. If only 5000 samples are taken then the transfer times are 5 seconds for 20K baud data rate and only 0.1 seconds at 1M baud.

If the system is to be used in an array of N units, then the waveforms will have to be loaded each time, into a different unit, and N-1 channels of received data sent to the PC at each test position. Under this arrangement data transfer time must be minimised. The least possible samples taken and the shortest waveforms loaded to memory.

Figure 175 Non-linear time reversal process time requirements

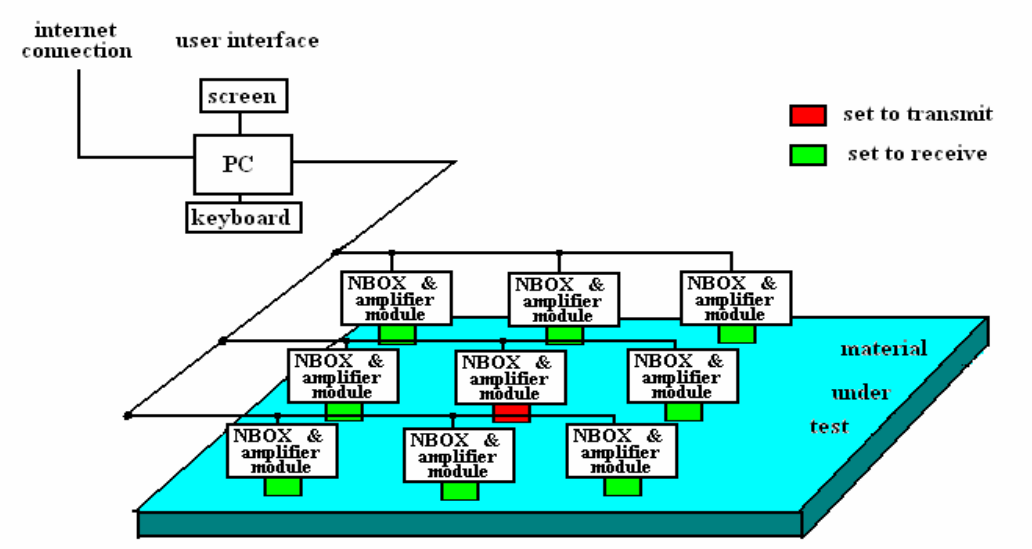

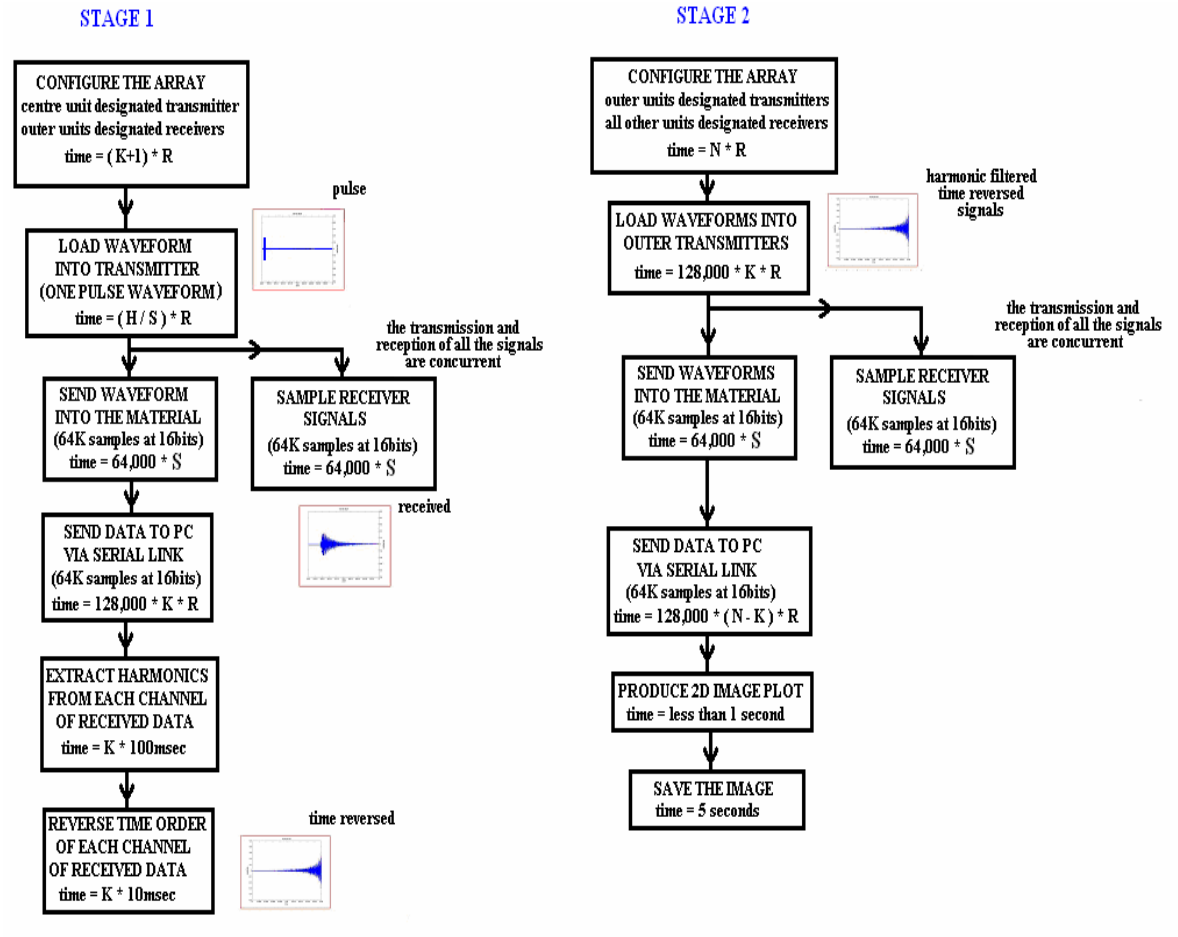

Definitions:-

N is the number of module units in the testing array.
N = X * Y where X is the number of units in the x direction, and Y is the number of units in the y direction.
If X = Y then the array is square.
If N is an odd number then the array will have one unit that is central to the array.
The number of units occupying the perimeter is K, = 2X + 2(Y-2)
H = required pulse length (in msecs)
S = sampling rate in usecs. (0.1usec for 10MHz clock, 0.025usec for 40MHz clock)
The number of samples to represent the pulse is then = H / S
R = data transmission period (time taken to send one worrd of data over a serial link).

It is assumed that the sampling of all receivers is 64,000 values at 16 bits
PC computer computation times have been estimated, based on a Pentium 1GHz machine.

Operational times for one sampling location:-

Operation	time
Configure the array (stage 1)	(K + 1) * R
Load pulse waveform	(H / S) * R
Send and receive waveforms (concurrent operation)	64,000 * S
Send received signal data to PC	128,000 * K * R
Extract harmonics from each receiver channel (on PC)	0.100 * K
Reverse the time order of each receiver channel (on PC)	0.01 * K
Configure the array (stage 2)	N * R
Load waveforms to outer transmitters	128,000 * K * R
Send and receive waveforms (concurrent operation)	64,000 * S
Send received signal data to PC	128000* (N – K) * R

Figure 176

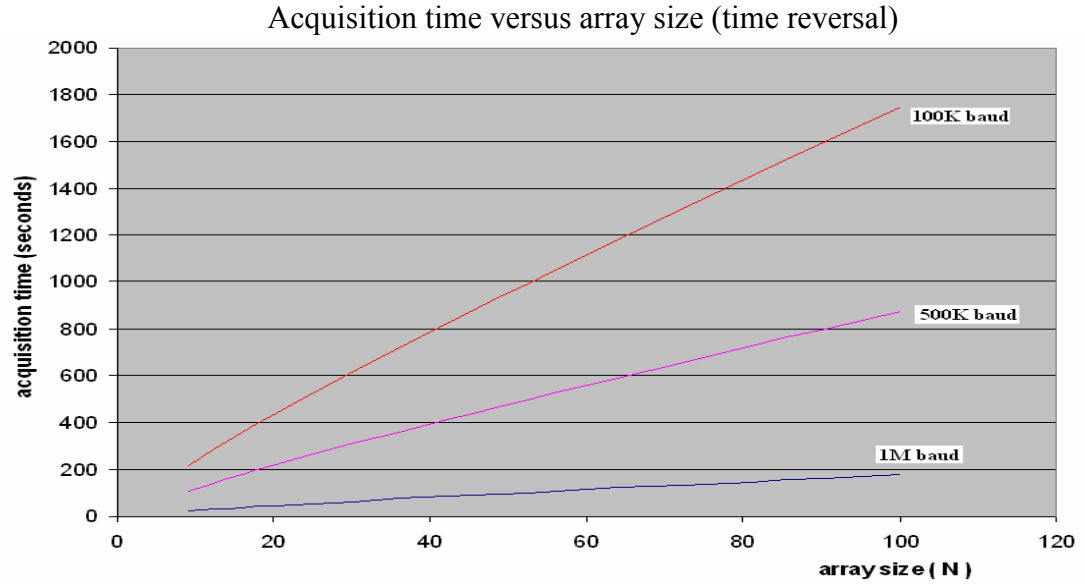

Figure 176 shows the effect of variations in the data rate R, for a fixed value of S and H.
S = 100nsec, for 10MHz clock, H = 1 microsecond.
R is the dominant factor, S and H have no significant effect on the acquisition time, for typical values of data baud rate.

Data acquisition time summary

Table 11 gives the values calculated for 100K baud data transfer rate and using a 10MHz sampling clock. The total time quoted is for one testing at a particular location. In Harmonics, Modulation and Pulse inversion the waveform need only be loaded once, since it stays in memory. For subsequent testing locations the waveform load time can be subtracted from the totals.

Table 11 A summary of data acquisition times

	HARMONICS		MODULATION				PULSE INVERSION	TIME REVERSAL		
	1	2	1	2	3	4				
Number of modules	2	2	3	3	2	2	2	9	16	25
Number of waveform samples	0	64K	128K	0	0	64K	64K	100	100	100
Number of data samples	1K	1K	1K	1K	1K	1K	64K	64K	64K	64K
Waveform load time (seconds)	1mS	12.8	25.6	2mS	2mS	12.8	12.8	102	154	205
Sampling time (seconds)	1mS	1mS	1mS	1mS	1mS	1mS	6.5mS	6.5mS	6.5mS	6.5mS
Data transfer time (seconds)	0.2	0.2	0.2	0.2	0.2	0.2	12.8	115	205	320
TOTAL TIME (seconds)	0.2	13	25.8	0.2	0.2	13	25.6	217	359	525
Options to reduce bottleneck	Higher data transfer rates		Higher data transfer rates				Use shorter waveform. Record less data	Higher data rates Record less data		

The sampling time has very little significance upon the system operation time. Once the data is in the PC the time to process is very short. The next bottleneck is the evaluation time. The graphical display of data is short. Operator decision time may be long, depending on whether we need an alarm to indicate fail or no fail situation (qualitative analysis) or an assessment of the state of the aircraft components health (quantitative evaluation. The data recording and logging, and communication to other experts via the internet will add time to the testing and assessment process.

REFERENCES

[1] Armitage P.R. Non destructive testing and imaging of concrete. Final report; December 1996. Brite-Euram Program II; Industrial and materials technology; Contract Number BRE2-CT4-1403; Project number CR-1292-91.

[2] Armitage P. R and Horwood J. M, The role of surface waves in assessing structural damage. Proceedings of the 5th International Conference on damage assessment of structures (DAMAS) Southampton, UK, 1st to 3rd July 2003.

[3] Harker A. H. Elastic Waves in Solids: 1988 British Gas plc
published: Eyre & Spottiswoode Ltd, Grosvenor press, Portsmouth. pages 37 to 38
ISBN 0 85274 582 6

[4] Kolsky H. Stress Waves in Solids, published: Clarendon Press Oxford 1953. pages 56 to 65

[5] Mason. P. Warren: Physical acoustics and properties of solids. pages 47 to 48 published: D. Van Nostrand Co Inc 1958. Lib Congress Cat No. 58-11114.

[6] Mircea Calomfirescu and Axel S. Herrmann: On the propagation of Lamb Waves in viscoelastic composites for SHM applications. Key Engineering Materials Vol. 347 (2007) pp. 543-548

[7] Harker A. H. Elastic Waves in Solids: 1988 British Gas plc
published: Eyre & Spottiswoode Ltd, Grosvenor press, Portsmouth. pages 40 to 47
ISBN 0 85274 582 6

[8] Grewal Dilawar. Improved Ultrasonic Testing of Railroad Rail forTransverse Discontinuities in the Rail Head Using Higher Order Rayleigh (M_{21}) Waves
1996 The American Society for non-destructive testing.

[9] Dobrin. Milton B, Introduction to geophysical prospecting, pages 38 to 39. Pub McGraw Hill international 1952 ISBN 0-07-017195-5

[10] Potel. C et al: Energetic Criterion for the Radiation of Floquet Waves in Infinite Anisotropic Periodically Multilayered Media.
published: Acustica vol 87(2001) 340-351

[11] Harker A. H. Elastic Waves in Solids: 1988 British Gas plc, pages 39 to 40.
published: Eyre & Spottiswoode Ltd, Grosvenor press, Portsmouth. pages 21 to 28
ISBN 0 85274 582 6

[12] Van Den Abeele K et al, Non-linear Elastic Wave Spectroscopy (NEWS) Techniques to Discern Material Damage, Part 1: Non-linear Wave Modulation Spectroscopy (NWMS). Research in Nondestructive Evaluation, Vol 12, 2000, pages 17-30

[13] Frouin J, Sathish D, Matikas T, Na J, "Ultrasonic linear and non-linear behavior of fatigued Ti-6Al-4V", J. of Mat. Res, 1999;14(4):1295.

[14] Johnson P A, NonDestructive Testing of Materials by Non-linear Elastic Wave Spectroscopy (NEWS), Non-linear Elasticity Mail Stop D443, Los Alamos Seismic Research Laboratory, Los Alamos National Laboratory.
Invited by *Materials World, the Journal of the Institute of Materials* for publication in the September 1999 issue.

[15] Conner F.R, Modulation, Introductory topics in electronics and telecommunication. pages 6 to 7. Published by Arnold Pty Ltd 1982, ISBN 0-7131-3457-7.

[16] Van Den Abeele; deliverable D4, section 5.4 Non-linear impact modulation spectroscopy, Aeronews, health monitoring of aircraft by non-linear elastic wave spectroscopy, EC sixth framework AT3-CT-2003-502927

[17] Van Den Abeele K et al, Non-linear Elastic Wave Spectroscopy (NEWS) Techniques to Discern Material Damage, Part II: Single-Mode Non-linear Resonance Acoustic Spectroscopy. Research in Nondestructive Evaluation,(2000) 12:31-42, pages 35-36.

[18] Mattei Christophe; deliverable D3. Pulse coded sequence technique, Aeronews, health monitoring of aircraft by non-linear elastic wave spectroscopy, EC sixth framework AT3-CT-2003-502927

[19] Armitage P R, UK patent, GB2383413, Detecting rail defects using acoustic surface waves, granted 26.9.2005.

[20] Dixon S et al, Inspection of rail track head surfaces using electromagnetic acoustic transducers (EMATs), Insight, Vol 46, pp326-330, 2004

[21] Dos Santos Serge and Van Den Abeele Koen ; deliverable D4. Non-linear time reversal acoustics, Aeronews, health monitoring of aircraft by non-linear elastic wave spectroscopy, EC sixth framework AT3-CT-2003-502927

[22] Van Den Abeele; Areonews deliverable D3, health monitoring of aircraft by non-linear elastic wave spectroscopy, EC sixth framework AT3-CT-2003-502927

[23] David P. Arnold , Sridhar Gururaj , Sunil Bhardwaj , Toshikazu Nishida , Mark Sheplak ; A piezoresistive microphone for aeroacoustic measurements. University of Florida, Gainesville, Proceedings of 2001 ASME International Mechanical Engineering Congress and Exposition November 11-16, 2001, New York.

[24] Lingenberg D, Meier R, New EMAT Probes useful for various Applications, NDTnet March 1998 vol 3 No.3

[25] Day Robert A, PVDF and array transducers, NDTnet Sept 1996 vol1 No.09

[26] Clark L.E and Hilliard J.K, Motion Picture Sound Engineering, Research council of the academy of motion picture arts and sciences, Hollywood, California. D. Van Nostrand Co, Inc. 1938. page 93 to 97.

[27] Goll J.H, the design of broad-band fluid-loaded ultrasonic transducers. IEEE trans vol.su-26. No.6 Nov 1979.

[28] Mook Gerhard, Pohl Jürgen, Michel Fritz, Benziger Thomas; From Non-Destructive inspection to health monitoring of SMART CFRP-Composies, (Otto-von-Guericke-Universität Magdeburg, IWW, GPO Box 4120, D-39016 Magdeburg, Germany)per presented at the 8th ECNDT, Barcelona, June 2002.

[29] Torben Amby Christensen, Active vibration control with macro fibre composites, MSc Mechatronics thesis 2005, MADS Clausen Institute SDU Sonderborg, Denmark.

[30] Moses Robert W; Aeroelasticity Branch, NASA Langley Research Center Presented at SPIE's 4th Annual Symposium on Smart Structures and Materials, Industrial and Commercial Applications of Smart Structures Technologies, Conference 3044, March 4-6, 1997, San Diego, CA.

[31] Kessler S.S., Spearing, S.M. and C. Soutis. "Damage Detection in Composite Materials using Lamb Wave Methods." Proceedings of the American Society for Composites, 9-12 September 2001, Blacksburg, VA.

[32] Chang Fu-Kuo, Demands and Challenges for Structural Health Monitoring, Dept. of Aeronautics and Astronautics Stanford University, The First Australia Structural Health Monitoring Workshop Nov. 25-26, 2002

[33] Krantz Donald(1), John Belk(2), Paul J. Biermann(3), Joel Dubow(4), Lee W. Gause(5), Ramesh Harjani(6), Susan Mantell(6), Dennis Polla(6), Philip Troyk(7) Applied Research on Remotely-Queried Embedded Microsensors, 1 MTS Systems Corporation, 2 The Boeing Company, 3 Applied Physics Laboratory of Johns Hopkins University,4 University of Utah, 5 Naval Research Laboratory, 6 University of Minnesota, 7 Illinois Institute of Technology. (Internet source).

[34] Wang Haifeng , Ritter Tim, Cao Wenwu, and Shung K. Kirk, Passive Materials for High Frequency Ultrasound Transducers, NIH Transducer Resource, The Pennsylvania State University, University Park, PA 16802) paper published :- 1999 SPIE Conference Proceedings

[35] Grewe Martha G, Gururaja T.R., Shrout Thomas R and Newnham Robert E, Acoustic properties of particle/polymer composites for ultrasonic transducer backing applications. :- IEEE transactions on ultrasonics, ferroelectrics and frequency control vol 37 No.6 November 1990.

[36] Van Dyke K. S 1925 The electric network equivalent of a piezo-electric resonator. Phys. Rev., 25, 895 (abstract).

[37] Krimholtz R, Leedom D. A, Matthaei G. L, New equivalent circuit for elementary piezoelectric transducers, Electronic letters 25th June 1970 vol6 No.13.

[38] Birnie P and Fairall J. An introduction to low power radio. Published by: RF solutions Ltd 2002.

[39] Armitage P R, The use of low-frequency Rayleigh waves to detect gauge corner cracking in railway lines, Insight, Vol 44, pp396-372, 2002

[40] Chung H & Law K, diagnosing in situ concrete by ultrasonic pulse technique: ACI concrete INT; design and construction vol 5 no. 10 Oct 1983.

[41] Gaydecki P & Burdekin F, magnetic/inductance imaging of reinforcement in concrete structures. Final report to the construction committee. SERC grant ref GR/H37860 Aug 1994.

[42] Maguire P. T, Computer aided design software for acoustic transducers, PhD thesis University of East Anglia Nov 1989.

[43] Gal'perina A. N, Equivalent-circuit analysis of complex ultrasonic vibratory systems, Sov. Phys. Acoust. 23(5) Sept-Oct 1977.

[44] Hartsuijker C, Welleman J, Engineering mechanics volume 2 (2001), published by Springer, ISBN 978-1-4020-5763-2 (e-book).

[45] Sengpielaudio, Studiotechnik Aufnahmetechnik Tontechnic forum. Currently as a web site :- www.sengpielaudio.com email:- eberhard@sengpielaudio.com

[46] Sensor Technology Ltd, 20 Stewart Rd, Collingwood. ON, Canada

[47] Morgan matroc Ltd, Vauxhall industrial Estate, Ruabon, Wrexham Clwyd Wales, Technical notes “piezoelectric ceramic products”.

[48] IEEE, Institution of Electrical and Electronic Engineers, standards association Corporate office 3 park avenue 17th floor New York NY 10016-5997 USA.

[49] Balanis C, Antenna theory analysis and design, published by Wiley 1997 chapter 2.

[50] Wikipedia, Window functions; compiled by many authors from a variety of sources principle reference quoted by authors :-
Harris, fredric j. (January 1978). On the use of Windows for Harmonic Analysis with the Discrete Fourier Transform. *Proceedings of the IEEE* 66 (1): 51–83.
Nuttall, Albert H. (February 1981). "Some Windows with Very Good Sidelobe Behavior". *IEEE Transactions on Acoustics, Speech, and Signal Processing 29*
Oppenheim, Alan V.; Schafer, Ronald W.; Buck, John A. (1999). *Discrete-time signal processing*. Upper Saddle River, N.J.: Prentice Hall. pp. 468–471. ISBN 0-13-754920-2

[51] Bores, FFT Window Functions Limits on FFT analysis, Bores Co Ltd, Forwater, Pond Road, Woking, Surrey, England.

[52] Melkonian Leon, Improving A/D converter performance by dither, National Semiconductor corporation application notes 804, Feb 1992.

BIBLIOGRAPHY

P.Vigoureux D.Sc. Ultrasonics. Royal Naval Scientific Service.
Publisher: Chapman and Hall 1950 cat No. 438/4

Kaye & Laby, Tables of physical and chemical constants. Pub; John Wiley & sons inc ISBN 0-582-46354-8

Read O and Welsh W. From tin foil to sterio. Pub: Howard W Sams & Co Inc. USA 1959. Library of congress cat No. 59-15832.